REGULATION OF MONOCARBOXYLATE TRANSPORTER 1 (MCT1) BY PROTEIN KINASE A (PKA), THE CANONICAL WNT/BETA-CATENIN, NOTCH SIGNALING PATHWAYS, AND BY A MCT METABOLIC BLOCKER

A DISSERTATION
SUBMITTED TO THE FACULTY OF THE GRADUATE SCHOOL
OF THE UNIVERSITY OF MINNESOTA
BY

Zejian Liu

IN PARTIAL FULFILLMENT OF THE REQUIREMENTS
FOR THE DEGREE OF
DOCTOR OF PHILOSOPHY

Advisor: Lester R. Drewes, Ph.D.

December, 2013

Acknowledgements

I deeply thank my thesis advisor, **Dr. Lester R. Drewes,** for the research projects that I enjoyed working on. Thank you very much for helping and inspiring me on the first important stage during my career. I appreciate all the studying experiences in Drewes lab that established my competitive academic background and grew me into a more mature researcher.

My great appreciation also goes to **Dr. Robert T. Cormier**. Bob, sincerely thank you for all your help and kind encouragements during my PhD years. Thank you for your always patience and considerate opinions as a chair, a teacher and a friend. Of course, great thanks for organizing and coordinating within my committee. It has been my great honor to have you as my chair!

My profound gratitude and thanks to the revered members of my thesis committee **Dr. Matthew T. Andrews, Dr. David A. Bernlohr, Dr. William F. Elmquist and Dr. Anika M. Hartz.** Many thanks for your generous contributions and invaluable instructions to my PhD studies. Special thanks to **Dr. David A. Bernlohr** and **Dr. Anika Hartz** for your critical comments on my thesis structure.

Huge thanks to **Dr. Patricia Scott** for instructing me in science during my first year rotation. It is my great honor to have you as my first mentor in the United States. My never enough gratitude goes to **Mrs. Mary Sneve** for her generous help in the lab as well as my life in Duluth. Mary, great thanks for encouraging me when I was in depress, tutoring me with my English and finally caring for me like one of your own children. Many thanks to **Dr. Joseph R. Prohaska, Dr. Kendall B. Wallace**, **Dr. Andrew J. Skildum, Dr. Teresa Rose-Hellekant** from the School of Medicine Duluth, **Dr. Bjoern Bauer** from the College of Pharmacy at University of Minnesota Duluth (UMD) and **Dr. Jeffrey P. Smith** from the Colorado State University-Pueblo for his generous support to my PhD research. A lot thanks to the faculty, staff, scientists and technical support people from the School of Medicine Duluth, Department of Biology and College of Pharmacy, who helped me greatly but their names cannot be listed here due to space limitation.

Thanks to the prestigious **University of Minnesota** for giving me such an invaluable life-time opportunity to pursue my PhD degree. My sincere appreciation also goes to **UMD** as my home campus. Great thanks to **Biochemistry, Molecular Biology & Biophysics (BMBB)** program and **Academic Heath Center Duluth (AHCD)** program for my admission and financial support. Sincere thanks to the **Department of Biology at UMD** for providing me with a Teaching Assistant position and great financial aid.

Lastly, but always most importantly, special thanks to my parents **Qiang Liu** and **Yuhui Liu** for raising me and supporting me. Your endeared love is my lifelong precious.

Dedication

This dissertation is dedicated to my beloved family

谨以此文，献给生养我的父母

Abstract

Monocarboxylate transporters (MCTs) are responsible for the bi-directional diffusion of monocarboxylic acids, such as lactate, pyruvate, β-hydroxybutyrate and acetate, across cellular membrane. As a result, they play essential roles in cellular metabolism and various biological processes. In this thesis, we first reported an update on the new developments and advances of MCTs families in the past decade, with an emphasis on their functional roles and regulation mechanisms. Then, we studied MCT1 and its regulation by protein kinase A (PKA), the canonical Wnt/β-catenin and Notch signaling pathways in an immortalized rat brain endothelial (RBE4) cell line. Our results showed that cAMP-dependent PKA activation caused dephosphorylation and subsequent internalization of MCT1 from plasma membrane into early endosomes. Wnt/β-catenin pathway failed to affect *Mct1* mRNA level, but increased its protein's expression on cellular surface. MCT1 in RBE4 cells is regulated by endosomal-lysosomal, but not proteasomal degradation. Inhibition of deubiquitinases (DUBs) caused an upregulation of MCT1, implying a possible involvement of ubiquitination in MCT1's regulation by Wnt pathway. Notch inhibition by a γ-secretase inhibitor (DAPT) also elevated MCT1 protein level, and an intact Notch activity was required for the upregulation of MCT1 by Wnt/β-catenin signaling, indicating a crosstalk between the two pathways. Furthermore, we tested a novel MCT inhibitor (MD1), a substantially more potent analog derived from α-cyano-4-hydroxycinnamic acid (α-CHC), in suppressing human peripheral blood mononuclear cells (hPBMCs) and selected tumor cells proliferation. Our findings showed that MD1 inhibited hPBMCs proliferation at concentrations no less than 50μM. Under hypoxic culturing condition, it suppressed SW480 colorectal cancer cells and H4IIE hepatoma cells proliferation starting at concentrations of 25μM and 5μM, respectively. The same effects were not observed under normoxia. Besides, hypoxic culturing may sensitize tumor cells to metabolic inhibition of MCT1. A potential combinatorial usage of MD1 with other chemotherapeutic drugs is implied to achieve improved clinical outcomes. In summary, our results showed, for the first time, the regulation of brain endothelial MCT1 by PKA, Wnt/β-catenin and Notch signaling pathways; we also evaluated the inhibitory role of MD1 in suppressing hPBMCs and tumor cells by blocking lactate transport.

Table of Contents

List of Tables

List of Figures

Chapter VI

Appendix I

Chapter I

Monocarboxylic Acid Transporters

(Book Chapter Review)

[Drug Transporters: Molecular Characterization and Role in Drug Disposition, Second Edition], Edited by [Guofeng You and Marilyn E. Morris].

ISBN 0-471-XXXXX-X

Monocarboxylic Acid Transporters[1]

Zejian Liu and Lester R. Drewes

University of Minnesota Medical School Duluth

Duluth, MN 55812

218-726-7925

ldrewes@umn.edu

218-726-8014 (fax)

[1] This chapter is based on the subject of "*Monocarboxylic Acid Transporters*" for inclusion in the forthcoming work tentatively entitled "*Drug Transporters: Molecular Characterization and Role in Drug Disposition, Second Edition*", edited by Guofeng You and Marilyn E. Morris. Here it is reprinted with kind permission from JOHN WILEY & SONS, INC.

1. INTRODUCTION.

Monocarboxylic acids are among the most common metabolic intermediates in living systems and exist in diverse forms. They comprise the products of major catabolic pathways and include lactic and pyruvic acids from glycolysis (sugars), acetoacetic, β-hydroxybutyric and butyric acids from β-oxidation (fatty acids) and fermentation (complex carbohydrates, dietary fiber) and α-ketoacids from protein degradation (ketogenic amino acids). Passage of these highly hydrophilic compounds through membranes separating cellular compartments is highly restricted. Therefore, membrane embedded proteins that function as transporters are essential for metabolite trafficking. Among the specialized proteins that function as small molecule carriers, there are three known protein families that transport monocarboxylic acids (MCAs). These are members of the solute carrier families known as SLC16, SLC5 and the mitochondrial pyruvate carrier (MPC) family. MCA transporters are significant for their role in intermediary metabolism, pathology and genetic diseases. They are also relevant to pharmacology because of their ability to transport carboxylated pharmaceuticals (drug delivery) and as targets of therapeutic agents. Some properties of the members of the SLC5 and the SLC16 families have recently been summarized (1-4). In this review, features of these transporters will be discussed with an emphasis on newer developments and advances in the past decade.

2. MITOCHONDRIAL PYRUVATE TRANSPORTER FAMILY.

Pyruvic acid generated by glycolysis must enter the mitochondria to reach the pyruvate dehydrogenase complex and assimilate into the tricarboxylic acid (TCA) cycle. That a pyruvate transporter existed in the inner mitochondrial membrane was hypothesized by transport kinetics and inhibitor studies almost 40 years ago (5). Despite expansion of the plasma membrane transporter field, the mitochondrial carrier remained elusive until recent studies using genetic tools in model organisms (6, 7). Evidence suggests that at least two proteins, MPC1 and MPC2 (originally designated BRP44 and BRP44L), participate in forming a large heterocomplex responsible for mitochondrial pyruvate import and are conserved in yeast, flies and mammals. Furthermore, mutation in the MPC1 gene is believed to lead to a dysfunctional carrier and a serious disease condition in humans (6).

The human MPC1 gene is located on chromosome 6 and encodes a 109 amino acid protein (MW 12,347Da) that is processed to a 66 amino acid mature form. The paralog of MPC1 is MPC2 and is a gene located on chromosome 1 and encodes a protein with 127 amino acids (MW 14,279Da). The mature MPC1 and MPC2 proteins each contains two transmembrane segments and is located in the inner mitochondrial membrane. The two proteins are believed to form a heterodimer and with other proteins form a 150kD complex that carries pyruvate into the mitochondria.

Recent reports have linked thiazolidinediones (TZDs) with the MPC complex (8, 9). TZDs, such as pioglitazone, are indicated for adult hyperglycemia because they prevent the conversion of this condition to type-2 diabetes and they increase insulin sensitivity. The target of TZDs now appears to be MPC1, thus suggesting that regulation of the complex is critical for glucose metabolism regulation and that the complex is a potential target for improving diabetes therapies. Future studies to characterize the MPC complex and its regulation promise to be revealing, if not critical for discovering new disease treatments.

3. SLC5 TRANSPORTER FAMILY.

3.1. Structure.

Based on sequence homologies the SLC5 transporter gene family consists of 12 members and their related protein products (Figure I-1). All members are symporters and have an obligate anion, Na^+, as a cotransported species. The substrate of several SLC5 transporters is a carbohydrate (glucose, myoinositol) and because of their role in energy metabolism, nutrition and disease (altered glucose metabolism, diabetes) and their electrogenic properties some SLC5 members have been subjected to intensive study both *in vitro* and *in vivo* (for review see (1, 10)). Two members, SLC5A8 and SLC5A12, transport physiological monocarboxylates including lactate, pyruvate and butyrate and are known as SMCT1 and SMCT2, respectively. In humans SMCT1 is composed of 610 amino acids (MW 66,447Da) and is located on chromosome 12 (12q23.1) while SMCT2 is composed of 618 amino acids (MW 67,516Da) and is located on chromosome 11 (11p14.2). The putative structures of SMCT1 and SMCT2 are

similar and both contain 13 transmembrane segments with the amino terminal (endofacial) and carboxyl terminal (exofacial) ends on opposite sides of the membrane. A 3D model structure can be predicted by threading the sequence to a previously structurally characterized transporter protein (Figure I-2).

3.2. Location and Function.

Cloning of the SMCT1 (SLC5A8) and SMCT2 (SLC5A12) open reading frames and examining the tissue distribution patterns provides insight into their biological functions (11, 12). SMCT1 is a higher affinity transporter for a substrate such as L-lactate with SMCT2 having a lower affinity, but often higher capacity. Based on careful examination using an oocyte expression system, the stoichiometry of SMCT1 is 2:1 with respect to sodium and lactate and the same is presumed to exist for SMCT2 (13). Transcript and protein analysis suggests that SMCT1 and SMCT2 play important roles in transepithelial cell transport in the kidney and in the gut.

A major function of the SMCTs is absorption of lactate from the renal ultrafiltrate as it passes through the kidney tubules. Reabsorption of lactate is mediated by the low-affinity Na^+-coupled lactate transporter SMCT2 in the initial part of the proximal tubule and by the high-affinity Na^+-coupled lactate transporter SMCT1 in the distal proximal tubule (14). The result is that the concentration of blood lactate is maintained at about 1.5 mM. Deletion of the SMCTs leads to very high excretion of lactate in the urine and also a lowering of lactate in the blood (11, 14-16). An interesting feature is that in renal tissues the SMCTs are transcriptional targets of the transcription activator, c/ebpδ (16). Thus, studies of homozygous deletion of the c/ebpδ gene leads to nearly total ablation of the SMCTs from the kidney tubules (essentially a tissue-specific double knockout) while non-renal tissue expression remains intact.

Immunohistochemical analysis indicates that SMCT1 is primarily located in the rat colon and distal end of the small intestine (17). By contrast, SMCT2 is primarily located further upstream in the proximal end of the jejunum near its entrance from the stomach. Functional transport studies have corroborated these observations (18). Closer localization studies reveal that the SMCTs are located on the apical side of the epithelial

cells in both the proximal tubules of the kidney and the intestinal brush border, thus, serving to capture carboxylic acids from the tubule and intestinal contents (11, 17).

3.3. Pharmaceutical Substrates and Disease.

Another substrate that is effectively transported by the SMCTs is nicotinic acid, a carboxylic acid and vitamin precursor of nicotinamide adenine dinucleotide (19) (14, 18, 20). Absorption of this vitamin B3 is accomplished primarily by SMCT1 along the intestinal tract and colon. Of importance is that transport is inhibited significantly by physiological carboxylates (lactate, β-hydroxybutyrate) and by short chain fatty acids and various monocarboxylate drugs such as benzoate, salicylate and 5-aminosalicylate (14). Many nonsteroidal anti-inflammatory drugs (NSAIDs) are monocarboxylates. In a study to examine interactions between NSAIDs and SMCT1 it was found that ibuprofen and structurally related compounds inhibit SMCT1 transport (21). However, despite its ability to block transport ibuprofen is not itself transported.

Evidence has also been reported that SMCT1 is essential for the transport of 5-oxoproline, an intermediate in the γ–glutamyl cycle in glutathione biosynthesis. Transport appears to function in kidney where robust reabsorption of 5-oxoproline occurs in the tubules (22). Furthermore, SMCT1 is expressed in the retinal pigment epithelium and other cells of the retina, a tissue that with age may suffer macular degeneration resulting in part from oxidative stress and low glutathione levels. As a therapeutic strategy glutathione levels may be enhanced by providing precursors or prodrugs such as 2-oxothiazonlidine-4-carboxylate (OTC). Following recent studies, it appears that OTC is an SMCT1 substrate and glutathione is elevated in retinal tissue following OTC treatment (23). Thus, the expression and function of SMCTs may be important factors in treating this debilitating disease.

SMCT1 (SLC5A8) is associated with cancerous tissues. In a study examining aberrantly methylated genes that result in gene silencing, it was discovered that the promoter region of SMCT1 is hypermethylated and is a common and early event in colon cancers (24). In over half of human colon cancers and related cell lines SMCT1 is silenced and, thus, SMCT1 is a tumor suppressor gene. This property is attributed to the fact that

SMCT1 is responsible for influx of butyrate into colonic epithelial calls and this monocarboxylic acid is a known potent inhibitor of histone deacetylases (HDACs) (25). In tumor cells, HDAC inhibition results in cellular differentiation and activation of cell death pathways (26). Tumor cell apoptosis involves cell specific induction of death receptor pathways and activation of pro-apoptotic proteins (27, 28). For some non-colonic tumors, pyruvate may be taken up by monocarboxylic acid transporters including SMCT1 and cause inhibition of HDACs and activate tumor cell apoptosis (29). New insights into the mechanisms of tumor cell differentiation and progression related to SMCTs (30) and their targeting by therapeutic drugs remain to be discovered.

4. SLC16 TRANSPORTER FAMILY.

4.1. Introduction.

The family of mammalian monocarboxylic acid transporters is officially assigned the name SLC16 and there are 14 unique members designated SLC16A1 through SLC16A14 (31). Before the genes were fully sequenced and annotated, several proteins from this family were independently reported in the literature using the abbreviations MCT1, MCT2 and so forth and, consequently, the numerical designations of the protein and gene names do not necessarily match. The MCT nomenclature is primarily used below.

Of the 14 members, five gene products appear capable of transporting the common short chain acids of lactate, pyruvate, butyrate, β-hydroxybutyrate, acetate, and similar carboxylic acids. The transporters MCT1, MCT2, MCT3 and MCT4 were first identified, characterized and continue to be the focus of many studies. Recently, evidence strongly suggesting that MCT7 (SLC16A6) plays an important role in monocarboxylic acid efflux from hepatocytes during fatty acid catabolism (fasting ketogenesis) was reported (32). Further studies to confirm this observation and to describe additional features are needed.

The MCTs typically contain 12 transmembrane segments with their carboxyl and amino termini on the cytoplasmic membrane side. To form a functional transporter unit MCTs combine with a member of the immunoglobulin superfamily such as basigin (CD147,

EMMPRIN) or embigin. Formation of this heterodimer appears to be essential for trafficking and insertion of the MCT into the plasma membrane. Current reviews are available that detail many additional characteristics of the structure and function of MCTs (2, 33, 34).

4.2. Functional Roles of MCTs under Physiological Conditions and in Drug Transport.

4.2.1. Brain Functions.

MCTs have been implicated in important brain functions because of their role in transporting lactate or other monocarboxylates between cell types. In the hypothalamus, the brain structure involved in sensing glucose levels, MCT1 and MCT4 are expressed on tanycytes (hypothalamic glial cells) while MCT2 is enriched on neurons (35). The glucose sensing mechanism is governed by a metabolic interaction between tanycytes and neurons via lactate efflux through MCT1 and MCT4 from the former cells and subsequent influx through MCT2 into the latter, in order to stimulate neuronal ATP synthesis and their activation (36). Furthermore, in long-term memory (LTM) formation, it is proposed that MCT1 and MCT4 transport lactate generated from hippocampal astrocytes into neighboring neurons that express MCT2 for importing this substrate. This metabolic interaction is essential for LTM by supporting neuronal synaptic plasticity as well as the formation of new synapses (37). In addition, oligodendrocytes support axonal survival and integrity by supplying energy metabolites and performing myelination. MCT1 is found highly enriched on these glial cells, and its disruption leads to axon damage and neuron loss in *Mct1* heterozygous knockout mice (*Mct1*+/-). In patients with amyotrophic lateral sclerosis, a reduction of MCT1 expression is observed in oligodendrocytes, suggesting a critical role for MCT1 on these glial cells in brain pathogenesis (38).

4.2.2. Obesity and Abnormal Insulin Secretion.

MCT1 is implicated in the metabolism of adipose tissue, whose dysfunction is a key factor associated with obesity and later occurrence of insulin resistance. Hypoxia, a critical feature of fat tissue proposed during its mass expansion in obesity, increases

MCT1, but decreases MCT2 expression in adipocytes. These changes are likely key adaptations of adipose tissue to low oxygen tension (39). Despite a universal expression across other tissues, *MCT1* is not normally transcribed in β cells, disallowing uptake of lactate/pyruvate, two ideal mitochondrial fuels for generation of ATP for insulin exocytosis. However, in β cells of patients with exercise-induced hyperinsulinism (EIHI) mutations identified within the *MCT1* promoter region result in marked transcriptional stimulation and expression of this gene. MCT1, thus enables pyruvate/lactate uptake from circulating blood and subsequent inappropriate release of insulin, which causes hypoglycemia (40). Transgenic mice that overexpress MCT1 in a β-cell specific manner recapitulate all the features of EIHI, including stimulated insulin secretion from β cells upon exercise exposure (41). All these findings demonstrate that silencing of MCT1 expression is critical for normal insulin secretion by β cells.

4.2.3. Drug Transport.

Many pharmaceutical agents contain a carboxylate group and, therefore, have structural similarities to MCT substrates such as the MCAs and short-chain fatty acids. The expression profile of MCT1 along the gastrointestinal tract, the neurovascular unit (blood-brain barrier) and other epithelial tissues makes this transporter an attractive route for passage of monocarboxylate-containing drugs through cellular membranes for absorption and for reaching their target sites. For example, benzoic acid is transported by porcine brain capillary endothelial cells (BCECs) in a saturable manner, with a K_m value of 3.05 mM (42). The same drug is reportedly transported by MCT1 in corneal epithelium where drug absorption is dominant, suggesting that MCT1 may play a role in the ocular drug absorption (43).

MCTs have also been documented as responsible for uptake of many other drugs across different biological membrane barriers. For example, as an antiepileptic drug, valproate must cross both the intestinal epithelial and blood-brain barrier for absorption and to reach the target cells in the central nervous system (CNS). In both Caco-2 and rat brain endothelial RBE4 cells, valproate transport is strongly stimulated by an inwardly directed H^+ gradient. The uptake rate is saturable with K_t values of 0.6mM and 0.8mM for Caco-2 and RBE4 cells, respectively. Lactate and pyruvate only inhibit its uptake at

RBE4 cells, but not at Caco-2 cells, indicating that MCT1 is responsible for valproate transport across blood-brain barrier, but suggesting the possibility for another yet unidentified H^+-dependent monocarboxylate transporter in intestinal epithelial cells (44). As an approved therapeutic agent for cataplexy with narcolepsy and a widely abused euphoriant, γ-hydroxybutyrate (GHB) uptake of GHB into Caco-2 cells is confirmed to be pH- and concentration-dependent and is best described by a Michaelis-Menten equation with K_m=17.6±10.5mM. Transport is inhibited by the known MCT inhibitor α-cyano-4-hydroxycinnamic acid (α-CHC). All of the above demonstrate that GHB uptake across Caco-2 cells is consistent with a proton-dependent MCT transport (45). Additional studies suggest that flavonoids (luteolin, phloretin and morin) may decrease the transport of GHB by MDA-MB231 cells transfected with the rat *Mct1* gene. Consistent with these *in vitro* studies, concomitant *in vivo* administration of GHB with luteolin increases its renal and total clearance, probably via inhibited renal reabsorption of GHB by luteolin (46). The interaction between these two drugs may suggest a potential clinical strategy to ameliorate GHB abuse (47).

With the aim to enhance drug uptake into CNS, betreliesoxybutyric acid (HBA) grafted docetaxel loaded solid lipid nanoparticles (HD-SLNs) have been explored to deliver docetaxel across blood-brain barrier. The HD-SLNs transportation relies on the transport of HBA through brain endothelial MCT1 and a significant resulting increase of accumulated docetaxel in the brain has been observed (48). More strikingly, a potent role of MCT1 as a drug transporter in treating cancers has been reported. The reprogrammed metabolism of tumor cells with a prominent glycolytic phenotype makes them sensitive to an anti-cancer reagent 3-bromopyruvate (3-BrPA), a drug that inhibits glycolysis (49). MCT1 is necessary and sufficient for 3-BrPA uptake by cancer cells, and its forced expression in 3-BrPA resistant cancer cells sensitizes tumor xenografts to the drug treatment *in vivo*. This reveals the concept that the selectivity of cancer-expressed transporters can be exploited for delivering toxic compounds to tumors.

4.3. Regulation of MCTs Activity

4.3.1. Regulation by Ancillary Proteins.

As membrane transporters with multiple transmembrane domains (TMs), MCTs require an association with a single TM glycosylated protein in order to be correctly targeted to plasma membrane. In most cases, this glycoprotein is CD147 (basigin, emmprin) for MCT1, MCT3 and MCT4, whereas it can be a different glycoprotein, embigin, in rat erythrocytes for MCT1 (50, 51). MCT2 requires embigin (also known as gp70) as its ancillary protein (52), although this transporter associates with CD147 in murine sperm (53). Enhanced association between MCT1 and CD147 has been reported to cause increased plasma membrane expression of this transporter protein (53, 54). Furthermore, silencing or knockout of CD147 in cultured cells or genetically modified animals results in decreased MCT1 plasma membrane localization, impaired MCT1:CD147 interaction, as well as altered tissue distribution of this transporter (55, 56). In malignant breast carcinoma cells, both MCT1 and MCT4 are associated with CD147 and another protein, CD44 (57). Interestingly, the destruction of CD44-hyaluronan interactions destabilizes assembly of the MCT1 and MCT4 complexes in the plasma membrane and the MCTs are retained in the cytosol. The molecular mechanism underlying MCTs' interaction with and regulation by CD147 involves hydrophobic residues residing in both the N-terminal and C-terminal ends of the single TM of CD147 (58). However, the conserved glutamate amino acid within the same TM domain, which was thought to be critical for mediating the interaction between these two proteins (59), now is reportedly not involved in this interaction (60, 61). MCT1 itself does not contain a basolateral sorting signal (BLSS) in its amino acid sequence. Therefore, its cellular polarity may be dictated by CD147 that has a weak BLSS that may be sufficient to shift some apical markers onto the basolateral membrane (62).

CD147 is also essential for maintaining protein expression levels of MCTs. For example, in human pancreatic ductal adenocarcinomas, silencing CD147 inhibits the expression and function of MCT1 and results in an increased intracellular lactate concentration (63). In addition, CD147 knockout animals show severely reduced intensity of MCT1 immunostaining in the regions where both CD147 and MCT1 are expressed (56). During tumorigenesis, the co-expression of MCT1, MCT4 and CD147 is commonly observed in cancer cells. Specifically, co-expression of MCT1 with CD147 is associated with low patient's overall survival in gastrointestinal stromal tumors (64). The expression of MCT1

and CD147 is correlated with primary and metastatic prostate cancer (65). In epithelial ovarian cancer (EOC) samples of primary tumors and in matched metastatic lesions, co-expression of CD147 with MCT1 and MCT4 is found and significantly associated with tumor stage, suggesting that over-expression of MCT1, MCT4 and CD147 is correlated with drug resistance during EOC metastasis. Thus MCT1 and MCT4 may be useful therapeutic targets (52, 66). Because of the close association, some inhibitors can target CD147 for suppressing MCTs transport function. For example, pCMBS inhibits MCT1 and MCT4 activity through targeting their common ancillary protein CD147, causing dissociation of these proteins by modifying the disulfide bridge in the Ig-like C2 domain of CD147 (52).

4.3.2. Regulation of MCT Intrinsic Activity.

Some studies have shown that the kinetics of MCTs transport can be modulated by signaling pathways and other intracellular molecules. For example, activation of the cAMP-dependent PKA pathway decreases MCT1's transport function [lower V_{max}, but no change in apparent Michaelis-Menten constant (K_m)] in RBE4 cells (67). Follow-up studies from the same group confirm that the observed reduction of MCT1 activity is due to dephosphorylation, and subsequent enhanced internalization of this transporter into early endosomes in a caveolae dependent manner (68). In Caco-2 intestinal epithelial cells, the p38 MAP kinase pathway increases the V_{max} of MCT1 transport by approximately two-fold without any changes in K_m. This higher transport activity is consistent with an increase in the apical membrane level of MCT1 parallel to a decrease of this protein in the intracellular pool (69). In addition, MCT1 transport activity of lactate in mouse cerebral astrocytes is augmented by carbonic anhydrase 2 (CAII). In a Xenopus expression system, MCT4 transport function is augmented by CAII as well (70). The mechanism is found to be independent of this enzyme's catalytic activity, but requires the binding of CAII to the C-terminus of MCTs, thus suppressing the formation of lactate microdomains at the transporter-core and therefore enhancing lactate flux (71). In other words, it is acting as an "H^+-collecting antenna". The amino acid His64 in the side chain of CAII is essential for this enhancement (72). MCT2's transport function can

be augmented by a different, extracellular membrane bound carbonic anhydrase isoform of CAIV, in a non-catalytic manner as well (73).

4.3.3. Regulation of MCT1 (SLC16A1) Gene Expression.

MCT1's expression has been associated with and thus regulated by tumorigenesis, with lines of evidence supporting both positive and negative modulations. A metabolic symbiosis has been suggested to explain enhanced glycolysis commonly observed during tumor progression, where lactate products from a highly glycolytic tumor core are extruded through MCT4 and then taken up via MCT1 into neighboring cells (74). As a result, increases in MCT1 expression, either mRNA or protein level or both, are observed in various tumors, e.g. breast (75-77), ovarian (66), prostate (78), melanoma (79, 80), non-small cell lung carcinoma (81) and leukemia (49). For example, MCT1 expression is elevated during nevus to melanoma progression as revealed by tissue microassay analysis, as well as in metastatic cells. Also, *MCT1* mRNA levels are found elevated in glycolytic leukemia. In contrast, MCT1 expression is down regulated in colorectal cancer, where butyrate (a substrate for MCT1) plays a critical role in maintaining colonocyte homeostasis (82-84). Compared with healthy colonic epithelium, MCT1 expression in the luminal membrane is decreased in colonic carcinoma (85) and in the transition to malignancy (86). In concurrence, MCT1 expression is not found on colorectal tumor vessels compared with normal tissues, although conflicting results are reported (87).

MCT1 is predominantly expressed in type I fibers in red skeletal muscle and in cardiac muscles, both of which have a more oxidative metabolic status (88-90) when compared to white muscles with more type II fibers and a glycolytic metabolism (91, 92). In developmental processes, MCT1 is detected as early as during oocyte maturation and its expression is maintained through the embryonic stage (93). In general, MCT1's expression level changes during development with a peak level at early postnatal life and rapidly declining towards adult age. Specifically, *Mct1* expression in mouse brain peaks around postnatal day 15, declining rapidly by 30 days at levels of adults (94). Similarly, 17-day old suckling rats have 25 times more MCT1 labeling than adults in the membranes of capillary endothelial cells, 15 times more in pericyte membranes and 19

times more in the membranes of astrocytic end feet adjacent to microvessels (95). Similar fluctuations of brain endothelial MCT1 levels are observed in both rodents and monkeys (96, 97). In mouse brown adipose tissue *Mct1* mRNA is more abundant in fetuses (E17.5) and neonates than in adult animals (98). In soleus muscle, MCT1 expression is lower in older rats than young rats, due to aging (99). However, in some other tissues, MCT1's regulation appears to be the opposite. For example, MCT1 expression is increased in adult bovine liver hepatocytes by 7-8 fold than in pre-ruminant animals (100). Furthermore, MCT1 protein levels are greater in horse gluteus medius muscle at 24 months compared to 2 months old (101). In conclusion, MCT1's regulation during development is complicated and variable in a tissue specific manner.

The expression levels of MCT1 have also been regulated by diets and nutrients. Specifically, a ketogenic diet increases MCT1 expression by 8-fold on rat brain endothelial cells and neuropil compared with animals on a normal control diet (102). This is supported by another study, where rat brain endothelial MCT1 level is elevated by 2-fold during a ketogenic diet (103) and suggests the neuroprotective potential of ketones (104, 105). Caloric restriction and protein malnutrition cause *Mct1* expression to decrease in Pla and EDL muscles, respectively (92, 106). In addition, folate deficiency causes reduced *MCT1* mRNA level in Caco-2 cells (107), whereas low digestible starch decreases MCT1 expression in ileum but increases its expression in colon (108). As for a regulatory role by hypoxia, 1% O_2 elevates *MCT1* mRNA and protein levels by 8.5- and 2.7-fold respectively in human adipose tissue, via a HIF-1 dependent manner (39, 109). In cervix, breast and colon cancer cell lines, MCT1 expression is also upregulated by hypoxia via NF-κB signaling pathway, but only in the absence of p53 (110).

Because MCT1 has been implicated in the alteration of cellular metabolism during many physiological progressions, its expression thus can be regulated by a variety of pathological conditions. In a rat focal ischemic hemisphere model, increase in *Mct1* mRNA expression is observed in cortex and hippocampus, as well as in peri-lesional macrophage/microglia (111). MCT1's regulation by insulin resistance during obesity/diabetes seems to be dependent on tissue types. MCT1 content of skeletal muscles in both STZ-induced diabetic rats and type 2 diabetic patients is reduced

compared with controls (112, 113). In contrast, elevated expression of brain MCT1, especially in the cortex and hippocampus, is observed in obese/diabetic mice (114). During hyperglycemia, rat brain MCT1 density is elevated by 12% within endothelial cells and astrocytes (115). Furthermore, epilepsy affects hippocampal MCT1 expression in patients with temporal lobe epilepsy by decreasing its expression on microvessels (116), but elevating that on astrocytes in epileptic models (117). Similarly, patients with temporal lobe epilepsy show decreased expression of endothelial MCT1 in hippocampus (116). In autoimmune diseases such as inflammatory bowel disease, MCT1 mRNA and protein levels in the inflamed colonic mucosa are markedly decreased (118).

MCT1's expression can also be modulated by a variety of signaling pathways. Protein kinase C (PKC) pathway increases MCT1 expression in colonic epithelial Caco-2 cells via the transcription factor activator protein 2 (AP2) (69). Similarly in muscle cells, phorbol 12-myristate 13-acetate (PMA) activates PKC, which then increases the V_{max} as well as the total expression level of MCT1 (119). PGC-1α, a key transcription factor for mitochondrial homeostasis, is positively correlated with and increases MCT1 expression levels in tibialis muscles (120, 121). NF-κB signaling is the mechanism of MCT1's regulation by butyrate in colonic Caco-2 cells (122, 123). Besides, activation of this pathway is required for MCT1 upregulation by hypoxia in p53-deficient cells (110). As MCT1's substrates, monocarboxylates (butyrate, lactate and pectin) can regulate its expression and function to adjust for metabolic needs. For example, butyrate has been known to increase MCT1's transcription and mRNA stabilization in colonic epithelial cells (122, 124), as well as this transporter's functional expression on plasma membrane in breast cancer cells (125). In skeletal muscle L6 cells, addition of lactate increases MCT1 expression at both mRNA and protein levels within 1h (126). Lactate produced by tumor cells and taken up by human mesenchymal stem cells increases their MCT1's expression (127).

4.3.4. Regulation of MCT2 (SLC16A7) Gene Expression.

Compared with normal tissues, MCT2 expression is consistent and ubiquitous in both prostate and gastrointestinal stromal tumor samples, demonstrating a significant elevation within cytoplasma granules (64, 128). Similar to MCT1, the expression pattern

of MCT2 in rodent brain during developmental processes peaks around early postnatal days and rapidly declines to the level observed at adulthood (94, 129). For example, neuronal MCT2 is most abundant in the first 3 postnatal weeks and thereafter decreases towards adulthood levels (130). The expression of MCT2 is also influenced by diets/nutrients. Studies have shown that fasting increases *Mct2* mRNA levels in the area postrema-solitary tract nucleus, whereas under-nutrition causes brain cortical MCT2 protein expression to be decreased (131, 132). In addition, pectin feeding increases MCT2 protein level in rat adrenal gland (133). Regulation of MCT2 by hormones has been reported. For instance, in cultured cortical neurons, brain-derived neurotrophic factor and insulin or IGF-1 significantly increase MCT2 protein levels at a translational level, requiring the PI3K-Akt-mTOR-S6K signaling axis (134, 135). Besides, removal of estrogen by ovariectomy induces the expression of neuronal MCT2 (136). In contrast, adrenalectomy decreases *Mct2* transcription in dorsal vagal complex of hypothalamus (137). MCT2 expression can also be regulated by various pathological conditions. For example, ischemic insult increases MCT2 protein expression in cells within the infarct and bordering the scar (138). In mice fed a high fat diet, genetically obese and diabetic mice, brain MCT2 expression is increased significantly as compared to controls (114). Finally, in a lithium-pilocarpine model of temporal lobe epilepsy, the expression of MCT2 is increased in adult animals and mostly enriched in the region of seizures (139).

4.3.5. Regulation of MCT4 (SLC16A3) Gene Expression.

As a prominent lactate extruder, MCT4 is associated with tumors and with tumor progression. These cancerous tissues are also characterized by the Warburg effect, a switch to aerobic glycolysis and lactate production and efflux. In prostate tumor samples, MCT4 expression in the cytoplasm of tumor cells is increased when compared with control tissue (128). In sections of human breast cancer samples, MCT4 immunostaining shows elevated expression level in the stroma, implying a metabolic reprogramming that supports tumor progression (75). The metastatic renal cell carcinomas have a significantly higher expression level of MCT4 compared with localized tissues, implying its significant role in metastasis (140). MCT4 has been considered to be the major efflux transporter of lactate from glycolytic muscles. As a result, its regulation in skeletal

muscles is correlated with type II fiber composition (141). The testosterone-induced increments of MCT4 expression are strongly correlated with fast-twitch fiber composition of rat muscles (89). Regulation of MCT4 expression by hormones has been documented substantially. T3 hormone increases both mRNA and protein expression levels of MCT4 in rat skeletal muscles (142). In human skin fibroblasts, T3 hormone induces MCT4 mRNA and protein expression in a PI3K signaling dependent manner (143). In human sertoli cells, insulin deprivation decreases *MCT4* transcription, consistent with an altered glucose metabolism (144).

MCT4 has been shown to be both positively and negatively regulated by exercise. Specifically, MCT4 protein expression is increased in rat red gastrocnemius and soleus muscles by a single bout of exercise, with peak expression 10h post training (145). Endurance training increases MCT4 expression in fasted skeletal muscles (146). After prolonged submaximal exercise in untrained volunteers, MCT4 expression in vastus lateralis is found modestly increased at recovery day 1 (147). In contrast, some studies have shown the opposite. In moderately endurance-trained runners, progressive sprint training does not result in any changes of MCT4 expression in vastus lateralis muscles before and after a single supramaximal running test to exhaustion (148). High-intensity training in women for five weeks fails to change MCT4 expression in vastus lateralis (149). MCT4 expression is influenced by a series of pathological conditions. In chronic obstructive pulmonary disease, MCT4 expression in vastus lateralis muscles is found to be 35% lower than control (150). In genetically obese or diabetic mice, increased brain MCT4 expression is observed compared to control animals (114). During ischemic insult, like MCT1 and MCT2, MCT4's expression also increases in cells within the infarct and bordering the scar after a permanent occlusion of the left middle cerebral artery (138).

There are many mechanisms for regulation of the MCTs expression and activity. Given the central role of monocarboxylic acids such as lactate and β-hydroxybutryate in cellular energy metabolism, it is not surprising that there are multiple types and levels of regulation. Further studies including examining micro-RNAs, protein-protein and protein-lipid interactions will be needed to provide a more complete picture of the role of MCTs

during development, under physiological and pathological conditions, and during delivery of drugs to the whole organism.

Table I-1: Representative substrates of MCTs and SMCTs

Transporter	Species	Expression System	Substrate	K_m (mM)	Refs
MCT1	Mouse	Ehrlich-Lettre cells	D/L-2-HB	2.62	(151-157)
	Rat	Xenopus Oocytes	Acetate L-Lactate D-Lactate Pyruvate	2.2 3.5 >60 1.01	
		REBC1	Benzoic acid	1.15	
		Red Blood Cells	GHB	2.2	
	Human	BCS-TC2 cells	Butyrate	0.0179	
MCT2	Rat	Xenopus Oocytes	Acetate L-Lactate D/L-β-HB Pyruvate	2.6 0.74 1.2 0.08	(156, 158, 159)
		Hepatocytes	HA	0.182-0.39	
MCT4	Human	Xenopus Oocytes	L-Lactate D-Lactate Pyruvate	28 519 153	(154, 160-162)
	Rat	Xenopus Oocytes	Acetate L-Lactate D-Lactate D/L-β-HB Pyruvate	>100 17 55 64.7 16.2	
		Mesangial cells	Lovastatin	37.3	
		Astrocytes	Nicotinate	2.8	
SMCT1	Human	Xenopus Oocytes	3-bromopyruvate Acetate Butyrate D-Lactate L-Lactate Nicotinate Pyruvate	0.5 2.46 0.08 1.09 0.18 0.23 0.39	(14, 163-166)
	Rat	Thyroid follicular cells	GHB	0.68	
SMCT2*	Human	hRPE cells	Lactate Butyrate Nicotinate	17-49 2.6-16 3.7-9.5	(12, 167)

RBEC1, rat brain endothelial cell line; BCS-TC2 cells, Colon adenocarcinoma cells; hRPE, human retinal pigmented epithelial cells; D/L-2-HB, D/L-2-Hydroxybutyrate; GHB, γ-Hydroxybutyrate; D/L-β-HB, D/L-β-Hydroxybutyrate; HA, Hippuric acid.

* Values derived from IC_{50}.

Table I-2: Representative inhibitors of MCTs, SMCTs and MPCs.

Transporter	Species	Expression System	Inhibitor	K_i or IC_{50} (μM)	Refs
MCT1	Mouse	Ehrlich-Lettre cells	α-CHC UK5099 DIDS Niflumic acid NPPB pCMBS	166 8.1 434 6.1 9.3 112	(46, 51, 168-171)
	Rat	Erythrocytes	GW604714X AR-C155858	<10 0.0023	
		MDA231 cells	Luteolin Phloretin	0.41 2.57	
	Human	Caco-2 cells	Naproxen Ketoprofen Naringenin Silybin	220 380 15.3 19.7	
MCT2	Rat	Xenopus Oocytes	α-CHC Phloretin Benzbromaron Quercetin	24 14 9 5	(151, 158)
		Hepatocytes	UK5099 DBDS Niflumic acid	45.2 181 20	
MCT4	Human	Xenopus Oocytes	α-CHC pCMBS Phloretin NPPB	991 21 41 240	(154, 172)
		LLC-PK1 cells	Fluvastatin Lovastatin acid	32.4 44.2	
SMCT1	Rat	Thyroid follicular cells	Ketoprofen Ibuprofen Probenecid	31.6 64.4 380	(21, 164, 173)
	Human	HRPE cells	Fenoprofen	119	
		IEC-6 cells	CDCA	n.a	
MPCs	Rat	Heart Mitochondria	α-CHC UK5099 α-Cyanocinnamate GW604714X	6.3 0.05 0.2 0.000057	(5, 169)

α-CHC, α-cyano-4-hydroxycinnamate; DIDS, 4,4'-Diisothiocyano-2,2'-stilbenedisulfonic acid; DBDS, 4,49-dibenzamidostilbene-2,29-disulfonate; NPPB, 5-nitro-2-(3-phenylpropylamino)benzoic acid; pCMBS, p-chloromercuribenzene sulfonate; CDCA, Chenodeoxycholic acid; n.a., not available

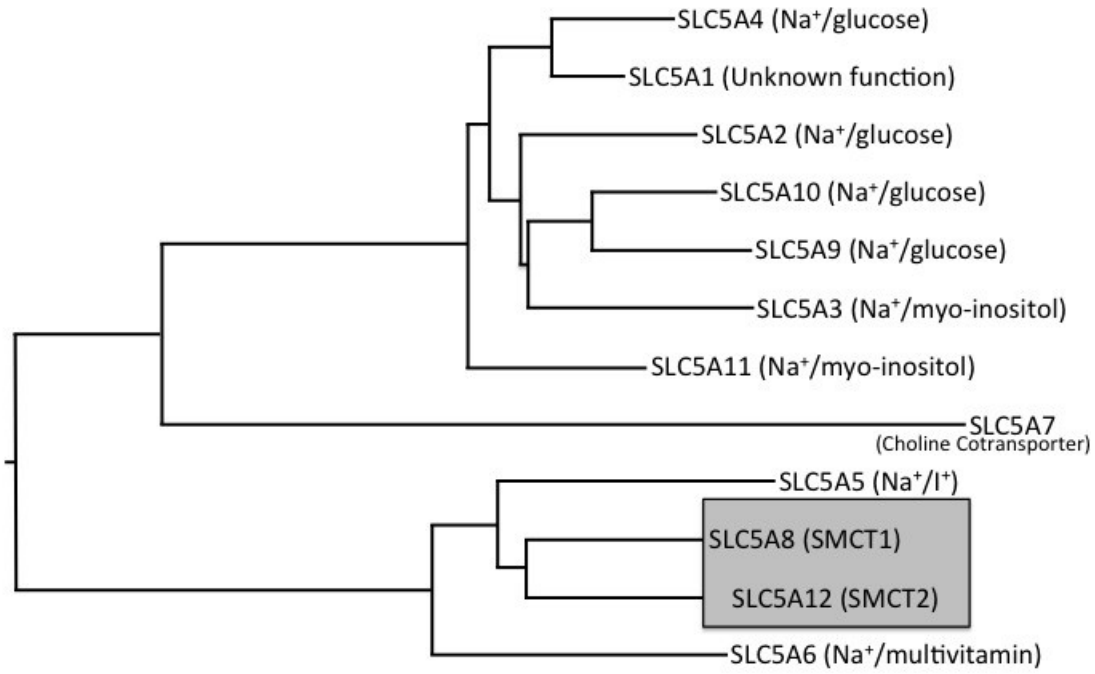

Figure I-1. Phylogenic Relationships of SLC5 Family Members. The carriers in this family that are sodium-dependent monocarboxylate transporters (SMCTs) are highlighted in the shaded box. Abbreviations for other SLC5 members and their substrates are also shown.

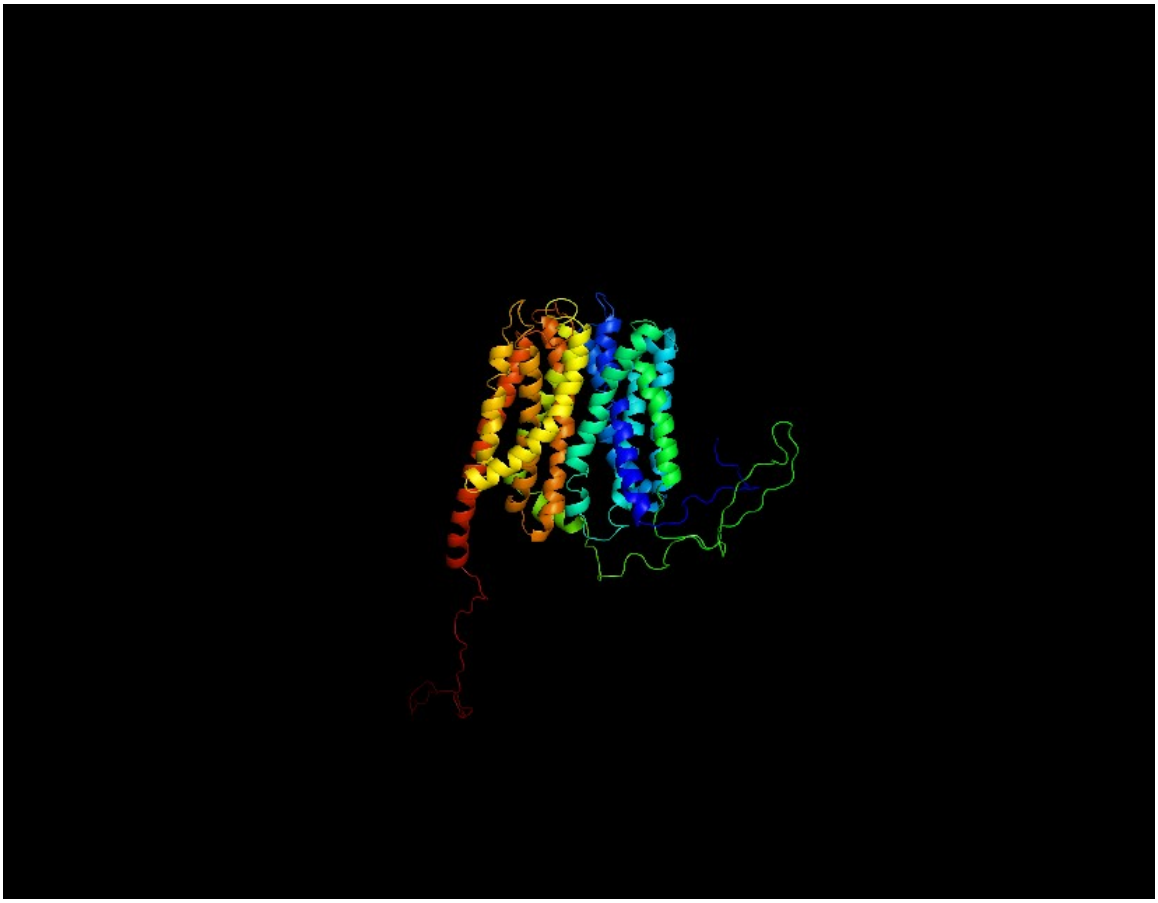

Figure I-2. Putative Membrane Structure of SMCT1. The amino acid sequence of SMCT1 was threaded onto a previously characterized 3D structure of a membrane transporter, the *Vibrio parahaemolyticus* sodium/galactose symporter (vSGLT), based on sequence homology. Each colored ribbon represents one of the thirteen transmembrane segments.

Chapter II

Regulation of brain endothelial MCT1 expression by cAMP-dependent pathway

Regulation of MCT1 by cAMP-dependent internalization in rat brain endothelial cells[2]

Jeffrey P. Smith[a,*], Amy L. Uhernik[a], Lun Li[a], Zejian Liu[b], Lester R. Drewes[b]

[a]Colorado State University-Pueblo, Department of Biology, 2200 Bonforte Blvd, Pueblo, CO 81001, USA [b]University of Minnesota Medical School Duluth, Department of Biomedical Sciences, 1035 University Drive, Duluth, MN 55812, USA

*Corresponding author:

Jeffrey P. Smith, Ph.D.

LS 224, Department of Biology

Colorado State University-Pueblo

2200 Bonforte Blvd, Pueblo, CO 81001, USA

Phone: (719)549-2420

Fax: (719)549-2993

Email: jeff.smith@colostate-pueblo.edu

---

[2] The expert technical assistance of Ms. Mary Sneve is greatly appreciated. This research was funded by American Heart Association grant 0855638G, and National Institutes of Health, National Institute of Neurological Disorders and Stroke, grant 1R15NS062404-01A2. This chapter is based on "*Regulation of Mct1 by cAMP-dependent internalization in rat brain endothelial cells*", published in *Brain Research* 1480 (2012) I-II. Here it is reprinted with kind permission from Elsevier publishing company. The original article can be found at http://www.sciencedirect.com/science/article/pii/S0006899312013595#

In the cerebrovascular endothelium, monocarboxylic acid transporter 1 (MCT1) controls blood–brain transport of short chain monocarboxylic and keto acids, including pyruvate and lactate, to support brain energy metabolism. MCT1 function is acutely decreased in rat brain cerebrovascular endothelial cells by β-adrenergic signaling through cyclic adenosine monophosphate (cAMP); however, the mechanism for this acute reduction in transport capacity is unknown. In this report, we demonstrate that cAMP induces the dephosphorylation and internalization of MCT1 from the plasma membrane into caveolae and early endosomes in the RBE4 rat brain cerebrovascular endothelial cell line. Additionally, we provide evidence that MCT1 constitutively cycles through clathrin vesicles and recycling endosomes in a pathway that is not dependent upon cAMP signaling in these cells. Our results are important because they show for the first time the regulated and unregulated vesicular trafficking of MCT1 in cerebrovascular endothelial cells; processes which have significance for better understanding normal brain energy metabolism, and the etiology and potential therapeutic approaches to treating brain diseases, such as stroke, in which lactic acidosis is a key component.

Introduction

Cerebral lactic acid levels are dependent on the activity of the monocarboxylic acid transporter 1 (MCT1) in the cerebral microvasculature where it is the only facilitator of lactic acid transport across the blood–brain barrier (174, 175). Because lactate is a critical energy substrate that has important roles in brain health and disease, understanding MCT1's physiological regulation in cerebrovascular endothelial cells is of great significance (67, 176). This is illustrated by the importance of MCT1 in controlling post-ischemic brain lactate concentrations, a key biochemical indicator of outcomes following stroke and brain injury (177-181). MCT1 is further implicated in metabolic coupling between astrocytes and neurons for brain energy metabolism, for regulating tumor growth, inflammatory responses, and for long term memory consolidation (37, 177-179, 181-185).

Previously, we have shown that the function of MCT1 is acutely regulated in a cerebrovascular endothelial cell line (RBE4) by a β-adrenergic receptor-mediated pathway that signals through adenylyl cyclase, cyclic adenosine monophosphate (cAMP), and protein kinase A (PKA). The regulation reduced the Michaelis–Menten parameter V_{max}, but not K_m, consistent with stimulus dependent reduction in the number of functional transporters on the cell surface (67). However, the mechanism linking PKA activation to reduced MCT1 function was not elucidated and questions remain regarding MCT1's plasma membrane location, phosphorylation status and trafficking.

PKA-dependent phosphorylation has been well characterized in having direct effects on the gating and kinetic function of various ion channels and transporters. This type of regulation is often associated with changes in K_m; however, this was not observed in our previous studies with RBE4 cells. Alternatively, phosphorylation-dependent vesicular trafficking to and from the plasma membrane also controls the cellular function of a diversity of membrane proteins and transporters, and is a plausible hypothesis for the cAMP-dependent changes in MCT1's V_{max} that we observed (186-190). Included among the transporters that are regulated by vesicular trafficking are monoamine transporters, aquaporins, sodium–hydrogen exchangers, proton pumps, and glucose transporters (19, 191-196). Vesicular trafficking occurs by different mechanisms including most notably

the clathrin and caveolin-dependent vesicular pathways. The caveolar pathway has been particularly well characterized in capillary endothelial cells, where it mediates not only the surface expression of proteins but also transcytosis of molecules between the luminal and abluminal surfaces of the endothelial barrier (197-199). Both clathrin- and caveolin-dependent endocytosis deliver protein cargos to various internal compartments including lysosomes, *trans*-Golgi, endoplasmic reticulum, and Rab 11 positive recycling endosomes. The specificity of protein trafficking to these organelles is controlled through processes involving early sorting endosomes, which are identified by their expression of the small GTPase Rab5, and EEA1. Therefore, we predicted that treatment of RBE4 cells with cAMP analogs would reduce the levels of MCT1 on the plasma membrane and increase MCT1 in clathrin coated pits or caveoli, early-sorting endosomes, and targeted cytoplasmic organelles. Identification of such a regulatory pathway, and whether direct MCT1 phosphorylation is involved, would greatly increase our understanding of the mechanism linking PKA activation to reduced MCT1 function, and could contribute to the development of new treatments for diseases in which monocarboxylate transport across the cerebral microvasculature is important.

Materials and Methods

RBE4 cell culture. RBE4 cells, a gift from F. Roux, were cultured as previously described (200-202). Briefly, cells were grown on collagen-coated polystyrene tissue culture dishes or collagen-coated number 1 coverslips in minimum essential medium alpha and F-10 nutrient (Ham's) (1:1) with 10% fetal bovine serum, 1% antibiotic–antimycotic, 0.3 mg/ml geneticin, and 1.0 ng/ml basic fibroblast growth factor. Cells were trypsinized, replated between 3 and 8 h prior to experimentation, and used at subconfluency.

Whole-cell protein isolation and western blot detection. Cells were lysed on ice for 45 min in pH 8 lysis buffer containing 10 mM Tris–Cl, 5 mM NaCl, 135 mM KCl, 2.5 mM EDTA, 2.5 mM iodoacetamide, 1% Triton X-100, 1 mM phenyl-methylsulfonyl fluoride (PMSF), protease inhibitor cocktail (Roche), and phosphatase inhibitor cocktail (Santa

Cruz Biotechnology). Lysates were sonicated for 10 min at 4^{o}C and centrifuged at 13,000 g for 8 min at 4^{o}C to remove debris and total protein was quantified with a BCA assay (Pierce Thermoscientific). Equivalent masses and volumes of protein were electrophoresed on 10% SDS-PAGE gels electrophoretically transferred to polyvinylidene fluoride membranes. Membranes were blocked in 50 mM Tris-buffered saline (pH=8.0), 5% non-fat milk, 1% Tween-20, and probed with primary antibodies overnight at 4^{o}C. Primary antibodies were diluted as follows: rabbit anti caveolin-1 (1:1000; Cell Signaling Technology), phospho-caveolin-1 (1:1000; Cell Signaling Technology), and chicken anti MCT1 antibody (1:5000) produced as previously described (102). Membranes were washed in blocking buffer and incubated in a goat anti-rabbit IgG-HRP to detect caveolin antibodies, (1:3000; Santa Cruz Biotechnology) or a rabbit anti chicken IgY-HRP (1:5000; Pierce Thermoscientific) to detect MCT1 antibodies. Blots were visualized using a Bio-Rad ABC chemiluminescence detection kit and imager.

Surface biotinylation and internalization. Cell surface proteins were biotinylated using reagents as described by the vendor's instructions (Pierce Thermoscientific; kit #89881) and quantified by immunoblotting. Briefly, RBE4 cell cultures (75 cm^2 flasks) were exposed for 30 min. at room temperature to Hepes Buffered Saline (HBS) or HBS containing 500 mM dibutyryl cyclic 3',5'-adenosine monophosphate (db-cAMP). Protein concentration was determined using the Pierce 660 nm Protein Assay kit including the Ionic Detergent Compatibility reagent (Pierce Thermoscientific). Proteins were run on SDS-Page gels, transferred to nitrocellulose membranes, blotted with chicken anti MCT1 IgY (1:5000) and mouse anti β-actin (1:10,000; Millipore). The proteins were detected using a secondary antibody consisting of HRP conjugated goat anti mouse IgG (1:10,000; Pierce Thermoscientific) or rabbit anti chicken IgY-HRP (1:5000; Pierce Thermoscientific) followed by Super Signal West Pico Chemiluminescent substrate (Pierce Thermoscientific). MCT1 and β-actin specific bands were imaged and quantified by spot densitometry using a ccd camera (Alpha Innotech) and related software.

MCT1 phosphorylation assay. RBE4 cell cultures (75 cm^2 flasks) were exposed for 30 min. at room temperature to HBS or HBS containing 500 mM db-cAMP followed by a

rinse with ice cold HBS. Cells were scraped in 800 μl homogenization buffer (20 mM Tris–Cl pH 7.4, 40 mM NaCl, 1 mM dithiothreitol with Complete Protease Inhibitor Cocktail (Roche)), homogenized using a motorized homogenizer, and ultracentrifuged at 50,000 rpm (100,000g) for 30 min. at 4^{o}C. Membrane pellets were solubilized and phosphoproteins separated using a Phosphoprotein Purification Kit according to the vendor's instructions (Qiagen). Briefly, solubilized membrane proteins were applied to an agarose column with high affinity for phosphoproteins. Unphosphorylated proteins do not bind and were present in the flow through. Bound phosphoproteins were eluted with high phosphate and high salt buffer. Protein determinations were made using a BCA protein assay (Pierce Thermoscientific). Representative aliquots of the flow through and eluate were subjected to SDS-PAGE gel electrophoresis, Western blotting, and quantitation by densitometry (normalized with actin) as described above. The phosphorylated fraction was reported as the percentage of the total MCT1 (see Figure II-1 legend).

Triton X-100 solubilization assay. Following treatment, RBE4 cells were lysed *in situ* on ice for 10 min in the lysis buffer described above. The supernatant (soluble fraction) was collected and the remaining insoluble cellular material was scraped from the culture substrate and resuspended in lysis buffer (insoluble fraction). Lysates were sonicated for 10 min at 4^{o}C. Equivalent volumes of each sample were mixed with DNase I (Invitrogen) and loaded onto gels for SDS-PAGE as described above.

Immunofluorescence staining. RBE4 cells were fixed in 3.7% formalin/PBS for 25 min followed by permeabilization with 0.5% Triton X-100 for 2.5 min at room temperature. Cells were rinsed with PBS, blocked with 1.5% goat serum, and stained with anti-MCT1 chicken diluted 1:1000 (Millipore) and anti-caveolin-1 rabbit diluted 1:700, anti-clathrin rabbit diluted 1:100, anti-EEA1 rabbit diluted 1:500, or anti-Rab11 rabbit diluted 1:300 primary antibodies (Cell Signaling) followed by detection with Alexafluor 488 diluted 1:125 and Alexafluor 568 diluted 1:75 secondary antibodies (Molecular Probes). Slides were mounted in ProLongs Gold Antifade Reagent (Molecular Probes).

Laser scanning confocal microscopy and colocalization analysis. Images were acquired using an Olympus FV10i laser scanning microscope using a 60x oil immersion objective and internally standardized illumination and detection-sensitivity parameters. Z-

slices were acquired at 0.646 mM/slice and Z-stacks spanned the thickness of each specimen. Colocalization analysis was performed using the colocalization function of Olympus Fluoview software version 3.1.

BCECF-AM ratiometric pH imaging. Internal pH measurements in RBE4 cells were made in HEPES-buffered saline (HBS) essentially as described previously (67, 202). Briefly, BCECF-AM loaded cells were exposed to 25 mM L-lactate and the initial rate of acidification was fit with a linear regression over the first ten seconds of the response. Image pairs, generated alternately with 440 and 495 nm excitation filters and 530 nm emission filter, were sampled at 60 Hz during the response. Following the response, the lactate-containing HBS was replaced with fresh HBS to allow the cells to recover and a two point calibration was made in nigericin-containing high K^+ HBS at pH 7.8 and 6.5. The ratio data was transformed to indicate intracellular pH by linear regression.

Drugs and statistics. All drugs were purchased from Sigma-Aldrich. Pearson's coefficients (203) were compared with a 2 sample t-test. Initial rates of L-lactate dependent acidification were measured in groups of a few hundred individual cells by BCECF imaging and binned by the intracellular pH determined at the start of each experiment in 0.01 increments. Responses from cells in each pH bin were averaged and the averages were paired across treatment groups for analysis using a paired t-test. Western blots were repeated at least 3 times and compared by a t-test.

Results

i. MCT1 phosphorylation and surface expression were reduced by cAMP

MCT1 transport function was reduced by more than 25% when RBE4 cells were treated for 10 min with membrane-permeant cAMP analogs (8-BrcAMP or db-cAMP), a result that is consistent with our previous report ((67); see also Figure II-6). Because we previously determined that this reduction was PKA-dependent, we assessed whether treatment with cAMP analogs causes a change in MCT1's phosphorylation status. This was achieved by purifying cellular membrane phosphoproteins from treated and

untreated RBE4 cell cultures followed by Western blot analysis and densitometry. Under basal conditions, 41% of the MCT1 signal was present in the phosphoprotein fraction and cAMP analogs reduced the signal to 29% (Figure II-1 A). This reduction was statistically significant ($p<0.05$), thus, cAMP signaling via PKA does not directly phosphorylate MCT1, but rather reduces the phosphorylation of MCT1.

Because the phosphorylation status of membrane proteins can control their surface expression, and because we previously showed that adrenergic signaling through cAMP decreases MCT1's Michaelis–Menten parameter V_{max} (67), we next assessed whether the surface expression of MCT1 was affected by elevated cytoplasmic cAMP. This was accomplished by brief treatment of RBE4 cells with cAMP analogs followed by biotinylation of the cell surface proteins that were isolated on streptavidin columns and subjected to Western blot detection and densitometry. Treatment resulted in a 16% reduction ($p<0.02$) in the level of MCT1 detected at the cell surface when compared to untreated controls or non-trafficking controls that were treated at 4^{o}C (Figure II-1 B). Therefore, our combined results (Figure II-1) demonstrate that elevated cytoplasmic cAMP causes dephosphorylation of MCT1 and that it becomes internalized from the surface of RBE4 cells. Thus, the cAMP dependent reduction of V_{max} is a result of MCT1 dephosphorylation and internalization.

ii. Colocalization of MCT1 with caveolin-1, but not clathrin, was increased by cAMP

To explore further the pathway for internalization of MCT1, we used dual immunostaining and fluorescence confocal imaging of MCT1 combined with either clathrin or caveolin-1 in RBE4 cells (Figure II-2). Widespread expression of MCT1 on the plasma membrane and especially at the leading edge of lamellipodia was observed. MCT1 was also detected across the cytoplasmic face in numerous puncta of different sizes and shapes as well as in a large perinuclear compartment that stained very brightly in most cells (Figures II-2 and -3, green). Clathrin-immunoreactivity (Figure II-2 A, red) was present in numerous round puncta that were distributed across the cytoplasmic face and in the large perinuclear compartment. Overlap between MCT1 and clathrin (yellow) was present in a subset of the round puncta that appeared to be very close to the

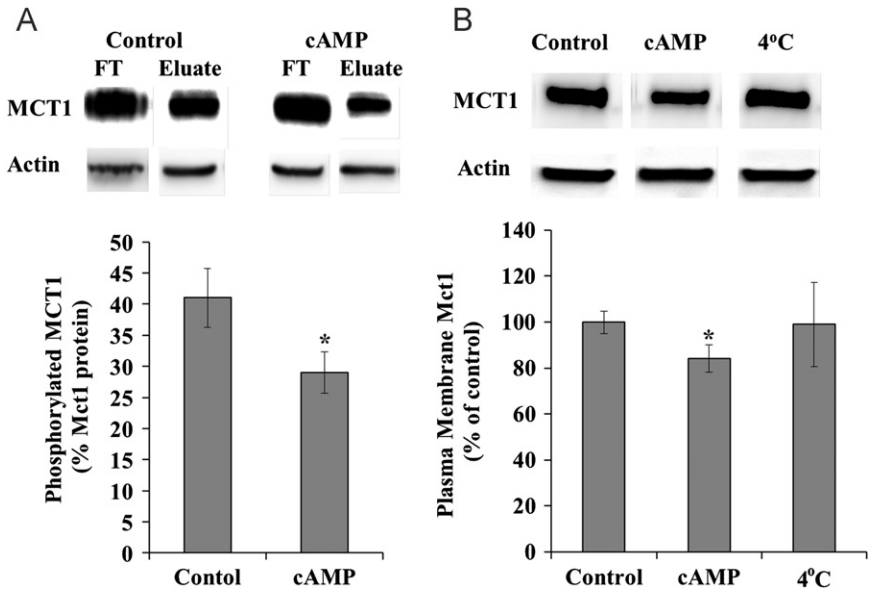

Figure II-1: MCT1 phosphorylation and surface expression were reduced by cAMP. (A) Cultured RBE4 cells were treated briefly with 500μM db-cAMP (cAMP) or with vehicle (control). Total cellular phosphoprotein was fractionated using a phosphoprotein purification column (Qiagen)-both flow through (unphosphorylated) and eluate (phosphoproteins) fractions were collected. MCT1 was detected in equal μg amounts of flow through and eluate proteins by Western blotting and quantified by densitometry using actin as a normalizing control. A representative blot is shown (above). The percentage of phosphorylated MCT1 was determined as elute/(elute+flow through) (below). The mean +/- s.e.m. from 4 independent experiments is shown and values were compared using the student's t test (*P<0.05). (B) The percentage of MCT1 in the plasma membrane was measured following treatment with cAMP analogs. Following treatment, surface proteins were biotinylated, solubilized, and purified on an avidin column. MCT1 was detected by Western blot and quantified by densitometry. A representative blot is shown (above). The amount of plasma membrane MCT1 was normalized to control. As an additional non-trafficking control some cells were treated with cAMP analogs but kept at 4^{o}C for the entire process to halt intracellular trafficking (4^{o}C). Values represent the mean +/- s.e.m. from 4 independent experiments. Differences in means were compared to control using the student's t test (*P<0.05).

plasma membrane, within the cytoplasm, and especially prominent in the brightly staining large central compartment. As has been reported in brain endothelial, smooth muscle, C6 glioma cells and neurons, treatment of the RBE4 cells with cAMP analogs caused them to round up, often accompanied by retraction of the lamellipodia (204, 205). However the overall patterns of MCT1, clathrin, and the overlap in staining, was not obviously changed. Pearson's coefficients of overlap (Rr) were calculated for Z stacks of multiple images and compared by two-sample t-tests. Rr values near 1 indicate the highest level of overlap and range to -1 when repulsion is present (203). Rr was near 0.8 for MCT1–clathrin pairs, consistent with MCT1's presence in clathrin coated vesicles; however, treatment with cAMP analogs did not appreciably change Rr (Figure II-4), suggesting that signaling through cAMP does not regulate MCT1's association with clathrin coated vesicles.

Caveolin-1 staining (Figure II-2 B, red) was present in vastly elongated regions on the plasma membrane, in numerous slightly elongated or round cytoplasmic puncta, and in larger clusters within the cytoplasm. It was largely absent in lammellipodia and the large central compartments that contained MCT1 and clathrin. In control cells, the overlap between MCT1 and caveolin-1 was diffusely localized in scattered cytoplasmic puncta and at the plasma membrane, particularly where some of the cells contacted one another. A cAMP-dependent increase in yellow overlap signal was obvious and widespread within intracellular puncta, cytoplasmic clusters, and in vastly elongated regions on the plasma membrane. The coefficient of overlap, Rr, for MCT1-caveolin-1 stained cells was in the range of 0.5 and was statistically significantly increased upon treatment with cAMP analogs (Figure II-4). Combined, the above results are consistent with a cAMP-dependent increase in endocytosis of MCT1 into caveolae via a clathrin-independent pathway.

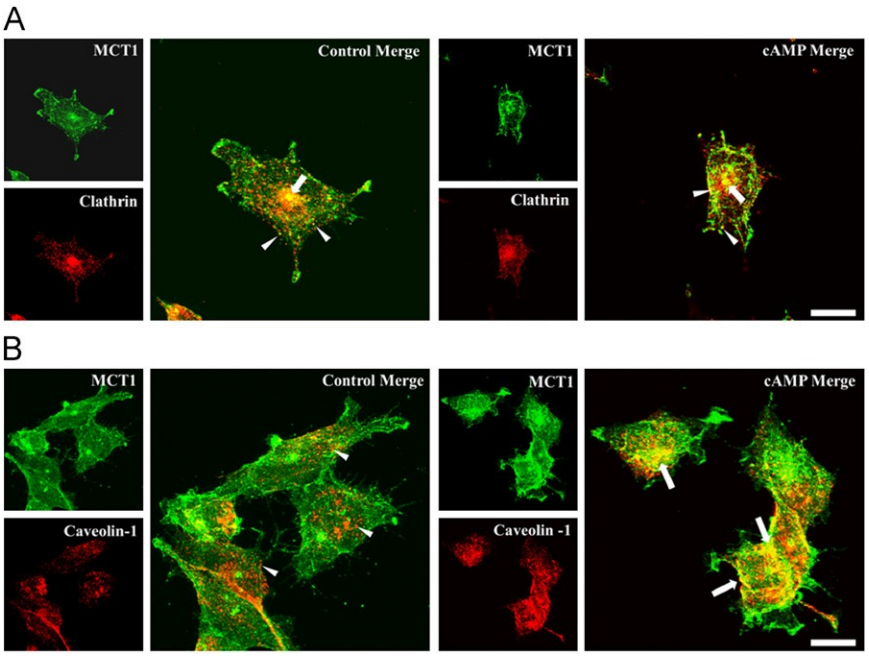

Figure II-2: Colocalization of MCT1 with caveolin-1, but not clathrin, was increased by cAMP. (A) Images of RBE4 cells that were dual-immunostained to visualize MCT1 (green) and clathrin (red) as indicated in the Figure. Merged images showed colocalization (yellow) in scattered puncta across the cytoplasmic face (arrowheads) and in a prominent perinuclear compartment (arrows) that was present in most cells. Treatment with 8Br-cAMP (right hand panels) did not appear to change the pattern of staining. (B) Images of RBE4 cells that were dual-immunostained to visualize MCT1 (green) and caveolin-1 (red) as indicated in the Figure. Caveolin-1 staining was present in localized areas close to the plasma membrane and in numerous slightly elongated puncta on the cytoplasmic face (arrowheads). Merged images from untreated cells showed less colocalization (yellow) in contrast to the more widespread colocalization observed in cells that were treated with cAMP analogs (arrows in right hand panel). Images are max-z projections of confocal images and the scale bar for merged images is 10 μm. (For interpretation of the references to color in this figure legend, the reader is referred to the web version of this article.)

iii. Colocalization of MCT1 with EEA1 but not Rab11 was increased by cAMP

The pathway of cAMP-induced internalization of MCT1 was further explored by confocal imaging of MCT1 with markers for early endosomes, EEA1 and Rab5, or with a marker for recycling endosomes, Rab11. EEA1 was readily detected in numerous round puncta that were spread across the cytoplasmic face and crowded along the perimeter of the plasma membrane of RBE4 cells (Figure II-3 A, red). Furthermore, EEA1 was present in the large perinuclear compartments described above. Colocalization between MCT1 and EEA1 was apparent in sparsely distributed puncta in the cytoplasm, near the plasma membrane, and in the large perinuclear compartment (Figure II-3 A). Supporting the notion of colocalization between MCT1 and EEA1, Rr for these images was near 0.7, and most importantly, a brief exposure to cAMP analogs significantly increased the Rr values for the MCT1–EEA1 pairs (Figure II-4). In many cells, the overlap appeared most prominent just adjacent to the plasma membrane (Figure II-3 A). Similar results were seen with immunostains for Rab5, a different marker of early endosomes; however, the change induced by cAMP did not reach statistical significance, possibly reflecting subtle differences among the endosomal populations identified or labeling efficacy achieved with the different markers (data not shown). Overall, these results are consistent with cAMP-dependent internalization of MCT1 into an EEA1-positive population of early-sorting endosomes.

As described above, MCT1 staining was very bright in a large and well-defined cytoplasmic region near the nucleus of many RBE4 cells. Clathrin, EEA1, and Rab5, invariably stained strongly in these regions as well; however, the boundaries of the region were broader and more diffuse for these markers than for MCT1. Interestingly, Rab11, a marker of recycling endosomes also strongly labeled these regions with a pattern similar to that seen for EEA1, Rab5 and clathrin (Figure II-3 B, red). Rab11 staining was also detected in fine puncta at the plasma membrane, and across the cytoplasmic face. In some images the cytoplasmic puncta appeared to form lines that radiated from the central region to the plasma membrane. Overlap between MCT1 and Rab11 was most prominent in the large cytoplasmic regions, and also occurred in finer puncta at the plasma membrane, cytoplasm, and along some of the radial lines. Rr

values for this pair were near 0.8; however, treatment with cAMP analogs did not cause an appreciable change in the level of overlap (Figure II-4). These results indicate that MCT1 was present in recycling endosomes, but that its presence therein was not regulated by cAMP.

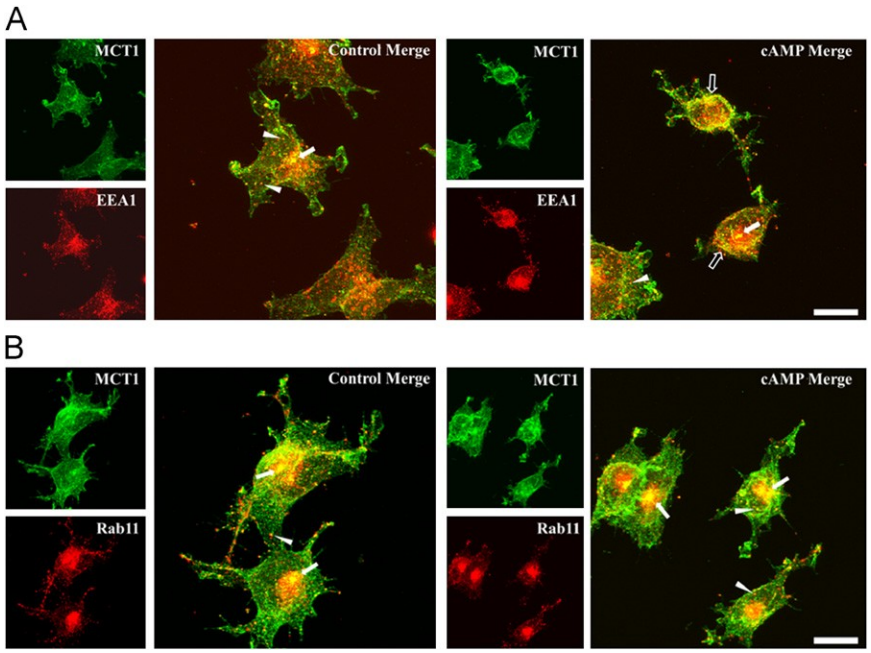

Figure II-3: Colocalization of MCT1 with EEA1 but not Rab11 was increased by cAMP. (A) Images of RBE4 cells that were dual-immunostained to visualize MCT1 (green) and EEA1 (red) as indicated in the Figure. Merged images showed colocalization (yellow) in scattered puncta across the cytoplasmic face (arrowheads) and in a prominent perinuclear compartment (solid arrows) that was present in most cells. Treatment with cAMP analogs appeared to increase colocalization near the plasma membrane of some cells (open arrows). (B) Images of RBE4 cells that were dual-immunostained to visualize MCT1 (green) and Rab11 (red) as indicated in the Figure. Merged images showed colocalization (yellow) in scattered puncta (arrowheads) and in a prominent perinuclear compartment (arrows) that was present in most cells and very strongly immunoreactive against Rab11 (a and b). Treatment with 8Br-cAMP did not appear to change the pattern of staining. Images are max-z projections of confocal images and the scale bar for merged images is 10 μm. (For interpretation of the references to color in this figure legend, the reader is referred to the web version of this article.)

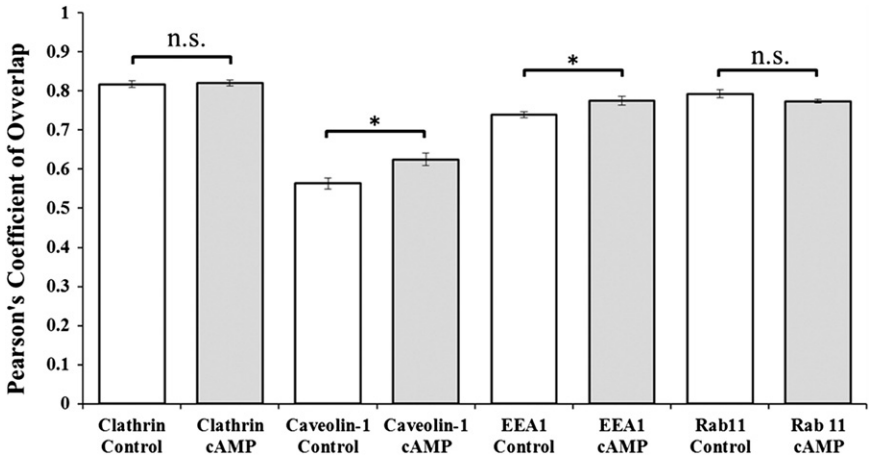

Figure II-4: Pearson's Coefficients of Overlap (Rr) for dual immunofluorescence images of untreated control and 8Br-cAMP treated RBE4 cells. In MCT1/clathrin stained cells Rr was 0.82+/-0.008 in control images and 0.082+/-0.007 in images from treated cells (p=0.775 showed no significant difference between groups, n.s.). In MCT1/caveolin-1 stained cells Rr was 0.56+/-0.014 in control images and 0.62+/-0.016 in images from treated cells (p=0.01). In MCT1/EEA1 stained cells Rr was 0.74+/-0.008 in control images and 0.78+/-0.012 in images from treated cells (p=0.02). In MCT1/Rab11 stained cells Rr was 0.79+/-0.01 in control images and 0.77+/-0.005 in images from treated cells (p=0.12, n.s.). For each bar, N=10 images like those represented in Figures II-3–6. Similar results were seen when these experiments were repeated.

iv. cAMP reduced the level of caveolin-1 phosphorylation

Because our results suggested that the major pathway for cAMP-dependent internalization of MCT1 from the plasma membrane of RBE4 cells is mediated through caveolae, and because phosphorylation of caveolin-1 changes its functional status, we used Western blotting to see whether phosphorylation of caveolin-1 changed in RBE4 cells after treatment with cAMP analogs. Under non-stimulated conditions caveolin-1 was detected in whole cell lysate from RBE4 cells using an antibody that recognizes the Y14 phosphorylated form of the protein (Figure II-5 A). Similarly we detected total

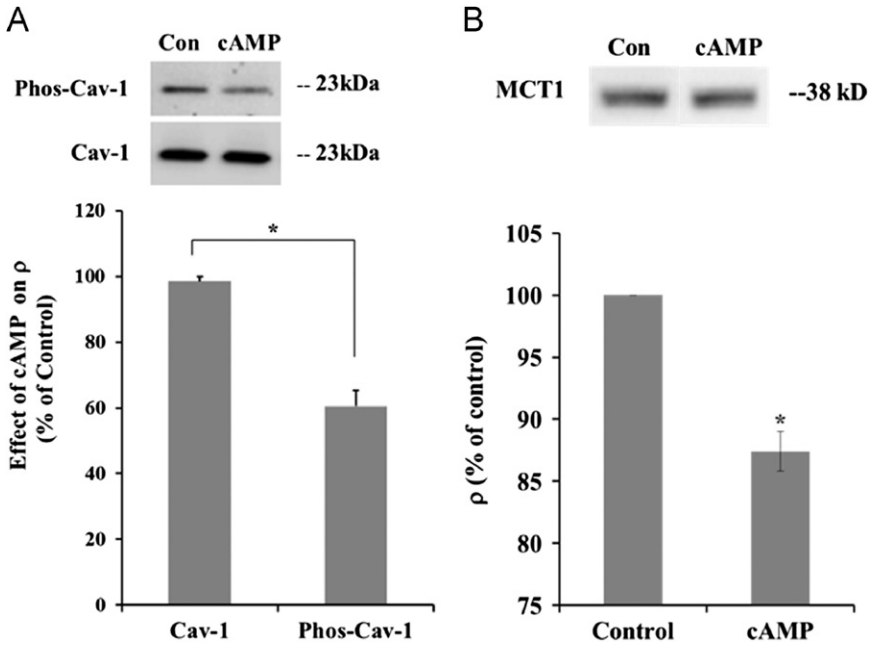

Figure II-5: cAMP reduced the levels of caveolin-1 phosphorylation and Triton X-100 soluble MCT1. (A) Cytoplasmic cAMP reduced caveolin-1 phosphorylation, a single band of 23 kD was detected with antibodies against phosphorylated caveolin-1 and caveolin-1 independent of its phosphorylation status. Treatment for 10 min with 500 μM 8-BrcAMP significantly reduced the level of phosphorylated caveolin-1, measured by the density of the band (ρ), by 40+/-5% (n=3 experiments, p=0.02). The level of total caveolin-1 that was detected was unchanged. (B) Adherent RBE4 cells were incubated in Triton X-100 and the supernatant was probed with an antibody against MCT1 to determine the level of MCT1 protein solubilized by this treatment. Cells that were treated for 10 min with 500 μM 8-BrcAMP showed a significant 12.5+/-1.6% decrease in MCT1 solubility (n=3 experiments, p=0.02).

caveolin-1 in these samples with an antibody that recognizes caveolin-1 independent of its phosphorylation status. Supporting the notion that cAMP leads to a change in caveolin-1 activity, brief cell treatment with cAMP analogs caused a statistically significant reduction in the phospho-caveolin-1 signal ($p<0.02$). However, the signal generated with the phosphorylation-independent antibody was unchanged. The specificity of the anti-phospho-caveolin-1 antibody and consistency in the loading of sample volumes was shown by the lack of a treatment-dependent change in the signal

generated with the control antibody. Thus, cAMP led to a change in the activation status of caveolin-1 consistent with its involvement in the regulation of MCT1.

v. cAMP reduced the level of Triton X-100 soluble MCT1

Next, whether cAMP signaling increases the association between MCT1 and caveolae was further investigated by taking advantage of the complete resistance of caveolae, and proteins associated with them, to solubilization in ice cold Triton X-100. Therefore, we extracted cAMP treated and untreated RBE4 cells with ice cold 1% Triton X-100 for 10 min and measured the level of MCT1 that was solubilized using Western blot and densitometry. The Triton X-100 solubility of MCT1 was significantly reduced in RBE4 cells that were treated for 10 min with 500 μM 8-BrcAMP (Figure II-5 B). This result is consistent with cAMP causing MCT1 to be internalized into caveolae and supports the findings of our confocal imaging data.

vi. Methyl-β-cyclodextrin and cAMP inhibited MCT1, but the inhibition was not additive

To evaluate further whether caveolae are involved in the functional regulation of MCT1 by cAMP, we conducted intracellular pH_i imaging experiments with BCECF to assess how MCT1 dependent transport of L-lactate was affected by cAMP and the cholesterol-depleting agent methyl-β-cyclodextrin (MβCD). MβCD has been shown to disrupt caveolae in numerous cell types. When RBE4 cells were exposed to 500 μM 8-BrcAMP for 10 min the transport rate was inhibited to 74+/-11% of control (Figure II-6, $p<0.01$). Treatment with 5 mg/ml MβCD for 30 min also inhibited MCT1 to 72+/-5% of control ($p<0.002$), and in experiments where MβCD was combined with 8-BrcAMP, MCT1 function was reduced to 77+/-5% of control ($p<0.01$). Because we have previously shown that MCT1's transport rates are heavily dependent on pH_i, in these experiments we paired the data by the resting pH_i to negate pH_i dependent effects that treatments or random variability may have produced (202). Thus, the effects of cAMP and MβCD were similar in magnitude, but not additive, consistent with both agents utilizing the same, caveoli-dependent, mechanism to reduce MCT1 function.

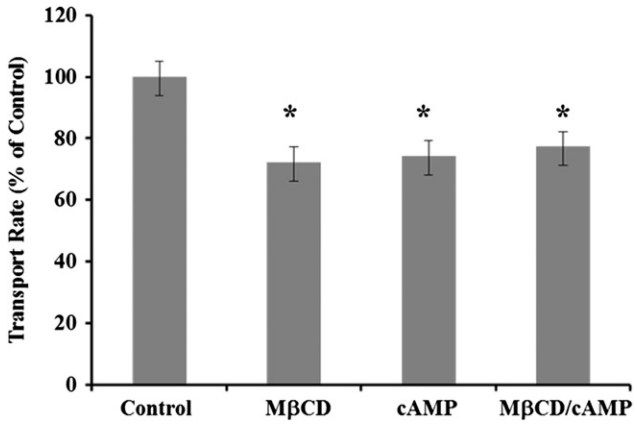

Figure II-6: cAMP and methyl-β-cyclodextrin (MβCD) inhibited MCT1 but the inhibition was not additive. In BCECF pH_i imaging experiments, all RBE4 cells responded to 25 mM L- lactate with an immediate cytoplasmic acidification. The acidification for each cell was fit with a linear regression over the first 10s of the response to quantify the transport rate. These rates were normalized to the average control rate and are presented in the upper panel +/- the SEM (n=177 to 225 cells per group combined from 4 experiments). Statistical significance in comparison to control is indicated by a star and described numerically in the text.

Discussion

Overview of the major results of this paper

Our previous work demonstrated a pathway in which β adrenergic signaling through adenylyl cyclase, cAMP, and PKA reduces V_{max} for MCT1, suggesting a mechanism involving a reduction in the cell surface expression of functional transporters (67). In this report we extend that result and show a detailed mechanism in which cAMP signaling causes dephosphorylation of MCT1 and caveolin-1 with an associated internalization of MCT1 from the plasma membrane into caveolae and EEA1 positive early/sorting endosomes. While caveolar pathways are less prominent in brain endothelium as compared to other endothelial cell types, the role of caveolae in regulating MCT1 is not surprising given (1) the prominent role that caveolae are known to play in endothelium in general, and (2) that major components of the β-adrenergic pathway, including β–adrenergic receptors, adenylyl cyclase, and PKA also localize to caveolae where they

are thought to form microdomains and focus the signaling pathway spatially and temporally (206, 207). Additionally, our data indicate that pathways involving clathrin dependent endocytosis and Rab11 positive recycling endosomes may be part of MCT1's trafficking pattern, but that this is constitutive and unregulated by cAMP. In this work, we chose RBE4 cells as a model for brain endothelial cells to be consistent in extending our previous work (67). RBE4 cells are a cell line derived by immortalization of rat brain endothelial cells and, therefore, represent an *in vitro* model useful in brain barrier research. A relatively short sub-culture period and the use of the cells at sub-confluence standardized our model as a more fundamental cellular, rather than barrier, model of brain endothelial cells which helped to avoid confusion associated with controversy surrounding the expression of MCT1 in the three dimensional blood–brain barrier (208).

Mechanism for cAMP dependent endocytosis of MCT1 into caveolae

The events in which cAMP leads to the removal of MCT1 from the membrane were consistent with activation of a phosphatase that dephosphorylated MCT1 and caveolin-1 concurrent with entry of MCT1 into caveolae. The identity of the phosphatase remains unknown, although, a number of prominent phosphor-serine,-threonine protein phosphatases and a phosphotyrosine phosphatase are known to be activated by PKA in endothelial cells, including alkaline phosphatase and myosin light chain phosphatase. The latter plays an important role in cytoskeleton remodeling and the breakdown in vascular barrier permeability during disease (209-211). Therefore, PKA-dependent dephosphorylation of MCT1 may be a component of such pathological processes and it will be important to identify the phosphatase in future studies.

In brain, MCT1 is phosphorylated at 11 different serine and threonine residues suggesting that dephosphorylation at one or more of these residues may facilitate its entry into caveolae (212). Two possible mechanisms are that (1) dephosphorylation increases MCT1's affinity for caveolae or (2) dephosphorylation decreases MCT1's affinity for a substrate that restricts its entry into caveolae. Regarding the first possibility, binding of cargo proteins to caveolin-1 facilitates their entry into caveolae; however, MCT1 does not contain one of the known φXXXφ motifs that facilitate direct interactions with caveolin-1, suggesting that this pathway is unlikely. On the other hand, MCT1's

molecular chaperone, CD147, contains an φXXXφ motif and it reportedly facilitates a specific interaction with caveolin-1 (207, 213, 214). Thus, similar to its known role as the determinant of apical/basolateral sorting of MCT1 in epithelial cells, one of CD147's functions may be to chaperone MCT1's entry into caveolae (62). Despite this, MCT1's interaction with CD147 involves transmembrane domains in the two proteins making regulation by dephosphorylation of MCT1 in a cytoplasmic domain less plausible (59). However, considering the second possible mechanics, dephosphorylation of MCT1 may cause it to be released from a factor that otherwise prevents it and CD147 from entering caveolae as a complex. Of the residues known to be phosphorylated in MCT1, S230 in its large intracellular loop, and S476 in the C-terminus, have the correct sequences to be binding motifs for type 4 WW domains, and Y11 in the N terminus is part of a PY domain which is a ligand for a type 1 WW domain. WW domains are analogous to SH3 and SH2 domains and mediate protein–protein interactions that can be regulated through phosphorylation, while PY motifs have been shown to bind to the WW domains of ubiquitin ligases and mediate phosphorylation dependent internalization and protein degradation (215). Also, S492 at the extreme C-terminus of MCT1 is within the correct sequence to be a PDZ ligand that could facilitate a dephosphorylation dependent release of MCT1 from a protein to protein interaction that otherwise prevents its translocation into caveolae. It is clear that the dynamics of MCT1/CD147 heterodimer formation and its interactions with membranes is complex and requires more detailed analysis in cerebrovascular endothelial cells.

Finally, our result that cAMP caused dephosphorylation of caveolin-1 at Y14 not only backs-up the idea that cAMP signaling activates a phosphatase in RBE4 cells, but also suggests a complementary role for caveolin-1 dephosphorylation in facilitating MCT1's entry into caveolae. Phosphorylation of caveolin-1 at Y14 is required for caveolin-1 to bind SH2 or PTB domain-containing proteins, so dephosphorylation at this site may prevent its binding to a protein that blocks interactions with CD147-MCT1 complexes. Release of such a block may allow binding to the scaffolding domain of caveolin-1 to facilitate entry of MCT1-CD147 into caveolae. These possibilities suggest a detailed plan for future work that will show the precise molecular determinants of cAMP dependent internalization of MCT1 into caveolae.

Intracellular pathways and potential significance of regulated MCT1 trafficking

A second major contribution of this work is showing basic trafficking patterns of MCT1 in brain endothelial cells for the first time. Our results showing a cAMP dependent reduction in MCT1 surface expression and increased colocalization with EEA1 and caveolin-1 demonstrates that the regulatory pathway includes increased trafficking of MCT1 through caveolae to early/sorting endosomes. That the regulation was mimicked by the caveolae disrupting compound MβCD, and the decreased solubility of MCT1 in TritonX-100 following 8Br-cAMP treatment further supported a role for caveolae in the regulatory pathway. On the other hand, the presence of MCT1 in Rab11 positive recycling endosomes and clathrin vesicles was not affected by cAMP in our colocalization analyses, suggesting that clathrin dependent endocytosis into recycling endosomes must be part of a constitutive MCT1 trafficking pathway that is not regulated by cAMP. Supporting this idea, MCT1 contains an YXXφ motif in its C terminus that would facilitate interactions with AP-2 complexes to promote clathrin dependent internalization (215). An illustration of the regulated and constituitive pathways of MCT1 trafficking reported here is presented (Figure II-7).

Finally, in a number of brain pathologies, lactic acidosis is either causal or a key indicator of brain damage. For example, in ischemic stroke, hyperglycemic stroke, and brain injury, the severity of lactic acidosis is a principle indicator of outcomes (177-179, 181, 216-221). MCT1 is ideally positioned in the cerebrovascular endothelial cells of the blood–brain barrier to counter lactic acidosis; however, lactic acid fails to flow readily from brain to blood during stroke and brain injury indicating that MCT1 is an ideal pharmacological target for modulating lactic acidosis in a novel therapeutic approach. Precedence for such a caveolar-based strategy comes from studies in cardiac tissue in which caveolae were targeted to modulate glucose transporter trafficking to improve reperfusion injury (222). The results presented here are also relevant for cancer because MCT1 controls lactate efflux from tumor cells, a factor that limits hyperplasia, and because CD147-caveolin-1 interactions reduce extracellular matrix remodeling which is necessary for tumor invasion (213, 223-225). Therefore, the results presented here advance our understanding of the biochemical regulatory mechanism by which cAMP

signaling controls MCT1 function in cerebrovascular endothelial cells, and is important for understanding molecular transport processes in the neurovascular unit in both health and disease.

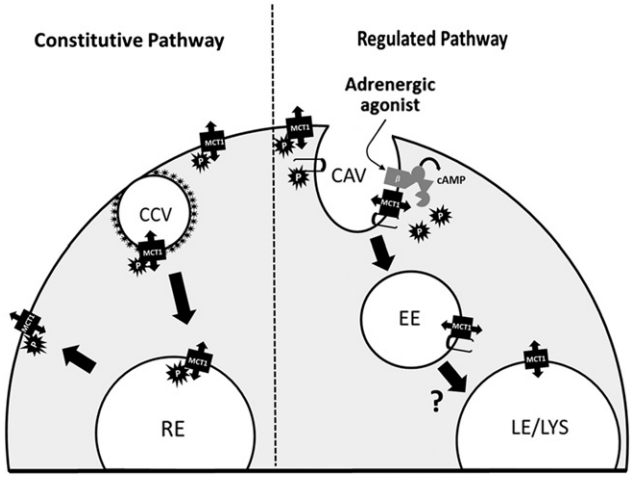

Figure II-7: Regulation of MCT1 by cAMP-dependent internalization into caveolae and early endosomes, and an unregulated clathrin-dependent recycling pathway. Right side: in the regulated pathway, activation of β-adrenergic receptors leads to cAMP production and activation of a phosphatase which dephosphorylates plasma membrane MCT1, and caveolin-1 (hairpin structures), facilitating an interaction between MCT1 and caveolin-1 to promote internalization of MCT1 into caveolae (CAV) and early endosomes (EE). From here MCT1 could be trafficked to various compartments such as late endosomes and lysosomes (LE/LYS), similar to the protein-kinase dependent trafficking of kainite receptors and aquaporins (226, 227). Left side: in the constitutive pathway, MCT1 is internalized into clathrin coated vesicles (CCV) where it is trafficked to recycling endosomes (RE) for redistribution on the plasma membrane, however, adrenergic signaling does not affect this trafficking pathway.

Contributions

In this paper, Z.Liu conducted the experiments of "MCT1's reduced phosphorylation and subsequently decreased surface expression on RBE4 cells after cAMP treatment" as demonstrated in Figure II-1.

Chapter III

Regulation of brain endothelial MCT1 expression by the canonical Wnt/β-catenin signaling pathway

Introduction:

Monocarboxylic acid transporters (MCTs) are responsible for rapid bi-directional facilitated diffusion of monocarboxylates, such as lactate, pyruvate, β-hydroxybutyrate (BHB) and acetate, across cellular membranes. They cotransport their ionic substrates with protons in a 1:1 stoichiometry manner, making the whole process electroneutral (228). The MCTs belong to the solute carrier (SLC16) family, of which 14 members (MCT1-14) have been identified. Only MCT1-4 and MCT7 have been demonstrated experimentally to facilitate the transport of monocarboxylates (3, 32). MCT8 transports thyroid hormones (T3 and T4) and its defects have been associated with the X-linked Allan-Herndon-Dudley Syndrome, where patients exhibit severe mental retardation, dysarthria, muscle hypoplasia and spastic paraplegia due to the lack of thyroid hormones transport into neurons (229). Single nucleotide polymorphisms (SNPs) within MCT9 gene can influence human serum uric acid levels, as revealed by meta-analysis of genome wide association scans (230). MCT10, also known as T type amino acid transporter 1 (TAT1), transports aromatic amino acids (231). Different MCTs have distinct tissue distribution patterns and their transport affinity/capacity for certain substrates can be quite different. As the prominent transporters for the thermogenic intermediate metabolites, MCT1, 2 and 4 have been most extensively studied and functionally characterized, whereas studies for MCT3, MCT7-8 and MCT10 are limited. The roles of MCT5-6 and MCT11-14 still remain elusive.

MCT1 is the first family member being identified as the transporter of lactate in rat erythrocytes as revealed by DIDS labeling (232). Its cDNA was then isolated from Chinese hamster ovarian (CHO) cells and the coded sequence was found to be identical to mevalonate transporter (Mev), except for one amino acid difference of Phe in MCT1 from that of Cys in Mev (233). Human *MCT1* gene lies on chromosome 1p13.2-p12 (234). Its transcription unit encompasses almost 44kb, and consists of 5 exons and 4 introns (Figure III-1; (235)). Rat MCT1 contains 494 amino acids, whose sequence shares 86% identity to that of human (236). The protein's calculated molecular weight is about 53kD with a migrating size of ~49kD on SDS-PAGE electrophoresis. Like other MCTs, MCT1 has 12 transmembrane domains (TMDs) with a large intracellular loop

between TMD 6 and 7. Both the N- and C-termini are located within the cytoplasm (237) (Figure III-14). The successful targeting of MCT1 from intracellular pools onto plasma membrane requires its association with an ancillary protein called CD147 (also known as Basigin and Emmprin), which is a single TM glycoprotein with extracellular IgG-like domains along with a short intracellular C-terminus (50).

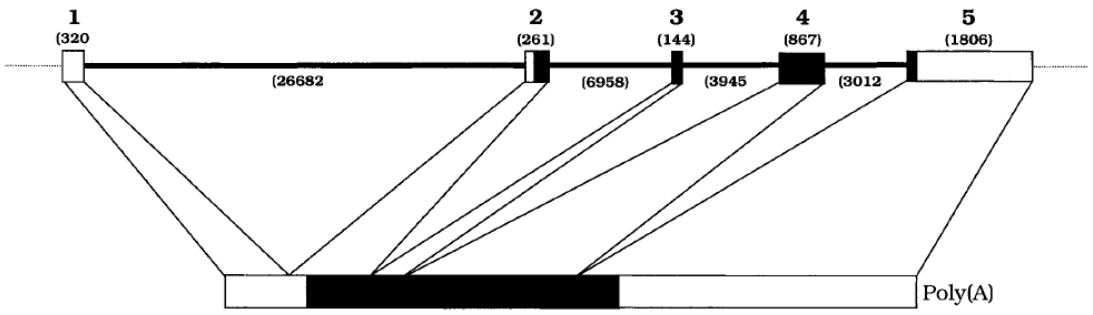

Figure III-1: Genomic organization of human MCT1 gene (Adapted and modified from (235)). The whole transcript unit spans about 44kb, contains 5 exons (numbered on the top) and 4 introns (thick black lines). Untranslated regions are represented by white boxes, while coding regions are indicated by black boxes. The size of each exon or intron is calculated and shown in parentheses. The complete mature transcript is shown at the bottom.

The substrates of MCT1 include important metabolic intermediates such as lactate, pyruvate, BHB, acetate and butyrate. Their affinities are declining in the order of butyrate (0.02mM), pyruvate (1mM), acetate and BHB (2.5mM) to L-lactate (3.5mM). As a result, MCT1 is closely related with diverse metabolic pathways including glycolysis, gluconeogenesis, ketone body metabolism and lipogenesis (237). MCT1 is the most universally expressed isoform, sometimes in conjunction with other MCTs whose distribution can be quite different among cell types to respond to local physiological transporting demands (3). Its expression is enriched in brain endothelial cells, particularly during postnatal development stages (94, 95). It is the predominant MCT transporter present at the blood-brain barrier (BBB) (67, 174), thus it is mainly

responsible for the exchange of monocarboxylates between central nervous system (CNS) and peripheral blood.

The function of MCT1 at BBB has many pathological implications. Firstly, during cerebral ischemia insult, the shortage of oxygen supply in arteries turns brain cells into an anaerobic metabolic state where glycolysis is the main route for ATP production. The concomitant byproduct, lactate, thus accumulates within CNS, a process called lactic acidosis that has been long observed and believed to contribute to the pathophysiology of ischemia (238, 239). Decrease in pH as a consequence of severe lactic acidosis injures and inactivates mitochondria, interferes with the function of enzymes and leads to irreversible damage of brain structures (240, 241). So, efficient clearance of excessive lactate from brain side into venous blood during and after ischemia is proposed to help alleviate its adverse effects on the CNS (242). In fact, higher cerebral lactate levels during incomplete ischemic anoxia are associated with worse brain injuries than in complete ischemia where lower lactate levels are observed (177, 178, 240, 242, 243). Secondly, MCT1 at BBB delivers ketone bodies that are generated by ketosis in liver as fuels into the brain. Glucose is the primary energy source for brain functions. However, the brain can also use monocarboxylates as metabolic substrates when the supply of sugars is low. For example, during suckling period, the mother's milk provides abundant lipids that can be converted to ketone bodies that the brain relies on for survival (244). During starvation and for epileptic patients on ketogenic diets, ketones can supply the most of brain's energy requirement as well as help to control occurrence of seizures, respectively (245, 246). In hibernating mammals with depressed body temperature and reduced metabolic rates, BHB is selectively used over glucose and metabolized by the tricarboxylic acid (TCA) cycle after its facilitated diffusion by brain endothelial MCT1 into the CNS. This adaptive mechanism implicates a potential use of BHB as therapeutic approach in treating pathologies like stroke, atrophies from muscle and hemorrhagic shock (247). Finally, MCT1 has been exploited as a drug transport route for delivering monocarboxylic acid like compounds into CNS. For example, the anticonvulsant reagent valproic acid (VA) has been widely used as an anti-epilepsy and anti-bipolar disorder drug (248). It has been well documented as a substrate for MCT1 in order to cross plasma membrane by a variety of studies (153, 249, 250). The predominant existence of

MCT1 at BBB ensures the rapid delivery of VA after oral administration into CNS (44). Other commonly used drugs that are known to be transported by MCT1 include but not limited to benzoic acid, salicylic acid and succinic acid (153, 251). Given the important roles of brain endothelial MCT1 in the above mentioned biological conditions, it is thus critical to better understand MCT1's regulation as well as its functional modulation at BBB by external stimuli and signaling pathways, especially under devastating pathological situations where its expression or function is commonly altered or can be beneficially exploited, such as stroke (138, 252), Alzheimer's disease (253, 254), epilepsy (116, 117) and diabetes (114, 115). A more detailed appreciation of the underlying mechanisms of its regulation can help restore or manipulate this transporter's function for therapeutic purpose.

The canonical Wnt/β-catenin signaling pathway was first discovered in *Drosophila* by genetic screening when the mutation of *Wingless* gene was found to cause a patterning defect during embryonic development (255). Its mammalian homologue, Wnt1, was identified couple years later by pro-viral tagging in breast carcinoma mouse model and became the founding member of the mammalian Wnt ligand family that contains 19 highly conserved secreted glycoproteins to date (256). Wnt ligands initiate their signaling transduction cascade by binding to the extracellular portion of a frizzled family of receptors (FZDs) as well as to a low density lipoprotein receptor-related protein (LRP) 5 or 6 as the co-receptor. 10 mammalian FZD genes have been identified, namely FZD1-10 (257). In the absence of Wnt signal, an intracellular destructive multi-protein complex, consisting of adenomatous polyposis coli (APC), Axin, glycogen synthase kinase-3 β (GSK-3 β) and casein kinase 1 α (CK1 α), recruits cytosolic β-catenin and mediates its phosphorylation by GSK-3 β and CK1 α at threonine 41, serines 33, 37 and 45 (258). This phosphorylated β-catenin is recognized by the E3 ubiquitin ligase β-Trcp, leading to its ubiquitination and subsequent proteasomal degradation (259) (Figure III-2 A). When Wnt ligands bind to FZD and LRP5 (6) receptor complex, a cytoplasmic scaffolding protein called Dsh/Dvl is recruited to plasma membrane and interacts with the phosphorylated intracellular domain of LRP5 (6). Axin binds with Dsh/Dvl readily and is

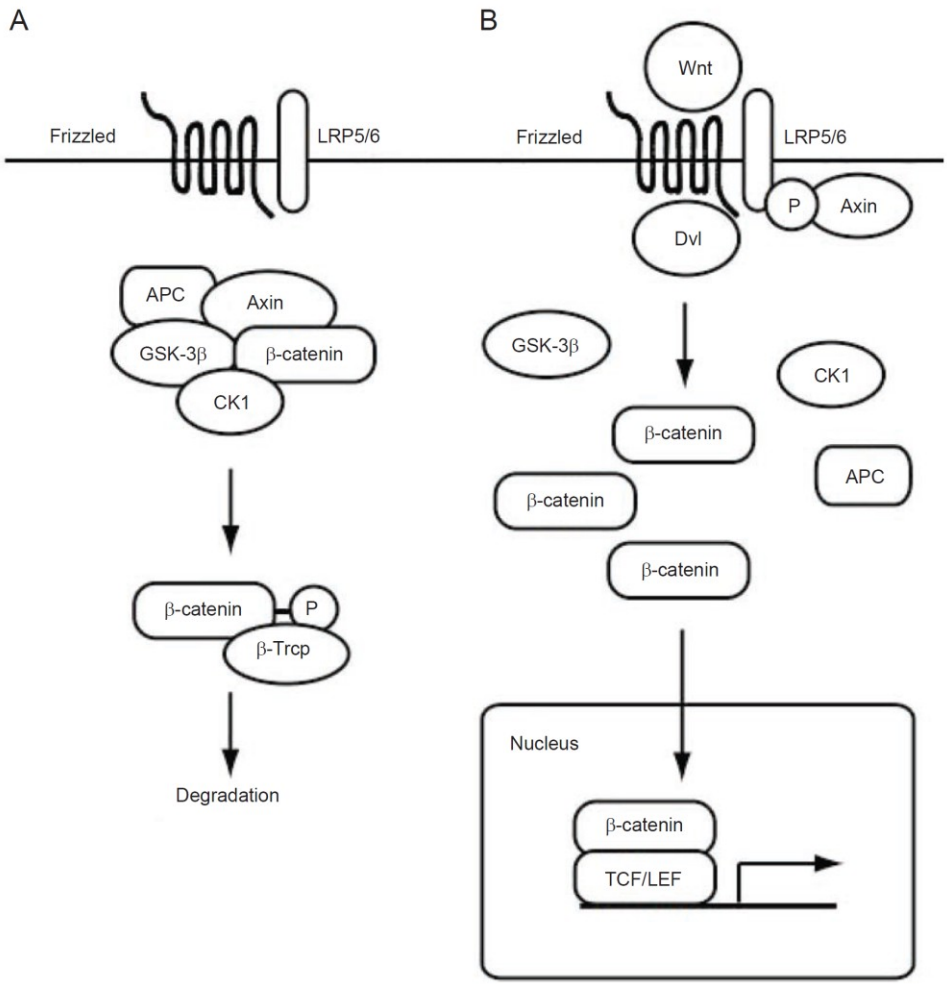

Figure III-2: A schematic diagram of the canonical Wnt/β-catenin signaling pathway (Adapted from (260)). (A) In the absence of Wnt ligands, an intracellular multi-protein complex, consisting of APC, Axin, GSK-3 β and CK1α, targets β-catenin for phosphorylation. This phosphorylated β–catenin can be recognized by an ubiquitin E3 ligase β-Trcp, and subjected to ubiquitination-dependent proteasomal degradation. (B) In the presence of Wnt ligands binding to FZD and LRP5 (6) co-receptor, the intracellular domain of LRP is phosphorylated by GSK-3 β, which recruits the scaffolding protein Axin from the destructive complex to plasma membrane. The loss of Axin disassembles the multi-protein complex, leading to the stabilization of cytoplasmic β-catenin and its subsequent translocation into nucleus, where it interacts with TCF/LEF co-transcription factors to promote target genes expression.

thus liberated from the β-catenin destructive complex that becomes disassembled. As a consequence, cytoplasmic β-catenin cannot be phosphorylated and is now stabilized, which then translocates into nucleus, interacts with TCF/LEF transcription factors and promotes Wnt target genes expression (261) (Figure III-2 B). Lithium has been known to inhibit the activity of GSK-3 both directly and by increasing its inhibitory phosphorylation. Consequently even though the structure of the destructive complex stays together, lithium can block GSK-3's capacity to phosphorylate β-catenin, thus causing β-catenin's accumulation in the cytosol and its entry into nucleus (262) (Figure III-3). The target genes that are regulated transcriptionally by Wnt/β-catenin pathway depend substantially on cell types that are exposed to different biological environments (263, 264), however, those that have been well established include CyclinD1 (265), LEF1 (266) and c-Myc (267) in general, as well as p-glycoprotein (Pgp) in brain endothelial cells (268).

The canonical Wnt/β-catenin signaling pathway has critical implications in a variety of biological processes, e.g. dorsal-ventral axis formation during embryonic development (269), human embryonic stem cells lineage-specific determination (270), cell proliferation (271), tissue self-renewal (272), *de novo* hair follicle regeneration (273) and cancer (especially colon cancer) progressions (274). Recently, it was discovered as a key requirement for initializing normal blood-brain barrier development and maturation in rodents (275, 276). Specifically on neural tube stage, secreted Wnt ligands from neuroepithelial cells act on the surrounding vascular endothelium, stimulate angiogenesis and new vasculature penetration into neuroepithelium, eventually leading to the formation of a mature BBB that are characterized by selective permeability, tight junctions as well as expression of nutrient transporters (e.g. GLUT1). Given the significance of brain endothelial MCT1 in CNS functions and the critical role Wnt/β-catenin plays in BBB normal development, we wanted to investigate whether MCT1 is regulated by this important signaling pathway in brain endothelial cells.

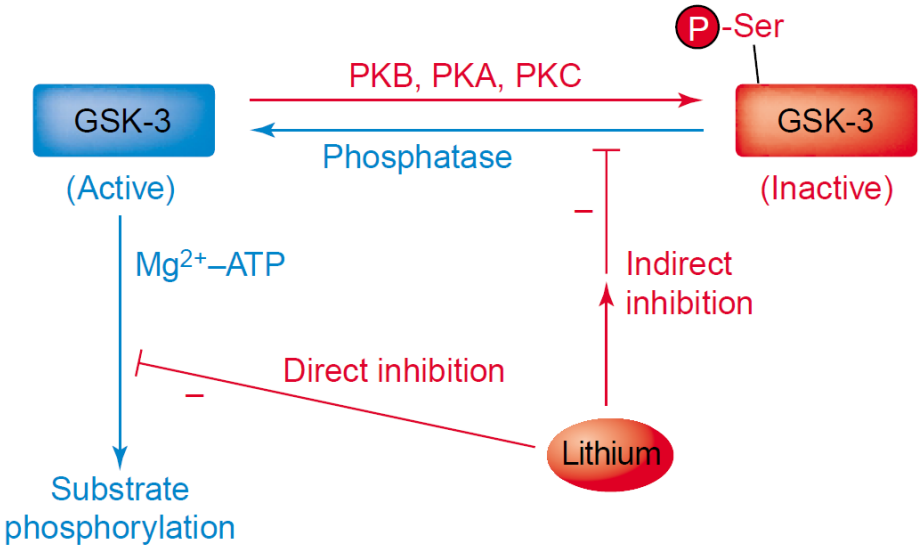

Figure III-3: Inhibitory effects of lithium on glycogen synthase kinase 3 (GSK-3) (Adapted from (262)). Active GSK-3 (shown in blue) catalyzes its many substrates phosphorylation, requiring the participation of both Mg^{2+} and ATP. Lithium can directly inhibit GSK-3's activity by competing with Mg^{2+}, thus dampening its catalytic capacity. On the other hand, GSK-3 can be phosphorylated at a serine residue in the N-terminal domain by several kinases, leading to its inactivation (Shown in red). This process can be reversed by a phosphatase, whose action is reduced by the presence of lithium. In summary, GSK-3 activity can be inhibited both by a direct action of lithium and indirectly by increased phosphorylation of serine.

Materials and Methods

Cell Culture. Immortalized rat brain endothelial (RBE4) cells were cultured in equal parts minimum essential medium alpha (MEM-α) (Invitrogen; #12561-056) and F-10 Nutrient (Ham's) (Invitrogen; #12390-035), supplemented with 10% fetal bovine serum (Atlanta Biologicals; #S11150H), 0.3 mg/ml geneticin (Sigma-Aldrich, #A1720), and 1.0 ng/ml basic fibroblast growth factor (Roche; #11363697001). 25-cm^2 polystyrene tissue culture flasks (Corning Inc.; #CLS430372) were first coated with collagen by treating the surface area with 50ng/ml rat tail collagen type I (BD Biosciences; #354236) in 0.013% cyanamide solution (Sigma-Aldrich; C87908) for 2 hours, followed by water rinsing of the

same volume twice. Cells were then cultured on these collagen coated flasks in a humidified incubator at 37^{o}C with 5% CO_2. All the experiments were conducted when the cells reached 80%-90% confluence.

Reagent Stocks. 1M lithium chloride (Sigma-Aldrich; #L-0505), 1M sodium chloride (Fisher Scientific; #S640-3) and 20mM chloroquine diphosphate (Sigma-Aldrich; #C6628) stocks were all made in H_2O, sterile filtered and stored in 4^{o}C. 1M quercetin dihydrate (EMD Millipore; #551600), 10mM MG132 (Sigma-Aldrich; #C2211), 10mM clasto-lactacystin beta-lactone (EMD Millipore; #426102), 1.5M N-Ethylmaleimide (NEM) (Sigma-Aldrich; #E3876) and 0.4M deubiquitinase inhibitor V, PR-619 (EMD Millipore; #662141) stocks were all made in DMSO (Sigma-Aldrich; #D2650) and stored in -80^{o}C until use.

Cellular proteins preparation. Cells were washed twice with 5ml ice-cold PBS (Mediatech, Inc.; #21-040-CV), supplemented with 1X protease inhibitor cocktail (Roche; #11697498001). Whole cellular protein samples were then prepared by direct in-flask scraping of cells within 100µl SDS boiling buffer (5% SDS, 10% v/v glycerol, 60mM Tris-Cl pH=6.8), transferred into 1.5ml eppendorf tubes (Sarstedt; #72690001), homogenized and centrifuged at 13,000 rpm for 10 minutes. Nuclear protein samples were prepared according to the procedures reported by (277). Briefly, monolayer cells were scraped off flasks and pelleted before being resuspended in NP-40 lysis buffer (0.3% NP-40, 1mM HEPES pH=7.9, 1.5mM $MgCl_2$, 10mM KCl, 0.5mM DTT and 1X protease inhibitor cocktail). After maximal centrifugation, pelleted nuclei were lysed using a high salt buffer (20mM HEPES pH=7.9, 25% v/v glycerol, 0.42M NaCl, 1.5mM $MgCl_2$ and 0.2mM EDTA). All the protein samples were stored in -80^{o}C until use.

RNA isolation, reverse transcription, polymerase chain reaction (PCR) and quantitative real time PCR (qRT-PCR). Total cellular RNAs were isolated using RNeasy Mini Kit (Qiagen; #74104) according to the manufacturer's instruction. After their concentrations being determined by ND-1000 NanoDrop spectrophotometer, the RNA samples were converted to cDNAs using QuantiTect Reverse Transcription Kit (Qiagen; #205311). Benchtop PCR was performed in a GeneAmp® PCR System 9700 machine using the Platinum Taq DNA polymerase (Invitrogen; #10966-034) within a 50µl reaction

volume: 1X PCR buffer (-Mg^{2+}), 0.2mM dNTP (each), 1.5mM $MgCl_2$, 0.2μM primer (each), 50ng template cDNA and 0.5 μl *Taq*. Cycling parameters used were: initial 94°C for 1 minute, followed by 30 cycles of 94°C for 30s and 72°C for 1.5 minutes, then an additional extension at 72°C for 7 minutes and finally holding at 4°C. The PCR products were analyzed by running at 90V on 1% (*Ubb* and *Ubc* products) or 1.5% (frizzled receptors PCR products) SeaKem agarose gel (Lonza; #50152) supplemented with ethidium bromide in 1X TAE buffer (40mM Tris, 20mM acetic acid, and 1mM EDTA). Rotor gene cyber green (Qiagen; #204074) based qRT-PCR was conducted on Rotor-Gene RG-3000 cycler (Corbett Research), using 50ng total cDNA per reaction with the following settings: 95°C 5 minutes, followed by 95°C 5s and 60°C 10s for 40 cycles. The qRT-PCR results were analyzed using the cycle threshold method (C_T, Applied Biosystems User Bulletin Number 2, P/N 4303859) and expressed as fold changes over controls. All the primers used here were designed through the PrimerQuest tool from Integrated DNA Technologies or IDT, and their sequences are summarized in Table III-1.

Restriction enzyme (RE) digestion. Restriction digestions of PCR products were performed by incubating at 37°C water bath for at least 2 hours in a 20μl reaction system: final 1X buffer, 2μl of PCR DNA product, 0.1μg/μl BSA and 0.5μl of specific RE. Details of buffer types for all the REs: Buffer A (Promega) for ApaI (Promega; #R6361) and HpaII (Promega; #R6311); buffer C (Promega) for MboI (Promega; #R6711); buffer D (Promega) for BstEII (Promega; #R6641); buffer E (Promega) for HindIII (Promega; #R6041); buffer H (Promega) for PstI (Promega; #R6111); buffer J (Promega) for SmaI (Promega; #R6121). The digests were analyzed by running at 90V on 1.5% SeaKem agarose gel (Lonza; #50152) supplemented with ethidium bromide in 1X TAE buffer (40mM Tris, 20mM acetic acid, and 1mM EDTA).

Protein assays and western blotting. Protein samples' concentrations were determined using Pierce BCA protein assay kit (Thermo Scientific; #23227) unless otherwise mentioned. Immunoblotting was performed as reported previously (278). Specifically, 10μg proteins from each sample were prepared and diluted 4:5 with homemade 5X sample loading buffer (10% SDS, 50% glycerol, 25% β- mercaptoethanol, 312.5mM Tris HCl and 0.01% bromophenol blue). Then they were subjected to SDS-

PAGE electrophoresis at 160V on Criterion TGX precast gels (Bio-Rad; #5671033), and transferred to supported nitrocellulose membranes (Bio-Rad; #162-0070) at constant 200mA for 90 minutes. The membranes were blocked at room temperature on an orbital shaker for 1 hour in SEA BLOCK (Thermo Scientific; #37527), followed by overnight incubation at 4^{o}C with primary antibody diluted 1:5,000 for anti-MCT1, 1:5,000 for anti-Actin (EMD Millipore; #MAB1501) and 1:20,000 for anti-β-catenin (EMD Millipore; #ABE208) in 1X TBST buffer (50 mM Tris base, pH 8.0, 0.9% NaCl, 0.1% Tween 20) supplemented with 1% SEA BLOCK. After washing in 1X TBST, the membranes were incubated at room temperature for 1 hour with rabbit anti-chicken IgY conjugated to horseradish peroxidase (Thermo Scientific; #31401) diluted 1:5,000 for MCT1, or goat anti-mouse IgG (Thermo Scientific; #31430) diluted 1:10,000 for Actin, or goat anti-rabbit IgG (Thermo Scientific; #31462) diluted 1:10,000 for β-catenin. Detection was accomplished after membranes being rinsed for 5 minutes in SuperSignal West Pico chemiluminescent Substrate (Thermo Scientific; #34080). The immunoblotting results were analyzed by densitometry, normalized to actin and then expressed as fold changes over control.

Plasmid transfection. Transfection of mCherry-MCT1 vectors (a gift from Dr. Jeffrey P. Smith) into RBE4 cells was conducted using Transfectamine LTX with Plus (Invitrogen; #15338-100), according to the manual's instruction. Briefly, the cells were exposed to the transfection complex, consisting of 1ng/μl DNA, 1μl/ml Plus Reagent and 4 μl/ml transfectamine LTX reagent in growth medium, for 4 hours and changed for fresh antibiotics-free medium. At least 18 hours later, transfected cells were trypsinized and reseeded at a density of $3x10^4$ cells /well into μ-Slide 8 well plates (Ibidi; #80821) that were pre-coated with collagen. These re-plated cells were allowed for additional 24 hours culture before they were treated with lithium chloride.

Confocal microscopy. Confocal images were collected on a laser scanning confocal microscope (Zeiss LSM710). Transfected RBE4 cells growing in μ-Slide 8 well plates were directly subjected to the microscope, using the following configurations: 40X objective with H_2O immersion; built-in settings for mCherry fluorescence (561nm laser);

scan mode as frame; frame size 512X512; averaging method as mean, number as 4 and mode as frame; 12 bit depth and 1 Airy Unit (AU).

Cell surface protein isolation. Cell surface proteins were labeled with biotin and then captured through avidin beads, using the Pierce Cell Surface Protein Isolation Kit (Thermo Scientific; #89881). Specifically, RBE4 cells growing in 75-cm^2 flasks (Corning Inc. #430725) were washed with ice-cold 1XPBS and incubated with 0.25mg/ml Sulfo-NHS-SS-Biotin dissolved in 1X PBS at 4^oC for 30 minutes on an orbital shaker. Then cells were scraped off, centrifuged to pellet and resuspended in 500µl provided lysis buffer for 60 minutes on ice with vortexing every 5 minutes. After that, the lysates were spun at 13,000rpm at 4^oC for 2 minutes and the supernatant was incubated with 500µl NeutrAvidin agarose at room temperature for 60 minutes with end-over-end mixing. After washing three times, biotinylated proteins were eluted using 450µl SDS-PAGE sample buffer (Thermo Scientific; #39001) supplemented with 50mM DTT at room temperature for 60 minutes with end-over-end mixing. Pierce 660nm protein assay (Thermo Scientific; #22662) was used for determining the eluates concentration.

Table III-1: (qRT-)PCR primers

Gene	Forward Primer	Reverse Primer
Mct1	GCTGCTTCTGTTGTTGCGAATGGA	AAAGGCAAATCCAAAGACTCCCGC
Lef1	TTCAGGCAAGCCTACCCATCTTCA	TTCTCTGTTCGTGCTCAGGCTTCA
CyclinD1	TGCTGCAAATGGAACTGCTTCTGG	AAGGTCTGTGCATGTTTGCGGATG
Pgp	TCTCCTATGCTGCTTGTTTCCGGT	TTCGCGTAGTCAGGAGCGAATGAA
Gapdh	ACAAGATGGTGAAGGTCGGTGTGA	AGCTTCCCATTCTCAGCCTTGACT
β-actin	TTGCTGACAGGATGCAGAAGGAGA	ACTCCTGCTTGCTGATCCACATCT
Ubb	GGCGGTTTGTTCCTTCATCGCATT	ATCCTGGATCTTGGCCTTCACGTT
Ubc	AAAGATCCAGGACAAGGAGGGCAT	TCTTGCCTGTCAGGGTCTTCACAA
Fzd1	AAGTGCAGCAAGCTTTGTGGGT	ACACACTGCCGTGAATCCAGACAA
Fzd2	TGCTGTGCTGCGCTTCTACTTT	TGTGCCGATGAACAGGTACACGAA
Fzd3	TTGCTGTTTCATGCCAGTGCCT	AGCTGGCCCATTCAAAGCATGT
Fzd4	TTGGAATGGCCAGCTCCATTTGGT	TTTCGTTGCCTTTCCCTGGCTT
Fzd5	ATTCTTGGTGCGCCTGGTTGTA	TGCCAATGCGGATCATGAGCTT
Fzd6	ACATTAGCGGCGTTTGCTTCGT	AGCCTGGTTTGCCATGCTTCTT
Fzd7	TCATGAAGCACGATGGCACCAA	AGCCAGCCCATGTCTTTCACAGTT
Fzd8	TGGTTCTTGGCGGCTGGTATGAAA	TTGGGCCTCCTTGTTGCTTGAT
Fzd9	TGTGGTCCGCGTTGTGTTTCTT	TGGTGCCGCCCGTCTTCATAATTT
Fzd10	ATGTGGGCAGCATGGATGTCAA	TGTTCTTGCAGTCAGCAGCCTT

Results:

i. Expression profile of Wnt frizzled receptors in RBE4 cells.[3]

In order to determine if Wnt signaling exists in RBE4 cells, the presence of its expressed frizzled (*Fzd*) receptors (*Fzd1* to *10*) was first examined via PCR using cDNA reverse transcribed from total RNA as template. The expected sizes of their PCR products are 547bp, 527bp, 544bp, 669bp, 503bp, 588bp, 647bp, 301bp, 600bp and 614 bp for *Fzd1, Fzd2, Fzd3, Fzd4, Fzd5, Fzd6, Fzd7, Fzd8, Fzd9 and Fzd10*, respectively (summarized in Table III-2). Subsequent agarose gel analysis revealed that all of the receptors except *Fzd10* are expressed in RBE4 cells, demonstrating that Wnt signaling could be activated readily (Figure III-4 A).

The specificity of each PCR product for truly representing individual receptor gene was confirmed by restriction enzyme digestion. Namely, BstEII splits *Fzd1* amplicon into 403bp and 144bp, *Fzd6* amplicon into 316bp and 272 bp; MboI splits *Fzd2* amplicon into 418bp and 109bp, *Fzd4* amplicon into 373bp and 296bp; HindIII splits *Fzd3* amplicon into 344bp and 200bp; ApaI splits *Fzd5* amplicon into 368bp and 135bp; SmaI splits *Fzd7* into 454bp and 193bp; HpaII splits *Fzd8* amplicon into 165bp and 136bp; PstI splits *Fzd9* amplicon into 317bp and 283bp. The enzymes used as well as the expected banding patterns after digestion for each PCR amplicon are summarized in Table III-2. Our results indicated that all of the digests gave expected bands for each gene being examined, confirming that the expression of frizzled receptors was truly represented by the presence of their PCR product bands (Figure III-4 B).

[3] We want to thank Thomas A. Haroldson for conducting the experiments of "Expression profile of Wnt frizzled receptors in RBE4 cells" and "commercial GSK-3β inhibitor SB216763" as shown in Figure III-4 and Figure III-6(B), respectively.

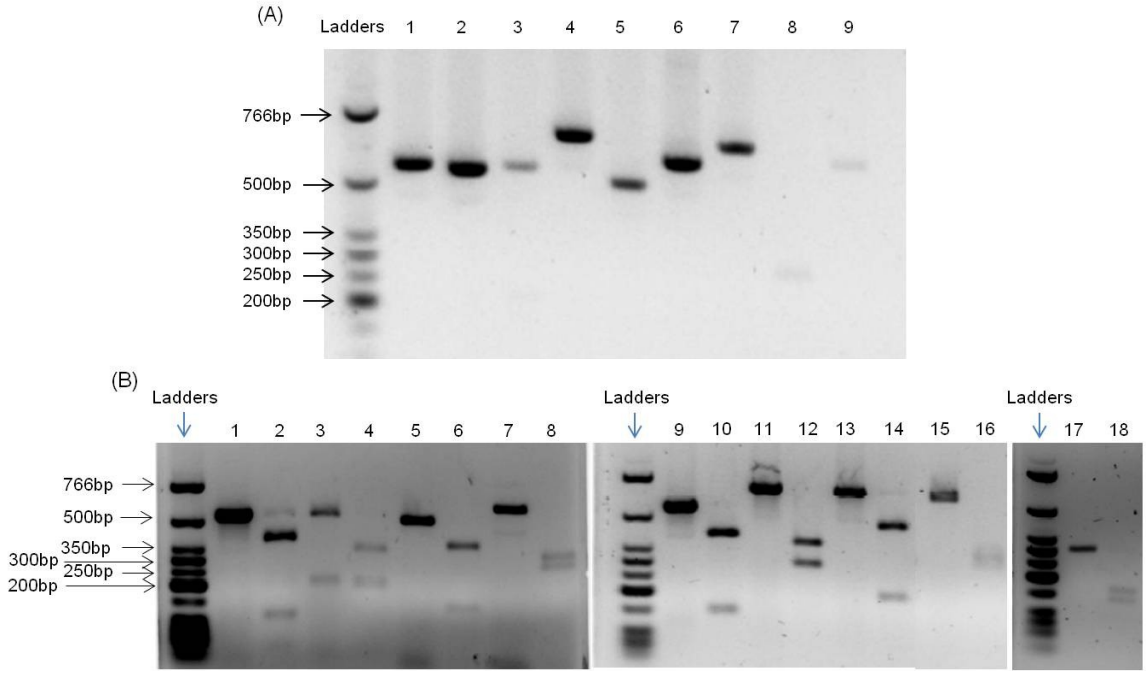

Figure III-4: Expression of Wnt frizzled (*Fzd*) receptors in brain endothelial cells. (A) Wnt *Fzd* receptor genes that are expressed in RBE4 cells were examined by PCR using cDNA as template, followed by 1.5% agarose gel analysis. *Fzd1* to *9,* from lane1 to 9 respectively, showed bands of the expected sizes as summarized in Table III-2. *Fzd10* PCR didn't give any visible bands (data not shown). (B) The specificity of each PCR product to that particular receptor gene was confirmed by using restriction enzyme digestion. All of the nine PCR digests showed expected banding patterns as indicated in Table III-2. Lane1: *Fzd2* PCR; lane2: *Fzd2* PCR+MboI digests; lane3: *Fzd3* PCR; lane4: *Fzd3* PCR+HindIII digests; Lane5: *Fzd5* PCR; lane6: *Fzd5* PCR+ApaI digests; lane7: *Fzd6* PCR; lane8: *Fzd6* PCR+BstEII digests; Lane9: *Fzd1* PCR; lane10: *Fzd1* PCR+BstEII digests; lane11: *Fzd4* PCR; lane12: *Fzd4* PCR+MboI digests; lane13: *Fzd7* PCR; lane14: *Fzd7* PCR+SmaI digests; lane15: *Fzd8* PCR; lane16: *Fzd8* PCR+HpaII digests; lane17: *Fzd9* PCR; lane18: *Fzd9* PCR+PstI digests. All of the ladders used here were Low Molecular weight DNA ladders (New England; #N3233).

Table III-2.Expected sizes of PCR products and RE digests for Fzd receptors

Receptor gene	Expected size of PCR product (bp)	RE for amplicon verification	Banding pattern after digestion (bp)
Fzd1	547	BstEII	403, 144
Fzd2	527	MboI	418, 109
Fzd3	544	HindIII	344, 200
Fzd4	669	MboI	373, 296
Fzd5	503	ApaI	368, 135
Fzd6	588	BstEII	316, 272
Fzd7	647	SmaI	454, 193
Fzd8	301	HpaII	165, 136
Fzd9	600	PstI	317, 283
Fzd10	614	BstEII	497, 117

ii. Canonical Wnt/β-catenin signaling pathway upregulates MCT1 protein expression in RBE4 cells.

In order to determine the optimal working condition for LiCl to regulate MCT1 expression through activating Wnt/β-catenin pathway, both dosage response (control, 5mM, 10mM, 20mM and 30mM) and time course (1h, 6h and 24h) studies were done in RBE4 cells at first, and their effects on MCT1's expression were examined by western blotting. Our results indicated that within 24h treatment, 20mM LiCl started to show increased MCT1 protein level compared with control, 5mM or 10mM group, whereas at 20mM LiCl concentration, 24h incubation time showed the maximal effect (Figure III-5 A). Then RBE4 cells were treated with vehicle control, or 20mM NaCl as osmotic control, or 20mM LiCl in the presence or absence of 80μM quercetin for 24h. Compared with NaCl, LiCl significantly increased MCT1 protein level by 75% (One-way ANOVA followed by Scheffe's post hoc test, $p<0.05$), which was negated by cotreatment with quercetin (One-way ANOVA followed by Fisher's LSD post hoc test, $p<0.05$), demonstrating the specific requirement of β-catenin mediated nuclear signaling transduction in the observed upregulation of MCT1 (Figure III-5 B).

In accordance, nuclear accumulation of β-catenin was increased by 300% after 20mM LiCl treatment for 24h, which was brought down to normal by cotreatment with 80μM quercetin (Figure III-6 A; One-way ANOVA followed by Bonferroni post hoc test, n=3,

p<0.05), confirming the earlier observation that MCT1 is upregulated by LiCl in a β-catenin signaling dependent manner. Similarly, treatment of RBE4 cells for 48h with

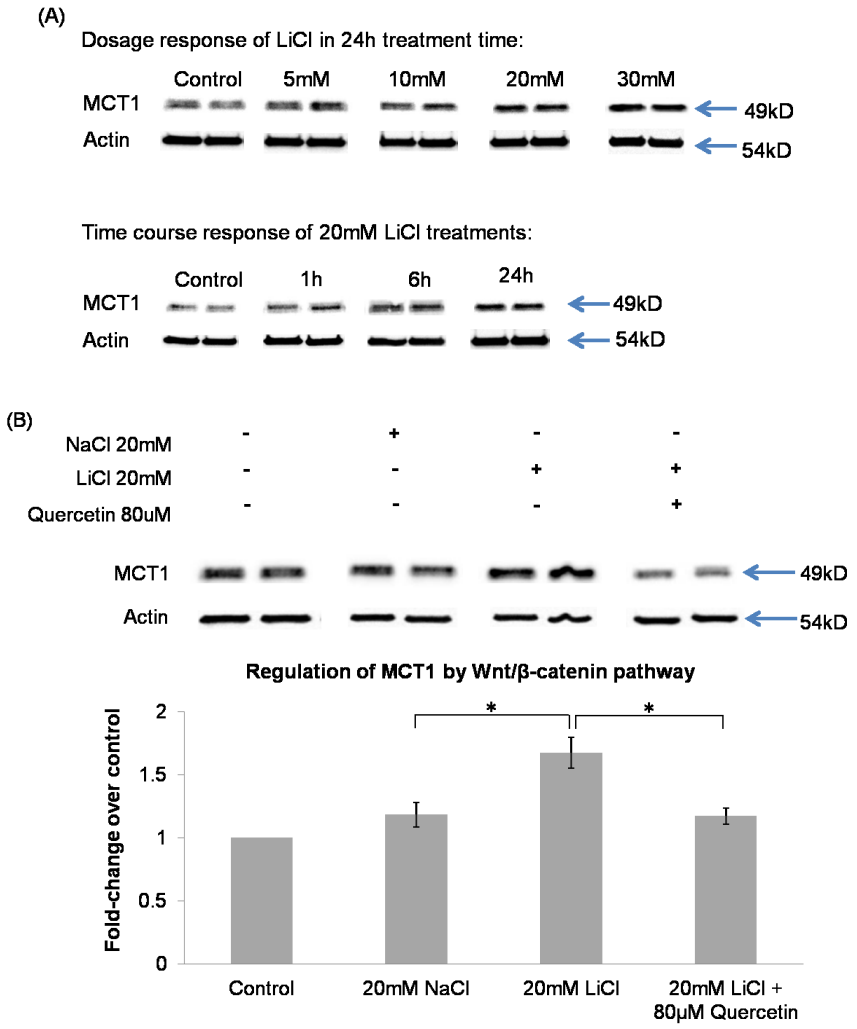

Figure III-5: Regulation of brain endothelial MCT1 expression by Wnt/β-catenin pathway. (A) Dosage and time course studies of LiCl in RBE4 cells to regulate MCT1's protein level. 20mM LiCl treatment for 24h gave the most significant increase. (B) RBE4 cells were treated with vehicle control, or 20mM NaCl osmotic control, or 20mM LiCl in the presence or absence of 80μM quercetin dihydrate, followed by western blotting analysis. Data are expressed as fold changes over control. MCT1 expression was found to be increased by Wnt pathway (75%, *P<0.05, one-way ANOVA followed by Scheffe's post hoc test; mean±SE), which was completely blocked by its antagonist (*P<0.05, one-way ANOVA followed by Fisher's LSD post hoc test; mean±SE).

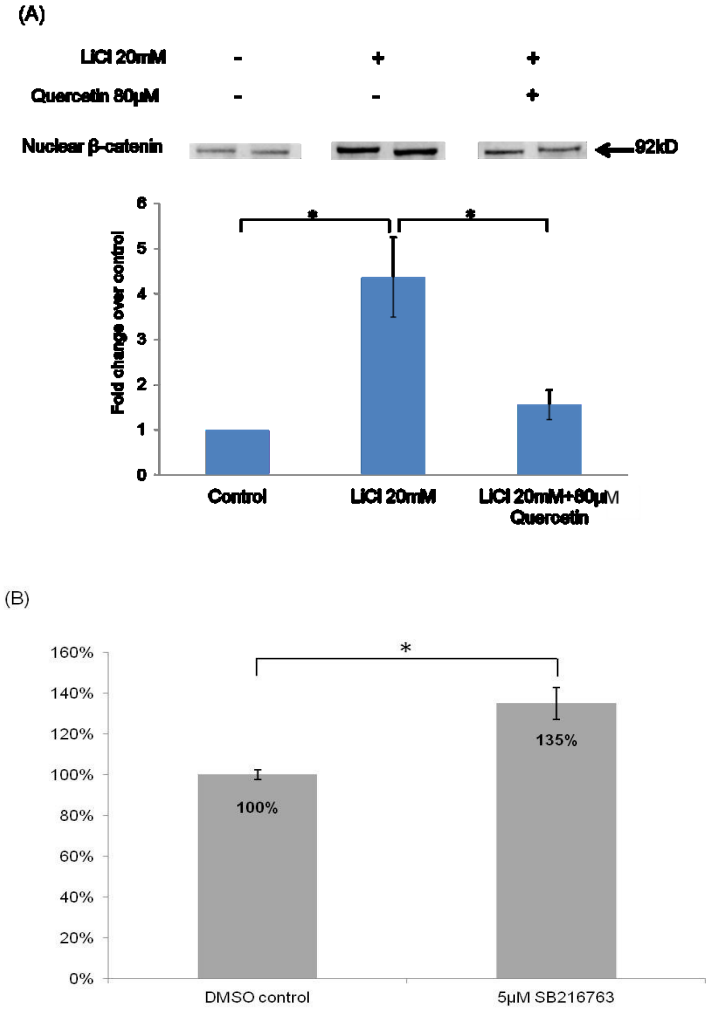

Figure III-6: Changes of nuclear β-catenin level by Wnt agonist and antagonist. (A) RBE4 cells were treated with or without 20mM LiCl in the presence of absence of 80μM quercetin for 24h. Then their nuclear portions were prepared and β-catenin level was examined by western blotting. Data are expressed as fold changes over control. LiCl increased nuclear β-catenin level (300%, *P<0.05, one-way ANOVA followed by Bonferroni post hoc test; mean±SE n=3), which was negated by Wnt blocker (150%, *P<0.05, one-way ANOVA followed by Bonferroni post hoc test; mean±SE n=3), indicating that our previous observation of MCT1's regulation correlate with β-catenin's functional localization. (B) RBE4 cells were treated for 48h with 5μM SB216763, a commercial GSK-3 β inhibitor. Western blotting showed that MCT1's protein level was increased by 35% (*P<0.003, student t test, mean±SE n=5), confirming the regulation of brain endothelial MCT1 by canonical Wnt pathway.

5μM SB216763, another commercial GSK-3β inhibitor, also increased MCT1 protein expression significantly (Figure III-6 B). In sum, the canonical Wnt/β-catenin signaling pathway elevates brain endothelial MCT1's protein level in a nuclear β-catenin-dependent manner.

iii. *Mct1*'s expression is not regulated transcriptionally by Wnt pathway.

Using version 8.3 of TRANSFAC database, analysis of 5kb DNA sequences upstream of *Mct1* transcription starting site revealed the presence of 7 putative TCF/LEF binding motifs (Figure III-7), raising the possibility that Wnt pathway might increase brain endothelial MCT1 protein expression by inducing its transcription. However, qRT-PCR results showed that compared with 20mM NaCl osmotic control, 20mM LiCl treatment in RBE4 cells for 24h didn't elevate *Mct1*'s mRNA level significantly, although some of the well-known target genes of Wnt pathway were upregulated as expected, e.g. *CyclinD1*, *Lef1* and P-glycoprotein (*Pgp*) (Figure III-8). In conclusion, the canonical Wnt/β-catenin signaling pathway upregulates brain endothelial MCT1 expression in a transcription independent manner.

iv. Brain endothelial MCT1 is regulated by lysosomal, but not proteasomal, degradation.

Because the observed upregulation of MCT1 by Wnt pathway is not due to increased transcription, its turnover rate might have been inhibited instead. Generally, cellular proteins can be degraded either in lysosome for membrane proteins, or in proteasome for intracellular proteins, or in both compartments. In order to determine how MCT1 is degraded in RBE4 cells, we first incubated cells with MG132, a commonly used proteasomal degradation inhibitor, at various concentrations for different time periods to test its toxicity on RBE4 cells. Our results indicated that the cells were viable in 0.2μM MG132 for up to 24h, whereas they are only healthy for up to 12h at 0.5μM, and 6h at 1μM or 2μM (Figure III-9). As a result, RBE4 cells were treated with 0.2μM MG132 for 6h, 12h or 24h, and 0.5μM for 6h or 12h, and 1μM or 2μM for 6h, followed by western blotting. We found no significant changes in MCT1's protein level in any of the above treatments (Figure III-10 A). This result was confirmed by using another more selective

proteasome inhibitor, clasto-lactacystin beta-lactone (CLBL), to treat RBE4 cells at 1μM for 6h, 12h or 24h, with no significant changes of MCT1's protein expression being observed (Figure III-10 B). The above results indicated that brain endothelial MCT1 is not regulated through proteasomal degradation. Next, we treated RBE4 cells for 24h with increasing concentrations of a lysosomal degradation inhibitor, chloroquine diphosphate (control, 50μM, 100μM and 200μM), and found a gradual elevation of MCT1's protein level, compared with control (Figure III-11). Specifically, treatment of 100μM chloroquine diphosphate for 24h significantly increased MCT1 protein expression by 100% in RBE4 cells (Figure III-11). In conclusion, brain endothelial MCT1 is regulated through lysosomal, but not proteasomal degradation route.

Figure III-7: Promoter region of *Mct1* contains putative TCF/LEF binding sites. Using a transcription factors binding prediction software (version 8.3 of TRANSFAC database), 5kb upstream of *Mct1*'s transcription starting site (+1) is found to contain seven TCF/LEF putative binding sites, the co-transcription factors critical for β-catenin signaling transduction, at around -905bp, -1287bp, -2602bp, -3395bp, -3910bp, -4137bp and -4990bp positions, implying a possible transcriptional regulation of *Mct1* by Wnt pathway.

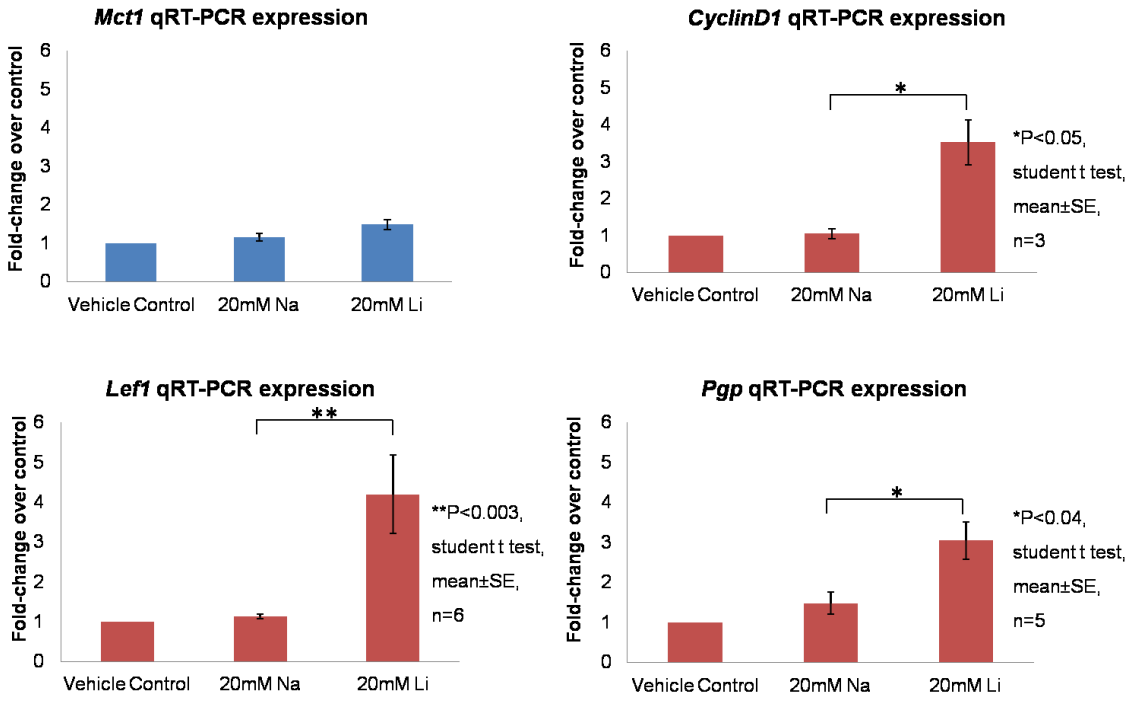

Figure III-8: Regulation of *Mct1* and Wnt target genes in brain endothelium by Wnt agonist. RBE4 cells were treated with vehicle control, 20mM NaCl or the agonist LiCl for 24h and subjected to qRT-PCR analysis. Results were first normalized to internal standard *Gapdh*, then expressed as fold changes over control as determined by $\Delta\Delta C_T$ method. LiCl failed to induce *Mct1*'s transcription (P>0.05, student t test, mean±SE, n=7), although it significantly increased Wnt target genes expression as expected (*CyclinD1* *P<0.05, student t test, mean±SE, n=3; *Lef1* **P<0.003, student t test, mean±SE, n=6; *Pgp* *P<0.04, student t test, mean±SE, n=5).

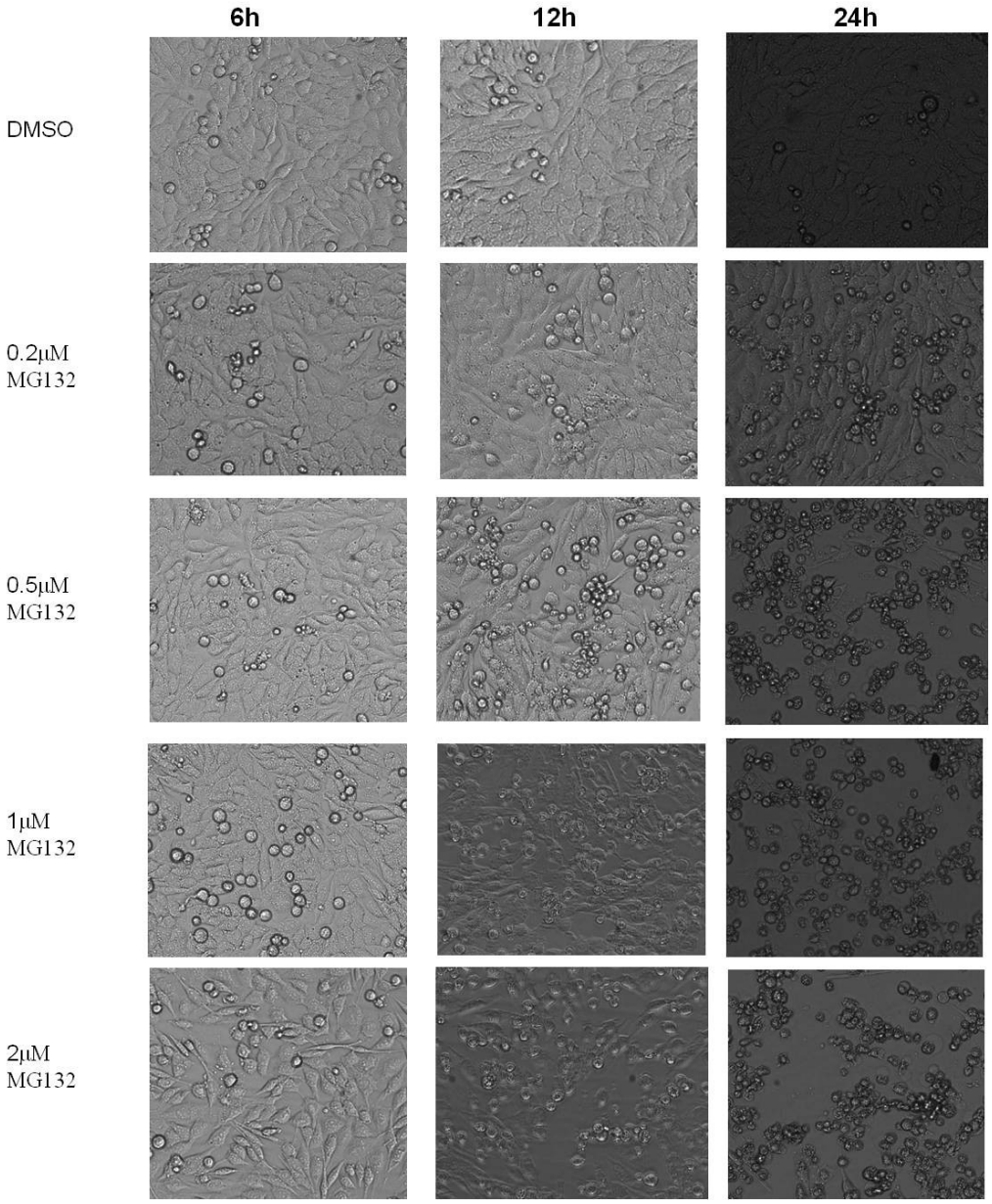

Figure III-9: Effects of MG132 on RBE4 cells' viability. RBE4 cells were cultured in 24-well plates with either DMSO control or different concentrations of MG132 (0.2μM, 0.5μM, 1μM and 2μM; shown on the left) for various hours (6h, 12h and 24h; shown on the top). Treatments started when cells were ~90% confluence. Images were taken at indicated time points. Cells were in good condition at DMSO for up to 24h, at 0.2μM MG132 for up to 24h, at 0.5μM for up to 12h and at 1μM as well as 2μM for 6h.

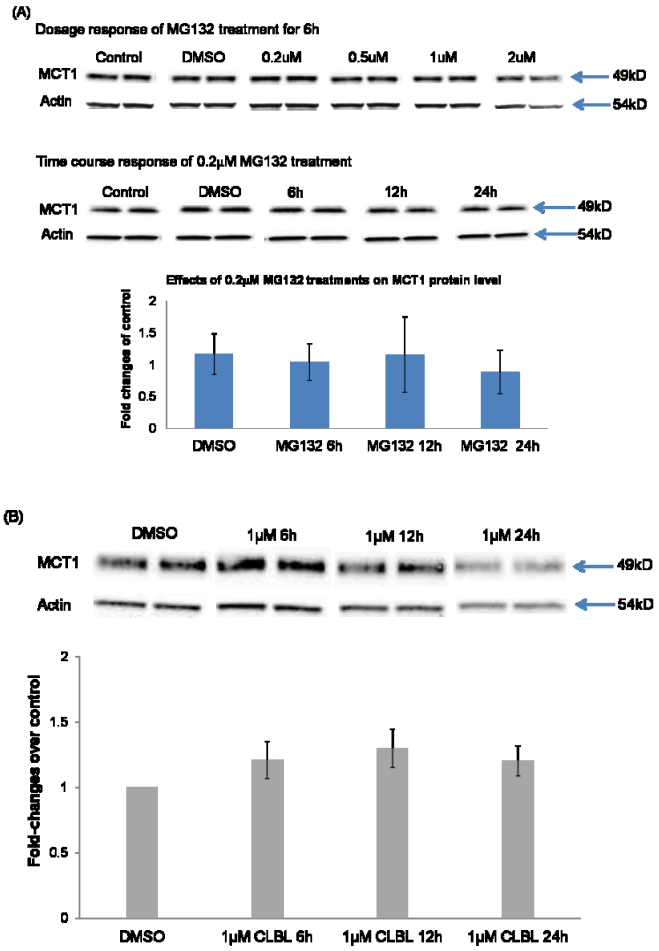

Figure III-10: Brain endothelial MCT1 is not regulated by proteasomal degradation route. (A) For the dosage response study, RBE4 cells were treated for 6h with DMSO, or MG132 at concentrations of 0.2μM, 0.5μM, 1μM or 2μM; for the time course study, RBE4 cells were treated with DMSO for 12h, or 0.2μM MG132 for 6h, 12h or 24h. Control groups had growth medium only and served as vehicle control. Immunoblotting on whole cellular protein was performed after each treatment against MCT1 and actin. No changes of MCT1 level was observed in any of these MG132 groups compared with DMSO. Statistical analysis (one-way ANOVA) did not find significant differences among groups of time course study, indicating that MCT1 in RBE4 cells is not regulated by proteasome. (B) RBE4 cells were treated with DMSO for 12h or 1μM clasto-lactacystin beta-lactone (CLBL) for 6h, 12h or 24h. Immunoblotting on whole cellular protein was performed after each treatment against MCT1 and actin. No changes of MCT1 level was observed in any of these CLBL treatment groups compared with DMSO (One-way ANOVA, P=0.34).

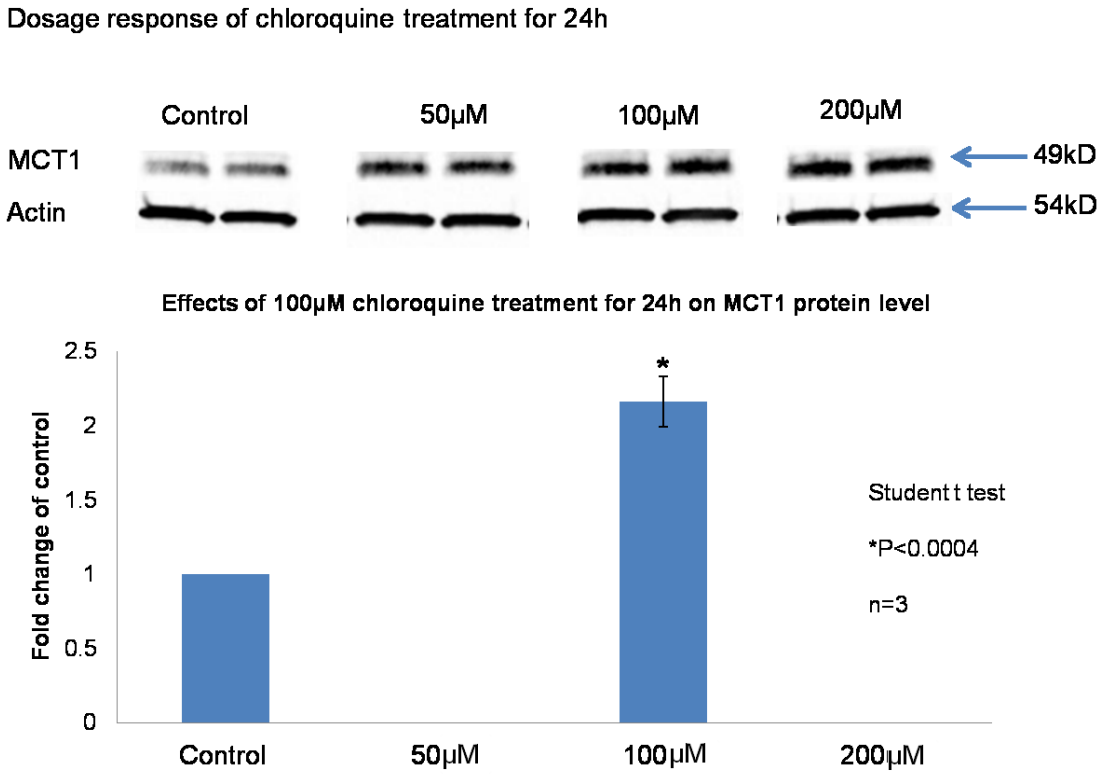

Figure III-11: Brain endothelial MCT1 is regulated by lysosomal degradation route. A dosage response study was performed by treating RBE4 cells for 24h with vehicle control or increasing concentrations of chloroquine (50μM, 100μM and 200μM), followed by immunoblotting on whole cell protein against MCT1 and actin. Our results revealed that chloroquine elevated MCT1 protein level in a dosage dependent manner. 100μM chloroquine significantly increased MCT1 protein level compared with control group (student t test, *P<0.0004, n=3, mean±SEM).

v. Functional expression of brain endothelial MCT1 on cellular surface is increased by Wnt pathway.

Our previous study has demonstrated an endosomal trafficking role of MCT1 in RBE4 cells, which is regulated by cAMP signaling pathway (68). In addition, MCT1 protein contains several motifs that are well known for being involved in endosomal sorting process, such as dileucine, YXXφ and acidic clusters (Figure III-14). Combined with our earlier observation that MCT1 is regulated by lysosomal degradation, we hypothesized that the canonical Wnt/β-catenin pathway stabilizes MCT1 through regulation of its trafficking in the endosomal-lysosomal system, leading to an increased expression on the surface membrane. In order to test this hypothesis, we biotinylated and purified RBE4 cell surface proteins, which were then subjected to SDS-PAGE electrophoresis followed by immunoblotting against MCT1. We found that 20mM LiCl treatment for 24h in RBE4 cells significantly increased MCT1's expression on surface membrane by ~200% (Figure III-12). This result was echoed by our confocal study, where mCherry-MCT1 plasmid was transfected into RBE4 cells, and the localization of red fluorescence tagged MCT1 on plasma membrane was found to be increased by 20mM LiCl treatment for 24h (Figure III-13). These data suggested that the functional expression of brain endothelial MCT1 on surface membrane was increased by the canonical Wnt/β-catenin signaling pathway.

vi. Ubiquitination is involved in brain endothelial MCT1's expression.

Ubiquitin has been known as a sorting signal not only for proteasomal degradation, but also implicated in the three major trafficking pathways: endocytosis, endosomal-lysosomal trafficking and trans-Golgi network sorting into endosomes (279). In addition, the analysis of MCT1 protein structure reveals a PY motif ("PPTY") on its N terminus that has been implicated in ubiquitin E3 ligase binding and late endosome/lysosome targeting (Figure III-14). In order to test the role of ubiquitination in brain endothelial MCT1's regulation, we first did viability screening by treating RBE4 cells with increasing concentrations of a commonly used deubiquitinases (DUBs) inhibitor, N-Ethylmaleimide

(NEM) at 2μM, 10μM or 20μM, for 2h, 6h or 12h time periods (Data not shown). After finding the optimal treatment condition, RBE4 cells were incubated with 10μM NEM for 6h, followed by SDS-PAGE and immunoblotting against MCT1. Our results showed that MCT1's protein level was upregulated by this DUBs inhibitor (Figure III-15 A). In order to confirm our results, we used another more specific commercial DUBs inhibitor, PR-619 DUB V, to treat RBE4 cells at 10μM for 12h. A significant upregulation of MCT1's protein level was observed again (Figure III-15 B). In sum, we conclude that brain endothelial MCT1 is modulated by ubiquitination.

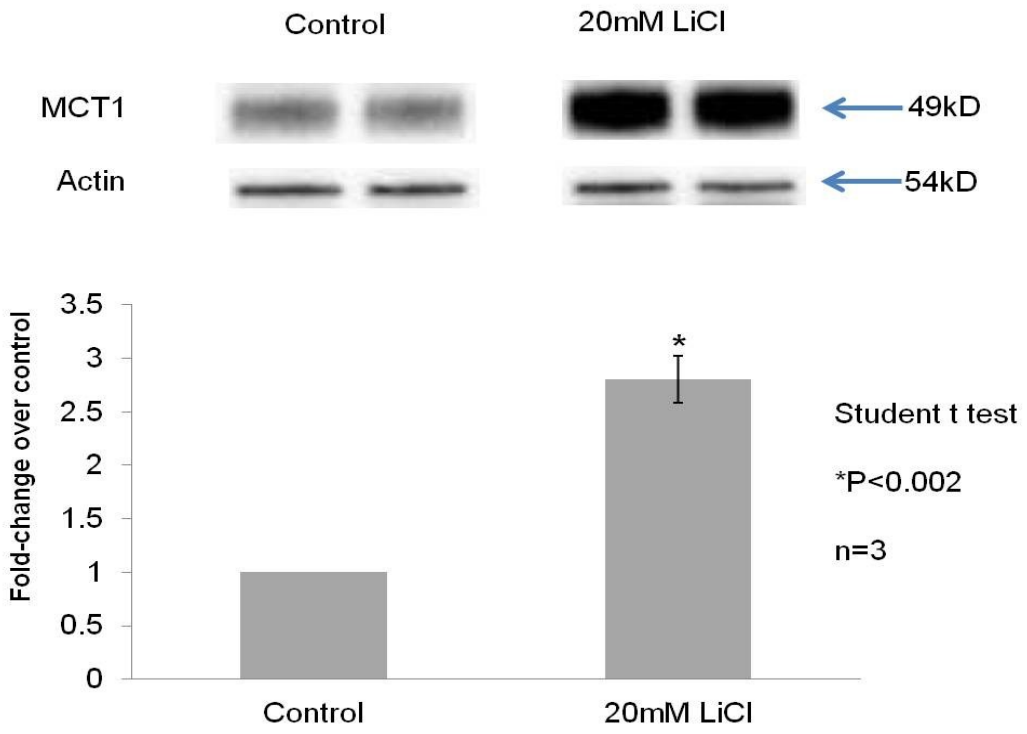

Figure III-12: Increased cellular surface expression of MCT1 by LiCl treatment in RBE4 cells. RBE4 cells were treated with or without 20mM LiCl for 24h. Then cellular surface proteins were labeled with biotin, captured/purified by avidin beads and subjected to SDS-PAGE separation, followed by immunoblotting against MCT1 and actin. Densitometry measurements and statistical analysis were performed, showing that Wnt activation by LiCl increased MCT1's expression on cellular surface membrane (Student t test, *P<0.002, n=3, mean±SEM).

Ubiquitin is encoded in mammals by 4 different genes. *Uba52* and *Rps27a* genes code for a single copy of ubiquitin fused to the ribosomal proteins L40 and S27a, respectively. The *Ubb* and *Ubc* genes code for polyubiquitin precursor proteins with 4 and 10 ubiquitin repeats respectively (280). In order to identify the ubiquitin gene isoform (s) present in RBE4 cells that are involved in protein trafficking, we used PCR to screen for *Ubb* and *Ubc* genes first, followed by agarose gel analysis. We found that all the expected bands from *Ubb* gene were clearly visible on the gel, whereas *Ubc* didn't give the expected banding pattern (Figure III-16). In conclusion, *Ubb* is the polyubiquitin gene isoform present in RBE4 cells.

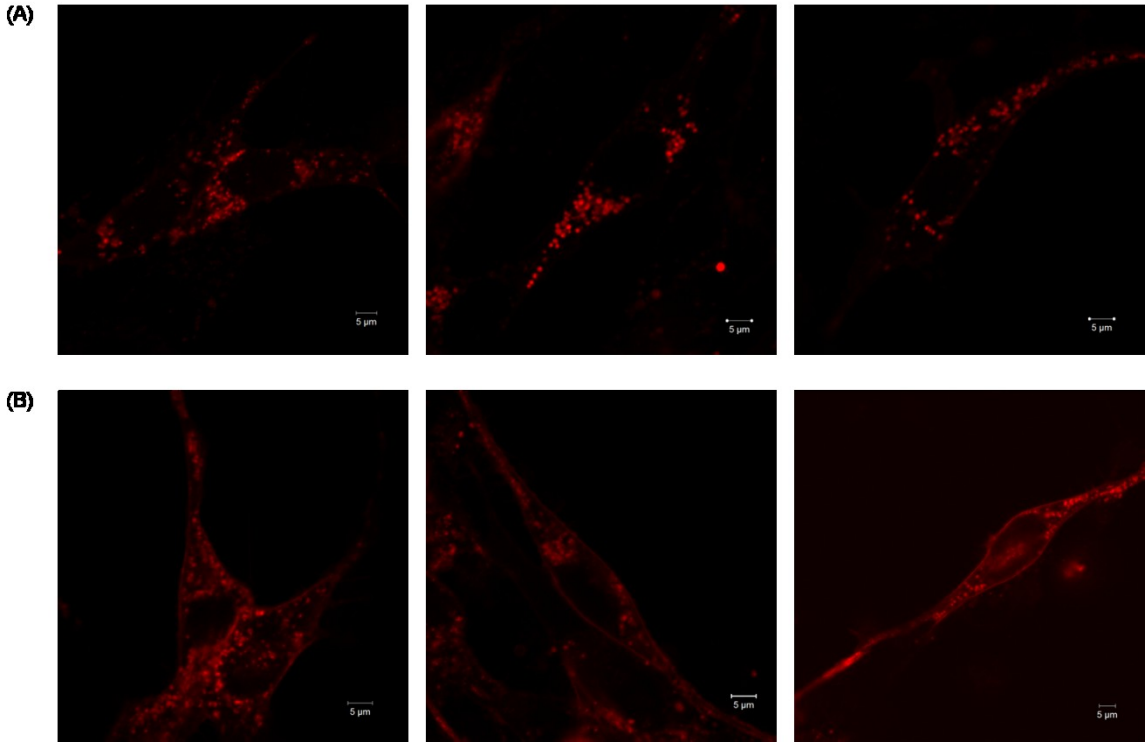

Figure III-13: LiCl caused brain endothelial MCT1 expression to be elevated on plasma membrane as revealed by confocal imaging. RBE4 cells were transfected with mCherry-MCT1 fusion plasmid (red fluorescence attached to N terminus of MCT1 protein); then cells were reseeded and grown in µ-Slide 8 well plates. They were either untreated (A) or treated with 20mM LiCl (B) for 24h to activate Wnt pathway. Our results indicate that MCT1 expression on plasma membrane increased upon LiCl treatment. White bar: 5µm.

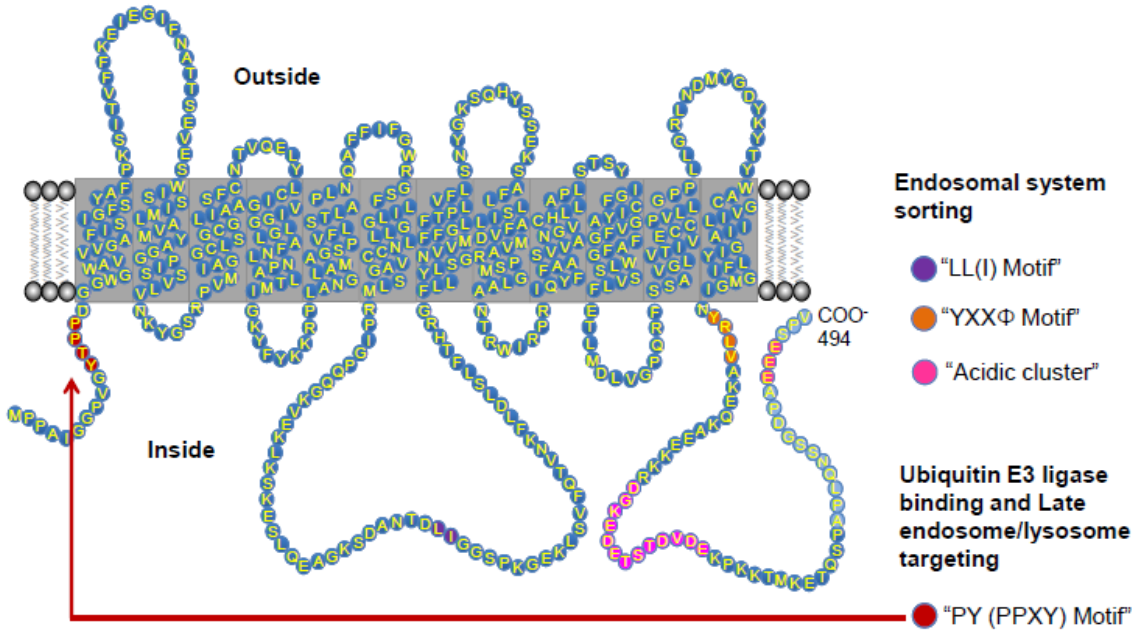

Figure III-14: Structure of rat MCT1 protein and the motifs implicated in intracellular trafficking. Rat MCT1 contains 494 amino acids, 12 transmembrane domains (TMDs) and one large intracellular loop. Both the C-terminal and N-terminal ends are inside the cell. Within the intracellular fragments, a "LL(I) motif (LI)" resides within the intracellular loop; a "YXXφ motif (YRLV)" and two "acidic clusters (EEE and DGKEDETSTDVDE)" are in the C-terminal end; one "PY motif (PPTY)" is found in the N-terminal end. "LL(I) motif", "YXXφ motif" and "acidic clusters" have been involved in endosomal system sorting process (281, 282), whereas "PY motif" is implicated in ubiquitin E3 ligase binding and late endosome/lysosome targeting (283).

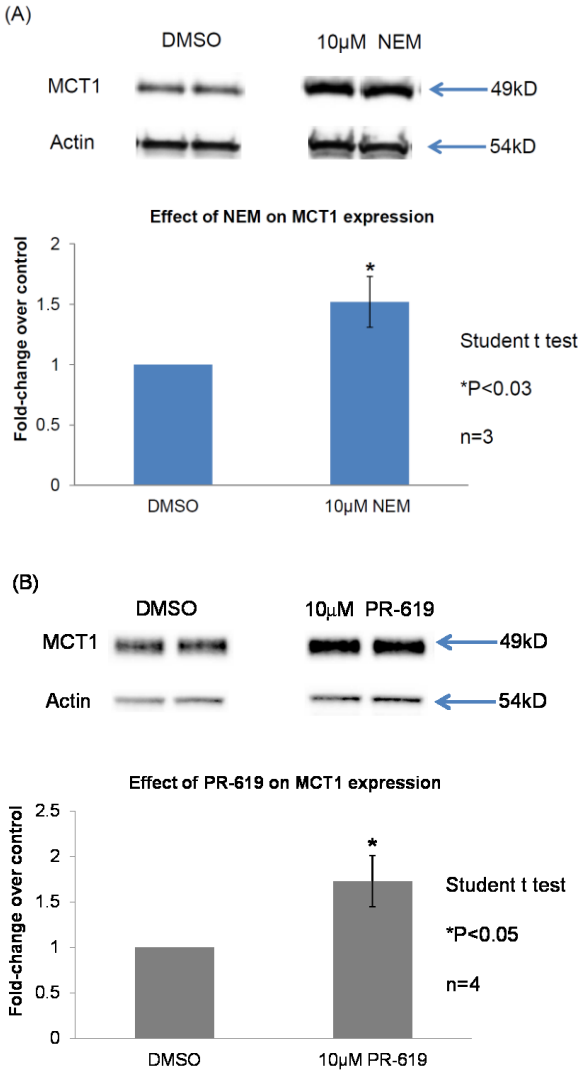

Figure III-15: Regulation of brain endothelial MCT1 by deubiquitinases (DUBs) inhibitors N-Ethylmaleimide (NEM) and PR-619 (DUB inhibitor V). (A) RBE4 cells were treated with either DMSO vehicle control or 10μM NEM for 6h. Whole cellular proteins were prepared and separated on SDS-PAGE gel, followed by immunoblotting against MCT1 and actin. Densitometry measurements and subsequent statistical analysis revealed that NEM upregulated MCT1 expression significantly (52%; student t test, *P<0.03, n=3, mean±SEM). (B) RBE4 cells were treated with either DMSO vehicle control or 10μM PR-619 for 12h. Whole cellular proteins were prepared and separated on SDS-PAGE gel, followed by immunoblotting against MCT1 and actin. Densitometry measurements and subsequent statistical analysis revealed that PR-619 also upregulated MCT1 expression significantly (73%; student t test, *P<0.05, n=4, mean±SEM).

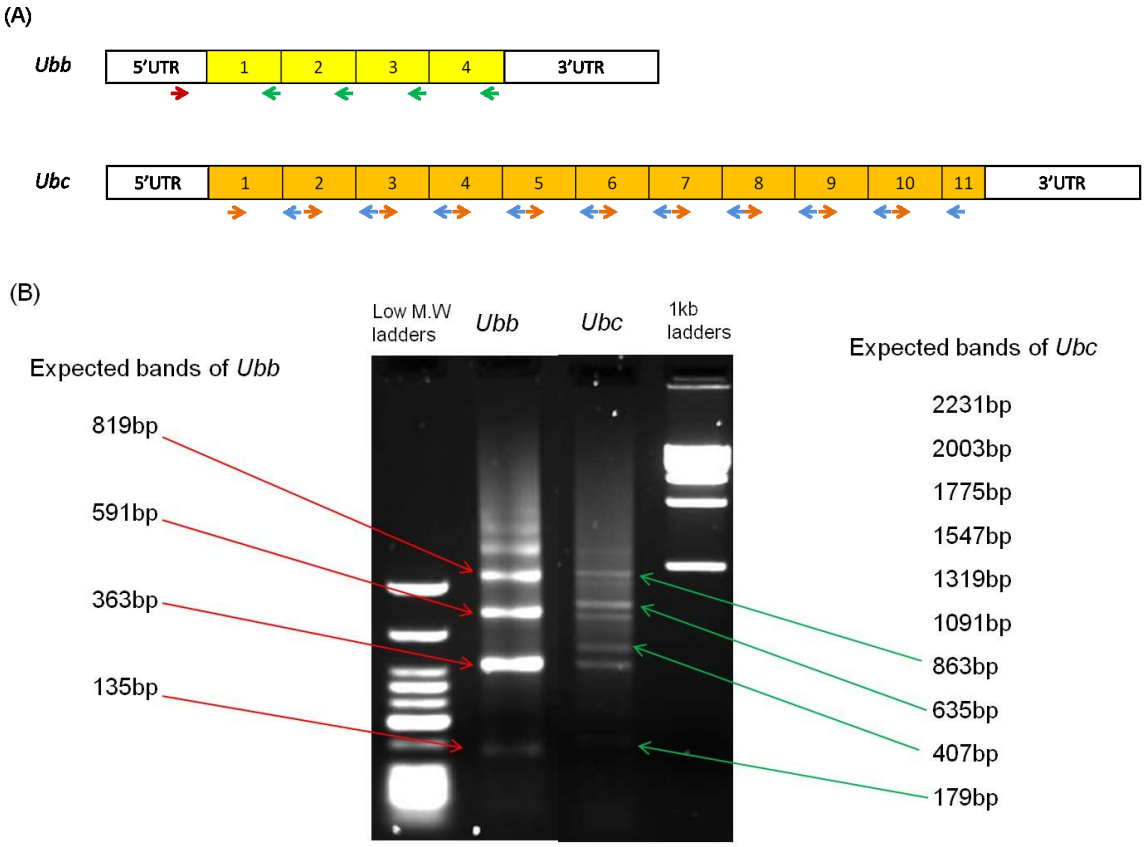

Figure III-16: PCR screening for *Ubb* and *Ubc* expression in RBE4 cells. (A) Schematic representation of PCR strategy. Specific primers were made for *Ubb* and *Ubc* genes respectively. There are multiple annealing sites for each primer pair within the gene because of the presence of polyubiquitin repeats. *Ubb* forward primer is shown in red, reverse primer in green; *Ubc* forward primer is in orange, reverse primer in blue. cDNA templates were used. (B) PCR products for *Ubb* and *Ubc* genes analyzed on 1.5% agarose gel. Expected PCR bands are listed on the left and right side of the image for *Ubb* and *Ubc*, respectively. "Low M.W. ladders": low molecular weight DNA ladders: (top 8 bands) 766bp, 500bp, 350bp, 300bp, 250bp, 200bp, 150bp and 100bp. "1kb ladders": (the first 3 from bottom) 1kb, 2kb and 3kb. The presence of each band is indicated by either red arrow for *Ubb* or green arrow for *Ubc*. Our results indicated that all of the expected bands for *Ubb* could be identified, but not for *Ubc*.

Discussion:

In this study, we report that brain endothelial MCT1 is upregulated by the canonical Wnt/β-catenin signaling pathway through enhanced plasma membrane expression and reduced degradation in the endosomal-lysosomal system, without an alteration of its mRNA level. We also found that MCT1 is regulated by the ubiquitin system, and the ubiquitination status of MCT1 may play a role in its observed regulation by Wnt pathway. This is the first report (to our knowledge) that examined the regulatory effect of Wnt pathway on MCT1, a key transporter for facilitated diffusion of critical metabolites, such as lactate, pyruvate and BHB. The role of canonical Wnt pathway in regulating MCT1 is not surprising given the fact that (1) Wnt signaling is necessary for normal blood-brain barrier development and maturation (275, 276), and (2) MCT1 is the major if not the only MCT isoform present at brain endothelial cells (67, 174). RBE4 cells are a cell line derived from immortalized rat brain endothelial cells, and thus served as a useful model for blood-brain barrier research, including transport and signaling studies (200, 201).

Regulation of brain endothelial MCT1 by lysosomal degradation

Our results on the β-catenin-dependent increase of MCT1 protein level but unaltered mRNA expression indicate that intracellular degradation routes are most likely the underlying mechanism of brain endothelial MCT1's regulation by the canonical Wnt pathway. Cellular proteins are degraded by either proteasomes or lysosomes. The former route is more responsible for degrading intracellular proteins, whereas the latter one is majorly for extracellular and transmembrane proteins that are taken up by endocytosis (284), although some proteins, e.g. EGFR, have been shown to be regulated by both routes (285). Our additional observation that MCT1 in RBE4 cells is responsive to chloroquine but insensitive to MG132 or clasto-lactacystin beta-lactone suggests that lysosomal, but not proteasomal, degradation plays a role in its turnover rate control. Lysosomes are cytoplasmic, membrane bound vesicles that contain proteases and hydrolytic enzymes. After internalization, endocytosed integral membrane proteins pass through early and late endosomes before final delivery to lysosomes (286). Recent research has shown for the first time that brain endothelial MCT1 is rapidly internalized into early endosomes following cAMP-dependent PKA signaling activation.

In addition, MCT1 is constitutively recycled through the clathrin vesicles into recycling endosomal system (68). MCT1 protein contains two acidic clusters and one YXXφ motif in its C-terminal end, as well as one dileucine (LL or LI) motif in the large intracellular loop (Figure III-14). Those motifs have been strongly associated with retention of transmembrane proteins into endosomal compartments (287), targeting of cellular surface proteins to lysosomes, endosomal compartments and *trans*-Golgi network (TGN) (281, 288, 289). For example, the intracellular sequestration of insulin-responsive glucose transporter GLUT4 in adipose tissue is found to be at least regulated by a LL domain (290) as well as an acidic-cluster-based motif in its C-terminus (291). Thus, our results are consistent with those previous findings that brain endothelial MCT1 is actively regulated through the endosomal-lysosomal sorting system.

Our results do not exclude the possibility that enhanced translation of *Mct1* mRNA contributes to the observed upregulation of MCT1 protein in the absence of transcriptional induction by the canonical Wnt pathway. Indeed, GSK-3 is able to phosphorylate and activate tuberous sclerosis complex 2 (TSC2), thus to inhibit mTORC1 activity (292). As a result, lithium can reverse GSK-3's inhibitory effect and activate mTOR signaling pathway, leading to the phosphorylation of the p70 ribosomal protein S6 kinase 1 (S6K1) and eukaryotic translation initiation factor 4E (eIF4E)-binding protein 1 (4E-BP1). The phosphorylation of 4E-BP1 prevents its binding to eIF4E, enabling eIF4E to promote cap-dependent translation. In addition, the stimulation of S6K1 by mTORC1 leads to increased synthesis of ribosomal proteins. Together they positively control the capacity of protein translational machinery (293). Previous studies on MCT2, the neuronal MCT isoform, found that its elevated expression by noradrenaline is mediated by translational activation via stimulation of mTOR/S6K pathway (294). However, the much greater upregulation of MCT1 observed on cellular plasma membrane than that from the whole cellular lysates favors the notion that its intracellular trafficking is more likely affected by the canonical Wnt pathway.

The role of post-translational modification in MCT1's intracellular trafficking

Our finding that both NEM and PR-619, two pharmaceutical inhibitors to DUBs, upregulated brain endothelial MCT1's protein level, demonstrates that ubiquitination is

likely to be involved in regulating MCT1's expression. As a major post-translational modification system, ubiquitin has been widely used as a sorting signal for targeting membrane proteins into endosomal-lysosomal system. It acts on many trafficking stages including initial clathrin-mediated internalization, sorting cargo proteins into multivesicular bodies (MVB) for subsequent infusion with lysosomes, directing damaged or functionally inappropriate proteins from TGN to endosomes and preventing their appearance on cell surface, and sequestering transmembrane proteins within recycling endosomes (279, 295-297). Although both monoubiquitination and K^{63}-polyubiquitination have been experimentally supported in mediating effective internalization of their substrates and subsequent sorting between endosomes, recent studies seem to favor the latter modification as a stronger signal (279). In consistence, our identification of *Ubb* gene in RBE4 cells further supports a potent role of polyubiquitination in modulating MCT1's endosomal-lysosomal trafficking. So it is likely that the enhanced localization of MCT1 onto plasma membrane after Wnt pathway activation is caused by at least one of the following: (1) reduced internalization of MCT1 from cellular membrane, or (2) suppressed cargo sorting into MVB intraluminal vesicles, which creates a "jam" along the trafficking path towards MVB-lysosome infusion and consequently slows down MCT1's detachment from cell surface, or (3) enhanced recycling rate back onto plasma membrane. Further studies on MCT1's ubiquitination status as well as its localization within endosomal system may shed lights on dissecting the molecular mechanisms underlying its regulation by Wnt pathway.

Generally, polyubiquitination is associated with favored protein sorting into MVB-lysosomes for degradation or sequestering within cytosolic vesicles (296, 298). DUBs remove ubiquitin moieties from targeted substrates and its inhibition helps retain an ubiquitination linkage state. Unexpectedly, our results showed that DUB inhibitors increase MCT1's protein expression in RBE4 cells. This phenomenon is not surprising given the fact that over 100 DUBs have been identified, each with the potential to remove or remodel ubiquitin chains in response to unique biological cues (299). Besides, DUBs can associate with either specific membrane proteins, or certain components from sorting machinery, in order to regulate lysosomal allocation of cargo proteins (279). It is possible that an unknown negative regulator of MCT1 is lightly ubiquitinated and

maintained active under normal conditions due to the action of one or more DUBs. Inhibiting these DUBs helps to retain polyubiquitin chains on this negative regulator, leading to its proteasomal or lysosomal degradation and subsequent increase in MCT1's level. For instance, some DUBs have been found to deubiquitinate and stabilize key ubiquitin-ligases that mediate cargo ubiquitination and degradation (300). In contrast, an intact ubiquitination status is required for some receptors to stay on cellular membrane. For example, PAR-1 is ubiquitinated in its basal state; receptor activation leads to the loss of ubiquitination and initiates its journey in ensosomal system. PAR-1 also undergoes constitutive internalization, a phenomenon that is enhanced in its mutant that lacks the major ubiquitinated lysine residues (301). The observed upregulation of brain endothelial MCT1 by DUBs inhibitors in our current study may belong to one of the above mentioned scenarios.

Our results do not exclude other possible post-translational modifications activated by Wnt pathway in assisting MCT1's intracellular trafficking onto or off plasma membrane, e.g. phosphorylation, association with ancillary proteins like CD147. Indeed, our previous research suggested that cAMP induces rapid dephosphorylation and subsequent caveolae-dependent internalization of brain endothelial MCT1 into early endosomes (68). This finding is supported by the same and other groups in that cAMP causes a reduction of V_{max} without changes of K_m in MCT1's transport properties (67, 119). Thus, it is possible that Wnt signaling activates a kinase that phosphorylates MCT1, which then is retained on the cell surface. The successful targeting of MCT1 onto plasma membrane requires its tight association with CD147, an ancillary glycoprotein that belongs to the IgG superfamily (50). Enhanced association between MCT1 and CD147 has been reported to cause increased plasma membrane expression of this transporter protein (53, 54), whereas silencing or knockout of CD147 in cultured cells or genetically modified animals results in decreased MCT1 plasma membrane localization, impaired MCT1:CD147 interaction, as well as altered tissue distribution of this transporter (55, 56). Future studies on MCT1's phosphorylation status and association with CD147 upon Wnt signaling activation shall help better understand MCT1's regulation by those post-translational modifications.

Clinical relevance of MCT1 regulation by the canonical Wnt pathway

A better understanding of MCT1's function and regulation along brain endothelial cell wall has many clinical implications. In addition to the above mentioned pathological conditions including lactic acidosis during ischemic stroke and brain injury, anti-epilepsy drug transport across BBB, as well as ketone bodies delivery during fasting and in epileptic patients on ketogenic diet, brain endothelial MCT1 has also been suggested to help protect brain cognition through transporting some of its substrates. Specifically, provision of alternate fuels, e.g. lactate and BHB, in to brain was found to improve cognitive dysfunctions during acute hypoglycemia in both healthy and diabetic subjects (302, 303). This may imply a potential use of monocarboxylic acids as protective agents against hypoglycemia in diabetic patients. The presence of MCT1 at BBB ideally provides a therapeutic target for accomplishing the above mentioned clinical benefits.

Beyond the BBB, both MCT1 and canonical Wnt pathway have been associated with the progression of many diseases, such as cancer, tissue self-renewal, and autoimmune disorders. For example, the canonical Wnt pathway has been long recognized as the single most dominant force in controlling cell fate along the crypt-villus axis within the intestinal system (304). Multiple mutations (e.g. APC, Axins and TCF) and aberrant modifications (e.g. hypermethylation) of players from this pathway have been well identified as causing reasons for the occurrence of colorectal cancer (305-308). Besides, other types of tumorigenesis, such as leukemia, hepatocelluar tumors, medulloblastoma and pediatric renal (Wilm's) tumor, are also commonly associated with dysregulated Wnt/β-catenin signaling (274, 309, 310). The metabolic phenotype of solid tumors is well characterized by large consumption of glucose and aerobic glycolysis, a phenomenon referred to as the "Warburg effect" (311). The resulting excessive lactate needs to be exported out readily through MCTs including MCT1, in order to maintain an amenable intracellular pH environment and to optimize bioenergetic metabolism (312). A metabolic symbiosis model emphasizes that cancer cells in the hypoxic core of a tumor convert glucose to lactate through enhanced glycolysis, which then is extruded by MCT4 and taken up via MCT1 by aerobic cancer cells on the periphery for mitochondrial oxidation (185). In fact, MCT1's expression level has been found to be upregulated, either mRNA

or protein or both, in various tumors, e.g. breast (75, 76), prostate (313), melanoma (79, 80) and leukemia (49). As a result, given the importance of both MCT1 and the canonical Wnt pathway in cancer progression, a good appreciation of their interaction/regulation can provide valuable information for therapeutic benefits.

Stem cells reside in renewing tissues (e.g. crypt-villus axis of the small intestine and hair follicle on epidermis) and possess the ability to differentiate into various cell types in response to external cues. Physiological signaling of the canonical Wnt pathway is tightly associated with maintaining cell fates within normal crypts or hair follicles, without promoting uncontrolled cell division leading to tumorigenesis (304, 314). Interestingly, immunostaining study in mouse showed a strong colocalization of MCT1 with both the crypts in gastrointestinal tract and the hair bulge, where stem cells are stored, respectively (315). In addition, Wnt signaling can affect the differentiation of naïve CD4+ T lymphocytes (316). In autoimmune diseases like rheumatoid arthritis and systemic lupus erythematosus, aberrant Wnt signaling has also been observed (317, 318). MCT1 on T cells was identified as a target for immunosuppression and its normal activity of extruding glycolytic lactate is required for immune activation in response to antigen stimulation (184). The close coexistence of MCT1 and Wnt signaling in stem cell derived tissue renewal as well as in immune reaction implies a possible crosstalk between the two during these pathological conditions and merits future research.

Our current study is the first one to examine a regulatory effect of Wnt signaling on MCT1 expression. This may lay down the first brick on the road to investigate regulation of this important metabolic transporter by a mighty signaling pathway that is essential for many biological processes. These results may have therapeutic implications in treating devastating diseases where the function of MCT1 is massively involved.

Chapter IV

Regulation of brain endothelial MCT1 expression by Notch pathway and its interaction with the canonical Wnt/β-catenin pathway in RBE4 cells

Introduction

Notch signaling pathway is highly conserved across the animal kingdom, from invertebrates like sea urchins and *Caenorhabditis. elegans*, to vertebrates such as *Drosophila melanogaster*, rodents and human (319). This pathway functions in determining cell fates during development through local cell-cell contact (320). In addition, Notch activity also contributes significantly to tissue self-renewal, proliferation, apoptosis and physiological disorders such as Alagille's syndrome (321, 322) and various cancers, e.g. colon cancer (323) as well as T cell acute lymphoblastic leukemia (324). In mammalian Notch pathway, four receptors (Notch1-4), five ligands (Jagged1 and 2, Dll1, 3 and 4) and two coligands (DLK-1 and -2) have been identified. Different receptors and ligands can have overlapping as well as distinct expression patterns during development and Notch receptors are found to have broad expression patterns in many tissues (320, 325). The Notch receptors are composed of a ligand-binding Notch extracelluar domain (NECD) that is noncovalently held together with a single-pass transmembrane signaling domain referred to as the Notch intracellular domain (NICD). The Notch pathway activation is mediated by a sequence of proteolytic events (Figure IV-1). Specifically, the binding of ligands on signal-sending cells to the receptors presented on the signal-receiving cells causes a cleavage of Notch at S2 site (~12 amino acids before the transmembrane domain) by ADAM metalloprotease (ADAM10 or TACE), followed by γ-secretase cleavage of the tethered receptor near the inner leaflet of the membrane (S3 site), creating a transiently active NICD that translocates into nucleus, interacts with the DNA-binding protein CSL (CBF1/RBPjκ/Su(H)/Lag-1), recruits the coactivator Mastermind (Mam or MAML in mammals) and induces upregulation of downstream target genes (320, 326), e.g. Hes1, 5 and 7, Hey1, 2 and L (327, 328).

The function of Notch signaling in the blood-brain barrier (BBB) mostly remains elusive. One study showed that activation of Notch pathway through Notch4 and Jagged1 in rat

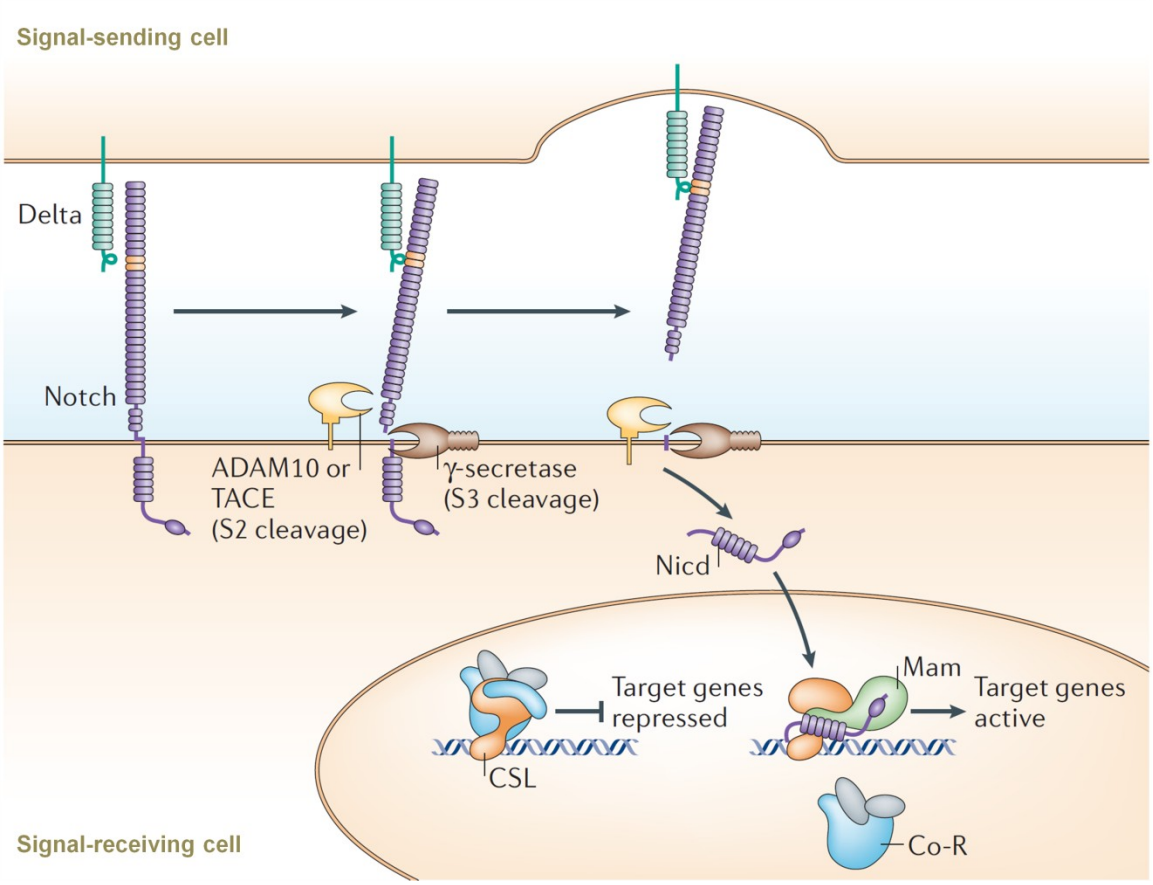

Figure IV-1: Schematic representation of Notch pathway (Adapted and modified from (325)). Binding of Notch ligand (Delta in this example) on the signal-sending cell to the Notch receptor on the signal-receiving cell causes a proteolytic cleavage by metalloprotease ADAM10 or TACE at S2 site, generating the substrate for S3 cleavage by γ-secretase. The resulting Notch intracellular domain (NICD) fragment translocates into nucleus, where it binds CSL, releases co-repressors and recruits the co-activator Mastermind (Mam) to promote target genes expression.

brain endothelial (RBE4) cells promotes endothelial cell differentiation and morphogenesis (329). Furthermore, Notch signaling appears to be one of the major forces involved in the stabilization growth of mature endothelium (330), and BBB endothelial dysfunction is correlated with an impaired expression of Notch4 after chronic exposure to nicotine (331). Other research in blood vessels revealed that during vascular development, the endothelial tip cells cap the migrating end of stalk cells, a

lumenized column of cells that form an angiogenic blood vessel (332). This precisely coordinated patterning of cells along the tubular structure is achieved through Notch-mediated lateral inhibition that prevents extra cells from assuming the lead portion in *Drosophila* tracheal branching (333). In mammals, Dll4 appears to be the major Notch ligand to regulate vascular development in a dosage-dependent manner (334, 335). Rodent Dll4-Notch1 signaling was found to be a negative regulator in determining the number of tip cells during angiogenesis to control vessel sprouting and branching (336, 337). The above observations are not surprising given the well-known role of Notch signaling as a determinant of cell fates.

Morphogenesis, cell fates, cell proliferation and apoptosis during the developmental course are iteratively governed by a combinatorial use of a small number of conserved signaling pathways, including Notch, Wnt, Hedgehog, transforming growth factor-β (TGF-β) and a few others (320, 325, 326). In accordance, a strong interaction, either positive or negative, between Notch and Wnt signaling pathways has been demonstrated in a variety of biological conditions, such as colorectal cancer (338-341), breast cancer (342, 343), intestinal epithelia and osteoblast differentiation (344, 345), as well as stem cells and progenitor cells biology (346). Specifically, the oncogenic conversion of human breast epithelial cells by ectopically increased Wnt signaling requires the normal function of Notch pathway (342). In addition, a synergistic relationship exists between Wnt and Notch activities in the oncogenic progression of rodent intestinal tumorigenesis, as well as in the development of *Drosophila* eye (347). In contrast, antagonizing effects between these two signaling pathways have also been observed in many other studies. For instance, in colorectal cancer, Notch1 counteracts the canonical Wnt pathway by suppressing the expression of Wnt target genes through epigenetic modification (338). Notch antagonizes Wnt activity during *Drosophila* development through modulating the levels of active β-catenin (348). Particularly in vascular developmental process, canonical Wnt and Notch signaling have been found functionally connected and controlling each other. Specifically, endothelial stabilization of Wnt/β-catenin signaling during early embryonic development alters expression of Dll4 ligand and causes vascular phenotype that is similar to what is observed by aberrant Notch pathway activation (349). The same functionality of Wnt/β-catenin-Dll4/Notch

signaling axis is also present in glioblastoma angiogenesis and responsible for the generation of a more normalized tumor vasculature phenotype (350).

Given the critical role of Notch signaling in vasculature development and cell fates determination, and the lack of information on BBB modulation by Notch pathway, we decided to examine whether or not brain endothelial MCT1, one of the important nutrient transporters along BBB, is regulated by Notch signaling. In addition, a well-known keen interaction between canonical Wnt and Notch pathways inspired us to ask whether such a crosstalk exists in brain endothelial MCT1's regulation.

Materials and Methods:

Cell Culture. Immortalized rat brain endothelial (RBE4) cells were cultured in equal parts minimum essential medium alpha (MEM-α) (Invitrogen; #12561-056) and F-10 Nutrient (Ham's) (Invitrogen; #12390-035), supplemented with 10% fetal bovine serum (Atlanta Biologicals; #S11150H), 0.3 mg/ml geneticin (Sigma-Aldrich, #A1720), and 1.0 ng/ml basic fibroblast growth factor (Roche; #11363697001). 25-cm^2 polystyrene tissue culture flasks (Corning Inc.; #CLS430372) were first coated with collagen by treating the surface area with 50ng/ml rat tail collagen type I (BD Biosciences; #354236) in 0.013% cyanamide solution (Sigma-Aldrich; C87908) for 2 hours, followed by water rinsing of the same volume twice. Cells were then cultured on these collagen coated flasks in a humidified incubator at 37^oC with 5% CO_2. All the experiments were conducted when the cells reached light (≥90%) confluence.

Reagent Stocks. 1M lithium chloride (Sigma-Aldrich; #L-0505) stock was made in H_2O and stored in 4^oC. 50mM DAPT (Sigma-Aldrich; #5942) stock was made in DMSO (Sigma-Aldrich; #D2650) and stored in -80^oC until use.

Cellular proteins preparation. Cells were washed twice with 5ml ice-cold PBS (Mediatech, Inc.; #21-040-CV), supplemented with 1X protease inhibitor cocktail (Roche; #11697498001). Whole cellular protein samples were then prepared by direct in-flask scraping of cells within 100µl SDS boiling buffer (5% SDS, 10% v/v glycerol, 60mM Tris-

Cl pH=6.8), transferred into 1.5ml eppendorf tubes (Sarstedt; #72690001), homogenized and centrifuged at 13,000 rpm for 10 minutes.

RNA isolation, reverse transcription and quantitative real time PCR (qRT-PCR). Total cellular RNAs were isolated using RNeasy Mini Kit (Qiagen; #74104) according to the manufacturer's instruction. After their concentrations being determined by ND-1000 NanoDrop spectrophotometer, the RNA samples were converted to cDNAs using QuantiTect Reverse Transcription Kit (Qiagen; #205311). Rotor gene cyber green (Qiagen; #204074) based qRT-PCR was conducted on Rotor-Gene RG-3000 cycler (Corbett Research), using 50ng total cDNA per reaction with the following settings: 95^{o}C 5 minutes, followed by 95^{o}C 5s and 60^{o}C 10s for 40 cycles. The qRT-PCR results were analyzed using the cycle threshold method (C_T, Applied Biosystems User Bulletin Number 2, P/N 4303859) and expressed as fold changes over controls. All the primers used here were designed through the PrimerQuest tool from IDT, and their sequences are summarized in Table IV-3.

Protein assays and western blotting. Protein samples' concentrations were determined using Pierce BCA protein assay kit (Thermo Scientific; #23227) unless otherwise mentioned. Immunoblotting was performed as reported previously (278). Specifically, 10μg proteins from each sample were prepared and diluted 4:5 with homemade 5X sample loading buffer (10% SDS, 50% glycerol, 25% β- mercaptoethanol, 312.5mM Tris HCl and 0.01% bromphenol blue). Then they were subjected to SDS-PAGE electrophoresis at 160V on Criterion TGX precast gels (Bio-Rad; #5671033), and transferred to supported nitrocellulose membranes (Bio-Rad; #162-0070) at constant 200mA for 90 minutes. The membranes were blocked at room temperature on an orbital shaker for 1 hour in SEA BLOCK (Thermo Scientific; #37527), followed by overnight incubation at 4^{o}C with primary antibody diluted 1:5,000 for anti-MCT1 and 1:5,000 for anti-Actin (EMD Millipore; #MAB1501) in 1X TBST buffer (50 mM Tris base, pH 8.0, 0.9% NaCl, 0.1% Tween 20) supplemented with 1% SEA BLOCK. After washing in 1X TBST, the membranes were incubated at room temperature for 1 hour with rabbit anti-chicken IgY conjugated to horseradish peroxidase (Thermo Scientific; #31401) diluted 1:5,000 for MCT1, or goat anti-mouse IgG (Thermo Scientific; #31430) diluted 1:10,000 for Actin.

Detection was accomplished after membranes being rinsed for 5 minutes in SuperSignal West Pico chemiluminescent Substrate (Thermo Scientific; #34080). The immunoblotting results were analyzed by densitometry, normalized to actin and then expressed as fold changes over control.

Table IV-1: qRT-PCR primers

Gene	Forward Primer	Reverse Primer
Notch1	CACCTGCACTGACTATCT	TAGGCACTCGTTGATCTC
Notch2	CTTTGAATGCCAGAGGAATAG	CGTTGTTGCATCCCTTATC
Notch3	CGGCTTGATTTCCCATAC	GAAGATGACCAGCAGAAAG
Notch4	GTGAACGCGACGTCAATGAATGCT	ATTGAGACAGGTTCCAGGAAGGCA
Jagged1	CAGAATGGCGCCCAATGCTACAAT	AGTGGTCTTTCAGGTGTGAGCAGT
Jagged2	ATCACCCAGAGAGGAAAC	GGAAGAGCCACCCATAA
Dll1	CTCTGTAGGAGAAGAGAAGAG	CTTGGTGTCCTTTGAAGTAG
Dll3	GGGACTCTCGATCTATTTATGT	TCATTCAGGCTCCATCTC
Dll4	GAACCACACACTGGACTA	GGCACCTTCTCTCCTAAA
Dlk1	CCAGGCCCTTCTACATTA	GTTCACTAGATTCCACACAAG
Dlk2	ATCAGGAGTGTCAGGTTAG	AGGTGAAAGGAGGTAAGG
Hes1	CAACACGACACCGGACAAACCAAA	TGGAATGCCGGGAGCTATCTTTCT
Hes5	CTACAGCGAGGGTTACT	CGCTGGAAGTGGTAAAG
Hes7	GCCTAGAAGAGCTGAGG	GCGAACTCCAGTATCTCT
Hey1	CTGAAGTTGCCCGTTATC	GGATGCGTAGTTGTTGAG
Hey2	CCATCCAGTAGTGCATTTATAC	GTTCAGGCACTTAGGAAAC
HeyL	GGTCACTCAGAGGACAATA	TCCTACCTAGCCAGAAATAC
Gapdh	ACAAGATGGTGAAGGTCGGTGTGA	AGCTTCCCATTCTCAGCCTTGACT
β-actin	TTGCTGACAGGATGCAGAAGGAGA	ACTCCTGCTTGCTGATCCACATCT

Results:

i. Notch receptors, ligands and target genes in RBE4 cells.

The presence of Notch receptors (*Notch1-4*), ligands (*Jagged1* and *2*; *Dll1,3* and *4*; *Dlk1* and *2*) and some of its known target genes (*Hes1*, *5* and *7*; *Hey1* and *2*; *HeyL*) in RBE4 cells were first investigated using quantitative real time PCR (qRT-PCR). Their abundances were shown as ratios to the expression level of internal standard gene *Gapdh*. Our results indicated that *Notch2* is the most abundant receptor, followed by

Notch3, 1 and *4*. *Jagged 1* has the highest expression level compared with other ligands. *Hes1* and *Hey2* are the two most prominent target genes (Figure IV-2).

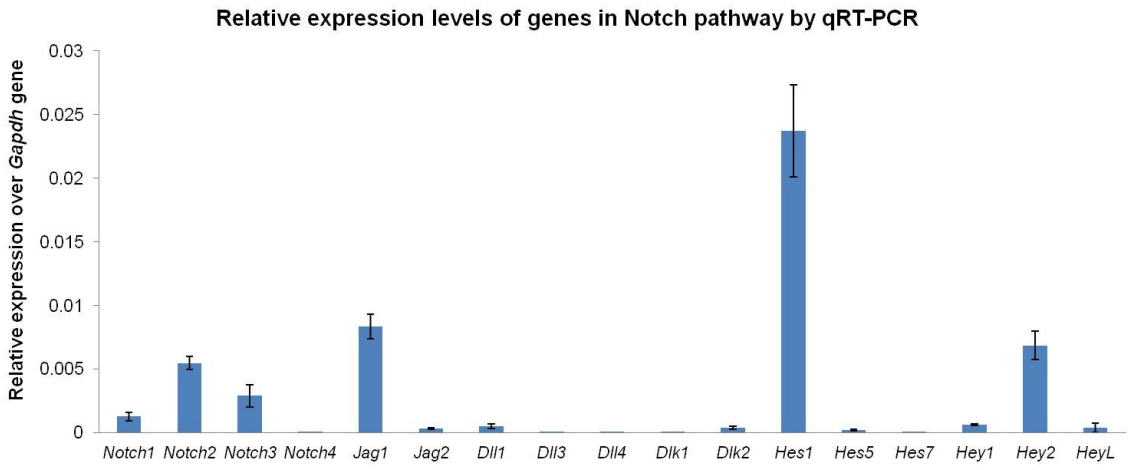

Figure IV-2: Expression profiles of Notch receptors, ligands and selected target genes in RBE4 cells. Total RNA was prepared from RBE4 cells and converted to cDNA, which was then used as template in qRT-PCR. The relative amount of each gene's expression level was roughly expressed as ratios to *Gapdh* gene, using $\Delta\Delta C_T$ method with the formula of $2^{(C_{TX} - C_{TGapdh})}$. Data were summarized as mean±SEM. C_{TX}: threshold cycle number of individual gene; C_{TGapdh}: threshold cycle number of *Gapdh* internal standard. Our data suggested that *Notch2* is the most abundant receptor, followed by *Notch3* and *Notch1*, whereas *Notch4* showed trace level. *Jagged1* is the most abundant ligand, whereas all the rest showed residual expression. *Hes1* is the predominant target gene, followed by *Hey2* that is at significantly higher expression level than the others.

ii. Inhibition of Notch pathway increased MCT1's protein level in RBE4 cells.

In order to see if brain endothelial MCT1 is regulated by Notch signaling, we used a common γ-secretase inhibitor DAPT to inhibit this pathway. Cell viability tests were first conducted with increasing concentrations of DAPT (control, 1μM, 5μM, 25μM and 100μM) for different time periods (6h and 24h) to find the maximal concentrations that do not cause significant cell death. Our results showed that 25μM is the highest concentration still with good cell viability (Figure IV-3). So, we treated RBE4 cells with

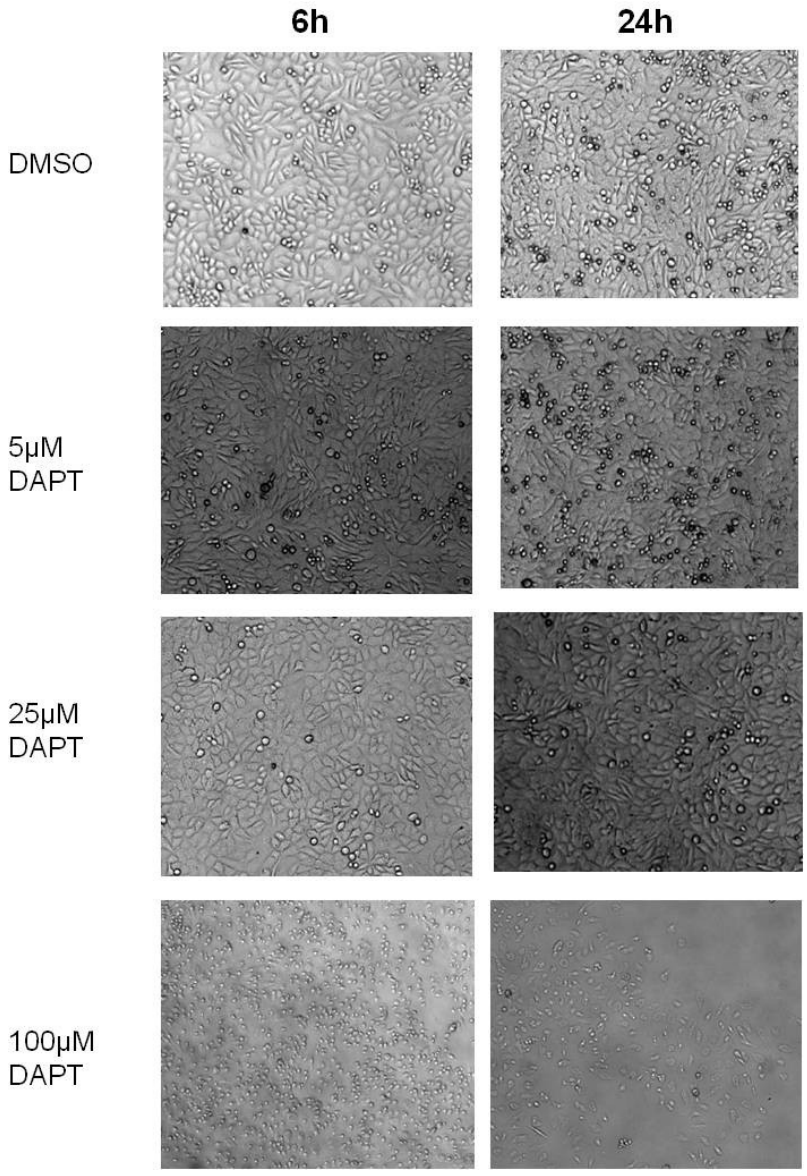

Figure IV-3: Effects of DAPT on RBE4 cells' viability. RBE4 cells were cultured in 24-well plates with either DMSO control or different concentrations of DAPT (5μM, 25μM and 100μM; shown on the left) for 6h or 24h shown on the top. Treatments started when cells were ~90% confluence. Images were taken at indicated time points. Cells were in good condition at DMSO, 5μM and 25μM DAPT for up to 24h. Severe cell death was observed with 100μM DAPT treatment starting at 6h.

5μM DAPT for 24h or 48h, or 25μM DAPT for 12h or 24h, followed by SDS-PAGE analysis of whole cellular proteins and subsequent immunoblotting against MCT1. We found that compared with DMSO vehicle control, 5μM DAPT treatment for 24h and 25μM DAPT treatment for 12h significantly increased MCT1's protein expression by 26% and 41%, respectively (Figure IV-4). qRT-PCR analysis of RNA samples from those two DAPT treatment groups showed significant downregulation of the two most abundant target genes in RBE4 cells, *Hes1* and *Hey2*, demonstrating that the observed upregulation of MCT1 by DAPT was due to inhibition of Notch signaling (Figure IV-5).

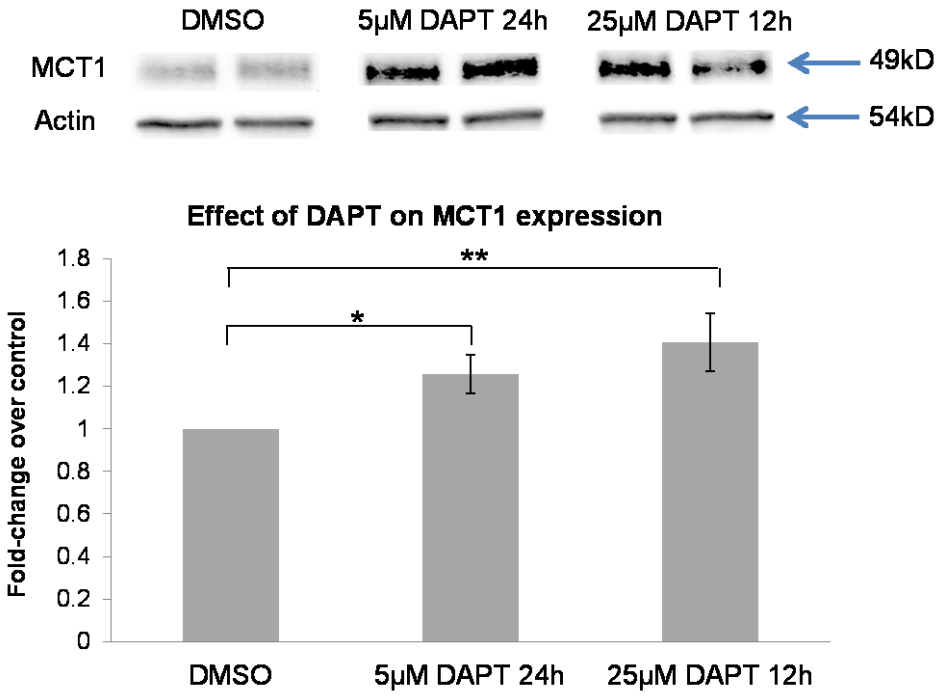

Figure IV-4: Effects of Notch inhibition by DAPT on brain endothelial MCT1 expression. Based on viability screening study with DAPT, RBE4 cells were treated with either 5μM DAPT for 24h or 25μM DAPT for 12h, followed by SDS-PAGE separation and immunoblotting against MCT1 and actin. The results were expressed as fold-changes over DMSO control. Statistical analysis showed that MCT1 protein level was upregulated by both DAPT treatments (5μM DAPT 24h: 26%; 25μM DAPT 12h: 41%; one-way ANOVA followed by Bonferroni post hoc test: *P<0.02, **P<0.01; mean±SEM).

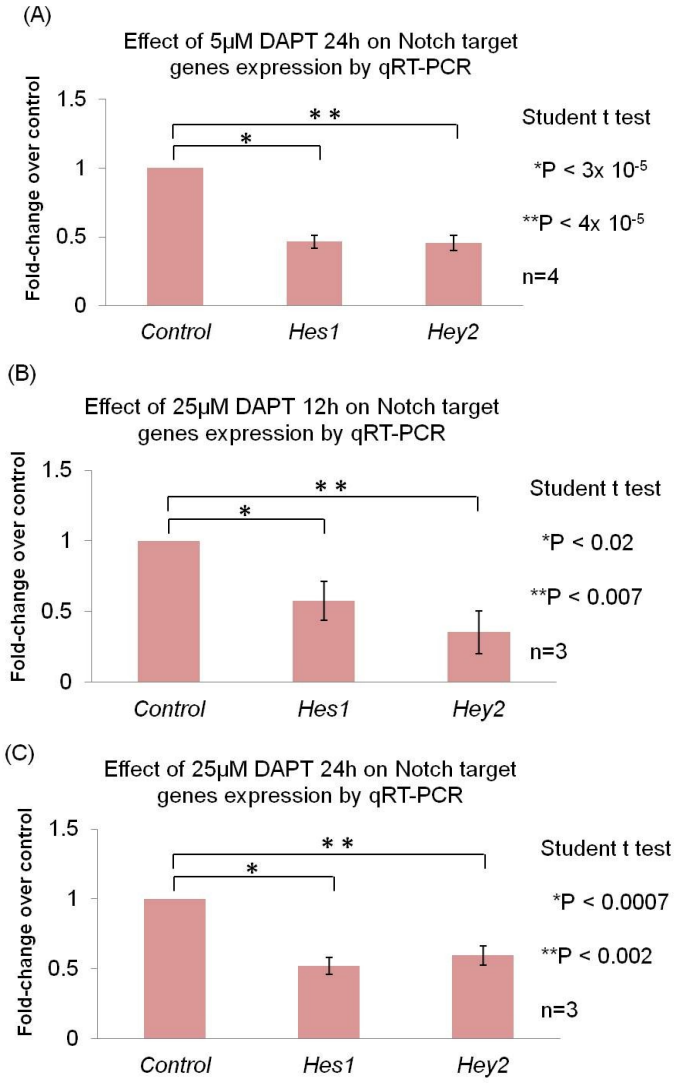

Figure IV-5: Notch target genes were downregulated by DAPT. RBE4 cells were treated with either 5μM DAPT for 24h (A), or 25μM DAPT for 12h (B) or 24h (C). After total RNA harvest and reverse transcription, qRT-PCR was performed to examine *Hes1* and *Hey2* expression. The data were first normalized to β-actin, and then expressed as fold-changes over control. $\Delta\Delta C_T$ method was used for quantification. Mean±SEM. Our results indicated that *Hes1* and *Hey2* were downregulated by: (A) 53% (student t test, *P<3X10^{-5}, n=4) and 54% (student t test, **P<4X10^{-5}, n=4) respectively in 5μM DAPT treatment for 24h, (B) 43% (student t test, *P<0.02, n=3) and 65% (student t test, **P<0.007, n=3) respectively in 25μM DAPT treatment for 12h, and (C) 48% (student t test, *P<0.0007, n=3) and 41% (student t test, **P<0.002, n=3) respectively in 25μM DAPT treatment for 24h.

iii. Upregulation of MCT1 by the canonical Wnt/β-catenin signaling pathway requires Notch participation in RBE4 cells.

Numerous studies have suggested a crosstalk between Wnt and Notch signaling pathways in a variety of biological conditions, either repressively or cooperatively. Here we wanted to ask if an interaction between the two pathways also exists in RBE4 cells in regulating MCT1's protein expression. Cells were co-treated with 20mM LiCl and 5μM or 25μM DAPT for 24h. Western blotting showed that the expected upregulation of MCT1's protein level by 20mM LiCl was reduced by co-treatment with 5μM DAPT and negated by 25μM DAPT (Figure IV-6). These results indicated that although inhibition of Notch pathway by DAPT alone increased MCT1's protein expression, intact Notch activity is required for MCT1's upregulation by the Wnt pathway, implying a cooperative role between them.

In order to confirm the observed interaction between Wnt and Notch pathways in RBE4 cells, we treated cells with either 20mM NaCl or LiCl for 24h; then qRT-PCR was performed to examine any changes in the expression levels of players in Notch pathway, namely receptors, ligands and target genes. Our results showed that compared with NaCl control, LiCl upregulated *Notch4*, *Dll3*, *Dll4* and *Hes7* expression significantly, thus promoting Notch signaling transduction (Figure IV-7 A-D). Surprisingly, another Notch target gene, *Hey2*, was found to be downregulated by LiCl treatment (Figure IV-7 E). In conclusion, the interplay between Wnt and Notch pathways is complicated in RBE4 cells, with evidences supporting both a cooperative and a repressive role.

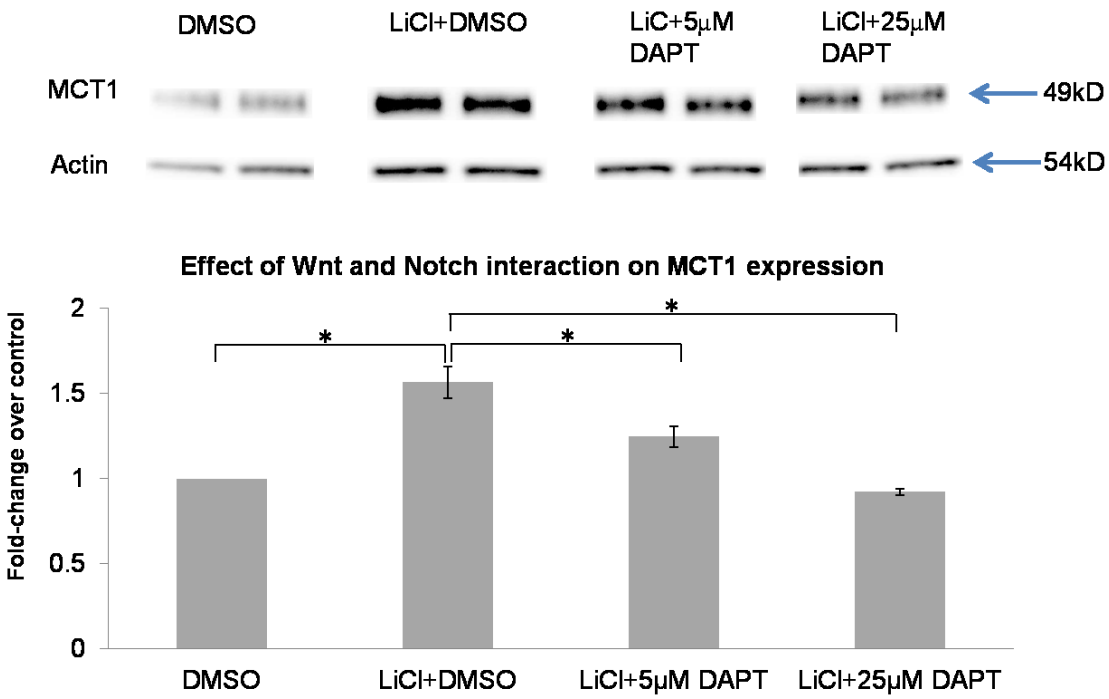

Figure IV-6: Interaction between Wnt and Notch pathways in regulating brain endothelial MCT1 expression. RBE4 cells were treated for 24h with or without 20mM LiCl, in the presence or absence of 5μM or 25μM DAPT. Whole cellular proteins were then prepared and separated on SDS-PAGE, followed by immunoblotting against MCT1 and actin. Densitometry was used for quantification and expression changes were manifested as fold-changes over DMSO control. Mean±SEM. Our results indicated that 20mM LiCl elevated MCT1 expression by 57%, which was reduced by cotreatment with 5μM (25%) or 25μM (-8%) DAPT. (One-way ANOVA followed by Scheffe's post hoc test, *P<0.05)

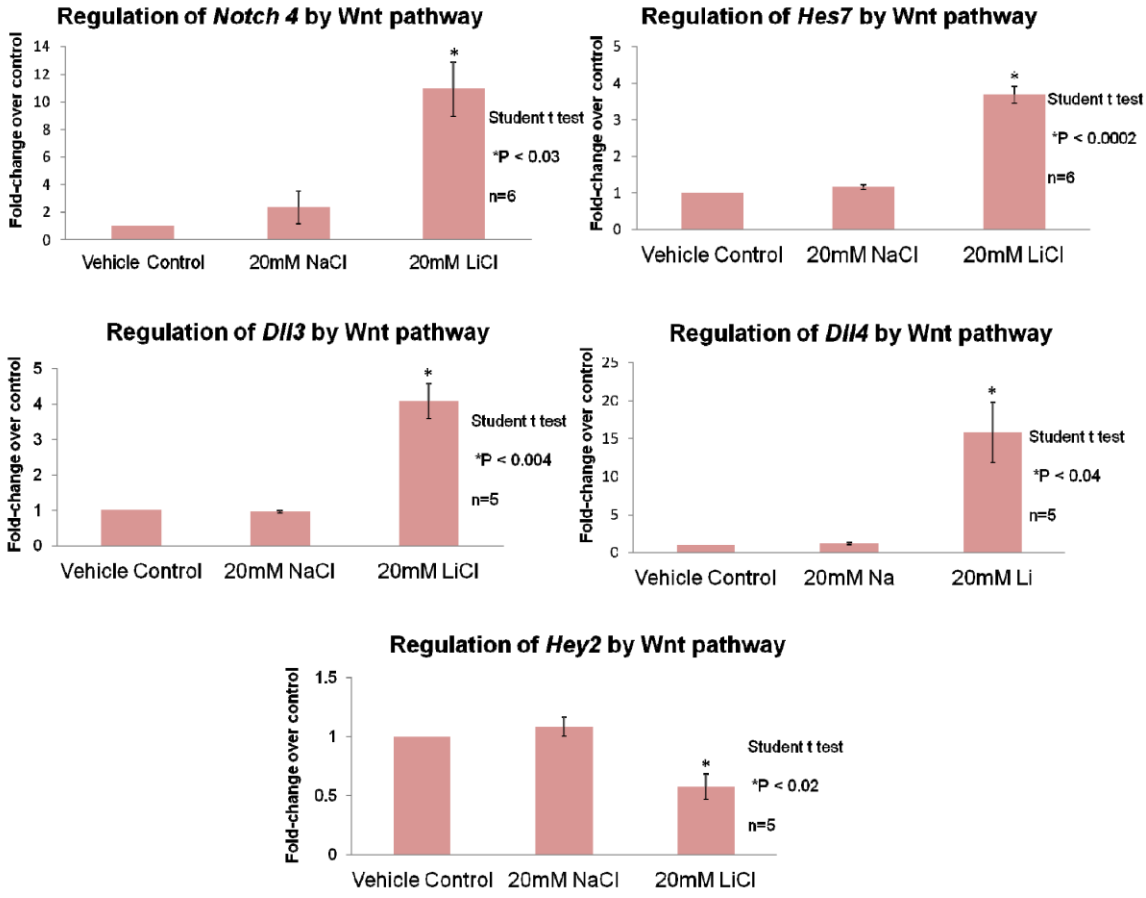

Figure IV-7: Regulation of Notch pathway by the canonical Wnt/β-catenin signaling. RBE4 cells were treated with either vehicle control, or 20mM NaCl (osmotic control) or 20mM LiCl for 24h. Total RNA was prepared and reverse transcribed. qRT-PCR results were first normalized to the internal standard *Gapdh* and then expressed as fold-changes over control, followed by $\Delta\Delta C_T$ method for quantifiaction. Mean±SEM. Our results showed that Wnt pathway significantly upregulated the expression of: (A) *Notch4* to 10-fold (student t test, *P<0.03, n=6); (B) *Hes7* to 3.5-fold (student t test, *P<0.0002, n=6); (C) *Dll3* to 4-fold (student t test, *P<0.004, n=5); and (D) *Dll4* to 16-fold (student t test, *P<0.04, n=5). In contrary, Wnt was found to downregulate another targe gene (E) *Hey2* to 0.42-fold (student t test, *P<0.02, n=5).

Discussion:

In this report, we investigated the regulatory effects of Notch pathway on brain endothelial MCT1's expression. Blockage of Notch signaling via the γ-secretase inhibitor DAPT increased MCT1's protein level, while in the meantime it suppressed Notch target genes expression as expected. In addition, a cooperative interaction was observed between Wnt and Notch signaling pathways on modulating brain endothelial MCT1's expression. Specifically, the observed upregulation of MCT1 by Wnt requires Notch activity, as inhibition of the latter by γ-secretase inhibitor (GSI) DAPT negates Wnt's effect (Figure IV-8). Our findings of the modulatory effect of Notch activity on a nutrient transporter in brain endothelial cells are not surprising given the important role of this pathway in the normal development of vasculature (351). In addition, modulation of Notch activity in endothelial cells can control glycolytic switch via different signaling processes, one of which is downregulation of p53 signaling after Notch inhibition (352, 353). In fact, MCT1 expression was found to be upregulated by hypoxia only in the absence of p53, mediated via NF-kB signaling pathway in cervix, breast and colon cancer cell lines (110). Lactate can accumulate intensively after glycolysis as well as within hypoxic conditions. In skeletal muscle L6 cells, addition of lactate increased MCT1 expression at both mRNA and protein levels within 1h (126). Besides, lactate produced by tumor cells can be uptaken by human mesenchymal stem cells to increase their MCT1's expression (127). Further research should shed lights on better understanding the molecular mechanisms of how Notch signaling modulates brain endothelial MCT1, e.g. transcriptionally, post-transcriptionally or post-translationally.

The cooperative interaction between Wnt and Notch pathways on regulating brain endothelial MCT1 observed in our study is supported by the well established notion that these two signaling processes cross talk with each other in a variety of biological conditions, as covered in the *Introduction* session at the beginning. In accordance with our observation that the upregulation of brain endothelial MCT1 requires the participation of Notch signaling, previous research in mouse embryonic stem cells found that inhibition of Notch by DAPT caused a significant reduction of active β-catenin activity and its protein levels (346), thus quenching Wnt signaling transduction. Besides, Notch

is found downstream of Wnt in colorectal cancer cells through β-catenin-mediated transcriptional activation of Notch-ligand Jagged 1. The fully bloomed intestinal tumorigenesis by genetically activated Wnt/β-catenin signaling requires Notch activity (341). Further research showed that the effect of Wnt activation via LiCl on cell cycle progression in non-small-cell lung cancer cells was attenuated by siRNA knockdown of Notch3 signaling, confirming that a cooperative interaction exists between Wnt and Notch (354). Conversely, in the absence of DAPT, which guarantees an intact Notch signaling transduction, Wnt activation successfully increased MCT1's expression, whereas in the presence of that γ-secretase inhibitor, this modulatory effect disappeared. As a consequence, another way of interpretating our results is that the canonical Wnt/β-catenin pathway needs to act under the umbrella of an intact Notch signaling in order to regulate MCT1 in RBE4 cells. Indeed, Notch1 signaling was found to act upstream of Wnt pathway by stabilizing β-catenin during the progression of primary melanoma (355). Inhibition of γ-secretase causes the cellular equilibium between membrane bound Notch receptors and those undergoing proteolytic cleavage to be in favor of the former. Notch receptors within the plasma membrane were found to bind active β-catenin; together they go into lysosomal degradation system, thus reducing cytoplasmic β-catenin level (346). Further confirming a reciprocal reliance of Wnt and Notch pathways, previous research in colorectal tumorigenesis showed that intestinal proliferation phenotype induced by activation of Notch requires TCF4, the important Wnt effector, indicating that only cells in which the Wnt signaling remains "intact" are competent to respond to Notch stimulation (347).

Our additional qRT-PCR data showing the upregulation of *Notch4*, *Dll3*, *Dll4* and *Hes7* by Wnt activation (Figure IV-7 A-D), correlate well with: (1) the critical role of canonical Wnt signaling in normal blood-brain barrier development (275, 276) and the essential function of Notch signaling in vasculature formation, especially mediated through Notch4 receptor (351, 356) and Dll4 ligand (334, 335); (2) the cooperative interaction between Wnt and Notch signaling activity. Surprisingly, Wnt activation didn't change *Hes1*'s transcriptional level (data not shown), the classic Notch target gene that was actually found decreased by DAPT treatment in our current study (Figure IV-5). In addition, another Notch target *Hey2* was found downregulated by Wnt pathway, suggesting an

antagonizing role of Wnt on Notch signaling (Figure IV-7 E). In fact, not all the Notch components are regulated by the Wnt/β-catenin signaling. For example, in adenomas from genetically modified $APC^{+/-}$ mice, only a subset of Notch receptors (Notch1, 2 and 4) and ligands (Jagged1 and 2, Dll4) were upregulated by loss of APC allele (340). Additionally, human Notch1, Jagged2, and Hey1 do not contain any putative LEF-1/TCF-site. Semi-quantitative PCR results showed that suppression of Wnt activity by ectopically expressing wild type APC in HT29 cells failed to change most of Notch pathway genes transcriptional level, even though they contain putative LEF-1/TCF elements in their promoters (357). Even strikingly, Hes7, one of Notch targets and also upregulated in our data by Wnt signaling, was found to inhibit periodically selected Notch downstream target genes transcription e.g. Hes7 itself and Lfng, during the control of segamentation clock (358). This finding supports our observation that Hey2 was suppressed by Wnt pathway, possibly as a result of Notch feedback regulation. Another possible explanation for heterogeneous responses of Notch pathway genes to Wnt activation arises from the way it was manipulated. LiCl targets and inhibits GSK3-β, a convergent point of multiple signaling pathways in addition to β-catenin, such as PKA, PI3K-AKT, MAPK-MAPKPK1, mTORC1 and Myc transcription factor (359). Alteration of GSK3-β activity in our study may cause other associated signaling routes to respond accordingly in order to maintain the final expression levels of particular target genes. So it is very likely that inhibiting GSK3-β causes integration of other signaling branches to negate any effects caused by one of them. Indeed, Hes1 can be activated by other pathways besides Notch, like Sonic Hedgehog, IkBa and Ras/MAPK (340). Application of downstream activators more specific to Wnt pathway may help resolve this issue.

The molecular mechanisms underlying the complicated cross-talk between Wnt and Notch pathways have received intensive investigations and generated a better understanding. For example, early insights on how Wnt signaling exerts an inhibitory effect on Notch signaling came from studies in *Drosophila*, where a physical binding of Dishevelled to NICD inhibits the latter-mediated Notch activity by disrupting the ability of NICD to act as a transcriptional regulatory factor in the nucleus (360). Besides, GSK3-β was found to bind and phosphorylate Notch1 intracellular domain, leading to the stabilization of NICD by preventing its entry into proteasomal degradation (361). One

mechanism of Wnt activating Notch was demonstrated as downregulating one of the latter's negative target Atoh1 (340). Conversely, Notch1 signaling suppressed the expression of Wnt target genes in colorectal cancer via epigenetic modification through recruiting histone methyltransferase (338). In addition, these two pathways have been shown to share common cofactors in the nucleus, such as Mastermind (MAML) (362). Although a wealth of knowledge has been obtained on Wnt-Notch interaction, the detailed mechanism of how they precisely orchestrate each other in order to determine cell fates during development and tissue self-renewal still remains elusive and merits further research.

Another contribution of our work here is to generate for the first time a complete gene expression profile of Notch ligands, receptors and some of the major downstream target genes in RBE4 cells, an *in vitro* model of BBB. These data shall be the basis for future studies on Notch signaling in brain endothelial cells.

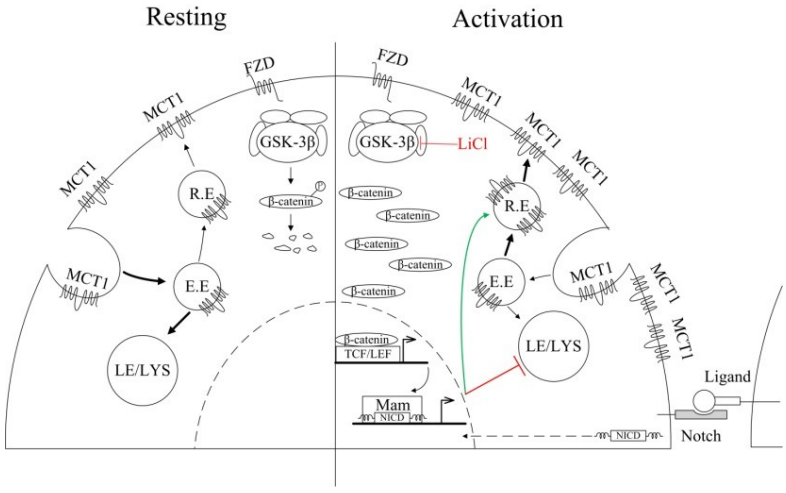

Figure IV-8: Summary of MCT1's regluation within the endosomal-lysosomal system by the canonical Wnt/β-catenin and Notch signaling pathways. Left side: in resting cells, MCT1 is first internalized into early endosomes (E.E). From here, MCT1 could be sorted into either recycling endosomes (R.E) for its redistribution on the plasma membrane, or into late endosomes and lysosomes (LE/LYS) for degradation. Right side: Activation of Wnt pathway through inhibiting GSK-3β by LiCl leads to nuclear β-catenin signaling and increased expression of MCT1 on the plasma membrane, presumably through either enhanced recycling rate via R.E or reduced degradation in LE/LYS or both. This regulation of MCT1 by Wnt pathway acts in a Notch signaling-dependent manner. FZD: Frizzled receptor; NICD: Notch intracellular domain; Mam: Mastermind.

Chapter V

Inhibition of MCT1 by small molecules: Metabolic blockage of MCT1 in human peripheral blood mononuclear cells (hPBMCs)

Introduction:

Metabolism is one of the most ancient functional features of cells to fulfill bioenergetic and biosynthetic demands, especially during active processes such as cellular growth and proliferation (363). As the primary source of nutrient under normal circumstances, intracellular glucose is usually broken down first by glycolysis to generate pyruvate through multiple intermediate metabolites that can be harnessed by different synthetic pathways as building blocks for bio-molecules, such as nucleotides via pentose phosphate pathway, amino acids using glycerate-3-phosphate and hexosamine from fructose-6-phosphate. In the presence of oxygen, pyruvate is fully consumed within mitochondria through tricarboxylic acid (TCA) cycle followed by oxidative phosphorylation to generate affluent ATP. In contrast, lack of oxygen diverts pyruvate into fermentative reaction and produces only 2 net ATP per glucose entry. Thus, glycolysis is generally considered as an inefficient way of generating cellular energy.

As the central part of adaptive immune response, T lymphocytes (naïve and memory T cells) undergo rapid and extensive clonal expansion after receiving antigen stimulation, accompanied by a metabolic switch from β-oxidation of fatty acids to glycolysis and glutaminolysis in order to support their proliferation, growth as well as effector functions (364, 365). Increased glucose utilization through glycolysis in activated T cells, even in the presence of plenty oxygen, is believed to provide metabolic intermediates to elevate biosynthetic machineries for the production of proteins, nucleic acids, lipids and other building blocks for cellular growth as well as for generating new cells (363). The energy demand of T cells under reprogrammed metabolism that impairs normal energy production from oxidative phosphorylation, is partially rescued by ATP molecules generated during aerobic glycolysis as well as those from mitochondrial function fueled by α-ketoglutarate that is derived from glutamine (366). The enhanced aerobic glycolysis results in extensive intracellular accumulation of lactate, which must be removed quickly, presumably by MCTs, to prevent feedback inhibition on glycolytic pathway as well as a detrimental acidic environment. Indeed, both MCT1 and 4 were found to be present on T lymphocytes and their expression levels were elevated upon T cells activation (184). Strikingly, MCT1 on activated T cells was demonstrated to be a novel target for

suppressing their proliferation at the extremely rapid phase triggered by antigens (184). As a result, MCT1 possesses the potential to be a therapeutic target for immunosuppressant during acute immune reactions, such as organ transplantation.

The most commonly used MCT inhibitor, alpha-cyano-4-hydroxycinnamate (α-CHC), was first identified as an inhibitor to mitochondrial pyruvate transport (367). Later kinetics studies demonstrated that the $K_{0.5}$ of α-CHC on 5mM L-lactate transport through MCT1 was 166μM (223). Besides, α-CHC is not specific to MCT1, but it also inhibits other MCTs, such as MCT2 and MCT4 (151, 160). In order to find more potent inhibitors that can block MCT1, more than 250 α-CHC analogues were synthesized and tested on RBE4 cells for their capacity to inhibit L-lactate transport. RBE4 cells predominantly express MCT1 than other MCT isoforms (67, 174), thus they are ideal model to screen for MCT1 inhibitors. Three potent lead compounds with high affinity and low EC_{50} values in the range of 3-8nM were discovered. Their structures have more than 20,000 times greater affinity than α-CHC for MCT1 and are designated MD1, MD2 and MD3. In this study, we examined MD1's potency in suppressing human peripheral blood mononuclear cells (hPBMCs) proliferation upon antigen stimulation by phorbol myristate acetate (PMA) and ionomycin. hPBMCs are a group of blood cells, including lymphocytes, monocytes and macrophages, which are critical component in the immune system to fight infection and have been used as a model to study adaptive immune response to antigen challenging (184).

Materials and Methods:

Human Peripheral Blood Mononuclear Cells (hPBMCs) preparation and culture.

hPBMCs were isolated from blood samples of a healthy male donor, using the Lymphoprep™ Tube (Cosmo Bio USA; #AXS-1019818). Specifically, fresh blood samples were first mixed with 20% volume anticoagulant ACD-A (22g/L sodium citrate tribasic dihydrate; 7.3g/L Citric acid anhydrous; 24.5g/L dextrose); then they were diluted 1:1 with equal volume of sterile 0.9% saline solution. After that, the diluted blood was applied to Lymphoprep™ Tubes and centrifuged at room temperature for 15min at 800xg.

hPBMCs were thus collected from a distinct layer within the tube. They were frozen in growth medium plus 10% DMSO (Sigma-Aldrich; #D2650) and stored in liquid nitrogen until use.

hPBMCs were cultured in their growth medium consisting of RPMI 1640 medium (Invitrogen; # 11835-030), supplemented with 10% FBS (Atlanta Biologicals; #S11150H), 2mM L-glutamine (Invitrogen; # 25030081), 1X Non-Essential Amino Acids (Invitrogen; # 11140-050), 1mM sodium pyruvate (Invitrogen; # 11360070) and 1X β-mercaptoethanol (Invitrogen; # 21985-023). Cells were kept in a humidified incubator at 37^{o}C with 5% CO_2.

Reagent stocks. 1mg/ml phorbol myristate acetate (PMA) (Sigma-Aldrich; #P8139), 1mg/ml ionomycin (Sigma-Aldrich; #I0634), 40mM cyclosporin A (Sigma-Aldrich; #30024) and 100mM MD1 (University of Minnesota Duluth; V.Mereddy's lab) stocks were all dissolved in DMSO and stored in -80^{o}C freezer until use, except for MD1 that was stored at room temperature.

Proliferation assays. 2X 10^5 hPBMCs cells were plated into each well of 96-well plates (Corning; #3595). The next day, equal volume of growth medium containing 1ng/ml phorbol myristate acetate (PMA) and 1μg/ml ionomycin, with either DMSO vehicle control or 2X MD1 compound was added into each well, making the final growth medium with 0.5ng/ml PMA and 500ng/ml ionomycin, with either DMSO vehicle control or MD1 compound at the desired concentration (2nM, 10nM, 50nM, 250nM, 1μM, 5μM, 25μM, 50μM, 75μM or 100μM). Cyclosporin A was used instead of MD1 as a positive control at a final concentration of 2nM, 10nM, 50nM, 250nM, 1μM, 5μM or 25μM. Cells were incubated for 72 hours, after which they were aspirated off the old medium and frozen at -80^{o}C overnight up to two weeks. Cyquant proliferation assay was conducted according to the manufacturer's instruction (Invitrogen; #7026). Basically, the whole 96-well plates were thawed at room temperature and incubated with 200μl per well of the provided 1X lysis buffer supplemented with 1X green fluorescent GR dye that binds nucleic acids. The samples fluorescence then was measured directly at a Synergy 2 multi-mode microplate reader (Biotek) with filters for ~480nm excitation and ~520nm emission.

Results:

In order to test our novel MCT1 inhibitor (MD1)'s potency in suppressing immune response, human peripheral blood mononuclear cells (hPBMCs) were isolated from a healthy donor, and stimulated by antigens of 0.5ng/ml PMA and 500ng/ml ionomycin for 72 hours, in the presence or absence of MD1 at various concentrations (2nM, 10nM, 50nM, 250nM, 1μM, 5μM, 25μM, 50μM, 75μM or 100μM). In the control group, hPBMCs remained in a quiescent state without any changes in the quantity of cells. Addition of antigens stimulated hPBMCs to proliferate and thus aggregate into small individual clusters (clonal expansion), as observed under light microscope (Figure V-1 A and B). However, cotreatment with MD1 inhibitors at various concentrations didn't change the proliferation status of hPBMCs stimulated by antigens (Figure V-1 C-I), unless relatively high concentrations were applied (Figure V-1 J-L). Cyquant proliferation assay results corroborated our microscopic observation and showed that PMA/ionomycin successfully stimulated hPBMCs to proliferate by ~175%, which was only inhibited by cotreatment with MD1 at concentrations ≥50μM. Specifically, 50μM, 75μM, and 100μM MD1 caused 63%, 62% and 95% inhibition on hPBMCs proliferation that was stimulated by antigens (Figure V-2). Cyclosporin A, a commonly used immunosuppressant drug, was able to inhibit hPBMCs proliferation by antigens at expected concentrations as low as 50nM, which was presented by both microscopy (Figure V-3) and Cyquant assay (Figure V-4), indicating that the novel MCT1 inhibitor, MD1, is less potent than cyclosporin A in suppressing immune response of hPBMCs.

Discussion:

Our results showed that a novel MCT1 inhibitor (MD1) suppressed proliferation of hPBMCs stimulated by PMA/ionomycin, only at high concentrations above 50μM, despite of the fact that it could inhibit L-lactate transport with an EC_{50} value of 6nM in RBE4 cells. Cyclosoprin A was included as a positive control in our current study, because it has been widely used as an immunosuppressant drug in clinic. The working concentration of cyclosporin A (≥50nM) in blocking PBMCs proliferation correlates well

with its role as a strong T-cell receptor signaling blocker and supported by previous similar research conducted by Astra Zeneca (184). In that same study, the authors used their newly designed immunosuppressive drugs to inhibit T lymphocytes proliferation by targeting MCT1 with an IC_{50} value being ~10nM. The EC_{50} value of that compound analogue was found to be 0.28-0.44nM for inhibiting lactate transport out of activated hPBMCs.

The huge difference between EC_{50} of MD1 in inhibiting lactate transport in RBE4 cells (6nM) and its working concentration for suppressing activated hPBMCs proliferation (50μM) as observed in the current study, suggests that our compound may work differently from the ones developed by Astra Zeneca. In fact, α-CHC was first described as a potent mitochondrial pyruvate transport inhibitor (K_i=6μM); in addition, it inhibits pyruvate transport into human erythrocytes more strongly than lactate (367). It is thus likely that our MD1, an analog of α-CHC, may function similarly in activated T cells by preferentially binding with pyruvate transporters on mitochondria, sparing MCT1 on cellular surface intact. MCT2 has a much higher affinity for monocarboxylate substrates, such as lactate and pyruvate, than MCT1. The same difference has been observed for the MCT inhibitor α-CHC (IC_{50}=425μM for rat MCT1 vs IC_{50}=24μM for rat MCT2) (368). Amazingly, Murray et al (184) showed that MCT2 ectopic expression in INS1 cells didn't contribute to L-lactate transport. Besides, their compounds were found to bind selectively with MCT1 over MCT2, partially explaining for the high sensitivity of activated T lymphocytes to their novel compounds. In contrast, our MD1 compound may be enriched at MCT2 binding sites on activated T lymphocytes and thus does not affect lactate transport via MCT1 when administrated at low concentrations. Additional kinetics studies of our MD compounds on different MCT isoforms (e.g. affinities, specificities et al) shall help shed lights on the mechanisms of their actions.

Although MCTs are generally considered as bi-directional facilitators for monocarboxylates down their concentration gradient across cellular membrane, MCT1 is thought to be more prone for importing substrates, whereas MCT4 assumes more an exporting role. Initial insights came from studies where MCT1 was found more predominantly expressed on type I fibers in red skeletal muscle as well as in cardical

muscles (88-90), while MCT4 was correlated with type II fiber composition in glycolytic white muscles (141). Maybe the inhibition of MCT1 by MD1 in the context of glycolytic burst within activated T cells, where efflux of lactate predominates, is not so sensitive to the other direction in lactate uptake assay originally conducted in RBE4 cells. MCTs require ancillary proteins for assisted trafficking from intracellular compartments onto plasma membrane, such as CD147 or embigin for MCT1 and MCT4 (50), embigin or CD147 for MCT2 (52, 53). As a consequence, some inhibitors can target the ancillary proteins for suppressing MCTs transport function. For example, pCMBS inhibits MCT1 and MCT4 activity through targeting CD147, causing dissociation of these proteins by modifying the disulfide bridge in the Ig-like C2 domain of CD147 (52). So it is possible that MD1 inhibits MCT1 though targeting its ancillary proteins with different capacities in RBE4 cells and activated T lymphocytes.

Our results that coincubation of antigens with MD1 didn't inhibit T lymphocytes activation in 72 hours, can be supported by the observation from Murray et al (184) that, incubation of T cells with their potent compounds from the time of activation showed no change in intracellular pH (pHi) compared with control cells over 72 hours. This puzzling phenomenon may indicate that inhibition of MCT1 by our MD1 stimulates other pathways within T cells to compensate for lactic acidosis-induced pH drop as well as proliferation arrest. In addition, our MD1 compound may act through modulating other signaling pathways, e.g. cytokine (interleukin-2) production or CD25 expression to shut down immune response, than simply blocking lactate efflux on cellular surface. Different mechanisms may require diverse thresholds of MD1 to be effective. Future research on lactate production, intracellular accumulation and MD1 binding assays during T cells activation are necessary to clarify the novel inhibitor's working mechanism.

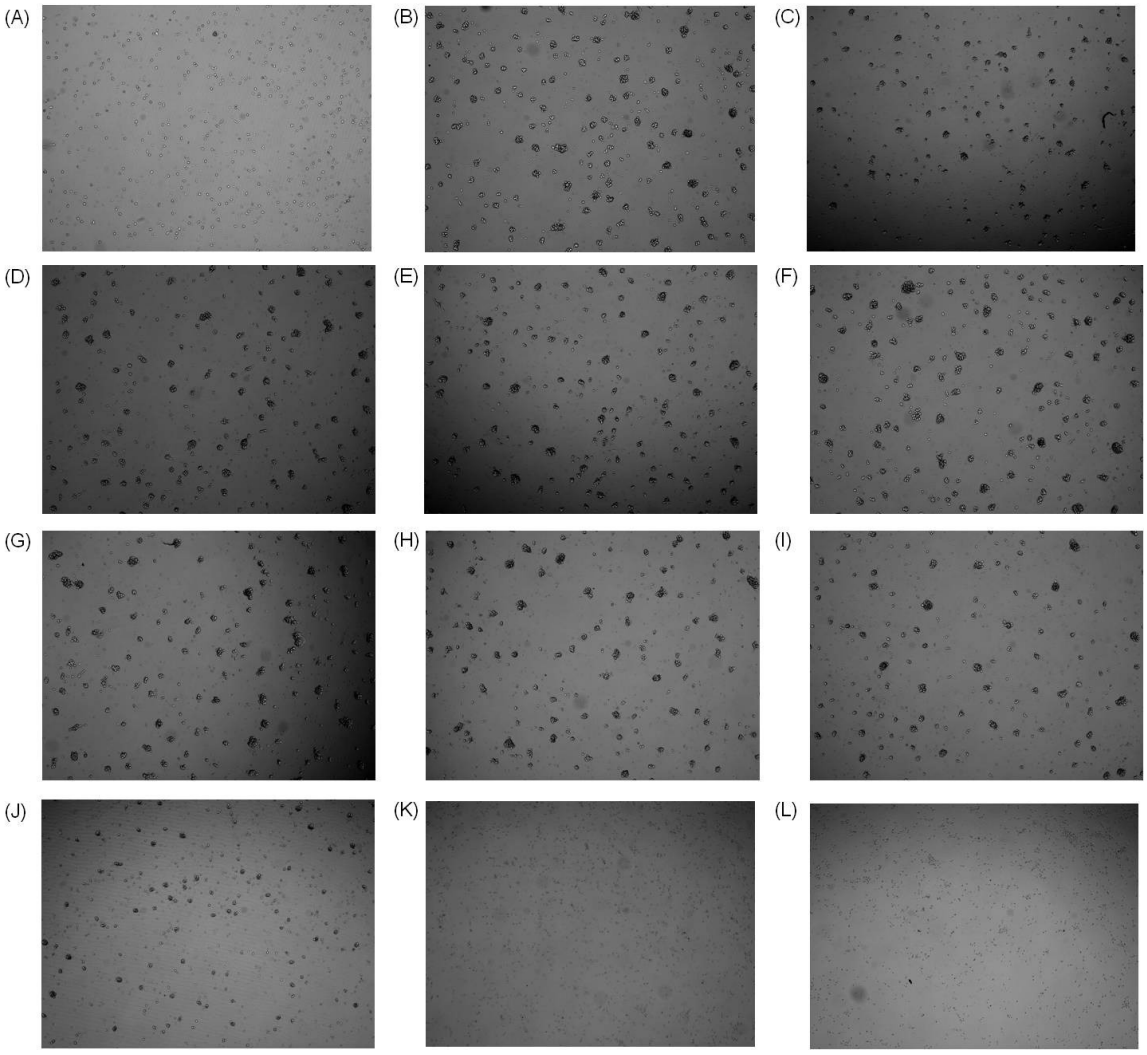

Figure V-1. Microscopic images of hPBMCs stimulated by antigens with or without MD1. $2x10^5$ hPBMCs were cultured for 72 h in the growth medium supplemented with DMSO (A), or stimulated with 0.5ng/ml PMA and 500ng/ml ionomycin (B-L) in the presence of DMSO vehicle control (B), or MD1 at concentrations of 2nM (C), 10nM (D), 50nM (E), 250nM (F), 1μM (G), 5μM (H), 25μM (I), 50μM (J), 75μM (K) or 100μM (L). Our observations indicated that, compared with resting control (A), antigens stimulated hPBMCs proliferation and subsequent aggregation (B), which was only suppressed by cotreatment with MD1 starting from 50μM (J-L).

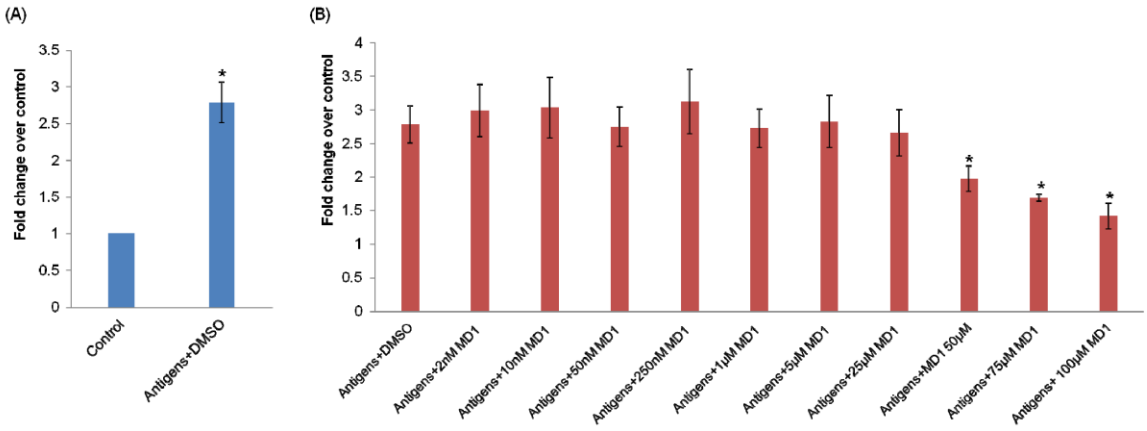

Figure V-2. Effects of MD1 on hPBMCs proliferation. hPBMCs proliferation was measured by DNA content using Cyquant assay. Data were expressed as fold-changes over control and presented as mean±SEM. (A) hPBMCs were cultured for 72h in the growth medium supplemented with DMSO, or stimulated with 0.5ng/ml PMA and 500ng/ml ionomycin (referred to as antigens). Antigens stimulated hPBMCs to proliferate up to 2.8-fold (Student t test, *P<0.0001, n=7). (B) Antigens were coincubated with DMSO or MD1 at concentrations indicated on the x-axis. MD1 was able to suppress hPBMCs proliferation capacities only at 50μM or higher. Specifically, 50μM MD1 reduced the proliferation capacity of stimulated hPBMCs to 1.98-fold (63% inhibition); 75μM MD1 reduced that to 1.69-fold (62% inhibition) and 100μM reduced that to 1.42-fold (95% inhibition) (one-way ANOVA, followed by Fisher's LSD post hoc test, *P <0.05, n≥4).

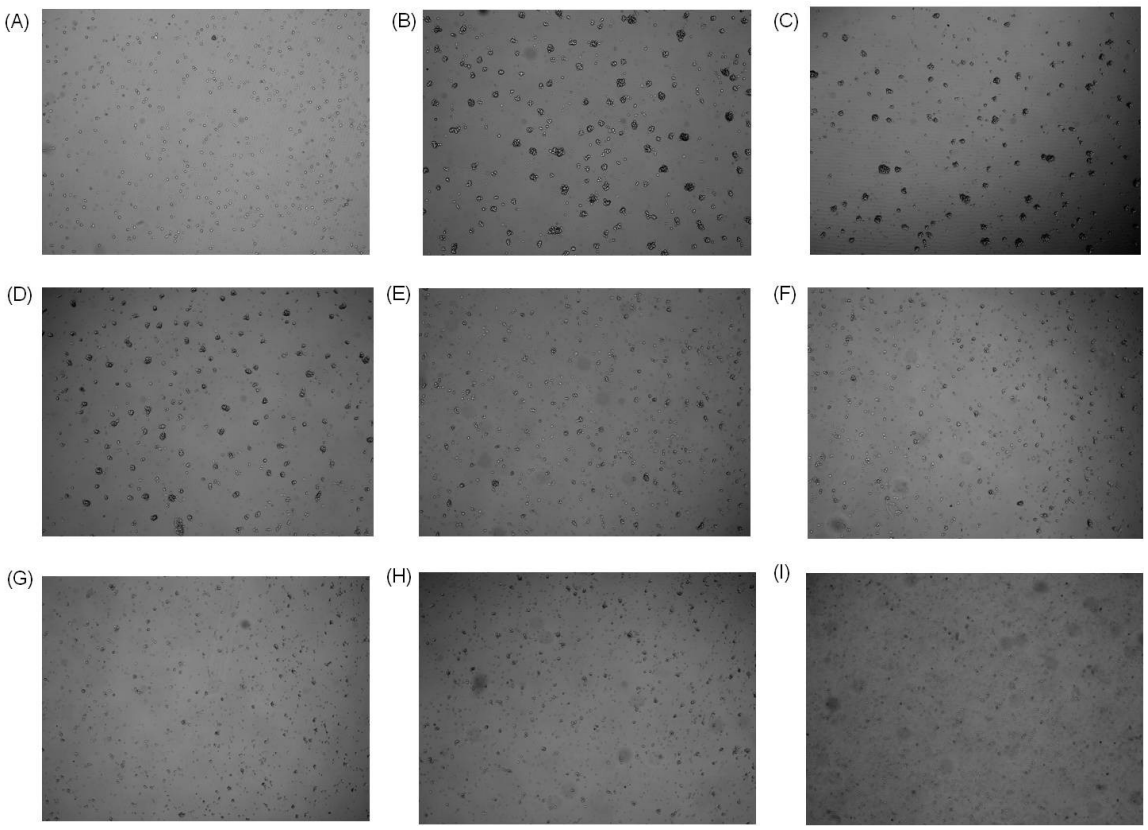

Figure V-3. Microscopic images of hPBMCs stimulated by antigens with or without cyclosporin A. $2x10^5$ hPBMCs were cultured for 72 h in the growth medium supplemented with DMSO (A), or stimulated with 0.5ng/ml PMA and 500ng/ml ionomycin (B-I) in the presence of DMSO vehicle control (B), or cyclosporin A at concentrations of 2nM (C), 10nM (D), 50nM (E), 250nM (F), 1μM (G), 5μM (H), 25μM (I). Our observations indicated that, compared with resting control (A), antigens stimulated hPBMCs proliferation and subsequent aggregation (B), which was suppressed by cotreatment with cyclosporin A starting from as low as 50nM (E), as expected.

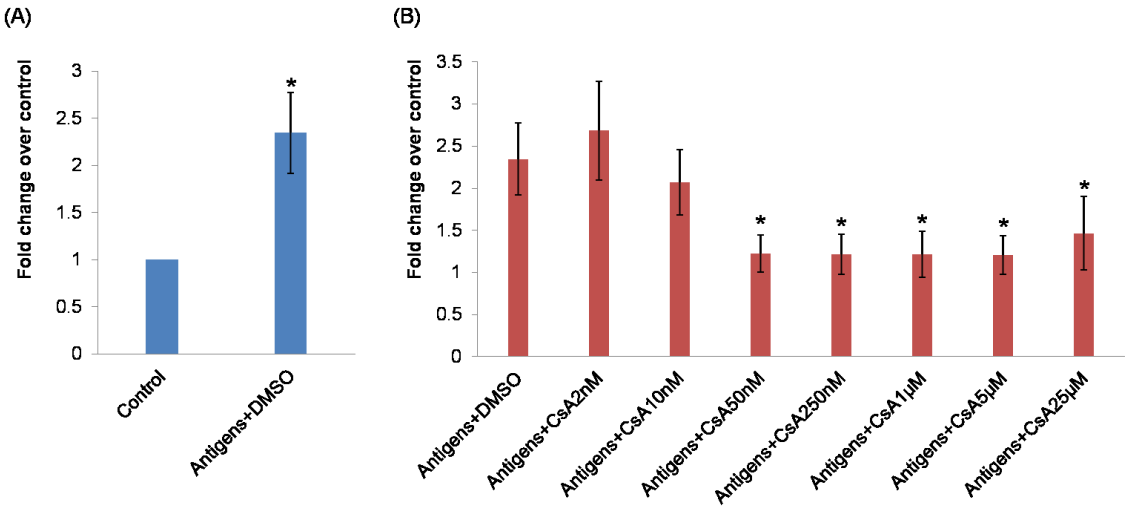

Figure V-4. Effects of cyclosporin A (CsA) on hPBMCs proliferation. hPBMCs proliferation was measured by DNA content using Cyquant assay. Data were expressed as fold-changes over control and presented as mean±SEM. (A) hPBMCs were cultured for 72h in the growth medium supplemented with DMSO, or stimulated with 0.5ng/ml PMA and 500ng/ml ionomycin (referred to as antigens). Antigens stimulated hPBMCs to proliferate up to 2.4-fold (Student t test, *P<0.04, n=3). (B) Antigens were coincubated with DMSO or CsA at concentrations indicated on the x-axis. CsA was able to suppress hPBMCs proliferation capacities at expected concentrations as low as 50nM. Specifically, 50nM CsA reduced the proliferation capacity of stimulated hPBMCs to 1.22-fold; 250nM CsA reduced that to 1.22-fold; 1μM reduced that to 1.22-fold; 5μM reduced that to 1.21-fold and 25μM reduced that to 1.47-fold (one-way ANOVA, followed by Tukey post hoc test, *P <0.05, n=3).

Chapter VI

Inhibition of MCT1 by small molecules: Metabolic blockage of MCT1 on tumor cells proliferation in selected cancer cell lines

Introduction:

Cancer cells rely on aerobic glycolysis, a reprogrammed metabolic phenotype adopted by fast dividing cells, to support their rapid proliferation rate and anabolic demands, a phenomenon known as “Warburg effect” (311). Although glucose consumed in this way rapidly generates ATP in a relatively inefficient manner, glycolytic intermediates along the pathway can be enriched and diverted into various precursors as “building blocks” for synthesizing big biomolecules that are necessary for cell dividing or growth, such as lipids, nucleic acids and proteins (369). As a consequence of this metabolic switch, glucose is preferentially catabolized to lactate, rather than being fully oxidized in mitochondria. In addition, glutamine in cancer cells can be first converted to glutamate, then α-ketoglutarate and thus serves as an important carbon source to sustain mitochondrial TCA cycle as well as to maintain redox homeostasis (370). Malate generated from this α-ketoglutarate can exit the TCA cycle and be converted to pyruvate, which then can be converted to lactate by lactate dehydrogenase A (LDHA). Overall, lactate is excessively produced in cancer cells due to altered metabolism. The maintenance of a normal lactate homeostasis that is critical for an intracellular environment with physiological pH, requires its prompt transport together with a proton out of cells via MCTs (371).

Conversely, the influx of lactate through MCTs has also been strongly implicated in tumorigenesis and cancer progression. Imported lactate can be used as an energy source for oxidation, promoting tumor inflammation, stimulating tumor angiogenesis as well as functioning as a signaling molecule that regulates multiple signaling pathways (74, 75, 87, 185). Three lactate shuttles have been proposed in cancerous condition. The first reverse Warburg effect model suggests that cancer cells secret hydrogen peroxide to create a pseudo-hypoxic environment to neighboring stromal cells, which are then adapted for aerobic glycolysis and export lactate back to cancer cells as oxidative fuel. The second metabolic symbiosis model indicates that cancer cells in hypoxic core of a tumor consume glucose through glycolysis to generate lactate, which is then excreted out into peripheral cancer cells with an oxidative metabolism. The third vascular-endothelial model implies that lactate generated from tumor cells through

glycolysis is delivered into endothelial cells, where it functions as a signaling molecule after being converted to pyruvate. The underlying mechanism is believed to be via the inhibitory effect of pyruvate on prolylhydroxylases (PHDs), the negative regulator of HIF-1α pathway. MCT1 and 4 actively participate in the above mentioned models by facilitating lactate influx and efflux, respectively. As a result, they possess great therapeutic potentials as the targeting sites for cancer treatment (371).

Previous research has investigated the effect of blocking MCTs and their ancillary chaperones on tumor cells, through both genetic knockdown and development of small-molecule inhibitors. Specifically, application of α-CHC in glioblastoma (GLB) cells impaired their proliferation, migration and survival (372, 373). Furthermore, α-CHC inhibited lactic acid extrusion from GLB cells implanted into immunodeficient rats and reduced their invasion (374). In a mouse model of lung carcinoma and xenotransplanted human colorectal adenocarcinoma cells, administration of α-CHC retarded tumor growth, due to a forced metabolic switch from lactate-fueled respiration to glycolysis in oxygenated tumor cells (185). More strikingly, one of the highly potent MCT1/MCT2 inhibitors (AZD3965) originally developed by Astra Zeneca is now under Phase I clinical trials for advanced solid tumors, prostate cancer, gastric cancer and diffuse-Large B cell lymphoma (375). Our novel MD inhibitors were analogs originally derived from α-CHC but exhibited substantially stronger potency in blocking L-lactate transport. Besides, based on T lymphocytes proliferation assay, our MD1 compound seems to work differently from the inhibitors developed by Astra Zeneca. As a consequence, we decided to study MD1's role in suppressing proliferation of multiple cancer cell lines under both normoxic and hypoxic culturing conditions.

Materials and Methods:

Normoxic and hypoxic cell culture.[4] SW480 cells were cultured in DMEM (Invitrogen #12491-015), supplemented with 10% FBS and 2mM L-Glutamine. MDA231 and GL261 cells were cultured in DMEM supplemented with 10% FBS. H4IIE cells were cultured in MEM-α, supplemented with 10% FBS. For normoxic culturing condition, cells were kept in a humidified incubator at 37°C with 5% CO_2, whereas for hypoxic culturing, a humidified modular incubator chamber (Billups-rothenberg) was sealed with hypoxic air (Praxair; 1% oxygen, 5% CO2 and 94% nitrogen) and put inside a 37°C environment.

Proliferation assay. $1X10^4$ cells were seeded into each well of 96-well plates (Corning; #3595) and cultured under normoxic condition first. At least 18 hours later, cells were treated with either DMSO control or various concentrations of MD1 (2nM, 10nM, 50nM, 250nM, 1μM, 5μM and 25μM) for 48 hours, at either normoxic or hypoxic culturing condition. Then the cells were derived of old medium and frozen in -80°C for at least 24 hours up to a week. Cyquant proliferation assay was conducted according to the manufacturer's instruction (Invitrogen; #7026). Basically, the whole 96-well plates were thawed at room temperature and incubated with 200μl per well of the provided 1X lysis buffer supplemented with 1X green fluorescent GR dye that binds nucleic acids. The samples fluorescence then was measured directly at a Synergy 2 multi-mode microplate reader (Biotek) with filters for ~480nm excitation and ~520nm emission.

Results:

To test our novel MCT1 inhibitor (MD1)'s ability to affect tumor cells proliferation capacity, we treated SW480 human colorectal cancer cells, MDA231 human breast cancer cells, GL261 mouse glioma cells and H4IIE rat hepatoma cells with either DMSO control or MD1 at various concentrations (1μM, 5μM or 25μM) and put them in either normoxia or hypoxic culturing conditions to proliferate for 48 hours. Both bright light microscopy

[4] We deeply thank Dr. R. Cormier, Dr. T. Rose-Hellekant, Dr. A. Johnson and Dr. K. Wallace for providing SW480, MDA231, GL261 and H4IIE cell lines, respectively.

imaging and cyquant assay were then applied to evaluate those cells proliferation capacities. Our results indicated that MD1 inhibited SW480 cells proliferation only at 25μM concentration under hypoxic conditions (Figure VI-2 A and D), although an obvious reduction of cell numbers was also observed in normoxic groups (Figure VI-1 A and D), as revealed by microscopy. These results were corroborated by Cyquant proliferation assay, where compared with DMSO control, 25μM MD1 inhibited SW480 cells proliferation under hypoxic condition (Figure VI-3, *P<0.05). Interestingly, although no significant inhibition by MD1 was observed at lower concentrations under hypoxic culturing condition, hypoxia generally tends to sensitize SW480 cells to MCT1 inhibition (Figure VI-3, $F_{(1,24)}$=3.1, P=0.08).

H4IIE cells proliferation was not inhibited by MD1 at any of the concentrations used here under normoxic condition (Figure VI-4 A-D), whereas in hypoxic culturing, they were effectively inhibited at both 5μM and 25μM concentrations (Figure VI-5 A-D; Figure VI-6; *P<0.05). Strikingly, hypoxia significantly sensitized H4IIE cells to MCT1 inhibition (Figure VI-6, $F_{(1,24)}$=16, φP=0.0005). However, no significant inhibition by MD1 was observed in MDA231 or GL261 cells under either culturing condition (Figure VI-7 and 8). Unexpectedly, 1μM MD1 was found to stimulate tumor cells proliferation in both SW480 (Figure VI-3, *P<0.05) and H4IIE cells (Figure VI-6, *P<0.05) under normoxic condition.

Discussion:

In this study, we investigated the inhibitory effect of MD1, a more potent analog of α-CHC, on the proliferation capacity of different tumor cell lines under either normoxic or hypoxic culturing condition, presumably through disrupting MCTs function. Our results showed that MD1 suppressed the proliferation capacity of SW480 colorectal cancer cells at 25μM under hypoxic condition, but not in normoxic condition. Similarly, it also inhibited H4IIE hepatoma cells at both 5μM and 25μM only under hypoxic condition. These findings are consistent with: (1) lactate homeostasis in tumor cells via its transport by MCTs plays a critical role in maintaining their reprogrammed metabolic phenotype that is required for fast proliferation (371); (2) hypoxia represents or emulates the *in vivo* tumor

environment and sensitizes tumor cells to therapeutic intervention aimed at targeting hypoxic metabolism. The latter is supported by the metabolic symbiosis model, where a tumor is composed of a hypoxic core and normoxic periphery. Hypoxic cells catabolize glucose molecules through glycolysis and export lactate for oxidation by peripheral cells (185). In fact, we found that compared with normoxic condition, hypoxia caused H4IIE cells and SW480 cells to be or tend to be sensitive to the same MD1 administrations.

α-CHC has been tested as a therapeutic drug to arrest the proliferation, migration and invastion of glioblastoma cells in culture (372). Besides, after α-CHC treatment and subsequent exposure to low-dose irradiation, U87-MG gliomas became more susceptible to apoptosis (373). Temozolomide (TMZ) is widely used in clinic as an anti-glioblastoma drug. A synergic interaction was observed between α-CHC and TMZ, where the former potentiates the latter, decreasing its IC_{50} value (372). Because of the low potency of α-CHC on inhibiting lactate transport, a relatively high working concentration range was used in the above studies, such as 5mM-25mM. Our MD1 compound has a substantially stronger potency and was shown to inhibit tumor cells proliferation at concentrations as low as 25μM in the current study. Besides, according to our earlier findings from hPBMCs activation, MD1 at 25μM is not enough to inhibit T cells mediated immune response, which needs at least 50μM. Taken together, our novel MD1 compound possesses great therapeutic potentials for treating aggressive tumors, while in the meantime, does not compromise immune system.

Surprisingly, MDA231 breast cancer cells and GL261 mouse glioblastoma cells didn't change their proliferation rates after MD1 treatment up to 25μM under normoxic or hypoxic culturing condition. This may be due to their low expression levels of MCT1 that is supposed to be the target of MD1. In fact, MDA231 cells have been shown to express predominantly MCT4 over MCT1 (376, 377), while MCTs expression profile in GL261 cells is largely unknown. However, the affinity of MCT4 to α-CHC is known to be very low with IC_{50} being 350μM-1mM (154, 160), indicating that cells carrying abundant MCT4 may not be so sensitive to either α-CHC or its analogs. Although previous research has shown that glioblastoma cell lines could be inhibited by α-CHC to block their proliferation and invasion, they did not respond uniformly at all. For example, U251

cells were most sensitive to α-CHC with IC_{50} being 5.1mM, while another glioblastoma cell line SW1088 was the least sensitive cell line with an IC_{50} value of 10.8mM. The above mentioned difference is likely due to different levels of cellular surface MCT1 expression (372). Similar difference was also observed in breast cancer cell lines. For instance, the metastatic MDA231 cells express limited amount of MCT1, while MCF-7 breast cancer cells express abundant MCT1 (376). As a consequence, GL261 cell line may be among the glioblastoma cell lines that are least sensitive to MCT1 intervention. Our observation that H4IIE hepatoma cells responded most sensitively to MD1 intervention under hypoxic condition correlates well with the previous finding that these cells contain significant amount of MCT1, as demonstrated in MCT:CD147 association study (50). Another explanation could be that MCT2 is much more sensitive to α-CHC inhibition than other MCTs, and MCT2 is readily expressed in liver cells (151, 378, 379).

Another unexpected finding is that under normoxic condition, lower concentrations of MD1 treatment at 1μM caused increased proliferation in both SW480 and H4IIE cells. This may be explained by uncoupled glycolysis and mitochondrial oxidation through MD1 blocking pyruvate's entry into mitochondria TCA cycle via mitochondrial pyruvate carriers (MPCs), which were originally demonstrated to have much higher affinity to α-CHC than lactate (367). As a result, intracellular pyruvate generated from glycolysis is diverted to lactate, resembling aerobic glycolysis to support tumor cell growth and proliferation, like the role of pyruvate kinase 2 (380, 381). Further research on dissecting more possible targets of MD1 and its action sites in the cells would shed lights on and direct future studies to clarifying all the research questions mentioned above.

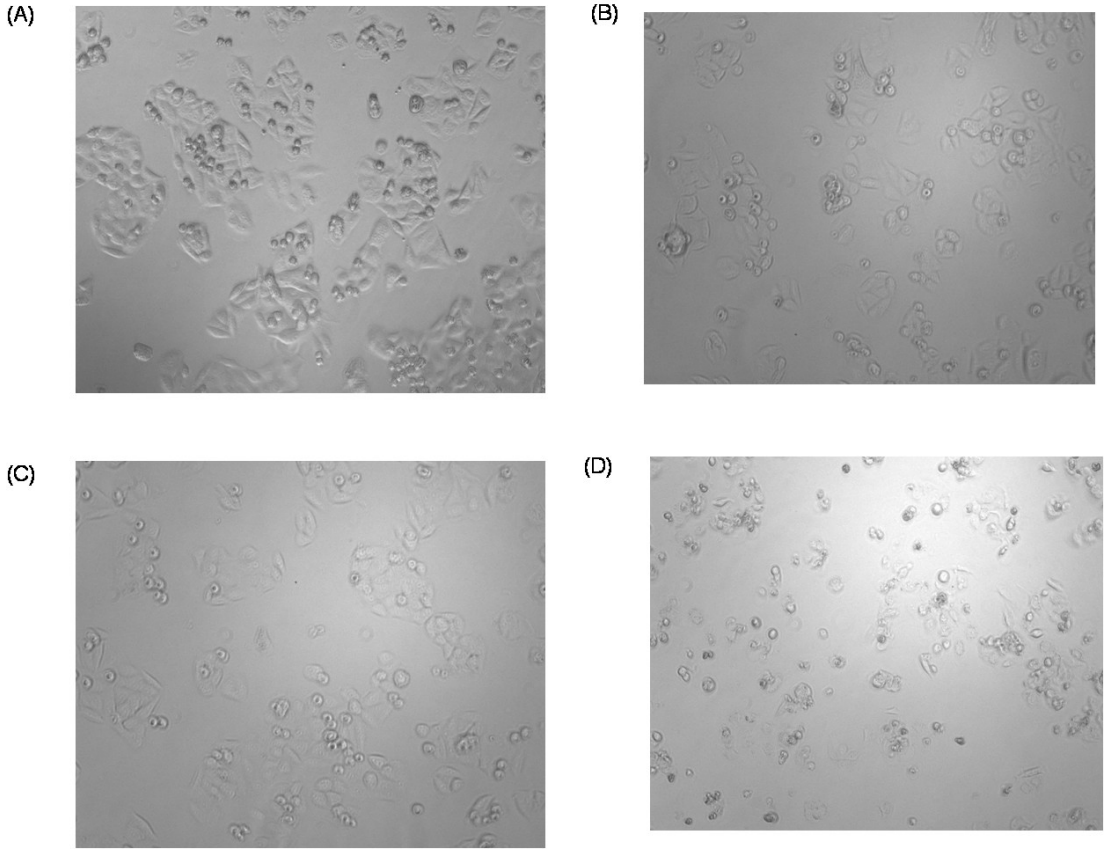

Figure VI-1: Microscopic images of SW480 cells with or without MD1 under normoxic culturing condition. $1x10^4$ cells per well were cultured in 96-well plate for 48h in the growth medium with DMSO (A), or in the presence of MD1 at concentrations of 1μM (B), 5μM (C), or 25μM (D). Our observations indicated that, compared with control (A), the proliferation capacity of SW480 cells was not suppressed significantly by increasing concentrations of MD1.

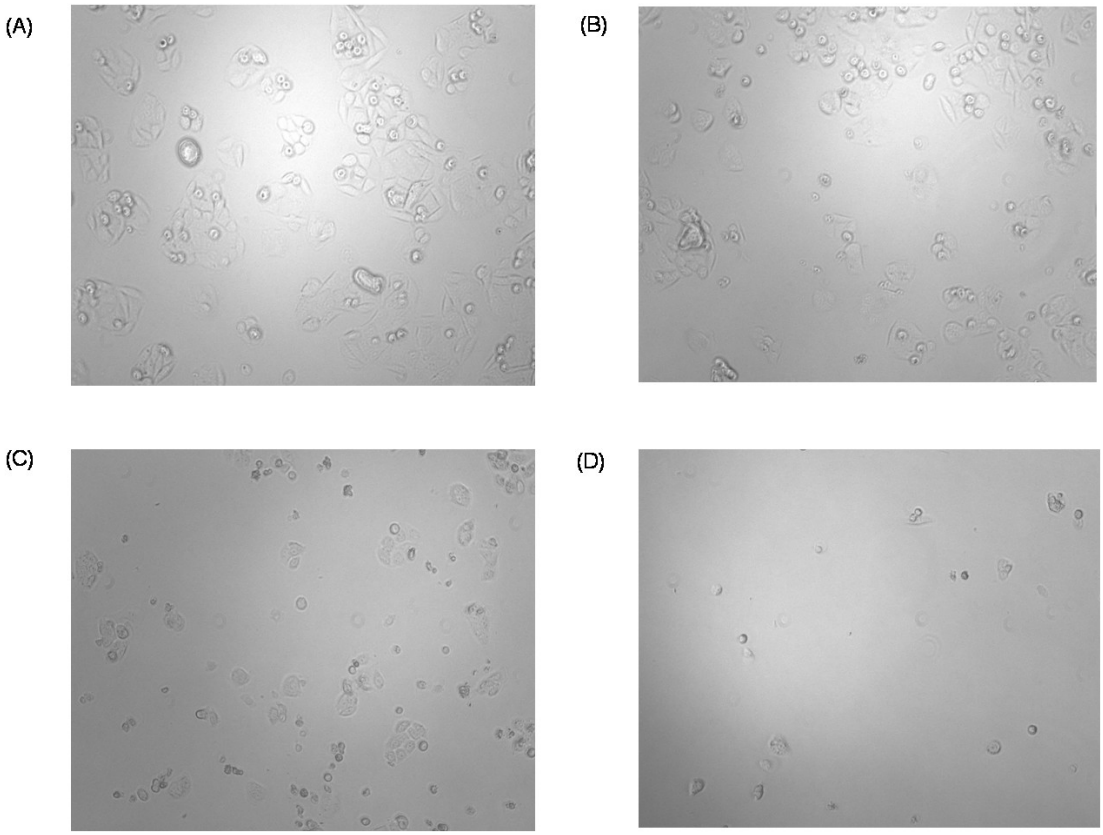

Figure VI-2: Microscopic images of SW480 cells with or without MD1 under hypoxic culturing condition. $1x10^4$ cells per well were cultured in 96-well plate for 48h in the growth medium with DMSO (A), or in the presence of MD1 at concentrations of 1μM (B), 5μM (C), or 25μM (D). Our observations indicated that, compared with control (A), the proliferation capacity of SW480 was suppressed by high concentrations of MD1.

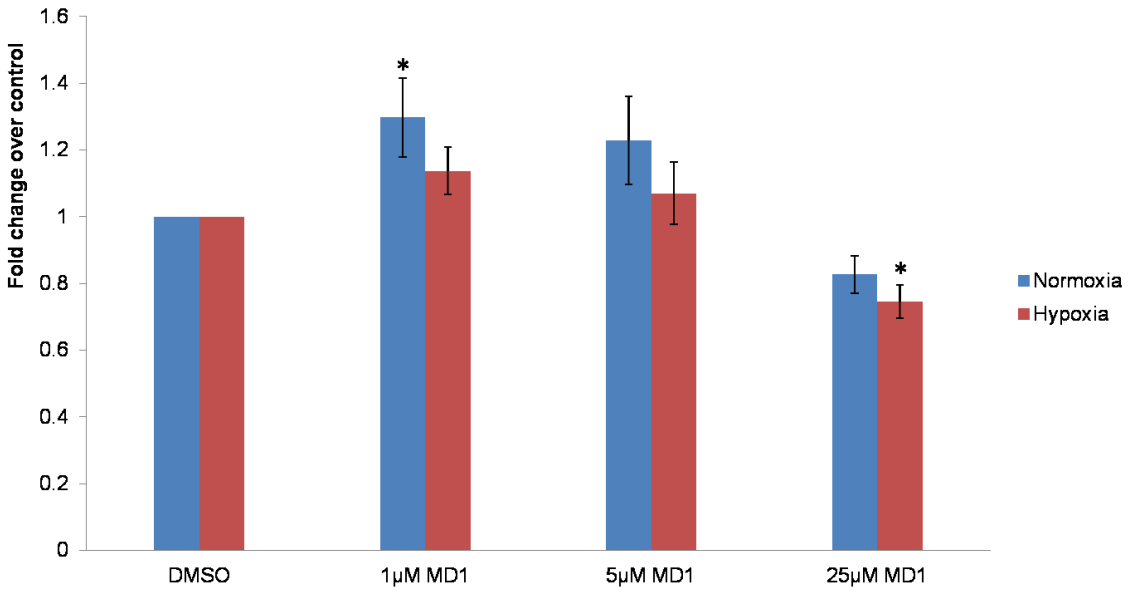

Figure VI-3: Effects of MD1 on SW480 cells proliferation capacity. $1X10^4$ cells were seeded into each well of 96-well plate and cultured for 48h in the growth medium with DMSO, or in the presence of MD1 at concentrations of 1μM, 5μM, or 25μM, as shown on the x-axis. Results were presented as mean±SEM. Compared with baseline level, 25μM MD1 under hypoxic culturing condition (in darkred) reduced the proliferation of SW480 cells by 25% (Two-way ANOVA, followed by Fisher's LSD post hoc test, *P<0.05). Compared with normoxic condition, hypoxia tend to sensitize SW480 cells response to MCT1 inhibition, thus to decrease their proliferation capacity (Two-way ANOVA, $F_{(1,24)}$=3.1, P=0.08). Under normoxic condition (in blue), no reduction of cell numbers was observed by any of the MD1 treatments. In contrast, 1μM MD1 was found to increase SW480 cells proliferation rate by 30% (Two-way ANOVA, followed by Fisher's LSD post hoc test, *P<0.05).

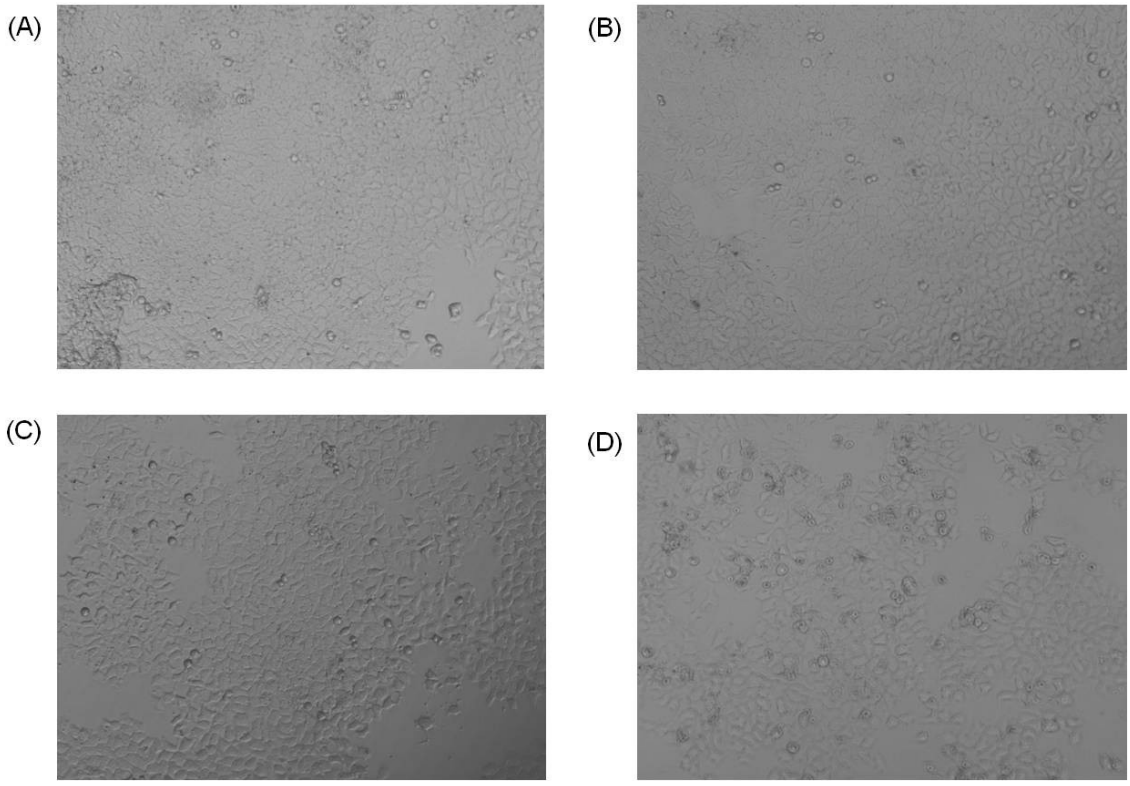

Figure VI-4: Microscopic images of H4IIE cells with or without MD1 under normoxic culturing condition. $1x10^4$ cells per well were cultured in 96-well plate for 48h in the growth medium with DMSO (A), or in the presence of MD1 at concentrations of 1μM (B), 5μM (C), or 25μM (D). Our observations indicated that, compared with control (A), the proliferation capacity of H4IIE, under normoxic condition, was not suppressed by MD1.

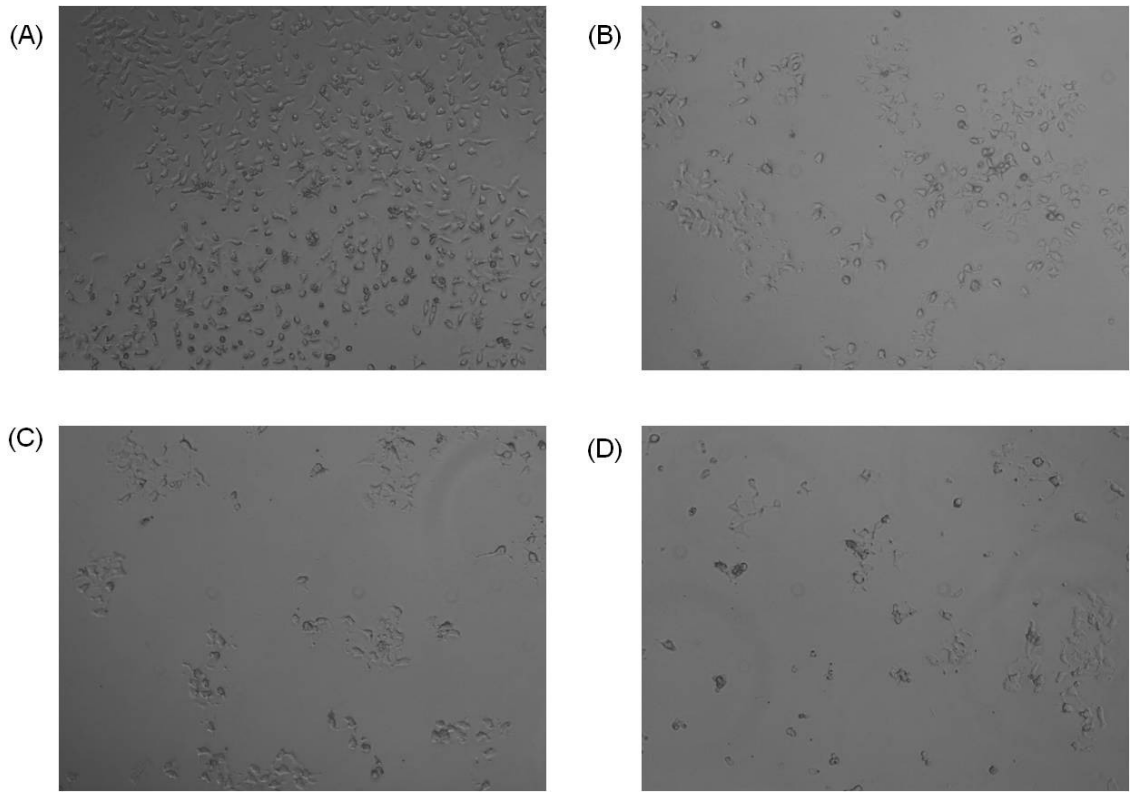

Figure VI-5: Microscopic images of H4IIE cells with or without MD1 under hypoxic culturing condition. $1x10^4$ cells per well were cultured in 96-well plate for 48h in the growth medium with DMSO (A), or in the presence of MD1 at concentrations of 1μM (B), 5μM (C), or 25μM (D). Our observations indicated that, compared with control (A), the proliferation capacity of H4IIE, under hypoxic condition, was obviously suppressed by increasing concentrations of MD1.

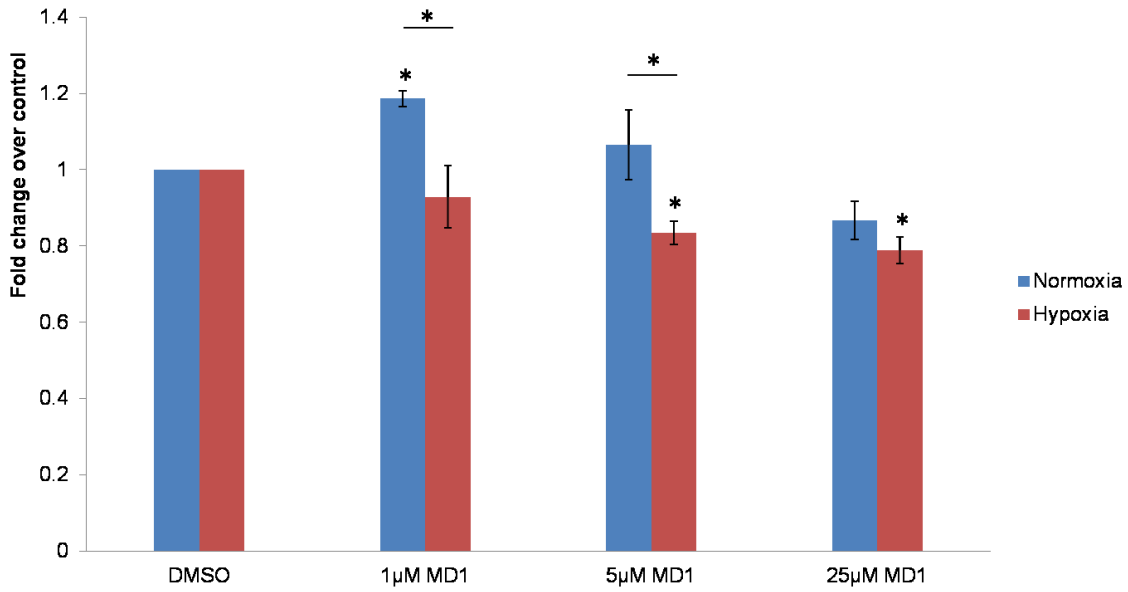

Figure VI-6: Effects of MD1 on H4IIE cells proliferation capacity. $1X10^4$ cells were seeded into each well of 96-well plate and cultured for 48h in the growth medium with DMSO, or in the presence of MD1 at concentrations of 1μM, 5μM, or 25μM, as shown on the x-axis. Results were presented as mean±SEM. Compared with baseline level, 5μM and 25μM MD1 under hypoxic culturing condition (in darkred) reduced the proliferation of H4IIE cells by 17% and 21%, respectively (Two-way ANOVA, followed by Fisher's LSD post hoc test, *P<0.05). Compared with normoxic condition, hypoxia sensitized H4IIE cells response to MCT1 inhibition, thus to decrease their proliferation capacity (Two-way ANOVA, $F_{(1,24)}$=16, P=0.0005, followed by Fisher's LSD post hoc test, *P<0.05). Under normoxic condition (in blue), no reduction of cell numbers was observed by any of the MD1 treatments. In contrast, 1μM MD1 was also found to increase H4IIE cells proliferation rate by 19% (Two-way ANOVA, followed by Fisher's LSD post hoc test, *P<0.05).

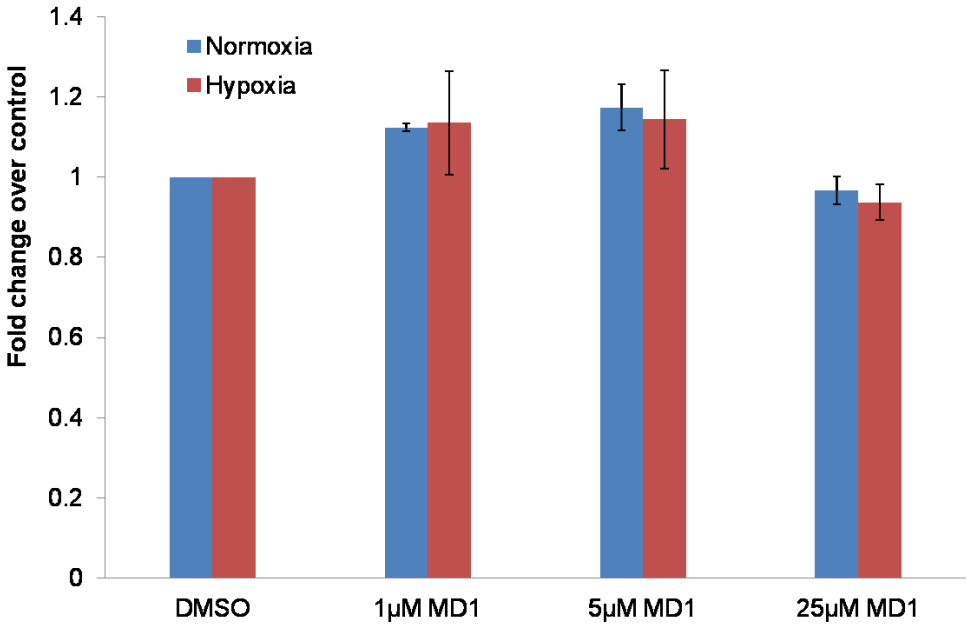

Figure VI-7. Effects of MD1 on MDA231 cells proliferation capacity. 1X10^4 cells were seeded into each well of 96-well plate and cultured for 48h in the growth medium with DMSO, or in the presence of MD1 at concentrations of 1μM, 5μM, or 25μM, as shown on the x-axis. Results were presented as mean±SEM. Two-way ANOVA followed with Fisher's LSD post hoc test showed that compared with DMSO baseline control, MD1 failed to affect MDA231 cells proliferation capacity at the given concentrations under either normoxic or hypoxic condition. In addition, hypoxia had no effect on MDA231 cells proliferation response to MCT1 inhibition (Two-way ANOVA, P=0.8>0.05).

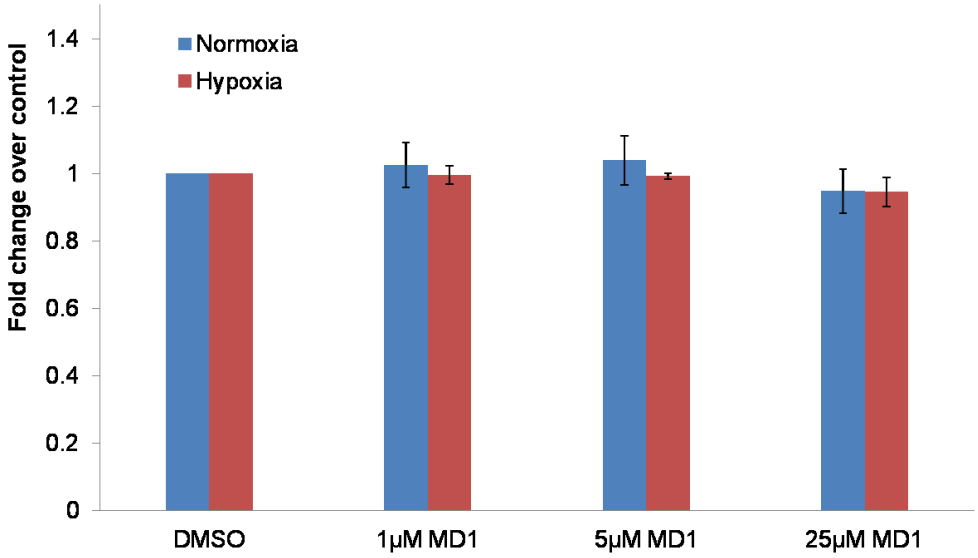

Figure VI-8: Effects of MD1 on GL261 cells proliferation capacity. 1X10^4 cells were seeded into each well of 96-well plate and cultured for 48h in the growth medium with DMSO, or in the presence of MD1 at concentrations of 1μM, 5μM, or 25μM, as shown on the x-axis. Results were presented as mean±SEM. Two-way ANOVA showed that compared with DMSO baseline control, MD1 failed to affect GL231 cells proliferation capacity at the given concentrations under either normoxic or hypoxic condition (P=0.56>0.05). In addition, hypoxia had no effect on GL261 cells proliferation response to MCT1 inhibition (Two-way ANOVA, P=0.6>0.05).

Chapter VII

Discussion

Summary

The overall aim of this thesis was to elucidate multifunctional roles of monocarboxylate transporters (MCTs) and their diverse regulatory mechanisms. Within Chapter I, an updated review to all the known MCTs was presented, including solute carrier families SLC5, SLC16 as well as mitochondrial pyruvate carrier (MPC) family. We summarized their basic biological properties, various physiological functions, pharmaceutical drug transport potentials as well as numerous regulatory mechanisms. This chapter raises stimulation for novel research efforts to better understand and exploit these transporters functions.

After that in Chapters II, III and IV, MCT1, the most ubiquitously expressed member was examined for its regulation by signaling pathways, such as cAMP-PKA, the canonical Wnt/β-catenin and Notch in immortalized rat brain endothelial cells. Specifically, we found that PKA activity led to a rapidly decreased phosphorylation and subsequent internalization of cellular surface MCT1 into early endosomes. This finding is consistent with and explanatory to our earlier observation that PKA caused a reduction of V_{max} in MCT1-mediated lactate transporting kinetics in the same cell line. Additionally, as a potent modulator of blood-brain barrier development, Wnt/β-catenin signaling was hypothesized to regulate brain endothelial MCT1 expression. No changes in *Mct1*'s mRNA level were observed in this study. Instead, our findings indicated that this pathway increased MCT1's protein level by decreasing its entry into endosomal-lysosomal degradation system, thus retaining this transporter more on the cellular surface membrane. Ubiquitination may play an essential role during this process, because deubiquitinases (DUBs) inhibitors were also found able to positively modulate MCT1's protein level. Accordingly, a polyubiquitin chain coding gene *Ubb* was identified by PCR analysis in RBE4 cells. To further our understanding of MCT1's regulation by Wnt/β-catenin signaling, and given the well-known fact that a crosstalk has been demonstrated between the canonical Wnt/β-catenin and Notch pathways, we studied the regulatory effects of Notch on brain endothelial MCT1 expression. Our results showed that inhibition of Notch activity by a γ-secretase inhibitor DAPT enhanced MCT1's protein expression. Interestingly, we also found that the previously observed regulatory

effect of Wnt/β-catenin on MCT1 requires an intact Notch activity, since MCT1's upregulation by Wnt/β-catenin activation was negated in the presence of DAPT. This observed interaction was supported by our additional finding that activation of Wnt/β-catenin modulated genes expression of Notch pathway in brain endothelium.

In Chapter V and VI, we studied the role of MD1, an analog with substantially greater potency derived from the classic MCTs inhibitor α-CHC, in suppressing T cells mediated immune reaction and tumor cells proliferation, respectively. The biochemical basis underlying acquired immune response is that aerobic glycolysis and subsequent release of lactate through MCT1 is essential for T cells activation. Although MD1 could inhibit lactate uptake with an EC_{50} value being 6nM, it inhibited human peripheral blood mononuclear cells (hPBMCs) proliferation at concentrations no less than 50μM. The presence of a hypoxic core in solid tumors as well as the proposal of a "symbiosis metabolic model" where hypoxic tumor cells break glucose molecules via glycolysis and export produced lactate that is then imported into peripheral normoxic tumor cells for oxidation, promoted us to examine MD1's inhibitory role in tumor cells proliferation under either normoxic or hypoxic culturing conditions. Our results indicated that under hypoxic culturing condition, MD1 inhibited SW480 colorectal cancer cells proliferation at no less than 25μM, whereas it started inhibiting H4IIE rat hepatoma cells proliferation at 5μM. Additionally, hypoxic condition sensitized H4IIE cell line to MCT1 inhibition. Interestingly, a transient increase in proliferation was observed in both tumor cell lines when treated with low concentration of MD1 at 1μM. No significant changes were observed for either MDA231 breast cancer cells or GL261 mouse glioblastoma cells under either culturing condition.

Future directions

cAMP-dependent PKA signaling regulation

Our observation of reduced MCT1 phosphorylation upon PKA stimulation is consistent with an activated phosphotase that dephosphorylated MCT1 on cellular surface membrane. It would be important to identify such unknown phosphotase in future

research. Besides, MCT1 has 11 serine and threonine residues that can be phosphorylated, and dephosphorylation at one or more of these sites may mediate the observed internalization of MCT1 from plasma membrane. Future efforts to identify the critical residues through point mutation/amino acids substitution analysis may help dissect the molecular details of MCT1's regulatory mechanism by PKA and broaden our understanding of this important transporter's modification by one of the most widely existing post-translational mechanisms. Besides, CD147 has been known to facilitate MCT1's trafficking onto plasma membrane as an ancillary protein and loss of its function jeopardized MCT1's expression both on cellular surface and in intracellular pools. Whether or not CD147's association capacity with MCT1 is altered upon PKA activation would be another interesting research area to pursue in the future.

Wnt/β-catenin signaling regulation

Enhanced MCT1 expression on plasma membrane by Wnt/β-catenin signaling pathway observed in our current study could be due to multiple mechanisms. First, because ubiquitination of substrate proteins has been well-known as a sorting signal within endosomal-lysosmal system, it would be interesting to examine MCT1's ubiquitination status upon the activation of Wnt signaling. Secondly, thus far we don't know whether the increased cell surface expression of MCT1 is caused by reduced internalization from the plasma membrane, or increased recycling rate from recycling endosomes, or disturbed trafficking into lysosomal compartments. Co-localization immunostaining studies in the future would shed lights on the underlying mechanisms of MCT1's regulation by Wnt pathway.

Notch signaling regulation and its crosstalk with Wnt pathway

In addition, how Notch pathway modulates MCT1's expression would be another important research topic to investigate, e.g. transcriptionally or post-translationally. Furthermore, how Notch and Wnt signaling corporate to upregulate MCT1 would be an inspiring project for future investigation as well. For example, as a critical determinant in Wnt pathway, whether or not β-catenin expression level or its nuclear activity upon Notch inhibition is altered would be a good starting point to gain a better understanding

of the integration between those two signaling pathways. Knowledge obtained from this study would also provide insights to understanding how blood-brain barrier (BBB) is dynamically maintained by different signaling inputs such as Wnt, Notch and Hedgehog, and how modulation of their interaction can help improve the functional output of BBB under pathological conditions.

MCT1 inhibition by a novel MD1 compound

Our novel MD1 analog showed stronger capacity to suppressing tumor cells proliferation, compared with its precedent compound α-CHC. It would be exciting to test whether the combinatorial use of MD1 with other chemotherapeutic drugs (e.g. Temozolomide) improves therapeutic benefits to the patients. One advantage of the MD1 compound may be that it inhibited tumor cells proliferation at concentrations that do not compromise T cells mediated immune response. Because different tumor cells tend to possess different profiles of MCTs expression, plus the fact that distinct MCTs can show different affinities to the same substrate, it would be good to test the specificity of MD1 compound to various MCT isoforms in the future, raising the possibility of combining different MCTs inhibitors as a customized therapeutic approach in accordance with MCT expression profiles in individual types of tumor. Additionally, our finding that MD1 inhibited hPBMCs proliferation at much higher concentration than its EC_{50} value observed in RBE4 cells, suggests that MD1 may inhibit lactate transport through different mechanisms in these two biological systems. As a consequence, it would be informative to figure out the principle of MD1 inhibiting MCT1 transport activity.

Final conclusions

In this report, we provided an updated summary of recent developments and insights on MCTs as well as their implications in physiological functions & diseases. In addition, we unraveled the mechanisms by which brain endothelial MCT1 can be regulated by diverse signaling pathways. Our studies are the first to investigate MCT1 intracellular trafficking within brain endothelium, which can be critically relevant for nutrients transport or pharmaceutical administration into CNS. A crosstalk between Wnt and Notch

signaling was also proposed, and provides an important piece of information for further studying signaling integration in brain endothelium. Furthermore, our promising findings of the novel MCT1 inhibitor in immune response and cancer biology through metabolic blockage, opens a new revenue for developing therapeutic intervention for treating many devastating disorders, such as autoimmune diseases, cancers and diabetes. Overall, our current study and, more importantly, continued future research, is necessary to achieve a more complete understanding of MCT1 as an important regulator in cellular metabolism and tissue homeostasis.

Bibliography

1. Wright EM. Glucose transport families SLC5 and SLC50. Mol Aspects Med. 2013;34(2-3):183-96.
2. Halestrap AP. The SLC16 gene family - structure, role and regulation in health and disease. Mol Aspects Med. 2013;34(2-3):337-49.
3. Halestrap AP, Wilson MC. The monocarboxylate transporter family--role and regulation. IUBMB life. 2012;64(2):109-19.
4. Halestrap AP. The monocarboxylate transporter family--Structure and functional characterization. IUBMB life. 2012;64(1):1-9.
5. Halestrap AP. The mitochondrial pyruvate carrier. Kinetics and specificity for substrates and inhibitors. Biochem J. 1975;148(1):85-96.
6. Bricker DK, Taylor EB, Schell JC, Orsak T, Boutron A, Chen YC, et al. A mitochondrial pyruvate carrier required for pyruvate uptake in yeast, Drosophila, and humans. Science. 2012;337(6090):96-100.
7. Herzig S, Raemy E, Montessuit S, Veuthey JL, Zamboni N, Westermann B, et al. Identification and functional expression of the mitochondrial pyruvate carrier. Science. 2012;337(6090):93-6.
8. Divakaruni AS, Wiley SE, Rogers GW, Andreyev AY, Petrosyan S, Loviscach M, et al. Thiazolidinediones are acute, specific inhibitors of the mitochondrial pyruvate carrier. Proceedings of the National Academy of Sciences of the United States of America. 2013;110(14):5422-7.
9. Colca JR, McDonald WG, Cavey GS, Cole SL, Holewa DD, Brightwell-Conrad AS, et al. Identification of a mitochondrial target of thiazolidinedione insulin sensitizers (mTOT)--relationship to newly identified mitochondrial pyruvate carrier proteins. PloS one. 2013;8(5):e61551.
10. Wright EM, Loo DD, Hirayama BA. Biology of human sodium glucose transporters. Physiol Rev. 2011;91(2):733-94.

11. Gopal E, Fei YJ, Sugawara M, Miyauchi S, Zhuang L, Martin P, et al. Expression of slc5a8 in kidney and its role in Na(+)-coupled transport of lactate. The Journal of biological chemistry. 2004;279(43):44522-32.
12. Gopal E, Umapathy NS, Martin PM, Ananth S, Gnana-Prakasam JP, Becker H, et al. Cloning and functional characterization of human SMCT2 (SLC5A12) and expression pattern of the transporter in kidney. Biochimica et biophysica acta. 2007;1768(11):2690-7.
13. Coady MJ, Wallendorff B, Bourgeois F, Charron F, Lapointe JY. Establishing a definitive stoichiometry for the Na+/monocarboxylate cotransporter SMCT1. Biophysical journal. 2007;93(7):2325-31.
14. Gopal E, Miyauchi S, Martin PM, Ananth S, Roon P, Smith SB, et al. Transport of nicotinate and structurally related compounds by human SMCT1 (SLC5A8) and its relevance to drug transport in the mammalian intestinal tract. Pharm Res-Dordr. 2007;24(3):575-84.
15. Frank H, Groger N, Diener M, Becker C, Braun T, Boettger T. Lactaturia and loss of sodium-dependent lactate uptake in the colon of SLC5A8-deficient mice. The Journal of biological chemistry. 2008;283(36):24729-37.
16. Thangaraju M, Ananth S, Martin PM, Roon P, Smith SB, Sterneck E, et al. c/ebpdelta Null mouse as a model for the double knock-out of slc5a8 and slc5a12 in kidney. The Journal of biological chemistry. 2006;281(37):26769-73.
17. Teramae H, Yoshikawa T, Inoue R, Ushida K, Takebe K, Nio-Kobayashi J, et al. The cellular expression of SMCT2 and its comparison with other transporters for monocarboxylates in the mouse digestive tract. Biomedical research. 2010;31(4):239-49.
18. Ohkubo M, Ohta K, Inoue K, Yuasa H. Nicotinate uptake by two kinetically distinct Na/-dependent carrier-mediated transport systems in the rat small intestine. Drug Metab Pharmacokinet. 2012;27(2):255-62.
19. Lukashova V, Szabo EZ, Jinadasa T, Mokhov A, Litchfield DW, Orlowski J. CK2 phosphorylation of an acidic Ser/Thr di-isoleucine motif in the Na+/H+ exchanger NHE5 isoform promotes association with beta-arrestin2 and endocytosis. The Journal of biological chemistry. 2011;286(13):11456-68.

20. Gopal E, Fei YJ, Miyauchi S, Zhuang L, Prasad PD, Ganapathy V. Sodium-coupled and electrogenic transport of B-complex vitamin nicotinic acid by slc5a8, a member of the Na/glucose co-transporter gene family. The Biochemical journal. 2005;388(Pt 1):309-16.

21. Itagaki S, Gopal E, Zhuang L, Fei YJ, Miyauchi S, Prasad PD, et al. Interaction of ibuprofen and other structurally related NSAIDs with the sodium-coupled monocarboxylate transporter SMCT1 (SLC5A8). Pharm Res-Dordr. 2006;23(6):1209-16.

22. Miyauchi S, Gopal E, Babu E, Srinivas SR, Kubo Y, Umapathy NS, et al. Sodium-coupled electrogenic transport of pyroglutamate (5-oxoproline) via SLC5A8, a monocarboxylate transporter. Biochimica et biophysica acta. 2010;1798(6):1164-71.

23. Babu E, Mareeswaran PM, Rajagopal S. Highly sensitive optical biosensor for thrombin based on structure switching aptamer-luminescent silica nanoparticles. J Fluoresc. 2013;23(1):137-46.

24. Li H, Myeroff L, Smiraglia D, Romero MF, Pretlow TP, Kasturi L, et al. SLC5A8, a sodium transporter, is a tumor suppressor gene silenced by methylation in human colon aberrant crypt foci and cancers. Proceedings of the National Academy of Sciences of the United States of America. 2003;100(14):8412-7.

25. Gupta N, Martin PM, Prasad PD, Ganapathy V. SLC5A8 (SMCT1)-mediated transport of butyrate forms the basis for the tumor suppressive function of the transporter. Life Sci. 2006;78(21):2419-25.

26. Davie JR. Inhibition of histone deacetylase activity by butyrate. J Nutr. 2003;133(7 Suppl):2485S-93S.

27. Insinga A, Monestiroli S, Ronzoni S, Gelmetti V, Marchesi F, Viale A, et al. Inhibitors of histone deacetylases induce tumor-selective apoptosis through activation of the death receptor pathway. Nature medicine. 2005;11(1):71-6.

28. Nakata S, Yoshida T, Horinaka M, Shiraishi T, Wakada M, Sakai T. Histone deacetylase inhibitors upregulate death receptor 5/TRAIL-R2 and sensitize apoptosis induced by TRAIL/APO2-L in human malignant tumor cells. Oncogene. 2004;23(37):6261-71.

29. Thangaraju M, Gopal E, Martin PM, Ananth S, Smith SB, Prasad PD, et al. SLC5A8 triggers tumor cell apoptosis through pyruvate-dependent inhibition of histone deacetylases. Cancer research. 2006;66(24):11560-4.
30. Elangovan S, Pathania R, Ramachandran S, Ananth S, Padia RN, Srinivas SR, et al. Molecular Mechanism of SLC5A8-Inactivation in Breast Cancer. Mol Cell Biol. 2013.
31. Halestrap AP, Meredith D. The SLC16 gene family--from monocarboxylate transporters (MCTs) to aromatic amino acid transporters and beyond. Pflugers Arch – Eur J Physiol. 2004;447(5):619-28.
32. Hugo SE, Cruz-Garcia L, Karanth S, Anderson RM, Stainier DY, Schlegel A. A monocarboxylate transporter required for hepatocyte secretion of ketone bodies during fasting. Genes & development. 2012;26(3):282-93.
33. Vijay N, Morris ME. Role of Monocarboxylate Transporters in Drug Delivery to the Brain. Curr Pharm Des. 2013.
34. Adijanto J, Philp NJ. The SLC16A family of monocarboxylate transporters (MCTs)--physiology and function in cellular metabolism, pH homeostasis, and fluid transport. Curr Top Membr. 2012;70:275-311.
35. Cortes-Campos C, Elizondo R, Llanos P, Uranga RM, Nualart F, Garcia MA. MCT expression and lactate influx/efflux in tanycytes involved in glia-neuron metabolic interaction. PloS one. 2011;6(1):e16411.
36. Cortes-Campos C, Elizondo R, Carril C, Martinez F, Boric K, Nualart F, et al. MCT2 expression and lactate influx in anorexigenic and orexigenic neurons of the arcuate nucleus. PloS one. 2013;8(4):e62532.
37. Suzuki A, Stern SA, Bozdagi O, Huntley GW, Walker RH, Magistretti PJ, et al. Astrocyte-neuron lactate transport is required for long-term memory formation. Cell. 2011;144(5):810-23.
38. Lee Y, Morrison BM, Li Y, Lengacher S, Farah MH, Hoffman PN, et al. Oligodendroglia metabolically support axons and contribute to neurodegeneration. Nature. 2012;487(7408):443-8.

39. Perez de Heredia F, Wood IS, Trayhurn P. Hypoxia stimulates lactate release and modulates monocarboxylate transporter (MCT1, MCT2, and MCT4) expression in human adipocytes. Pflugers Arch. 2010;459(3):509-18.
40. Otonkoski T, Jiao H, Kaminen-Ahola N, Tapia-Paez I, Ullah MS, Parton LE, et al. Physical exercise-induced hypoglycemia caused by failed silencing of monocarboxylate transporter 1 in pancreatic beta cells. American journal of human genetics. 2007;81(3):467-74.
41. Pullen TJ, Sylow L, Sun G, Halestrap AP, Richter EA, Rutter GA. Overexpression of monocarboxylate transporter-1 (SLC16A1) in mouse pancreatic beta-cells leads to relative hyperinsulinism during exercise. Diabetes. 2012;61(7):1719-25.
42. Kido Y, Tamai I, Nakanishi T, Kagami T, Hirosawa I, Sai Y, et al. Evaluation of blood-brain barrier transporters by co-culture of brain capillary endothelial cells with astrocytes. Drug Metab Pharmacokinet. 2002;17(1):34-41.
43. Vellonen KS, Hakli M, Merezhinskaya N, Tervo T, Honkakoski P, Urtti A. Monocarboxylate transport in human corneal epithelium and cell lines. Eur J Pharm Sci. 2010;39(4):241-7.
44. Fischer W, Praetor K, Metzner L, Neubert RH, Brandsch M. Transport of valproate at intestinal epithelial (Caco-2) and brain endothelial (RBE4) cells: mechanism and substrate specificity. European journal of pharmaceutics and biopharmaceutics : official journal of Arbeitsgemeinschaft fur Pharmazeutische Verfahrenstechnik eV. 2008;70(2):486-92.
45. Lam WK, Felmlee MA, Morris ME. Monocarboxylate transporter-mediated transport of gamma-hydroxybutyric acid in human intestinal Caco-2 cells. Drug Metab Dispos. 2010;38(3):441-7.
46. Wang Q, Morris ME. Flavonoids modulate monocarboxylate transporter-1-mediated transport of gamma-hydroxybutyrate in vitro and in vivo. Drug Metab Dispos. 2007;35(2):201-8.
47. Wang X, Wang Q, Morris ME. Pharmacokinetic interaction between the flavonoid luteolin and gamma-hydroxybutyrate in rats: potential involvement of monocarboxylate transporters. The AAPS journal. 2008;10(1):47-55.

48. Venishetty VK, Samala R, Komuravelli R, Kuncha M, Sistla R, Diwan PV. beta-Hydroxybutyric acid grafted solid lipid nanoparticles: a novel strategy to improve drug delivery to brain. Nanomedicine. 2013;9(3):388-97.
49. Birsoy K, Wang T, Possemato R, Yilmaz OH, Koch CE, Chen WW, et al. MCT1-mediated transport of a toxic molecule is an effective strategy for targeting glycolytic tumors. Nature genetics. 2013;45(1):104-8.
50. Kirk P, Wilson MC, Heddle C, Brown MH, Barclay AN, Halestrap AP. CD147 is tightly associated with lactate transporters MCT1 and MCT4 and facilitates their cell surface expression. Embo J. 2000;19(15):3896-904.
51. Ovens MJ, Manoharan C, Wilson MC, Murray CM, Halestrap AP. The inhibition of monocarboxylate transporter 2 (MCT2) by AR-C155858 is modulated by the associated ancillary protein. The Biochemical journal. 2010;431(2):217-25.
52. Wilson MC, Meredith D, Fox JE, Manoharan C, Davies AJ, Halestrap AP. Basigin (CD147) is the target for organomercurial inhibition of monocarboxylate transporter isoforms 1 and 4: the ancillary protein for the insensitive MCT2 is EMBIGIN (gp70). The Journal of biological chemistry. 2005;280(29):27213-21.
53. Mannowetz N, Wandernoth P, Wennemuth G. Basigin interacts with both MCT1 and MCT2 in murine spermatozoa. Journal of cellular physiology. 2012;227(5):2154-62.
54. Saksena S, Theegala S, Bansal N, Gill RK, Tyagi S, Alrefai WA, et al. Mechanisms underlying modulation of monocarboxylate transporter 1 (MCT1) by somatostatin in human intestinal epithelial cells. Am J Physiol-Gastr L. 2009;297(5):G878-G85.
55. Su J, Chen X, Kanekura T. A CD147-targeting siRNA inhibits the proliferation, invasiveness, and VEGF production of human malignant melanoma cells by down-regulating glycolysis. Cancer letters. 2009;273(1):140-7.
56. Nakai M, Chen L, Nowak RA. Tissue distribution of basigin and monocarboxylate transporter 1 in the adult male mouse: a study using the wild-type and basigin gene knockout mice. The anatomical record Part A, Discoveries in molecular, cellular, and evolutionary biology. 2006;288(5):527-35.
57. Slomiany MG, Grass GD, Robertson AD, Yang XY, Maria BL, Beeson C, et al. Hyaluronan, CD44, and emmprin regulate lactate efflux and membrane localization of

monocarboxylate transporters in human breast carcinoma cells. Cancer research. 2009;69(4):1293-301.

58. Finch NA, Linser PJ, Ochrietor JD. Hydrophobic interactions stabilize the basigin-MCT1 complex. Protein J. 2009;28(7-8):362-8.

59. Wilson MC, Meredith D, Halestrap AP. Fluorescence resonance energy transfer studies on the interaction between the lactate transporter MCT1 and CD147 provide information on the topology and stoichiometry of the complex in situ. The Journal of biological chemistry. 2002;277(5):3666-72.

60. Deora AA, Philp N, Hu J, Bok D, Rodriguez-Boulan E. Mechanisms regulating tissue-specific polarity of monocarboxylate transporters and their chaperone CD147 in kidney and retinal epithelia. Proceedings of the National Academy of Sciences of the United States of America. 2005;102(45):16245-50.

61. Manoharan C, Wilson MC, Sessions RB, Halestrap AP. The role of charged residues in the transmembrane helices of monocarboxylate transporter 1 and its ancillary protein basigin in determining plasma membrane expression and catalytic activity. Mol Membr Biol. 2006;23(6):486-98.

62. Castorino JJ, Deborde S, Deora A, Schreiner R, Gallagher-Colombo SM, Rodriguez-Boulan E, et al. Basolateral sorting signals regulating tissue-specific polarity of heteromeric monocarboxylate transporters in epithelia. Traffic. 2011;12(4):483-98.

63. Schneiderhan W, Scheler M, Holzmann KH, Marx M, Gschwend JE, Bucholz M, et al. CD147 silencing inhibits lactate transport and reduces malignant potential of pancreatic cancer cells in in vivo and in vitro models. Gut. 2009;58(10):1391-8.

64. de Oliveira AT, Pinheiro C, Longatto-Filho A, Brito MJ, Martinho O, Matos D, et al. Co-expression of monocarboxylate transporter 1 (MCT1) and its chaperone (CD147) is associated with low survival in patients with gastrointestinal stromal tumors (GISTs). J Bioenerg Biomembr. 2012;44(1):171-8.

65. Hao J, Chen H, Madigan MC, Cozzi PJ, Beretov J, Xiao W, et al. Co-expression of CD147 (EMMPRIN), CD44v3-10, MDR1 and monocarboxylate transporters is associated with prostate cancer drug resistance and progression. British journal of cancer. 2010;103(7):1008-18.

66. Chen H, Wang L, Beretov J, Hao J, Xiao W, Li Y. Co-expression of CD147/EMMPRIN with monocarboxylate transporters and multiple drug resistance proteins is associated with epithelial ovarian cancer progression. Clin Exp Metastasis. 2010;27(8):557-69.

67. Smith JP, Drewes LR. Modulation of monocarboxylic acid transporter-1 kinetic function by the cAMP signaling pathway in rat brain endothelial cells. The Journal of biological chemistry. 2006;281(4):2053-60.

68. Smith JP, Uhernik AL, Li L, Liu Z, Drewes LR. Regulation of Mct1 by cAMP-dependent internalization in rat brain endothelial cells. Brain Res. 2012;1480:1-11.

69. Saksena S, Dwivedi A, Gill RK, Singla A, Alrefai WA, Malakooti J, et al. PKC-dependent stimulation of the human MCT1 promoter involves transcription factor AP2. Am J Physiol Gastrointest Liver Physiol. 2009;296(2):G275-83.

70. Becker HM, Klier M, Deitmer JW. Nonenzymatic augmentation of lactate transport via monocarboxylate transporter isoform 4 by carbonic anhydrase II. J Membr Biol. 2010;234(2):125-35.

71. Stridh MH, Alt MD, Wittmann S, Heidtmann H, Aggarwal M, Riederer B, et al. Lactate flux in astrocytes is enhanced by a non-catalytic action of carbonic anhydrase II. The Journal of physiology. 2012;590(Pt 10):2333-51.

72. Becker HM, Klier M, Schuler C, McKenna R, Deitmer JW. Intramolecular proton shuttle supports not only catalytic but also noncatalytic function of carbonic anhydrase II. Proceedings of the National Academy of Sciences of the United States of America. 2011;108(7):3071-6.

73. Klier M, Schuler C, Halestrap AP, Sly WS, Deitmer JW, Becker HM. Transport activity of the high-affinity monocarboxylate transporter MCT2 is enhanced by extracellular carbonic anhydrase IV but not by intracellular carbonic anhydrase II. The Journal of biological chemistry. 2011;286(31):27781-91.

74. Sonveaux P, Copetti T, De Saedeleer CJ, Vegran F, Verrax J, Kennedy KM, et al. Targeting the lactate transporter MCT1 in endothelial cells inhibits lactate-induced HIF-1 activation and tumor angiogenesis. PloS one. 2012;7(3):e33418.

75. Whitaker-Menezes D, Martinez-Outschoorn UE, Lin Z, Ertel A, Flomenberg N, Witkiewicz AK, et al. Evidence for a stromal-epithelial “lactate shuttle” in human tumors:

MCT4 is a marker of oxidative stress in cancer-associated fibroblasts. Cell Cycle. 2011;10(11):1772-83.

76. Pinheiro C, Albergaria A, Paredes J, Sousa B, Dufloth R, Vieira D, et al. Monocarboxylate transporter 1 is up-regulated in basal-like breast carcinoma. Histopathology. 2010;56(7):860-7.

77. Pinheiro C, Reis RM, Ricardo S, Longatto-Filho A, Schmitt F, Baltazar F. Expression of monocarboxylate transporters 1, 2, and 4 in human tumours and their association with CD147 and CD44. J Biomed Biotechnol. 2010;2010:427694.

78. Fiaschi T, Chiarugi P. Oxidative stress, tumor microenvironment, and metabolic reprogramming: a diabolic liaison. Int J Cell Biol. 2012;2012:762825.

79. Shimoyama Y, Akihara Y, Kirat D, Iwano H, Hirayama K, Kagawa Y, et al. Expression of monocarboxylate transporter 1 in oral and ocular canine melanocytic tumors. Veterinary pathology. 2007;44(4):449-57.

80. Ho J, de Moura MB, Lin Y, Vincent G, Thorne S, Duncan LM, et al. Importance of glycolysis and oxidative phosphorylation in advanced melanoma. Molecular cancer. 2012;11:76.

81. Lee GH, Kim DS, Chung MJ, Chae SW, Kim HR, Chae HJ. Lysyl oxidase-like-1 enhances lung metastasis when lactate accumulation and monocarboxylate transporter expression are involved. Oncol Lett. 2011;2(5):831-8.

82. Treem WR, Ahsan N, Shoup M, Hyams JS. Fecal short-chain fatty acids in children with inflammatory bowel disease. J Pediatr Gastroenterol Nutr. 1994;18(2):159-64.

83. Koukourakis MI, Giatromanolaki A, Harris AL, Sivridis E. Comparison of metabolic pathways between cancer cells and stromal cells in colorectal carcinomas: a metabolic survival role for tumor-associated stroma. Cancer research. 2006;66(2):632-7.

84. Pinheiro C, Longatto-Filho A, Nogueira R, Schmitt F, Baltazar F. Lactate-induced IL-8 pathway in endothelial cells--letter. Cancer research. 2012;72(7):1901-2; author reply 3-4.

85. Ritzhaupt A, Wood IS, Ellis A, Hosie KB, Shirazi-Beechey SP. Identification and characterization of a monocarboxylate transporter (MCT1) in pig and human colon: its

potential to transport L-lactate as well as butyrate. The Journal of physiology. 1998;513 (Pt 3):719-32.

86. Lambert DW, Wood IS, Ellis A, Shirazi-Beechey SP. Molecular changes in the expression of human colonic nutrient transporters during the transition from normality to malignancy. British journal of cancer. 2002;86(8):1262-9.

87. Vegran F, Boidot R, Michiels C, Sonveaux P, Feron O. Lactate influx through the endothelial cell monocarboxylate transporter MCT1 supports an NF-kappaB/IL-8 pathway that drives tumor angiogenesis. Cancer research. 2011;71(7):2550-60.

88. Kobayashi M. Fiber type-specific localization of monocarboxylate transporters MCT1 and MCT4 in rat skeletal muscle. The Kurume medical journal. 2004;51(3-4):253-61.

89. Enoki T, Yoshida Y, Lally J, Hatta H, Bonen A. Testosterone increases lactate transport, monocarboxylate transporter (MCT) 1 and MCT4 in rat skeletal muscle. The Journal of physiology. 2006;577(Pt 1):433-43.

90. Mykkanen AK, Hyyppa S, Poso AR, Roneus N, Essen-Gustavsson B. Immunohistochemical analysis of MCT1 and CD147 in equine skeletal muscle fibres. Research in veterinary science. 2010;89(3):432-7.

91. Revold T, Mykkanen AK, Karlstrom K, Ihler CF, Poso AR, Essen-Gustavsson B. Effects of training on equine muscle fibres and monocarboxylate transporters in young Coldblooded Trotters. Equine Vet J Suppl. 2010(38):289-95.

92. Py G, Eydoux N, Lambert K, Chapot R, Koulmann N, Sanchez H, et al. Role of hypoxia-induced anorexia and right ventricular hypertrophy on lactate transport and MCT expression in rat muscle. Metabolism: clinical and experimental. 2005;54(5):634-44.

93. Kitaura T, Tsunekawa N, Hatta H. Decreased monocarboxylate transporter 1 in rat soleus and EDL muscles exposed to clenbuterol. J Appl Physiol. 2001;91(1):85-90.

94. Pellerin L, Pellegri G, Martin JL, Magistretti PJ. Expression of monocarboxylate transporter mRNAs in mouse brain: support for a distinct role of lactate as an energy substrate for the neonatal vs. adult brain. Proceedings of the National Academy of Sciences of the United States of America. 1998;95(7):3990-5.

95. Leino RL, Gerhart DZ, Drewes LR. Monocarboxylate transporter (MCT1) abundance in brains of suckling and adult rats: a quantitative electron microscopic immunogold study. Brain research Developmental brain research. 1999;113(1-2):47-54.
96. Vannucci SJ, Simpson IA. Developmental switch in brain nutrient transporter expression in the rat. Am J Physiol Endocrinol Metab. 2003;285(5):E1127-34.
97. Ito K, Uchida Y, Ohtsuki S, Aizawa S, Kawakami H, Katsukura Y, et al. Quantitative membrane protein expression at the blood-brain barrier of adult and younger cynomolgus monkeys. J Pharm Sci. 2011;100(9):3939-50.
98. Iwanaga T, Kuchiiwa T, Saito M. Histochemical demonstration of monocarboxylate transporters in mouse brown adipose tissue. Biomedical research. 2009;30(4):217-25.
99. Masuda S, Hayashi T, Egawa T, Taguchi S. Evidence for differential regulation of lactate metabolic properties in aged and unloaded rat skeletal muscle. Exp Gerontol. 2009;44(4):280-8.
100. Kirat D, Inoue H, Iwano H, Yokota H, Taniyama H, Kato S. Monocarboxylate transporter 1 (MCT1) in the liver of pre-ruminant and adult bovines. Vet J. 2007;173(1):124-30.
101. Kitaoka Y, Hoshino D, Mukai K, Hiraga A, Takemasa T, Hatta H. Effect of growth on monocarboxylate transporters and indicators of energy metabolism in the gluteus medius muscle of Thoroughbreds. Am J Vet Res. 2011;72(8):1107-11.
102. Leino RL, Gerhart DZ, Duelli R, Enerson BE, Drewes LR. Diet-induced ketosis increases monocarboxylate transporter (MCT1) levels in rat brain. Neurochem Int. 2001;38(6):519-27.
103. Pifferi F, Tremblay S, Croteau E, Fortier M, Tremblay-Mercier J, Lecomte R, et al. Mild experimental ketosis increases brain uptake of 11C-acetoacetate and 18F-fluorodeoxyglucose: a dual-tracer PET imaging study in rats. Nutr Neurosci. 2011;14(2):51-8.
104. Puchowicz MA, Zechel JL, Valerio J, Emancipator DS, Xu K, Pundik S, et al. Neuroprotection in diet-induced ketotic rat brain after focal ischemia. Journal of cerebral blood flow and metabolism : official journal of the International Society of Cerebral Blood Flow and Metabolism. 2008;28(12):1907-16.

105. Xu K, Lamanna JC, Puchowicz MA. Neuroprotective properties of ketone bodies. Adv Exp Med Biol. 2012;737:97-102.
106. Jouaville LF, Fellmann N, Coudert J, Clottes E. Skeletal muscle expression of LDH and monocarboxylate transporters in growing rats submitted to protein malnutrition. Eur J Nutr. 2006;45(6):355-62.
107. Tavares S, Sousa J, Goncalves P, Araujo JR, Martel F. The effect of folate status on the uptake of physiologically relevant compounds by Caco-2 cells. Eur J Pharmacol. 2010;640(1-3):29-37.
108. Woodward AD, Regmi PR, Ganzle MG, van Kempen TA, Zijlstra RT. Slowly digestible starch influences mRNA abundance of glucose and short-chain fatty acid transporters in the porcine distal intestinal tract. J Anim Sci. 2012;90 Suppl 4:80-2.
109. Wood IS, Stezhka T, Trayhurn P. Modulation of adipokine production, glucose uptake and lactate release in human adipocytes by small changes in oxygen tension. Pflugers Arch. 2011;462(3):469-77.
110. Boidot R, Vegran F, Meulle A, Le Breton A, Dessy C, Sonveaux P, et al. Regulation of monocarboxylate transporter MCT1 expression by p53 mediates inward and outward lactate fluxes in tumors. Cancer research. 2012;72(4):939-48.
111. Moreira TJ, Pierre K, Maekawa F, Repond C, Cebere A, Liljequist S, et al. Enhanced cerebral expression of MCT1 and MCT2 in a rat ischemia model occurs in activated microglial cells. Journal of cerebral blood flow and metabolism : official journal of the International Society of Cerebral Blood Flow and Metabolism. 2009;29(7):1273-83.
112. Enoki T, Yoshida Y, Hatta H, Bonen A. Exercise training alleviates MCT1 and MCT4 reductions in heart and skeletal muscles of STZ-induced diabetic rats. J Appl Physiol. 2003;94(6):2433-8.
113. Juel C, Holten MK, Dela F. Effects of strength training on muscle lactate release and MCT1 and MCT4 content in healthy and type 2 diabetic humans. The Journal of physiology. 2004;556(Pt 1):297-304.
114. Pierre K, Parent A, Jayet PY, Halestrap AP, Scherrer U, Pellerin L. Enhanced expression of three monocarboxylate transporter isoforms in the brain of obese mice. The Journal of physiology. 2007;583(Pt 2):469-86.

115. Canis M, Maurer MH, Kuschinsky W, Duembgen L, Duelli R. Increased densities of monocarboxylate transporter MCT1 after chronic hyperglycemia in rat brain. Brain Res. 2009;1257:32-9.
116. Lauritzen F, de Lanerolle NC, Lee TS, Spencer DD, Kim JH, Bergersen LH, et al. Monocarboxylate transporter 1 is deficient on microvessels in the human epileptogenic hippocampus. Neurobiology of disease. 2011;41(2):577-84.
117. Lauritzen F, Perez EL, Melillo ER, Roh JM, Zaveri HP, Lee TS, et al. Altered expression of brain monocarboxylate transporter 1 in models of temporal lobe epilepsy. Neurobiology of disease. 2012;45(1):165-76.
118. Thibault R, De Coppet P, Daly K, Bourreille A, Cuff M, Bonnet C, et al. Down-regulation of the monocarboxylate transporter 1 is involved in butyrate deficiency during intestinal inflammation. Gastroenterology. 2007;133(6):1916-27.
119. Narumi K, Furugen A, Kobayashi M, Otake S, Itagaki S, Iseki K. Regulation of monocarboxylate transporter 1 in skeletal muscle cells by intracellular signaling pathways. Biological & pharmaceutical bulletin. 2010;33(9):1568-73.
120. Benton CR, Yoshida Y, Lally J, Han XX, Hatta H, Bonen A. PGC-1alpha increases skeletal muscle lactate uptake by increasing the expression of MCT1 but not MCT2 or MCT4. Physiological genomics. 2008;35(1):45-54.
121. Hoshino D, Yoshida Y, Holloway GP, Lally J, Hatta H, Bonen A. Clenbuterol, a beta2-adrenergic agonist, reciprocally alters PGC-1 alpha and RIP140 and reduces fatty acid and pyruvate oxidation in rat skeletal muscle. American journal of physiology Regulatory, integrative and comparative physiology. 2012;302(3):R373-84.
122. Borthakur A, Saksena S, Gill RK, Alrefai WA, Ramaswamy K, Dudeja PK. Regulation of monocarboxylate transporter 1 (MCT1) promoter by butyrate in human intestinal epithelial cells: involvement of NF-kappaB pathway. Journal of cellular biochemistry. 2008;103(5):1452-63.
123. Boidot R, Vegran F, Meulle A, Le Breton A, Dessy C, Sonveaux P, et al. Regulation of monocarboxylate transporter MCT1 expression by p53 mediates inward and outward lactate fluxes in tumors. Cancer Res. 2012;72(4):939-48.

124. Cuff MA, Lambert DW, Shirazi-Beechey SP. Substrate-induced regulation of the human colonic monocarboxylate transporter, MCT1. The Journal of physiology. 2002;539(Pt 2):361-71.
125. Queiros O, Preto A, Pacheco A, Pinheiro C, Azevedo-Silva J, Moreira R, et al. Butyrate activates the monocarboxylate transporter MCT4 expression in breast cancer cells and enhances the antitumor activity of 3-bromopyruvate. J Bioenerg Biomembr. 2012;44(1):141-53.
126. Hashimoto T, Hussien R, Oommen S, Gohil K, Brooks GA. Lactate sensitive transcription factor network in L6 cells: activation of MCT1 and mitochondrial biogenesis. FASEB journal : official publication of the Federation of American Societies for Experimental Biology. 2007;21(10):2602-12.
127. Rattigan YI, Patel BB, Ackerstaff E, Sukenick G, Koutcher JA, Glod JW, et al. Lactate is a mediator of metabolic cooperation between stromal carcinoma associated fibroblasts and glycolytic tumor cells in the tumor microenvironment. Experimental cell research. 2012;318(4):326-35.
128. Pertega-Gomes N, Vizcaino JR, Miranda-Goncalves V, Pinheiro C, Silva J, Pereira H, et al. Monocarboxylate transporter 4 (MCT4) and CD147 overexpression is associated with poor prognosis in prostate cancer. BMC Cancer. 2011;11:312.
129. Mac M, Nalecz KA. Expression of monocarboxylic acid transporters (MCT) in brain cells. Implication for branched chain alpha-ketoacids transport in neurons. Neurochem Int. 2003;43(4-5):305-9.
130. Rafiki A, Boulland JL, Halestrap AP, Ottersen OP, Bergersen L. Highly differential expression of the monocarboxylate transporters MCT2 and MCT4 in the developing rat brain. Neuroscience. 2003;122(3):677-88.
131. Matsuyama S, Ohkura S, Iwata K, Uenoyama Y, Tsukamura H, Maeda K, et al. Food deprivation induces monocarboxylate transporter 2 expression in the brainstem of female rat. J Reprod Dev. 2009;55(3):256-61.
132. Lizarraga-Mollinedo E, Fernandez-Millan E, Martin Jde T, Martinez-Honduvilla C, Escriva F, Alvarez C. Early undernutrition induces glucagon resistance and insulin hypersensitivity in the liver of suckling rats. Am J Physiol Endocrinol Metab. 2012;302(9):E1070-7.

133. Kirat D. Effect of pectin feeding on monocarboxylate transporters in rat adrenal gland. J Comp Physiol B. 2010;180(1):57-65.
134. Chenal J, Pierre K, Pellerin L. Insulin and IGF-1 enhance the expression of the neuronal monocarboxylate transporter MCT2 by translational activation via stimulation of the phosphoinositide 3-kinase-Akt-mammalian target of rapamycin pathway. Eur J Neurosci. 2008;27(1):53-65.
135. Robinet C, Pellerin L. Brain-derived neurotrophic factor enhances the expression of the monocarboxylate transporter 2 through translational activation in mouse cultured cortical neurons. Journal of cerebral blood flow and metabolism : official journal of the International Society of Cerebral Blood Flow and Metabolism. 2010;30(2):286-98.
136. Ding F, Yao J, Zhao L, Mao Z, Chen S, Brinton RD. Ovariectomy induces a shift in fuel availability and metabolism in the hippocampus of the female transgenic model of familial Alzheimer's. PloS one. 2013;8(3):e59825.
137. Cherian AK, Briski KP. Effects of adrenalectomy on neuronal substrate fuel transporter and energy transducer gene expression in hypothalamic and hindbrain metabolic monitoring sites. Neuroendocrinology. 2010;91(1):56-63.
138. Zhang F, Vannucci SJ, Philp NJ, Simpson IA. Monocarboxylate transporter expression in the spontaneous hypertensive rat: effect of stroke. Journal of neuroscience research. 2005;79(1-2):139-45.
139. Leroy C, Pierre K, Simpson IA, Pellerin L, Vannucci SJ, Nehlig A. Temporal changes in mRNA expression of the brain nutrient transporters in the lithium-pilocarpine model of epilepsy in the immature and adult rat. Neurobiology of disease. 2011;43(3):588-97.
140. Keshari KR, Sriram R, Koelsch BL, Van Criekinge M, Wilson DM, Kurhanewicz J, et al. Hyperpolarized 13C-pyruvate magnetic resonance reveals rapid lactate export in metastatic renal cell carcinomas. Cancer research. 2013;73(2):529-38.
141. Pilegaard H, Terzis G, Halestrap A, Juel C. Distribution of the lactate/H+ transporter isoforms MCT1 and MCT4 in human skeletal muscle. Am J Physiol. 1999;276(5 Pt 1):E843-8.

142. Wang Y, Tonouchi M, Miskovic D, Hatta H, Bonen A. T3 increases lactate transport and the expression of MCT4, but not MCT1, in rat skeletal muscle. Am J Physiol Endocrinol Metab. 2003;285(3):E622-8.
143. Moeller LC, Dumitrescu AM, Refetoff S. Cytosolic action of thyroid hormone leads to induction of hypoxia-inducible factor-1alpha and glycolytic genes. Mol Endocrinol. 2005;19(12):2955-63.
144. Oliveira PF, Alves MG, Rato L, Laurentino S, Silva J, Sa R, et al. Effect of insulin deprivation on metabolism and metabolism-associated gene transcript levels of in vitro cultured human Sertoli cells. Biochimica et biophysica acta. 2012;1820(2):84-9.
145. Coles L, Litt J, Hatta H, Bonen A. Exercise rapidly increases expression of the monocarboxylate transporters MCT1 and MCT4 in rat muscle. The Journal of physiology. 2004;561(Pt 1):253-61.
146. Neal CM, Hunter AM, Brennan L, O'Sullivan A, Hamilton DL, De Vito G, et al. Six weeks of a polarized training-intensity distribution leads to greater physiological and performance adaptations than a threshold model in trained cyclists. J Appl Physiol. 2013;114(4):461-71.
147. Green HJ, Bombardier E, Duhamel TA, Stewart RD, Tupling AR, Ouyang J. Metabolic, enzymatic, and transporter responses in human muscle during three consecutive days of exercise and recovery. American journal of physiology Regulatory, integrative and comparative physiology. 2008;295(4):R1238-50.
148. Bickham DC, Bentley DJ, Le Rossignol PF, Cameron-Smith D. The effects of short-term sprint training on MCT expression in moderately endurance-trained runners. Eur J Appl Physiol. 2006;96(6):636-43.
149. Bishop D, Edge J, Thomas C, Mercier J. Effects of high-intensity training on muscle lactate transporters and postexercise recovery of muscle lactate and hydrogen ions in women. American journal of physiology Regulatory, integrative and comparative physiology. 2008;295(6):R1991-8.
150. Green HJ, Burnett ME, D'Arsigny CL, O'Donnell DE, Ouyang J, Webb KA. Altered metabolic and transporter characteristics of vastus lateralis in chronic obstructive pulmonary disease. J Appl Physiol. 2008;105(3):879-86.

151. Jackson VN, Halestrap AP. The kinetics, substrate, and inhibitor specificity of the monocarboxylate (lactate) transporter of rat liver cells determined using the fluorescent intracellular pH indicator, 2',7'-bis(carboxyethyl)-5(6)-carboxyfluorescein. Journal of Biological Chemistry. 1996;271(2):861-8.

152. Broer S, Schneider HP, Broer A, Rahman B, Hamprecht B, Deitmer JW. Characterization of the monocarboxylate transporter 1 expressed in Xenopus laevis oocytes by changes in cytosolic pH. Biochem J. 1998;333 (Pt 1):167-74.

153. Kido Y, Tamai I, Okamoto M, Suzuki F, Tsuji A. Functional clarification of MCT1-mediated transport of monocarboxylic acids at the blood-brain barrier using in vitro cultured cells and in vivo BUI studies. Pharm Res-Dordr. 2000;17(1):55-62.

154. Manning Fox JE, Meredith D, Halestrap AP. Characterisation of human monocarboxylate transporter 4 substantiates its role in lactic acid efflux from skeletal muscle. The Journal of physiology. 2000;529 Pt 2:285-93.

155. Lecona E, Olmo N, Turnay J, Santiago-Gomez A, Lopez de Silanes I, Gorospe M, et al. Kinetic analysis of butyrate transport in human colon adenocarcinoma cells reveals two different carrier-mediated mechanisms. The Biochemical journal. 2008;409(1):311-20.

156. Moschen I, Broer A, Galic S, Lang F, Broer S. Significance of short chain fatty acid transport by members of the monocarboxylate transporter family (MCT). Neurochem Res. 2012;37(11):2562-8.

157. Morse BL, Felmlee MA, Morris ME. gamma-Hydroxybutyrate blood/plasma partitioning: effect of physiologic pH on transport by monocarboxylate transporters. Drug Metab Dispos. 2012;40(1):64-9.

158. Broer S, Broer A, Schneider HP, Stegen C, Halestrap AP, Deitmer JW. Characterization of the high-affinity monocarboxylate transporter MCT2 in Xenopus laevis oocytes. Biochem J. 1999;341 (Pt 3):529-35.

159. Yoshimura T, Schwab AJ, Tao L, Barker F, Pang KS. Hepatic uptake of hippurate: a multiple-indicator dilution, perfused rat liver study. The American journal of physiology. 1998;274(1 Pt 1):G10-20.

160. Dimmer KS, Friedrich B, Lang F, Deitmer JW, Broer S. The low-affinity monocarboxylate transporter MCT4 is adapted to the export of lactate in highly glycolytic cells. Biochem J. 2000;350:219-27.
161. Nagasawa K, Nagai K, Ishimoto A, Fujimoto S. Transport mechanism for lovastatin acid in bovine kidney NBL-1 cells: kinetic evidences imply involvement of monocarboxylate transporter 4. Int J Pharm. 2003;262(1-2):63-73.
162. Shimada A, Nakagawa Y, Morishige H, Yamamoto A, Fujita T. Functional characteristics of H+ -dependent nicotinate transport in primary cultures of astrocytes from rat cerebral cortex. Neurosci Lett. 2006;392(3):207-12.
163. Miyauchi S, Gopal E, Fei YJ, Ganapathy V. Functional identification of SLC5A8, a tumor suppressor down-regulated in colon cancer, as a Na(+)-coupled transporter for short-chain fatty acids. The Journal of biological chemistry. 2004;279(14):13293-6.
164. Cui D, Morris ME. The drug of abuse gamma-hydroxybutyrate is a substrate for sodium-coupled monocarboxylate transporter (SMCT) 1 (SLC5A8): characterization of SMCT-mediated uptake and inhibition. Drug Metab Dispos. 2009;37(7):1404-10.
165. Martin PM, Gopal E, Ananth S, Zhuang L, Itagaki S, Prasad BM, et al. Identity of SMCT1 (SLC5A8) as a neuron-specific Na+-coupled transporter for active uptake of L-lactate and ketone bodies in the brain. Journal of neurochemistry. 2006;98(1):279-88.
166. Thangaraju M, Karunakaran SK, Itagaki S, Gopal E, Elangovan S, Prasad PD, et al. Transport by SLC5A8 with subsequent inhibition of histone deacetylase 1 (HDAC1) and HDAC3 underlies the antitumor activity of 3-bromopyruvate. Cancer. 2009;115(20):4655-66.
167. Srinivas SR, Gopal E, Zhuang L, Itagaki S, Martin PM, Fei YJ, et al. Cloning and functional identification of slc5a12 as a sodium-coupled low-affinity transporter for monocarboxylates (SMCT2). Biochem J. 2005;392(Pt 3):655-64.
168. Carpenter L, Halestrap AP. The kinetics, substrate and inhibitor specificity of the lactate transporter of Ehrlich-Lettre tumour cells studied with the intracellular pH indicator BCECF. Biochem J. 1994;304 (Pt 3):751-60.
169. Hildyard JC, Ammala C, Dukes ID, Thomson SA, Halestrap AP. Identification and characterisation of a new class of highly specific and potent inhibitors of the mitochondrial pyruvate carrier. Biochimica et biophysica acta. 2005;1707(2-3):221-30.

170. Choi JS, Jin MJ, Han HK. Role of monocarboxylic acid transporters in the cellular uptake of NSAIDs. The Journal of pharmacy and pharmacology. 2005;57(9):1185-9.
171. Shim CK, Cheon EP, Kang KW, Seo KS, Han HK. Inhibition effect of flavonoids on monocarboxylate transporter 1 (MCT1) in Caco-2 cells. J Pharm Pharmacol. 2007;59(11):1515-9.
172. Kobayashi M, Otsuka Y, Itagaki S, Hirano T, Iseki K. Inhibitory effects of statins on human monocarboxylate transporter 4. Int J Pharm. 2006;317(1):19-25.
173. Goncalves P, Catarino T, Gregorio I, Martel F. Inhibition of butyrate uptake by the primary bile salt chenodeoxycholic acid in intestinal epithelial cells. Journal of cellular biochemistry. 2012;113(9):2937-47.
174. Daneman R, Zhou L, Agalliu D, Cahoy JD, Kaushal A, Barres BA. The mouse blood-brain barrier transcriptome: a new resource for understanding the development and function of brain endothelial cells. PloS one. 2010;5(10):e13741.
175. Enerson BE, Drewes LR. The rat blood-brain barrier transcriptome. Journal of cerebral blood flow and metabolism : official journal of the International Society of Cerebral Blood Flow and Metabolism. 2006;26(7):959-73.
176. Gerhart DZ, Enerson BE, Zhdankina OY, Leino RL, Drewes LR. Expression of monocarboxylate transporter MCT1 by brain endothelium and glia in adult and suckling rats. Am J Physiol. 1997;273(1 Pt 1):E207-13.
177. Coon AL, Arias-Mendoza F, Colby GP, Cruz-Lobo J, Mocco J, Mack WJ, et al. Correlation of cerebral metabolites with functional outcome in experimental primate stroke using in vivo 1H-magnetic resonance spectroscopy. AJNR American journal of neuroradiology. 2006;27(5):1053-8.
178. Frykholm P, Hillered L, Langstrom B, Persson L, Valtysson J, Enblad P. Relationship between cerebral blood flow and oxygen metabolism, and extracellular glucose and lactate concentrations during middle cerebral artery occlusion and reperfusion: a microdialysis and positron emission tomography study in nonhuman primates. J Neurosurg. 2005;102(6):1076-84.
179. Wagner KR, Kleinholz M, de Courten-Myers GM, Myers RE. Hyperglycemic versus normoglycemic stroke: topography of brain metabolites, intracellular pH, and

infarct size. Journal of cerebral blood flow and metabolism : official journal of the International Society of Cerebral Blood Flow and Metabolism. 1992;12(2):213-22.

180. Wagner M, Schmid M, Juretschko S, Trebesius KH, Bubert A, Goebel W, et al. In situ detection of a virulence factor mRNA and 16S rRNA in Listeria monocytogenes. FEMS microbiology letters. 1998;160(1):159-68.

181. Wass CT, Lanier WL. Glucose modulation of ischemic brain injury: review and clinical recommendations. Mayo Clinic proceedings Mayo Clinic. 1996;71(8):801-12.

182. Belanger M, Allaman I, Magistretti PJ. Brain energy metabolism: focus on astrocyte-neuron metabolic cooperation. Cell metabolism. 2011;14(6):724-38.

183. Erlichman JS, Hewitt A, Damon TL, Hart M, Kurascz J, Li A, et al. Inhibition of monocarboxylate transporter 2 in the retrotrapezoid nucleus in rats: a test of the astrocyte-neuron lactate-shuttle hypothesis. The Journal of neuroscience : the official journal of the Society for Neuroscience. 2008;28(19):4888-96.

184. Murray CM, Hutchinson R, Bantick JR, Belfield GP, Benjamin AD, Brazma D, et al. Monocarboxylate transporter MCT1 is a target for immunosuppression. Nature Chemical Biology. 2005;1(7):371-6.

185. Sonveaux P, Vegran F, Schroeder T, Wergin MC, Verrax J, Rabbani ZN, et al. Targeting lactate-fueled respiration selectively kills hypoxic tumor cells in mice. The Journal of clinical investigation. 2008;118(12):3930-42.

186. Balklava Z, Grant BD. The regulation of endocytosis by kinases: cell biology meets genomics. Genome Biol. 2005;6(13):245.

187. Ceresa BP, Schmid SL. Regulation of signal transduction by endocytosis. Current opinion in cell biology. 2000;12(2):204-10.

188. Dart C. Lipid microdomains and the regulation of ion channel function. The Journal of physiology. 2010;588(Pt 17):3169-78.

189. Delom F, Fessart D. Role of Phosphorylation in the Control of Clathrin-Mediated Internalization of GPCR. Int J Cell Biol. 2011;2011:246954.

190. Melikian HE. Neurotransmitter transporter trafficking: endocytosis, recycling, and regulation. Pharmacology & therapeutics. 2004;104(1):17-27.

191. Jayanthi LD, Samuvel DJ, Ramamoorthy S. Regulated internalization and phosphorylation of the native norepinephrine transporter in response to phorbol esters.

Evidence for localization in lipid rafts and lipid raft-mediated internalization. The Journal of biological chemistry. 2004;279(18):19315-26.

192. Lau T, Horschitz S, Bartsch D, Schloss P. Monitoring mouse serotonin transporter internalization in stem cell-derived serotonergic neurons by confocal laser scanning microscopy. Neurochem Int. 2009;54(3-4):271-6.

193. Moeller HB, Olesen ET, Fenton RA. Regulation of the water channel aquaporin-2 by posttranslational modification. American journal of physiology Renal physiology. 2011;300(5):F1062-73.

194. Mortensen OV, Larsen MB, Prasad BM, Amara SG. Genetic complementation screen identifies a mitogen-activated protein kinase phosphatase, MKP3, as a regulator of dopamine transporter trafficking. Molecular biology of the cell. 2008;19(7):2818-29.

195. Reinhardt J, Kosch M, Lerner M, Bertram H, Lemke D, Oberleithner H. Stimulation of protein kinase C pathway mediates endocytosis of human nongastric H+-K+-ATPase, ATP1AL1. American journal of physiology Renal physiology. 2002;283(2):F335-43.

196. Yang J, Holman GD. Long-term metformin treatment stimulates cardiomyocyte glucose transport through an AMP-activated protein kinase-dependent reduction in GLUT4 endocytosis. Endocrinology. 2006;147(6):2728-36.

197. Demeule M, Jodoin J, Gingras D, Beliveau R. P-glycoprotein is localized in caveolae in resistant cells and in brain capillaries. FEBS letters. 2000;466(2-3):219-24.

198. Frank PG, Woodman SE, Park DS, Lisanti MP. Caveolin, caveolae, and endothelial cell function. Arteriosclerosis, thrombosis, and vascular biology. 2003;23(7):1161-8.

199. Stewart PA. Endothelial vesicles in the blood-brain barrier: are they related to permeability? Cell Mol Neurobiol. 2000;20(2):149-63.

200. Roux F, Durieu-Trautmann O, Chaverot N, Claire M, Mailly P, Bourre JM, et al. Regulation of gamma-glutamyl transpeptidase and alkaline phosphatase activities in immortalized rat brain microvessel endothelial cells. Journal of cellular physiology. 1994;159(1):101-13.

201. Roux F, Couraud PO. Rat brain endothelial cell lines for the study of blood-brain barrier permeability and transport functions. Cell Mol Neurobiol. 2005;25(1):41-58.

202. Uhernik AL, Tucker C, Smith JP. Control of MCT1 function in cerebrovascular endothelial cells by intracellular pH. Brain Res. 2011;1376:10-22.
203. Zinchuk V, Grossenbacher-Zinchuk O. Recent advances in quantitative colocalization analysis: focus on neuroscience. Progress in histochemistry and cytochemistry. 2009;44(3):125-72.
204. Kempski O, Wroblewska B, Spatz M. Effects of forskolin on growth and morphology of cultured glial and cerebrovascular endothelial and smooth muscle cells. International journal of developmental neuroscience : the official journal of the International Society for Developmental Neuroscience. 1987;5(5-6):435-45.
205. Hu W, Onuma T, Birukawa N, Abe M, Ito E, Chen Z, et al. Change of morphology and cytoskeletal protein gene expression during dibutyryl cAMP-induced differentiation in C6 glioma cells. Cell Mol Neurobiol. 2008;28(4):519-28.
206. Gratton JP, Bernatchez P, Sessa WC. Caveolae and caveolins in the cardiovascular system. Circulation research. 2004;94(11):1408-17.
207. Razani B, Woodman SE, Lisanti MP. Caveolae: from cell biology to animal physiology. Pharmacological reviews. 2002;54(3):431-67.
208. Cornford EM, Hyman S. Localization of brain endothelial luminal and abluminal transporters with immunogold electron microscopy. NeuroRx : the journal of the American Society for Experimental NeuroTherapeutics. 2005;2(1):27-43.
209. Aslam M, Hartel FV, Arshad M, Gunduz D, Abdallah Y, Sauer H, et al. cAMP/PKA antagonizes thrombin-induced inactivation of endothelial myosin light chain phosphatase: role of CPI-17. Cardiovascular research. 2010;87(2):375-84.
210. Beuckmann C, Hellwig S, Galla HJ. Induction of the blood/brain-barrier-associated enzyme alkaline phosphatase in endothelial cells from cerebral capillaries is mediated via cAMP. European journal of biochemistry / FEBS. 1995;229(3):641-4.
211. Goeckeler ZM, Wysolmerski RB. Myosin phosphatase and cofilin mediate cAMP/cAMP-dependent protein kinase-induced decline in endothelial cell isometric tension and myosin II regulatory light chain phosphorylation. The Journal of biological chemistry. 2005;280(38):33083-95.

212. Huttlin EL, Jedrychowski MP, Elias JE, Goswami T, Rad R, Beausoleil SA, et al. A tissue-specific atlas of mouse protein phosphorylation and expression. Cell. 2010;143(7):1174-89.
213. Tang W, Hemler ME. Caveolin-1 regulates matrix metalloproteinases-1 induction and CD147/EMMPRIN cell surface clustering. The Journal of biological chemistry. 2004;279(12):11112-8.
214. Tang W, Chang SB, Hemler ME. Links between CD147 function, glycosylation, and caveolin-1. Molecular biology of the cell. 2004;15(9):4043-50.
215. Staruschenko A, Pochynyuk O, Stockand JD. Regulation of epithelial Na+ channel activity by conserved serine/threonine switches within sorting signals. The Journal of biological chemistry. 2005;280(47):39161-7.
216. Schnaberth G, Brunner G, Scheiber V. [Lactate acidosis in the cerebrospinal fluid as a prognostic parameter of malacic cerebral insult (author's transl)]. Wiener klinische Wochenschrift. 1981;93(12):388-93.
217. Siesjo BK, Katsura K, Mellergard P, Ekholm A, Lundgren J, Smith ML. Acidosis-related brain damage. Progress in brain research. 1993;96:23-48.
218. Wei J, Cohen DM, Quast MJ. Effects of 2-deoxy-d-glucose on focal cerebral ischemia in hyperglycemic rats. Journal of cerebral blood flow and metabolism : official journal of the International Society of Cerebral Blood Flow and Metabolism. 2003;23(5):556-64.
219. Clausen T, Khaldi A, Zauner A, Reinert M, Doppenberg E, Menzel M, et al. Cerebral acid-base homeostasis after severe traumatic brain injury. J Neurosurg. 2005;103(4):597-607.
220. DeSalles AA, Kontos HA, Becker DP, Yang MS, Ward JD, Moulton R, et al. Prognostic significance of ventricular CSF lactic acidosis in severe head injury. J Neurosurg. 1986;65(5):615-24.
221. Unterberg AW, Stover J, Kress B, Kiening KL. Edema and brain trauma. Neuroscience. 2004;129(4):1021-9.
222. Roth DM, Patel HH. Role of caveolae in cardiac protection. Pediatric cardiology. 2011;32(3):329-33.

223. Carpenter L, Halestrap AP. The Kinetics, Substrate and Inhibitor Specificity of the Lactate Transporter of Ehrlich-Lettre Tumor-Cells Studied with the Intracellular Ph Indicator Bcecf. Biochem J. 1994;304:751-60.
224. Dai JY, Dou KF, Wang CH, Zhao P, Lau WB, Tao L, et al. The interaction of HAb18G/CD147 with integrin alpha6beta1 and its implications for the invasion potential of human hepatoma cells. BMC Cancer. 2009;9:337.
225. Weidle UH, Scheuer W, Eggle D, Klostermann S, Stockinger H. Cancer-related issues of CD147. Cancer genomics & proteomics. 2010;7(3):157-69.
226. Martin S, Henley JM. Activity-dependent endocytic sorting of kainate receptors to recycling or degradation pathways. Embo J. 2004;23(24):4749-59.
227. Sidhaye V, Hoffert JD, King LS. cAMP has distinct acute and chronic effects on aquaporin-5 in lung epithelial cells. The Journal of biological chemistry. 2005;280(5):3590-6.
228. Hertz L, Dienel GA. Lactate transport and transporters: general principles and functional roles in brain cells. Journal of neuroscience research. 2005;79(1-2):11-8.
229. Dumitrescu AM, Liao XH, Best TB, Brockmann K, Refetoff S. A novel syndrome combining thyroid and neurological abnormalities is associated with mutations in a monocarboxylate transporter gene. American journal of human genetics. 2004;74(1):168-75.
230. Kolz M, Johnson T, Sanna S, Teumer A, Vitart V, Perola M, et al. Meta-analysis of 28,141 individuals identifies common variants within five new loci that influence uric acid concentrations. PLoS genetics. 2009;5(6):e1000504.
231. Kim DK, Kanai Y, Chairoungdua A, Matsuo H, Cha SH, Endou H. Expression cloning of a Na+-independent aromatic amino acid transporter with structural similarity to H+/monocarboxylate transporters. The Journal of biological chemistry. 2001;276(20):17221-8.
232. Poole RC, Halestrap AP. Identification and partial purification of the erythrocyte L-lactate transporter. Biochem J. 1992;283 (Pt 3):855-62.
233. Garcia CK, Goldstein JL, Pathak RK, Anderson RG, Brown MS. Molecular characterization of a membrane transporter for lactate, pyruvate, and other monocarboxylates: implications for the Cori cycle. Cell. 1994;76(5):865-73.

234. Garcia CK, Li X, Luna J, Francke U. cDNA cloning of the human monocarboxylate transporter 1 and chromosomal localization of the SLC16A1 locus to 1p13.2-p12. Genomics. 1994;23(2):500-3.
235. Cuff MA, Shirazi-Beechey SP. The human monocarboxylate transporter, MCT1: genomic organization and promoter analysis. Biochemical and biophysical research communications. 2002;292(4):1048-56.
236. Jackson VN, Price NT, Halestrap AP. cDNA cloning of MCT1, a monocarboxylate transporter from rat skeletal muscle. Biochimica et biophysica acta. 1995;1238(2):193-6.
237. Halestrap AP, Price NT. The proton-linked monocarboxylate transporter (MCT) family: structure, function and regulation. Biochem J. 1999;343:281-99.
238. Frerichs KU, Lindsberg PJ, Hallenbeck JM, Feuerstein GZ. Increased cerebral lactate output to cerebral venous blood after forebrain ischemia in rats. Stroke. 1990;21(4):614-7.
239. Siesjo BK. Cell damage in the brain: a speculative synthesis. Journal of cerebral blood flow and metabolism : official journal of the International Society of Cerebral Blood Flow and Metabolism. 1981;1(2):155-85.
240. Rehncrona S, Kagstrom E. Tissue lactic acidosis and ischemic brain damage. The American journal of emergency medicine. 1983;1(2):168-74.
241. Rehncrona S. Brain acidosis. Annals of emergency medicine. 1985;14(8):770-6.
242. Biros MH, Dimlich RV, Barsan WG. Postinsult treatment of ischemia-induced cerebral lactic acidosis in the rat. Annals of emergency medicine. 1986;15(4):397-404.
243. Rehncrona S, Rosen I, Siesjo BK. Brain lactic acidosis and ischemic cell damage: 1. Biochemistry and neurophysiology. Journal of cerebral blood flow and metabolism : official journal of the International Society of Cerebral Blood Flow and Metabolism. 1981;1(3):297-311.
244. Nehlig A, Pereira de Vasconcelos A. Glucose and ketone body utilization by the brain of neonatal rats. Progress in neurobiology. 1993;40(2):163-221.
245. Owen OE, Morgan AP, Kemp HG, Sullivan JM, Herrera MG, Cahill GF, Jr. Brain metabolism during fasting. The Journal of clinical investigation. 1967;46(10):1589-95.

246. Freeman J, Veggiotti P, Lanzi G, Tagliabue A, Perucca E, Institute of Neurology ICMF. The ketogenic diet: from molecular mechanisms to clinical effects. Epilepsy Res. 2006;68(2):145-80.
247. Andrews MT, Russeth KP, Drewes LR, Henry PG. Adaptive mechanisms regulate preferred utilization of ketones in the heart and brain of a hibernating mammal during arousal from torpor. American journal of physiology Regulatory, integrative and comparative physiology. 2009;296(2):R383-93.
248. Bialer M, Yagen B. Valproic acid: Second generation. Neurotherapeutics. 2007;4(1):130-7.
249. Tamai I, Sai Y, Ono A, Kido Y, Yabuuchi H, Takanaga H, et al. Immunohistochemical and functional characterization of pH-dependent intestinal absorption of weak organic acids by the monocarboxylic acid transporter MCT1. The Journal of pharmacy and pharmacology. 1999;51(10):1113-21.
250. Hosoya K, Kondo T, Tomi M, Takanaga H, Ohtsuki S, Terasaki T. MCT1-mediated transport of L-lactic acid at the inner blood-retinal barrier: A possible route for delivery of monocarboxylic acid drugs to the retina. Pharm Res-Dordr. 2001;18(12):1669-76.
251. Shim CK, Cheon EP, Kang KW, Seo KS, Han HK. Inhibition effect of flavonoids on monocarboxylate transporter 1 (MCT1) in Caco-2 cells. The Journal of pharmacy and pharmacology. 2007;59(11):1515-9.
252. Yamagata K, Tagami M, Yamori Y. Nitric oxide reduces astrocytic lactate production and induces neuronal vulnerability in stroke-prone spontaneously hypertensive rats. Glia. 2008;56(4):387-93.
253. Reger MA, Henderson ST, Hale C, Cholerton B, Baker LD, Watson GS, et al. Effects of β-hydroxybutyrate on cognition in memory-impaired adults. Neurobiology of Aging. 2004;25(3):311-4.
254. Henderson ST. Ketone bodies as a therapeutic for Alzheimer's disease. Neurotherapeutics. 2008;5(3):470-80.
255. Nusslein-Volhard C, Wieschaus E. Mutations affecting segment number and polarity in Drosophila. Nature. 1980;287(5785):795-801.

256. Angers S, Moon RT. Proximal events in Wnt signal transduction. Nature reviews Molecular cell biology. 2009;10(7):468-77.
257. Huang HC, Klein PS. The Frizzled family: receptors for multiple signal transduction pathways. Genome Biol. 2004;5(7).
258. Kimelman D, Xu W. beta-catenin destruction complex: insights and questions from a structural perspective. Oncogene. 2006;25(57):7482-91.
259. MacDonald BT, Tamai K, He X. Wnt/beta-catenin signaling: components, mechanisms, and diseases. Developmental cell. 2009;17(1):9-26.
260. Nemeth MJ, Bodine DM. Regulation of hematopoiesis and the hematopoietic stem cell niche by Wnt signaling pathways. Cell research. 2007;17(9):746-58.
261. Vincan E. Wnt signaling. Pathway methods and mammalian models. Preface. Methods in molecular biology. 2008;468:v.
262. Jope RS. Lithium and GSK-3: one inhibitor, two inhibitory actions, multiple outcomes. Trends in Pharmacological Sciences. 2003;24(9):441-3.
263. Hlubek F, Brabletz T, Budczies J, Pfeiffer S, Jung A, Kirchner T. Heterogeneous expression of Wnt/beta-catenin target genes within colorectal cancer. International journal of cancer Journal international du cancer. 2007;121(9):1941-8.
264. Vlad A, Rohrs S, Klein-Hitpass L, Muller O. The first five years of the Wnt targetome. Cellular signalling. 2008;20(5):795-802.
265. Shtutman M, Zhurinsky J, Simcha I, Albanese C, D'Amico M, Pestell R, et al. The cyclin D1 gene is a target of the beta-catenin/LEF-1 pathway. Proceedings of the National Academy of Sciences of the United States of America. 1999;96(10):5522-7.
266. Hovanes K, Li TW, Munguia JE, Truong T, Milovanovic T, Lawrence Marsh J, et al. Beta-catenin-sensitive isoforms of lymphoid enhancer factor-1 are selectively expressed in colon cancer. Nature genetics. 2001;28(1):53-7.
267. He T. Identification of c-MYC as a Target of the APC Pathway. Science. 1998;281(5382):1509-12.
268. Lim JC, Kania KD, Wijesuriya H, Chawla S, Sethi JK, Pulaski L, et al. Activation of beta-catenin signalling by GSK-3 inhibition increases p-glycoprotein expression in brain endothelial cells. Journal of neurochemistry. 2008;106(4):1855-65.

269. Miller JR, Rowning BA, Larabell CA, Yang-Snyder JA, Bates RL, Moon RT. Establishment of the dorsal-ventral axis in Xenopus embryos coincides with the dorsal enrichment of dishevelled that is dependent on cortical rotation. The Journal of cell biology. 1999;146(2):427-37.
270. Blauwkamp TA, Nigam S, Ardehali R, Weissman IL, Nusse R. Endogenous Wnt signalling in human embryonic stem cells generates an equilibrium of distinct lineage-specified progenitors. Nature communications. 2012;3:1070.
271. Panhuysen M, Vogt Weisenhorn DM, Blanquet V, Brodski C, Heinzmann U, Beisker W, et al. Effects of Wnt1 signaling on proliferation in the developing mid-/hindbrain region. Molecular and cellular neurosciences. 2004;26(1):101-11.
272. Clevers H. Wnt/beta-catenin signaling in development and disease. Cell. 2006;127(3):469-80.
273. Ito M, Yang Z, Andl T, Cui C, Kim N, Millar SE, et al. Wnt-dependent de novo hair follicle regeneration in adult mouse skin after wounding. Nature. 2007;447(7142):316-20.
274. Polakis P. Wnt signaling in cancer. Cold Spring Harbor perspectives in biology. 2012;4(5).
275. Liebner S, Corada M, Bangsow T, Babbage J, Taddei A, Czupalla CJ, et al. Wnt/beta-catenin signaling controls development of the blood-brain barrier. The Journal of cell biology. 2008;183(3):409-17.
276. Stenman JM, Rajagopal J, Carroll TJ, Ishibashi M, McMahon J, McMahon AP. Canonical Wnt signaling regulates organ-specific assembly and differentiation of CNS vasculature. Science. 2008;322(5905):1247-50.
277. Tsai A, Carstens RP. An optimized protocol for protein purification in cultured mammalian cells using a tandem affinity purification approach. Nature protocols. 2006;1(6):2820-7.
278. Matson CT, Drewes LR. Immunoblot detection of brain vascular proteins. Methods in molecular medicine. 2003;89:479-87.
279. Piper RC, Lehner PJ. Endosomal transport via ubiquitination. Trends in cell biology. 2011;21(11):647-55.
280. Kimura Y, Tanaka K. Regulatory mechanisms involved in the control of ubiquitin homeostasis. Journal of biochemistry. 2010;147(6):793-8.

281. Marks MS, Woodruff L, Ohno H, Bonifacino JS. Protein targeting by tyrosine- and di-leucine-based signals: evidence for distinct saturable components. The Journal of cell biology. 1996;135(2):341-54.
282. Mellman I. Endocytosis and molecular sorting. Annual review of cell and developmental biology. 1996;12:575-625.
283. Lu C, Pribanic S, Debonneville A, Jiang C, Rotin D. The PY motif of ENaC, mutated in Liddle syndrome, regulates channel internalization, sorting and mobilization from subapical pool. Traffic. 2007;8(9):1246-64.
284. Adams J. The proteasome: a suitable antineoplastic target. Nature reviews Cancer. 2004;4(5):349-60.
285. Alwan HA, van Zoelen EJ, van Leeuwen JE. Ligand-induced lysosomal epidermal growth factor receptor (EGFR) degradation is preceded by proteasome-dependent EGFR de-ubiquitination. The Journal of biological chemistry. 2003;278(37):35781-90.
286. Luzio JP, Parkinson MD, Gray SR, Bright NA. The delivery of endocytosed cargo to lysosomes. Biochemical Society transactions. 2009;37(Pt 5):1019-21.
287. Johnson AO, Lampson MA, McGraw TE. A di-leucine sequence and a cluster of acidic amino acids are required for dynamic retention in the endosomal recycling compartment of fibroblasts. Molecular biology of the cell. 2001;12(2):367-81.
288. Storch S, Pohl S, Braulke T. A dileucine motif and a cluster of acidic amino acids in the second cytoplasmic domain of the batten disease-related CLN3 protein are required for efficient lysosomal targeting. The Journal of biological chemistry. 2004;279(51):53625-34.
289. Xia S, Dun XP, Hu PS, Kjaer S, Zheng K, Qian Y, et al. Postendocytotic traffic of the galanin R1 receptor: a lysosomal signal motif on the cytoplasmic terminus. Proceedings of the National Academy of Sciences of the United States of America. 2008;105(14):5609-13.
290. Corvera S, Chawla A, Chakrabarti R, Joly M, Buxton J, Czech MP. A double leucine within the GLUT4 glucose transporter COOH-terminal domain functions as an endocytosis signal. The Journal of cell biology. 1994;126(6):1625.

291. Shewan AM, Marsh BJ, Melvin DR, Martin S, Gould GW, James DE. The cytosolic C-terminus of the glucose transporter GLUT4 contains an acidic cluster endosomal targeting motif distal to the dileucine signal. Biochem J. 2000;350 Pt 1:99-107.

292. Inoki K, Ouyang H, Zhu T, Lindvall C, Wang Y, Zhang X, et al. TSC2 integrates Wnt and energy signals via a coordinated phosphorylation by AMPK and GSK3 to regulate cell growth. Cell. 2006;126(5):955-68.

293. Laplante M, Sabatini DM. mTOR signaling at a glance. J Cell Sci. 2009;122(20):3589-94.

294. Chenal J, Pellerin L. Noradrenaline enhances the expression of the neuronal monocarboxylate transporter MCT2 by translational activation via stimulation of PI3K/Akt and the mTOR/S6K pathway. Journal of neurochemistry. 2007;102(2):389-97.

295. Piper RC, Luzio JP. Ubiquitin-dependent sorting of integral membrane proteins for degradation in lysosomes. Current opinion in cell biology. 2007;19(4):459-65.

296. Yuasa-Kawada J, Kinoshita-Kawada M, Wu G, Rao Y, Wu JY. Midline crossing and Slit responsiveness of commissural axons require USP33. Nature neuroscience. 2009;12(9):1087-9.

297. Bomberger JM, Barnaby RL, Stanton BA. The deubiquitinating enzyme USP10 regulates the post-endocytic sorting of cystic fibrosis transmembrane conductance regulator in airway epithelial cells. The Journal of biological chemistry. 2009;284(28):18778-89.

298. Clague MJ, Urbe S. Endocytosis: the DUB version. Trends in cell biology. 2006;16(11):551-9.

299. Sowa ME, Bennett EJ, Gygi SP, Harper JW. Defining the human deubiquitinating enzyme interaction landscape. Cell. 2009;138(2):389-403.

300. Avvakumov GV, Walker JR, Xue S, Finerty PJ, Jr., Mackenzie F, Newman EM, et al. Amino-terminal dimerization, NRDP1-rhodanese interaction, and inhibited catalytic domain conformation of the ubiquitin-specific protease 8 (USP8). The Journal of biological chemistry. 2006;281(49):38061-70.

301. Wolfe BL, Marchese A, Trejo J. Ubiquitination differentially regulates clathrin-dependent internalization of protease-activated receptor-1. The Journal of cell biology. 2007;177(5):905-16.
302. Veneman T, Mitrakou A, Mokan M, Cryer P, Gerich J. Effect of hyperketonemia and hyperlacticacidemia on symptoms, cognitive dysfunction, and counterregulatory hormone responses during hypoglycemia in normal humans. Diabetes. 1994;43(11):1311-7.
303. Maran A, Crepaldi C, Trupiani S, Lucca T, Jori E, Macdonald IA, et al. Brain function rescue effect of lactate following hypoglycaemia is not an adaptation process in both normal and Type I diabetic subjects. Diabetologia. 2000;43(6):733-41.
304. Reya T, Clevers H. Wnt signalling in stem cells and cancer. Nature. 2005;434(7035):843-50.
305. Clements WM, Lowy AM, Groden J. Adenomatous Polyposis Coli/β-Catenin Interaction and Downstream Targets: Altered Gene Expression in Gastrointestinal Tumors. Clinical Colorectal Cancer. 2003;3(2):113-20.
306. Salahshor S, Woodgett JR. The links between axin and carcinogenesis. Journal of clinical pathology. 2005;58(3):225-36.
307. Bass AJ, Lawrence MS, Brace LE, Ramos AH, Drier Y, Cibulskis K, et al. Genomic sequencing of colorectal adenocarcinomas identifies a recurrent VTI1A-TCF7L2 fusion. Nature genetics. 2011;43(10):964-8.
308. Laird PW, Jackson-Grusby L, Fazeli A, Dickinson SL, Jung WE, Li E, et al. Suppression of intestinal neoplasia by DNA hypomethylation. Cell. 1995;81(2):197-205.
309. Satoh S, Daigo Y, Furukawa Y, Kato T, Miwa N, Nishiwaki T, et al. AXIN1 mutations in hepatocellular carcinomas, and growth suppression in cancer cells by virus-mediated transfer of AXIN1. Nature genetics. 2000;24(3):245-50.
310. Kongkham PN, Northcott PA, Croul SE, Smith CA, Taylor MD, Rutka JT. The SFRP family of WNT inhibitors function as novel tumor suppressor genes epigenetically silenced in medulloblastoma. Oncogene. 2010;29(20):3017-24.
311. Warburg O. On the origin of cancer cells. Science. 1956;123(3191):309-14.
312. Parks SK, Chiche J, Pouyssegur J. Disrupting proton dynamics and energy metabolism for cancer therapy. Nature reviews Cancer. 2013;13(9):611-23.

313. Fiaschi T, Marini A, Giannoni E, Taddei ML, Gandellini P, De Donatis A, et al. Reciprocal metabolic reprogramming through lactate shuttle coordinately influences tumor-stroma interplay. Cancer research. 2012;72(19):5130-40.
314. Zimmerman ZF, Moon RT, Chien AJ. Targeting Wnt pathways in disease. Cold Spring Harbor perspectives in biology. 2012;4(11).
315. Takebe K, Takahashi-Iwanaga H, Iwanaga T. Intensified expressions of a monocarboxylate transporter in consistently renewing tissues of the mouse. Biomedical research. 2011;32(4):293-301.
316. Notani D, Gottimukkala KP, Jayani RS, Limaye AS, Damle MV, Mehta S, et al. Global regulator SATB1 recruits beta-catenin and regulates T(H)2 differentiation in Wnt-dependent manner. PLoS biology. 2010;8(1):e1000296.
317. Sen M, Reifert J, Lauterbach K, Wolf V, Rubin JS, Corr M, et al. Regulation of fibronectin and metalloproteinase expression by Wnt signaling in rheumatoid arthritis synoviocytes. Arthritis and rheumatism. 2002;46(11):2867-77.
318. Sheng YJ, Gao JP, Li J, Han JW, Xu Q, Hu WL, et al. Follow-up study identifies two novel susceptibility loci PRKCB and 8p11.21 for systemic lupus erythematosus. Rheumatology. 2011;50(4):682-8.
319. Artavanis-Tsakonas S. Notch Signaling: Cell Fate Control and Signal Integration in Development. Science. 1999;284(5415):770-6.
320. Kopan R, Ilagan MX. The canonical Notch signaling pathway: unfolding the activation mechanism. Cell. 2009;137(2):216-33.
321. Oda T, Elkahloun AG, Pike BL, Okajima K, Krantz ID, Genin A, et al. Mutations in the human Jagged1 gene are responsible for Alagille syndrome. Nature genetics. 1997;16(3):235-42.
322. McDaniell R, Warthen DM, Sanchez-Lara PA, Pai A, Krantz ID, Piccoli DA, et al. NOTCH2 mutations cause Alagille syndrome, a heterogeneous disorder of the notch signaling pathway. American journal of human genetics. 2006;79(1):169-73.
323. van Es JH, van Gijn ME, Riccio O, van den Born M, Vooijs M, Begthel H, et al. Notch/gamma-secretase inhibition turns proliferative cells in intestinal crypts and adenomas into goblet cells. Nature. 2005;435(7044):959-63.

324. Weng AP, Ferrando AA, Lee W, Morris JPt, Silverman LB, Sanchez-Irizarry C, et al. Activating mutations of NOTCH1 in human T cell acute lymphoblastic leukemia. Science. 2004;306(5694):269-71.
325. Bray SJ. Notch signalling: a simple pathway becomes complex. Nature reviews Molecular cell biology. 2006;7(9):678-89.
326. Guruharsha KG, Kankel MW, Artavanis-Tsakonas S. The Notch signalling system: recent insights into the complexity of a conserved pathway. Nature reviews Genetics. 2012;13(9):654-66.
327. Maier MM, Gessler M. Comparative analysis of the human and mouse Hey1 promoter: Hey genes are new Notch target genes. Biochemical and biophysical research communications. 2000;275(2):652-60.
328. Dong Y, Jesse AM, Kohn A, Gunnell LM, Honjo T, Zuscik MJ, et al. RBPjkappa-dependent Notch signaling regulates mesenchymal progenitor cell proliferation and differentiation during skeletal development. Development. 2010;137(9):1461-71.
329. Uyttendaele H, Closson V, Wu G, Roux F, Weinmaster G, Kitajewski J. Notch4 and Jagged-1 induce microvessel differentiation of rat brain endothelial cells. Microvascular research. 2000;60(2):91-103.
330. Karsan A. The role of notch in modeling and maintaining the vasculature. Canadian journal of physiology and pharmacology. 2005;83(1):14-23.
331. Manda VK, Mittapalli RK, Geldenhuys WJ, Lockman PR. Chronic exposure to nicotine and saquinavir decreases endothelial Notch-4 expression and disrupts blood-brain barrier integrity. Journal of neurochemistry. 2010;115(2):515-25.
332. Tam SJ, Watts RJ. Connecting vascular and nervous system development: angiogenesis and the blood-brain barrier. Annual review of neuroscience. 2010;33:379-408.
333. Ghabrial AS, Krasnow MA. Social interactions among epithelial cells during tracheal branching morphogenesis. Nature. 2006;441(7094):746-9.
334. Duarte A, Hirashima M, Benedito R, Trindade A, Diniz P, Bekman E, et al. Dosage-sensitive requirement for mouse Dll4 in artery development. Genes & development. 2004;18(20):2474-8.

335. Gale NW, Dominguez MG, Noguera I, Pan L, Hughes V, Valenzuela DM, et al. Haploinsufficiency of delta-like 4 ligand results in embryonic lethality due to major defects in arterial and vascular development. Proceedings of the National Academy of Sciences of the United States of America. 2004;101(45):15949-54.
336. Hellstrom M, Phng LK, Hofmann JJ, Wallgard E, Coultas L, Lindblom P, et al. Dll4 signalling through Notch1 regulates formation of tip cells during angiogenesis. Nature. 2007;445(7129):776-80.
337. Suchting S, Freitas C, le Noble F, Benedito R, Breant C, Duarte A, et al. The Notch ligand Delta-like 4 negatively regulates endothelial tip cell formation and vessel branching. Proceedings of the National Academy of Sciences of the United States of America. 2007;104(9):3225-30.
338. Kim HA, Koo BK, Cho JH, Kim YY, Seong J, Chang HJ, et al. Notch1 counteracts WNT/beta-catenin signaling through chromatin modification in colorectal cancer. Journal of Clinical Investigation. 2012;122(9):3248-59.
339. Camps J, Pitt JJ, Emons G, Hummon AB, Case CM, Grade M, et al. Genetic amplification of the NOTCH modulator LNX2 upregulates the WNT/beta-catenin pathway in colorectal cancer. Cancer research. 2013;73(6):2003-13.
340. Peignon G, Durand A, Cacheux W, Ayrault O, Terris B, Laurent-Puig P, et al. Complex interplay between beta-catenin signalling and Notch effectors in intestinal tumorigenesis. Gut. 2011;60(2):166-76.
341. Rodilla V, Villanueva A, Obrador-Hevia A, Robert-Moreno A, Fernandez-Majada V, Grilli A, et al. Jagged1 is the pathological link between Wnt and Notch pathways in colorectal cancer. Proceedings of the National Academy of Sciences of the United States of America. 2009;106(15):6315-20.
342. Ayyanan A, Civenni G, Ciarloni L, Morel C, Mueller N, Lefort K, et al. Increased Wnt signaling triggers oncogenic conversion of human breast epithelial cells by a Notch-dependent mechanism. Proceedings of the National Academy of Sciences of the United States of America. 2006;103(10):3799-804.
343. Guo S, Liu M, Gonzalez-Perez RR. Role of Notch and its oncogenic signaling crosstalk in breast cancer. Biochimica et biophysica acta. 2011;1815(2):197-213.

344. Lin GL, Hankenson KD. Integration of BMP, Wnt, and notch signaling pathways in osteoblast differentiation. Journal of cellular biochemistry. 2011;112(12):3491-501.
345. Nakamura T, Tsuchiya K, Watanabe M. Crosstalk between Wnt and Notch signaling in intestinal epithelial cell fate decision. Journal of gastroenterology. 2007;42(9):705-10.
346. Kwon C, Cheng P, King IN, Andersen P, Shenje L, Nigam V, et al. Notch post-translationally regulates beta-catenin protein in stem and progenitor cells. Nature cell biology. 2011;13(10):1244-51.
347. Fre S, Pallavi SK, Huyghe M, Lae M, Janssen KP, Robine S, et al. Notch and Wnt signals cooperatively control cell proliferation and tumorigenesis in the intestine. Proceedings of the National Academy of Sciences of the United States of America. 2009;106(15):6309-14.
348. Hayward P, Brennan K, Sanders P, Balayo T, DasGupta R, Perrimon N, et al. Notch modulates Wnt signalling by associating with Armadillo/beta-catenin and regulating its transcriptional activity. Development. 2005;132(8):1819-30.
349. Corada M, Nyqvist D, Orsenigo F, Caprini A, Giampietro C, Taketo MM, et al. The Wnt/beta-catenin pathway modulates vascular remodeling and specification by upregulating Dll4/Notch signaling. Developmental cell. 2010;18(6):938-49.
350. Reis M, Czupalla CJ, Ziegler N, Devraj K, Zinke J, Seidel S, et al. Endothelial Wnt/beta-catenin signaling inhibits glioma angiogenesis and normalizes tumor blood vessels by inducing PDGF-B expression. The Journal of experimental medicine. 2012;209(9):1611-27.
351. Phng LK, Gerhardt H. Angiogenesis: a team effort coordinated by notch. Developmental cell. 2009;16(2):196-208.
352. Landor SK, Mutvei AP, Mamaeva V, Jin S, Busk M, Borra R, et al. Hypo- and hyperactivated Notch signaling induce a glycolytic switch through distinct mechanisms. Proceedings of the National Academy of Sciences of the United States of America. 2011;108(46):18814-9.
353. Harjes U, Bensaad K, Harris AL. Endothelial cell metabolism and implications for cancer therapy. British journal of cancer. 2012;107(8):1207-12.

354. Li C, Zhang Y, Lu Y, Cui Z, Yu M, Zhang S, et al. Evidence of the cross talk between Wnt and Notch signaling pathways in non-small-cell lung cancer (NSCLC): Notch3-siRNA weakens the effect of LiCl on the cell cycle of NSCLC cell lines. Journal of cancer research and clinical oncology. 2011;137(5):771-8.
355. Balint K, Xiao M, Pinnix CC, Soma A, Veres I, Juhasz I, et al. Activation of Notch1 signaling is required for beta-catenin-mediated human primary melanoma progression. The Journal of clinical investigation. 2005;115(11):3166-76.
356. Krebs LT, Xue YZ, Norton CR, Shutter JR, Maguire M, Sundberg JP, et al. Notch signaling is essential for vascular morphogenesis in mice. Genes & development. 2000;14(11):1343-52.
357. Ungerback J, Elander N, Grunberg J, Sigvardsson M, Soderkvist P. The Notch-2 Gene Is Regulated by Wnt Signaling in Cultured Colorectal Cancer Cells. PloS one. 2011;6(3).
358. Chalamalasetty RB, Dunty WC, Jr., Biris KK, Ajima R, Iacovino M, Beisaw A, et al. The Wnt3a/beta-catenin target gene Mesogenin1 controls the segmentation clock by activating a Notch signalling program. Nature communications. 2011;2:390.
359. Grimes CA, Jope RS. The multifaceted roles of glycogen synthase kinase 3beta in cellular signaling. Progress in neurobiology. 2001;65(4):391-426.
360. Axelrod JD, Matsuno K, ArtavanisTsakonas S, Perrimon N. Interaction between Wingless and Notch signaling pathways mediated by dishevelled. Science. 1996;271(5257):1826-32.
361. Foltz DR, Santiago MC, Berechid BE, Nye JS. Glycogen synthase kinase-3 beta modulates notch signaling and stability. Curr Biol. 2002;12(12):1006-11.
362. Alves-Guerra MC, Ronchini C, Capobianco AJ. Mastermind-like 1 Is a specific coactivator of beta-catenin transcription activation and is essential for colon carcinoma cell survival. Cancer research. 2007;67(18):8690-8.
363. Wang R, Green DR. Metabolic checkpoints in activated T cells. Nature immunology. 2012;13(10):907-15.
364. Krauss S, Brand MD, Buttgereit F. Signaling takes a breath - New quantitative perspectives on bioenergetics and signal transduction. Immunity. 2001;15(4):497-502.

365. Gerriets VA, Rathmell JC. Metabolic pathways in T cell fate and function. Trends in immunology. 2012;33(4):168-73.
366. Wang R, Dillon CP, Shi LZ, Milasta S, Carter R, Finkelstein D, et al. The transcription factor Myc controls metabolic reprogramming upon T lymphocyte activation. Immunity. 2011;35(6):871-82.
367. Halestrap AP, Denton RM. Specific inhibition of pyruvate transport in rat liver mitochondria and human erythrocytes by alpha-cyano-4-hydroxycinnamate. Biochem J. 1974;138(2):313-6.
368. Morris ME, Felmlee MA. Overview of the proton-coupled MCT (SLC16A) family of transporters: characterization, function and role in the transport of the drug of abuse gamma-hydroxybutyric acid. The AAPS journal. 2008;10(2):311-21.
369. Vander Heiden MG, Cantley LC, Thompson CB. Understanding the Warburg effect: the metabolic requirements of cell proliferation. Science. 2009;324(5930):1029-33.
370. DeBerardinis RJ, Mancuso A, Daikhin E, Nissim I, Yudkoff M, Wehrli S, et al. Beyond aerobic glycolysis: transformed cells can engage in glutamine metabolism that exceeds the requirement for protein and nucleotide synthesis. Proceedings of the National Academy of Sciences of the United States of America. 2007;104(49):19345-50.
371. Doherty JR, Cleveland JL. Targeting lactate metabolism for cancer therapeutics. The Journal of clinical investigation. 2013;123(9):3685-92.
372. Miranda-Goncalves V, Honavar M, Pinheiro C, Martinho O, Pires MM, Pinheiro C, et al. Monocarboxylate transporters (MCTs) in gliomas: expression and exploitation as therapeutic targets. Neuro-oncology. 2013;15(2):172-88.
373. Colen CB, Seraji-Bozorgzad N, Marples B, Galloway MP, Sloan AE, Mathupala SP. Metabolic remodeling of malignant gliomas for enhanced sensitization during radiotherapy: an in vitro study. Neurosurgery. 2006;59(6):1313-23; discussion 23-4.
374. Colen CB, Shen Y, Ghoddoussi F, Yu P, Francis TB, Koch BJ, et al. Metabolic targeting of lactate efflux by malignant glioma inhibits invasiveness and induces necrosis: an in vivo study. Neoplasia. 2011;13(7):620-32.
375. Cancer Research UK. A Phase I Trial of AZD3965 in Patients With Advanced Cancer. NIH Web site. http://www.clinicaltrials.gov/ct2/show/NCT01791595. Updated October 7, 2013.

376. Hussien R, Brooks GA. Mitochondrial and plasma membrane lactate transporter and lactate dehydrogenase isoform expression in breast cancer cell lines. Physiological genomics. 2011;43(5):255-64.
377. Asada K, Miyamoto K, Fukutomi T, Tsuda H, Yagi Y, Wakazono K, et al. Reduced Expression of GNA11 and Silencing of MCT1 in Human Breast Cancers. Oncology. 2003;64(4):380-8.
378. Fishbein WN, Merezhinskaya N, Foellmer JW. Relative distribution of three major lactate transporters in frozen human tissues and their localization in unfixed skeletal muscle. Muscle & nerve. 2002;26(1):101-12.
379. Bonen A, Heynen M, Hatta H. Distribution of monocarboxylate transporters MCT1-MCT8 in rat tissues and human skeletal muscle. Applied physiology, nutrition, and metabolism = Physiologie appliquee, nutrition et metabolisme. 2006;31(1):31-9.
380. Christofk HR, Vander Heiden MG, Harris MH, Ramanathan A, Gerszten RE, Wei R, et al. The M2 splice isoform of pyruvate kinase is important for cancer metabolism and tumour growth. Nature. 2008;452(7184):230-3.
381. Vander Heiden MG, Locasale JW, Swanson KD, Sharfi H, Heffron GJ, Amador-Noguez D, et al. Evidence for an alternative glycolytic pathway in rapidly proliferating cells. Science. 2010;329(5998):1492-9.
382. Herzog RI, Jiang L, Herman P, Zhao C, Sanganahalli BG, Mason GF, et al. Lactate preserves neuronal metabolism and function following antecedent recurrent hypoglycemia. The Journal of clinical investigation. 2013;123(5):1988-98.
383. Doyle A, McGarry MP, Lee NA, Lee JJ. The construction of transgenic and gene knockout/knockin mouse models of human disease. Transgenic research. 2012;21(2):327-49.
384. Rosenthal N, Brown S. The mouse ascending: perspectives for human-disease models. Nature cell biology. 2007;9(9):993-9.
385. Koretsky AP. Investigation of Cell Physiology in the Animal Using Transgenic Technology. Am J Physiol. 1992;262(2):C261-C75.
386. Roebroek AJ, Wu X, Bram RJ. Knockin approaches. Methods in molecular biology. 2003;209:187-200.

387. Evans MJ, Kaufman MH. Establishment in Culture of Pluripotential Cells from Mouse Embryos. Nature. 1981;292(5819):154-6.
388. Thomas KR, Capecchi MR. Site-Directed Mutagenesis by Gene Targeting in Mouse Embryo-Derived Stem-Cells. Cell. 1987;51(3):503-12.
389. Maniatis T. Targeting in mammalian cells. Nature. 1985;317(6034):205-6.
390. Hall B, Limaye A, Kulkarni AB. Overview: generation of gene knockout mice. Current protocols in cell biology / editorial board, Juan S Bonifacino [et al]. 2009;Chapter 19:Unit 19 2 2 1-7.
391. Lewandoski M. Conditional control of gene expression in the mouse. Nature reviews Genetics. 2001;2(10):743-55.
392. Skarnes WC, Rosen B, West AP, Koutsourakis M, Bushell W, Iyer V, et al. A conditional knockout resource for the genome-wide study of mouse gene function. Nature. 2011;474(7351):337-42.
393. Brauchi S, Rauch MC, Alfaro IE, Cea C, Concha, II, Benos DJ, et al. Kinetics, molecular basis, and differentiation of L-lactate transport in spermatogenic cells. American journal of physiology Cell physiology. 2005;288(3):C523-34.
394. Meier ID, Bernreuther C, Tilling T, Neidhardt J, Wong YW, Schulze C, et al. Short DNA sequences inserted for gene targeting can accidentally interfere with off-target gene expression. FASEB journal : official publication of the Federation of American Societies for Experimental Biology. 2010;24(6):1714-24.
395. Wang Z, Jaenisch R. At most three ES cells contribute to the somatic lineages of chimeric mice and of mice produced by ES-tetraploid complementation. Developmental biology. 2004;275(1):192-201.
396. Park IH, Arora N, Huo H, Maherali N, Ahfeldt T, Shimamura A, et al. Disease-specific induced pluripotent stem cells. Cell. 2008;134(5):877-86.

Appendix I:

Generation of *Mct1* conditional knockout mouse model

Introduction:

MCT1's multiple roles in cellular metabolism, drug transport and many pathological diseases make it an attractive target for intensive research. A better understanding of this monocarboxylate transporter's function in different biological contexts not only expands our knowledge of alternative fuels such as lactate, acetate and β-Hydroxybutyrate (BHB), but also facilitates the progression of deciphering the recent discovery of lactate's complex but poorly understood functional roles in diseases including cancer, amyotrophic lateral sclerosis and diabetes (38, 371, 382). Based on these research findings, therapeutic methods can be developed for debilitating disorders. For example, reprogrammed metabolism research found in cancer cells leads to the finding of MCT1 as a critical factor in maintaining tumorigenesis by exporting or importing lactate (74, 75, 87, 185); thus multiple MCT1 inhibitors have been proposed and employed as potential therapeutic intervention in treating cancer, such as the highly potent AZD3965 that is now under Phase I clinical trials for advanced solid tumors, prostate cancer, gastric cancer and diffuse-large B cell lymphoma (375). As a consequence, continued bulky research on MCT1 is necessary and requires combined approaches as well as interdisciplinary efforts.

Genetically modified mouse models have been studied for a variety of genes related to human diseases (383, 384). Approaches to study an *in vivo* gene's function include but not limited to: (1) Transgenic expression (385), where exogenous coding DNA sequence is injected into pronuclei of zygote-stage embryos that are implanted back later into pseudopregnant recipient females to develop into newborns; (2) gene knockin (386), where an endogenous genomic locus of interest is replaced by exogenous targeting DNA vector carrying a modified version of the same gene; and (3) gene knockout (387-389), which is similar to knockin approach, except that the genomic locus of interest is deleted or inactivated. Knockout mouse has become a valuable tool to discern the role of a gene during embryonic development, in normal physiological homeostasis as well as genetics diseases (390). More importantly, it allows researchers to delete and investigate genes in a tissue-dependent manner, where that particular gene is only

disrupted in certain types of cells. This can be achieved by *Cre-LoxP* conditional knockout system driven by the function of a cell type specific promoter (391).

Gene knockout takes advantage of homologous recombination between the genomic locus of interest (target gene) and exogenous targeting vector in embryonic stem (ES) cells. The vector is engineered in a way that it now contains a modified version of the same gene. Specifically, the new sequence is identical to the original gene as well as its immediate neighboring DNA fragments (5' and 3' homologous arms), except that the protein coding sequence between the two homologous arms has been changed so substantially that the original gene's function is inactivated (knocked-out). After introducing the targeting vector into ES cells, two homologous recombination events can happen at both the 5' arm and 3' arm sites, swapping DNA content between the endogenous locus on a chromosome and that residing on the vector. In this case, the original allele has been replaced with our modified/knocked-out version. These genetically engineered ES cells will be selected based on their resistance to neomycin, a capacity that is conferred by the Neo resistant gene originally present on and brought into genome by the targeting vector. Modified ES cells will then be injected into blastocysts derived from another mouse strain that exhibits a different coat color. As a result, any pups developed from those unique blastocysts will be chimeras, as demonstrated by their coats with mixed colors, and serve as founder strains. If their reproductive organs were developed from the genetically altered ES cells and they are crossbred with wild type animals, those chimeras can produce offspring that contain one copy of the knocked-out gene in their cells. When these heterozygous offspring are interbred, some of their progenies will inherit the knocked-out alleles from both parents and become homozygous knockout animals (Figure A-1). For conditional knockout, one or more exons of the target gene are flanked by two *LoxP* sites, 34bp palindromic DNA sequence. They can be recognized by *Cre* recombinase to initiate crossover between them. The ending result is the excision of exon(s) in between. As a consequence, mice carrying homozygous flanked exon(s) actually contain functional alleles of the target gene, unless they are challenged by the expression of *Cre* recombinase. Conditional knockout is conferred by mating those *LoxP* animals to others that only express *Cre* in certain tissues, like neurons, astrocytes or endothelial cells (Figuref A-2).

Although MCT1 has recently received intensive research attention because of its critical roles in cellular metabolism and therapeutic drugs transport, animal models with modified MCT1 gene are a limiting factor for further understanding of this important transporter. Indeed, very recently, only *Mct1*+/- heterozygous mice have been reported, where the gene's function in oligodentricytes during neurodegeneration was studied (38). Thus, we decided to generate homozygous *Mct1* conditional knockout (*Mct1*-/-) mouse model that would greatly advance research progression on deciphering this critical monocarboxylate transporter's function *in vivo*.

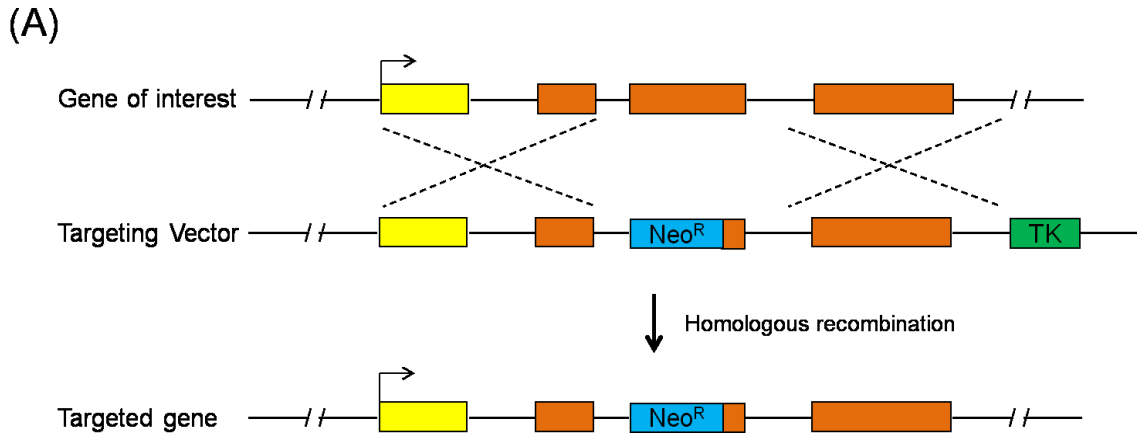

Figure A-1: Generation of knockout mice. (A) Gene targeting in ES cells through homologous recombination. The presence of neomycin resistant gene (Neo^R) in the vector replaces the original gene of interest (*Goi*)'s critical exon and inactivates its function. For detailed information, see text. (Panel B and its legends are shown on next page)

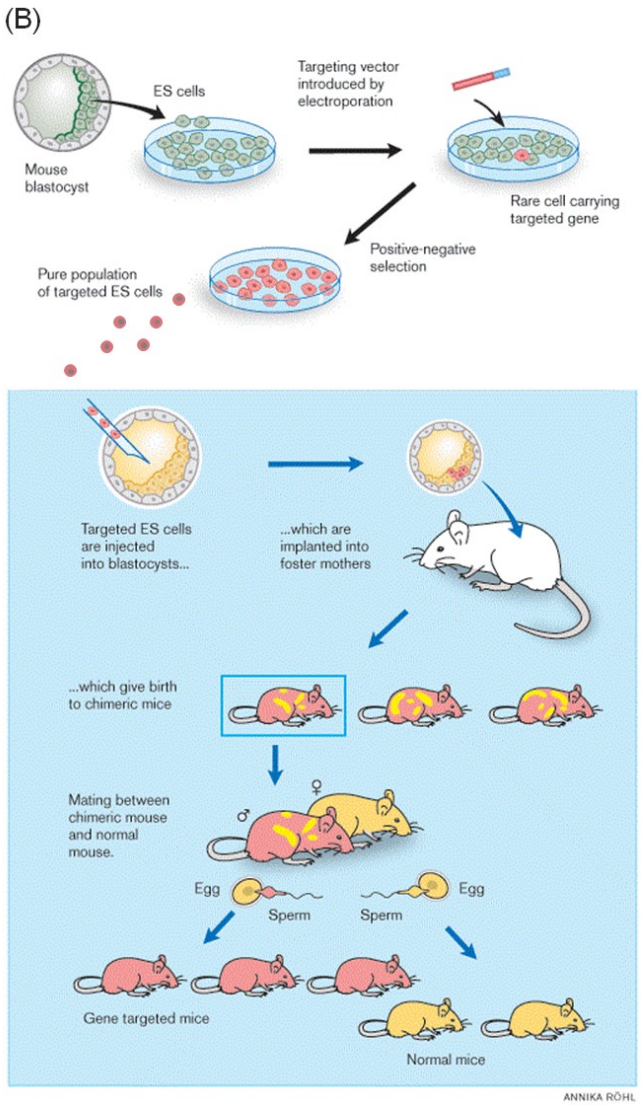

(B) Flow-chart of targeting ES cells in culture and subsequent breeding for homozygous null animals (Adapted and modified from © The Nobel Committee for Physiology Illustration: Annika Röhl). Briefly, identified positive ES cells from one strain (Red) with one modified allele are injected into blastocysts of another strain (Yellow). Those blastocysts with mixed ES cells are then transplanted into pseudopregnant females to generate chimeras in the next generation. Those male chimeras are crossbred with wild type females of yellow strain. Progenies (*Goi*$^{+/-}$) derived from fertilization of red sperms that contain genetic modification and yellow oocytes that are wild type, are then identified and subject to interbred to generate homozygous offspring (Not shown in the illustration).

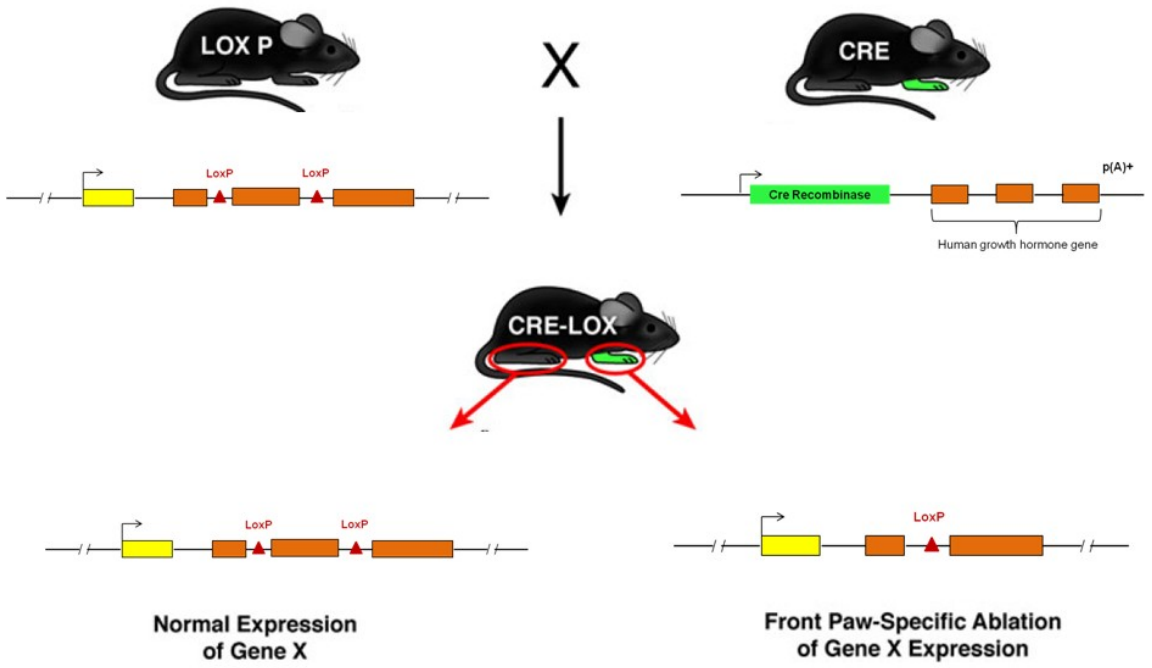

Figure A-2: Generation of conditional knockout mice (Adapted and modified from (383)). Homozygous mice with two *LoxP* sites flanking the critical exon in both alleles are generated from Figure A-1. In this case, the gene of interest can function normally because all the coding sequences are intact. In addition, a specialized transgenic mouse strain that express *Cre* recombinase (bright green) under the control of a tissue specific promoter (front paw specific in this example), is introduced to mate with the *LoxP* flanked animals. As a result, *Cre* recombinase is only expressed in front paw, thus the *Goi* is only deleted in a front paw-specific manner (indicated by green paw).

Materials and Methods

Mouse embryonic fibroblasts (MEFs) culture and inactivation. MEFs were cultured in 100mm x 20mm dishes (Corning #430167) within a humidified incubator at 37^{o}C supplemented with 5% CO_2.The growth medium was composed of DMEM (high glucose, Na Pyruvate and L-glutamine; Invitrogen #11960-044), 10% FBS (Atlanta Biologicals; #S10250), 1X Non-Essential Amino Acids (NEAA; Invitrogen #11140-50) and 1X L-

Glutamine (Invitrogen #25030-081). For inactivation, confluent MEFs were washed with 1X PBS (Invitrogen; #14190-144) once and then treated with 10μg/ml mitomycin-C (Sigma-Aldrich; #M4287) for 4h. After that, old medium was removed and cells were rinsed twice with 1X PBS before they were trypsinized (Invitrogen; #25200-056), quenched with growth medium and spun down to pellet. Inactivated MEFs were resuspended in ice-cold freezing medium (growth medium+10% DMSO (Sigma-Aldrich; #D2650)) to the concentration of $1x10^7$ cells/ml, placed into -80^oC freezer and then transferred to liquid nitrogen tank the next day for future use.

Embryonic stem (ES) cells culture. CJ7 ES cells from mouse strain 129 were provided by University of Minnesota Mouse Genetics Laboratory Shared Resource facility. Inactivated MEFs were first plated into 100mm x 20mm dishes (Corning #430167) as feeder cells at a concentration of 200,000 cells/ml two days in advance of the day 10,000 cells/ml ES cells were thawed and seeded. ES cells were cultured within a humidified incubator at 37^oC supplemented with 5% CO_2.The ES growth medium was composed of DMEM (high glucose, Na Pyruvate and L-glutamine; Invitrogen #11960-044), 17% FBS (Atlanta Biologicals; #S10250), 1X Non-Essential Amino Acids (NEAA; Invitrogen #11140-50), 1X L-Glutamine (Invitrogen #25030-081), 22nM (1X) β-Mercaptoethanol (Invitrogen; #21985-023), 2mM HEPES (Sigma # H6147) and 1000 units/ml LIF (Millipore # ESG007). ES cells were passaged or frozen down at 1:6 when they became confluent (40-50%).

Targeting vector transformation/preparation. *Mct1* targeting construct was purchased from European Conditional Mouse Mutagenesis Program (EUCOMM) (#40919), after which the plasmid was transformed into the MAX Efficiency DH-10β competent *E.coli* cells (Invitrogen; #18297-010) according to the manufacturer's instruction. Specifically, less than 20ng DNA was incubated with the thawed 50μl competent cells in each tube on ice for 30 minutes, heat-shocked for 30 seconds in a 42^oC water bath, returned on ice for additional 5 minutes before they were mixed with 250μl S.O.C. medium (Invitrogen; #15544-034) in a Falcon Round-Bottom Polystyrene tube (Fisher Scientific; #14-959-1B) and shaken at 225rpm (at 37^oC) for 1 hour. Then, 50μl transformants were pipetted onto a kanamycin (Fisher Scientific; #BP906-5) selective agar plate (15g/L agar, 10g/L

Tryptone, 10g/L NaCl, 5g/L Yeast Extract and 50μg/ml kanamycin) and spread out evenly across the surface using a sterile glass rod spreader. The whole plate was put into a 37^{o}C oven for 24h.

Candidate colonies that grew out on the plate were picked and inoculated into separate Falcon Round-Bottom Polystyrene tubes that had 2ml LB medium (10g/L Tryptone, 10g/L NaCl and 5g/L Yeast Extract), supplemented with 50μg/ml kanamycin. They were shaken at 37^{o}C, 225rpm for 16-18 hours. Plasmid DNA from each falcon tube was isolated by the MiniPrep Kit (Qiagen; #27104) according to its instruction. The integrity of each DNA preparation was verified using restriction enzymes digestion. The colony that passed the initial screen was subjected to 200ml LB culture supplemented with kanamycin at 37^{o}C, 225rpm for 16-18 hours. Its DNA was prepared using the PureYield™ Plasmid Maxiprep System (Promega; #A2392). The quality of this final DNA preparation was further confirmed by sequencing (University of Minnesota Genomics Center).

Restriction enzymes (REs) digestion. REs of EcoRI (Promega; #R6011), AvrII and SpeI (New England Biolabs; #R0174 and #R0133) were used separately to screen for *Mct1* targeting vectors after plasmid DNA MiniPreps from candidate colonies as well as to verify the integrity of final DNA MaxiPrep. The expected band patterns (in bp) for each enzyme after complete digestion of *Mct1* targeting vector are listed: AvrII (8134, 7014, 2580, 1856, 831); EcoRI (12740, 2937, 2042, 1772, 882) and SpeI (8644, 4523, 4069, 1864, 1315). The reaction conditions used were as followings: EcoRI in a 20μl volume with 1Xbuffer H, 1μg DNA, 10U RE and 0.1μg/ml BSA; SpeI in a 25μl volume with 1Xbuffer 4, 1μg DNA, 10U RE and 0.1μg/ml BSA; AvrII in a 25μl volume with 1Xbuffer 4, 1μg DNA and 10U RE. All the reactions were carried out in a 37^{o}C water bath for at least 4 hours. All the digests were analyzed on 1% agarose gels.

Targeting plasmid DNA linearization and precipitation. SgrAI (New England Biolabs; #R0603) was used to linearize the *Mct1* targeting vector by incubating 10μg DNA in a final 50μl reaction volume supplemented with 1Xbuffer 4 and 10U enzyme at 37^{o}C for 1h. The same procedures were repeated for additional 30μg DNA in 3 separate tubes, making the final amount of linearized DNA to be 40μg. All the digests were pooled

together to make a total volume of 200µl, which was then mixed with a final concentration of 0.3M NaAc/70% ethanol and incubated for 30 minutes at -20^{o}C. After that, the tube was centrifuged at 13,000rpm for 15 minutes at 4^{o}C. The resulting supernatant was discarded and pellet was washed three times with ice-cold 70% ethanol followed by centrifugation at 13,000rpm for 5 minutes each time. After discarding the 70% ethanol supernatant, the DNA pellet was washed with ice-cold 100% ethanol, dried in a sterile hood and redissolved in 25µl 1X PBS at 4^{o}C overnight. 0.2µg of the precipitated DNA was subjected to electrophoresis on a 0.5% agarose gel to check the successful linearization before being electroporated into ES cells.

Agarose gel electrophoresis. DNA electrophoresis analysis was performed using SeaKem agarose gel (Lonza; #50152) supplemented with ethidium bromide in 1X TAE running buffer (40mM Tris, 20mM acetic acid, and 1mM EDTA), at various densities of 1.5% for the PCR products of mycoplasma detection, 1% for restriction enzyme digestions, and 0.5% for linearized DNA vector confirmation as well as LA PCR products. All the experiments were run at 70V until the blue dye reached near the bottom of the gel, after which the whole gel was visualized under a UV imager.

Electroporation. Six 100mm x 20mm dishes were first coated with 0.1% gelatin solution (Sigma-Aldrich; #G1393) for 2 hours, washed with H_2O three times and dried in the hood for future use. Upon confluent (~50%), ES cells were trypsinized off the culture dish, spun to pellet and resuspended in 1X PBS (Ca^{2+}-, Mg^{2+}-; Invitrogen; #14190-144) to generate a single-cell solution of 1x10^{7} cells/ml. Then 8 million ES cells were mixed well and incubated with either 20µg linearized *Mct1* targeting vector DNA or equal amount of 1X PBS control in a 0.4cm cuvette. After standing at room temperature for 5 minutes, electroporation was performed at 250V/500µF with exponential curve setting on the Gene Pulser Xcell system machine (Bio-Rad; #165-2660), according to the manufacturer's instruction. The contents of the cuvette with DNA and half of the contents from the control cuvette were equally divided into four and two gelatin-coated dishes, respectively, which had inactivated MEFs plated already beforehand. 24 hours later, the plates started feeding with ES growth medium supplemented with 250µg/ml G418

(Sigma-Aldrich; #G8168) for selecting positive colonies. Change for fresh medium+G418 daily until all the cells from the control plates died out.

Picking candidate colonies. The picking process was performed on a cell culture light microscope sitting in a Laminar hood. Specifically, cells were deprived of old selective medium, washed once with and then kept in ES cell qualified 1X DPBS (Millipore; #BSS-1005-B). A positive colony was first separated from the adherent MEFs layer by physically scratching and breaking the MEFs feeder cells surrounding it using a sterile 10µl pipette tip. The subsequent floating loose colony was then pipetted up and transferred into a well of V-bottom 96 well plates (Sarstedt; #821583001) that contained 25µl ice-cold 0.25% trypsin (Invitrogen; #25200-056). The same steps were repeated until all the colonies from that dish had been picked, or 24 wells of a V-bottom plate had been filled up. The ES cells dish was replaced with fresh medium and returned back into the incubator if needed. The V-bottom 96-well plate with colonies in trypsin was incubated at 37^{o}C for 10 minutes; then the colonies were pipetted up and down until they disassociated into single cells. After that, these single cell suspensions were dispersed evenly into corresponding wells of a Corning Costar cell culture flat-bottom 96-well plate (Sigma-Aldrich; #CLS3585) that had already been gelatin-coated and seeded with 1.2x10^{4} inactivated MEF feeders in 150µl ES growth medium with G418. The growth medium was renewed daily until ES cells became confluent.

Freezing colonies and establishing cultures for DNA isolation. ES cells growing in flat-bottom 96-well plates reaching confluence were rinsed once with 1X PBS and incubated with 40µl 0.25% trypsin at 37^{o}C for 10 minutes, with pipetting up and down at the end to break up clumps into single cells. They were then quenched by 60µl additional growth medium. 33µl of the trypsinized ES cells was transferred to each of the duplicate flat-bottom 96-well plates that had 33µl ice-cold 2X freezing medium (ES growth medium with 20% DMSO) in the wells. Those duplicate plates were then stored in well sealed foam-box at -80^{o}C undisturbed. The remaining 33µl ES cells were mixed with 100µl fresh growth medium and put back into 37^{o}C incubator to grow to high densities for DNA isolation.

DNA preparation from 96-well plates. When ES cells grew confluent (100%), they were decanted of the old medium and washed twice with 1X PBS. Then they were incubated with 50µl lysis buffer (10mM Tris pH 7.5, 10mM EDTA pH 8.0, 10mM NaCl and 0.5% Sarcosyl (Sigma-Aldrich; #L7414)) supplemented with 1mg/ml proteinase K (Roche; #03115836001) within a humidified container at 55^{o}C overnight. Then 100µl of NaCl/Ethanol mixture (100mM NaCl and 100% Ethanol) was added into each well and the whole plate was incubated at -20^{o}C for 30 minutes or until precipitated DNA became visible. After washing three times with 70% ethanol and paper blotted by the end of the third wash, the plate was dried in hood for 15 minutes. 35µl TE buffer (10mM Tris, 1mM EDTA, pH 8.0) was then added to dissolve precipitated DNA in each well at 4^{o}C overnight.

Long range LA PCR screening. The correct targeting of *Mct1* at its genomic locus was confirmed by long range PCR (LA PCR) from both 5' and 3' homologous ends. The expected PCR product sizes after homologous recombination are 10,914bp for 5' end and 7,641bp for the 3' end. The primers used here are listed as followings: 5' forward primer: GGGAGTTACTTAGGACTCGTGGCATACCCGCCCAG, 5' reverse primer: GGACGACGACAGTATCGGCCTCAGGAAGATCGCAC, 3' forward primer: CGATGCCTGCTTGCCGAATATCATGGTGGA, 3' reverse primer: GGCGACTGTGCAGCTTTCATCGTCTCCTTT. The reaction was carried out in a final 50µl volume that comprised of 1X LA PCR buffer II, dNTP mixture (0.4mM each), forward primer (0.2µM), reverse primer (0.2µM), DNA template (<1µg) and 2.5U *Takara LA Taq* (Takara; #RR002). The cycling parameters used were: 94^{o}C 1min, 30 cycles of 94^{o}C 30s, 68^{o}C 10min and 72^{o}C 15min, 72^{o}C for 15min and 4^{o}C hold.

Expansion of positive ES colonies. 100µl pre-warmed ES medium was added into each well of the 96-well plates containing frozen ES cells from the -80^{o}C freezer. Then the whole plate was put into a pre-warmed tupperware/H_2O bath inside 37^{o}C incubator until the cells were completely thawed. All the contents were transferred into a 24-well MEF feeder plate filled with 2ml ES medium per well. Once those cells became confluent (50%), they were trypsinized and transferred into a 6-well MEF feeder plate filled with 3ml ES medium per well, after which they were further transferred into 100mm dishes

with MEF feeders plated beforehand. When confluent, those ES cells were passaged at 1:6 and stored in liquid nitrogen for future use. ES growth medium was renewed daily for all the cultures.

Mycoplasma detection, karyotyping analysis and blastocysts injection. Mycoplasma detection was performed using the VenorGem PCR-based Mycoplasma Detection Kit (Sigma-Aldrich; #MP0025) according to its instruction. Specifically, positive ES colonies were cultured without antibiotics to full confluence (100%) without changing medium in between in order to enrich possible mycoplasma in the supernatant, which was heated for 5min at 95^{o}C and served as DNA template. The PCR reaction volume was 25µl consisting of a Mastermix (provided by and prepared from the kit), 1 unit Jumpstart Taq polymerase (Sigma-Aldrich; #D9307) and a template being either H_2O (negative control), or the provided positive control DNA, or our sample supernatant. The thermal cycling parameters were: 94^{o}C for 2min, 39 cycles of 94^{o}C 30s, 55^{o}C 1min and 72^{o}C 30s, followed by 4^{o}C hold.

Karyotyping analysis of the positive ES colonies was conducted by University of Minnesota's Cytogenomics Laboratory. Blastocysts injection of ES cells was served by the Mouse Genetics Laboratory in the University of Minnesota.

Western blotting. Protein samples were prepared by solubilizing cells in 1X lysis buffer (63mM Tris pH=6.8, 2% SDS, 10% glycerol, 5% beta-mercaptoethonal, 1X Roche protease inhibitor cocktail and 1mM PMSF) for 5 minutes, followed by centrifugation at 13,000g for 8 minutes at 4^{0}C. The supernatant was collected and subjected to gel electrophoresis and subsequent MCT1 immunodetection as described in the Materials & Methods section of chapter III.

Results:

i. Cloning of *Mct1* targeting vector in competent *E.coli*.

In order to prepare the *Mct1* targeting vector after obtaining from EUCOMM, it was transformed into competent DH10β *E.coli* cells on kanamycin selective agar plates. The schematic diagram of the vector is shown in Figure A-3. The presence of a kanamycin resistant gene within the plasmid backbone allows its transformants to survive kanamycin stress. Four positive colonies were picked and their plasmid DNA was prepared for restriction enzymes (REs) digestions to analyze its integrity. Three REs were used for each clone: EcoRI, SpeI and AvrII. The expected banding pattern for each enzyme is summarized in Table A-1. Our results of all the REs digestions analyzed on 1% agarose gel indicated that colony #4 was the correct colony containing the expected *Mct1* targeting vector (Figure A-4, A-C). Subsequently, this colony was cultured in a larger volume and its plasmid DNA was isolated by MaxiPrep, the quality of which was finally confirmed by the same enzymes (Figure A-4, D) as well as by sequencing.

Table A-1: The expected banding patterns of REs on *Mct1* targeting vector

Enzyme name	Banding pattern (in bp)
EcoRI	12740, 2937, 2042, 1772, 882
SpeI	8644, 4523, 4069, 1864, 1315
AvrII	8134, 7014, 2580, 1856, 831

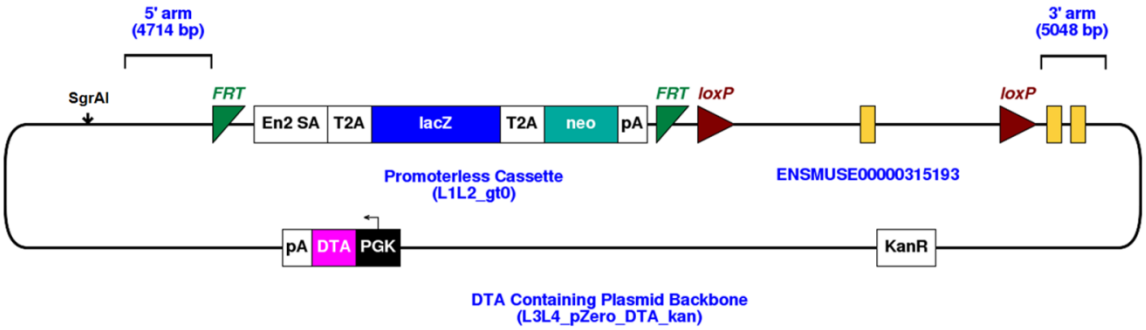

Figure A-3: Schematic representation of *Mct1* targeting vector (adapted and modified from EUCOMM). The total size of the vector is 20,415bp. SgrAI is the enzyme used to linearize the whole vector for electroporation into ES cells. 5' arm and 3' arm contain sequences identical to corresponding *Mct1* genomic loci that allow homologous recombination. *FRTs* are short DNA fragments that, upon exposure to *Flp* recombinase, align with each other and recombine to delete sequences in between that are referred to as "promoterless cassette" within the vector. This cassette contains "neo" gene that gives cells resistance to the drug G418 and serves as the basis of positive selection for correctly targeted ES cells. *LoxP* sites, like *FRTs*, each contains two sets of short palindromic sequences and also recombines with each other to delete DNA fragment in between in the presence of *Cre* recombinase. The three yellow boxes represent exons of *Mct1* gene, with the critical first one being flanked by *LoxP* sites. KanR is the resistant gene that allows bacterial cells carrying the vector to survive kanamycin selection. PGK-DTA-pA cassette is the negative selecting fragment, which eliminates positive ES colonies that are not due to homologous recombination.

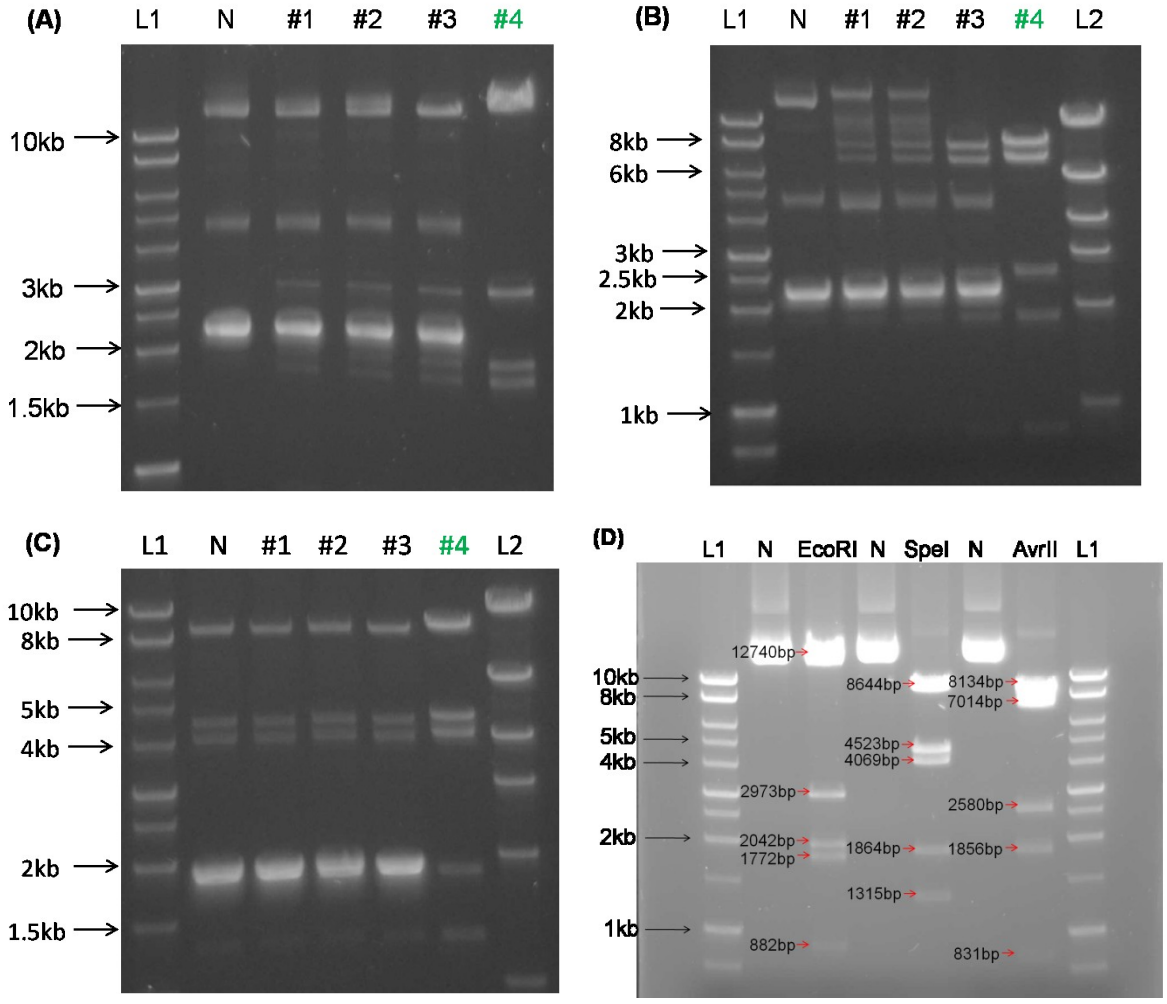

Figure A-4: Banding patterns of *Mct1* targeting vector prepared from candidate colonies after restriction enzymes digestions. The vector was isolated from four individual colonies that survived kanamycin selection, and all the four DNA samples were then cut separately by EcoRI (A), AvrII (B) and SpeI (C). The digests were analyzed on 1% agarose gels. The expected bands after each digestion are summarized in Table A-1. Accordingly, only colony #4 (shown in green) showed correct bands after digestion by each of the three enzymes and was considered as the right one. The further MaxiPrep DNA from this colony #4 was verified by digestions using the same individual enzymes as indicated in panel (D). L1: 1kb DNA ladders (Promega; #G5711); L2: Mass DNA 1kb ladders (NEB; #N3237); N: Vector DNA not cut.

ii. MCT1 protein is expressed in both mouse embryonic fibroblasts (MEFs) cells and 129 embryonic stem (ES) cells.

The promoterless selective cassette within *Mct1* targeting vector (Figure A-3) enables correctly targeted ES cells resistant to G418 selection with the help of neo gene, whose successful expression after homologous recombination requires the functionality of endogenous promoter of the gene being targeted, in our case, *Mct1*. As a result, the protein expression status of MCT1 in 129 ES cells was first examined by western blot. MEFs were expanded and inactivated by mitomycin C before they were used as feeders for ES cells culture. Then each of two identical MEF dishes was either seeded with 129 ES cells or left intact as control. When ES cells became 50% confluent, both dishes were incubated with 1X lysis buffer; then equal volumes of samples were subjected to SDS-PAGE electrophoresis, followed by immunoblotting against MCT1. As shown in Figure A-5, MCT1 protein (~45kD) has trace expression in MEF feeder cells and more abundant expression in MEFs seeded with ES cells, demonstrating that *Mct1* gene is transcribed in 129 ES cells. This result indicates that targeting *Mct1* gene in 129 ES cells using our vector is feasible.

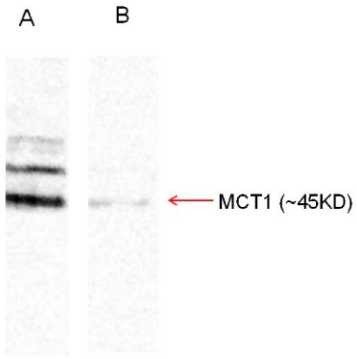

Figure A-5: MCT1 expression in MEFs and 129 ES cells. Two 100mm dishes were first plated with MEFs and then seeded with either 129 ES cells (A) or left intact (B). Cells from the two dishes were lysed in 1X lysis buffer and subjected to SDS-PAGE with equal sample volume loading, followed by immunoblotting against MCT1. MEFs showed baseline expression of MCT1 (B), whereas the co-culture with ES cells robustly increased its expression level (A), demonstrating that *Mct1* gene is transcribed in 129 ES cells.

iii. Gene targeting and identification of positive ES colonies

Linearized plasmid DNA tends to run slower on agarose gel than uncut control, because the latter usually possesses supercoil conformation and migrates faster. In order to target the *Mct1* genomic locus, the targeting vector was first linearized (Figure A-8), purified by NaAc/Ethanol precipitation and electroporated into cultured 129 ES cells. The presence of neo gene only allows ES cells that obtained the selective cassette from *Mct1* targeting vector to grow under G418 selection, whereas the expression of diphtheria toxin A (or DTA) gene in the vector backbone serves as a negative selection and eliminates false positive colonies that were generated independent of homologous recombination. After a week, 32 candidate colonies were picked up and grown in separate wells of a 96-well plate. When they grew confluent, all the colonies were carefully stored in -80^{o}C freezer for future use, while in the mean time, their individual genomic DNA was prepared and subjected to long range LA PCR for screening positive colonies. Correct targeting through homologous recombination replaces the portion of DNA fragment between the 5' and 3' homologous arms of genomic DNA with that in the targeting vector, creating new 5' and 3' genetic ends (Figure A-6). For LA PCR screening at 5' end, the forward primer anneals upstream of the 5' homologous arm, whereas reverse primer pairs with sequence from the selective cassette that is unique to the targeting vector but now present in the ES genome. The same thing is true for 3' screening although its forward and reverse primers anneal to the opposite direction of that at 5' end. In the wild type 129 ES DNA, neither of the two primer pairs is supposed to generate any PCR products (Figure A-7). Our LA PCR results indicated that two candidate colonies, named 3^{o} 1-D and 3^{o} 1-E (derived from their locations in the 96-well plate), showed correct genetic modification, generating a PCR band of ~10.9kb at 5' end and another band of ~7.6kb at the 3' end (Figure A-9). Those two colonies were thus thawed and expanded in culture from 24-well plates to 6-well plates and eventually to 100mm X 20mm dishes.

iv. Quality control tests of positive colonies

The quality of our positive ES colonies for blastocysts injection was investigated on three levels: morphology, mycoplasma and karyotype. First, these two colonies were cultured

on MEF feeder cells and both of them exhibited standard morphological hallmarks of undifferentiated state: compact, multicelluar colonies of cells with cobblestone shape, a high nucleus-cytoplasm ratio and a distinct colony border (Figure A-10). Then, the absence of mycoplasma contamination, which significantly decreases the germline transmission potency of contaminated ES cells, was confirmed by PCR using primers that are specific to the conserved 16S rRNA coding region in the mycoplasma genome and sufficient for detecting all the 24 known species. Enriched cell culture supernatant was collected and used as DNA template. Our results indicated the absence of any mycoplasma contamination in either of the two positive colonies (Figure A-11). After that, karyotyping service of the two colonies was conducted by a cytogenomics lab (University of Minnesota-Minneapolis). 20 metaphases were completely analyzed by G-banding for each of the colonies. Although 3^o 1-E cells showed no abnormalities on any of the 40 chromosomes (19 pair + X + Y), a small deletion within the proximal long arm of chromosome 17 was observed in 3^o 1-D colony (Figure A-12 A). Thus, 3^o 1-E was the colony good for blastocysts injection.

v. Blastocytes injection and breeding

At least 75 blastocysts were injected with our genetically modified 3^o 1-E ES cells and implanted into at least 5 pseudopregnant recipients. A total of 8 chimeric mice (6 males and 2 females) were generated afterwards, however none of them showed signs of germline transmission after breeding with C57/B6 mice.

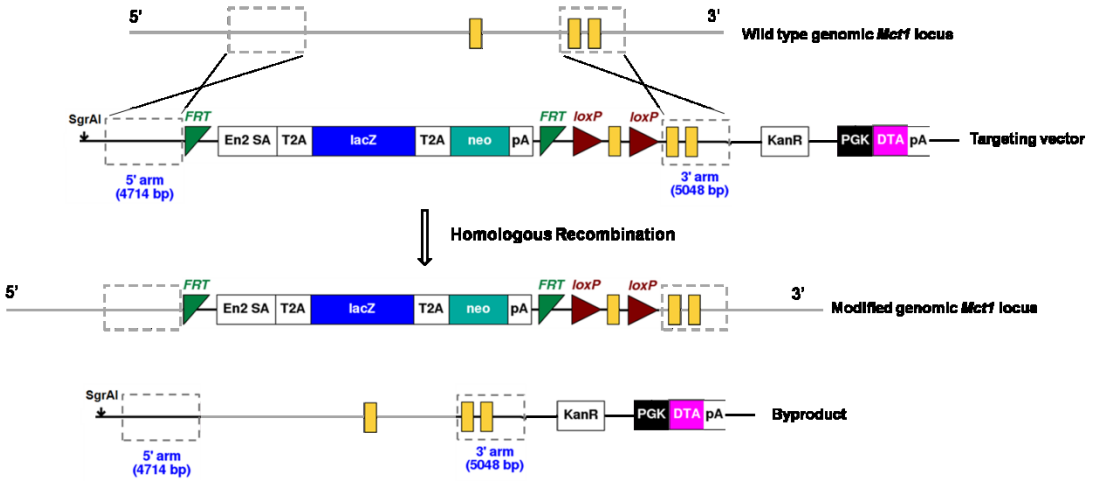

Figure A-6: Gene targeting scheme. The endogenous 129 ES cells genomic DNA is represented as solid grey lines, with polarity indicated at 5' and 3' ends, whereas DNA sequence from the targeting vector is represented in black lines. The homologous arms are enclosed by dashed grey lines, with 5' arm on the left and 3' arm on the right. Exons are represented by yellow boxes. The critical exon is flanked by *LoxP* sites. After homologous recombination, double crossovers (as indicated by crossing lines) happen between endogenous DNA and linearized targeting vector, one at the 5' end and the other at 3' end, which swaps the fragment between the two homologous arms in wild type DNA with that from the vector, generating the modified genomic *Mct1* sequence.

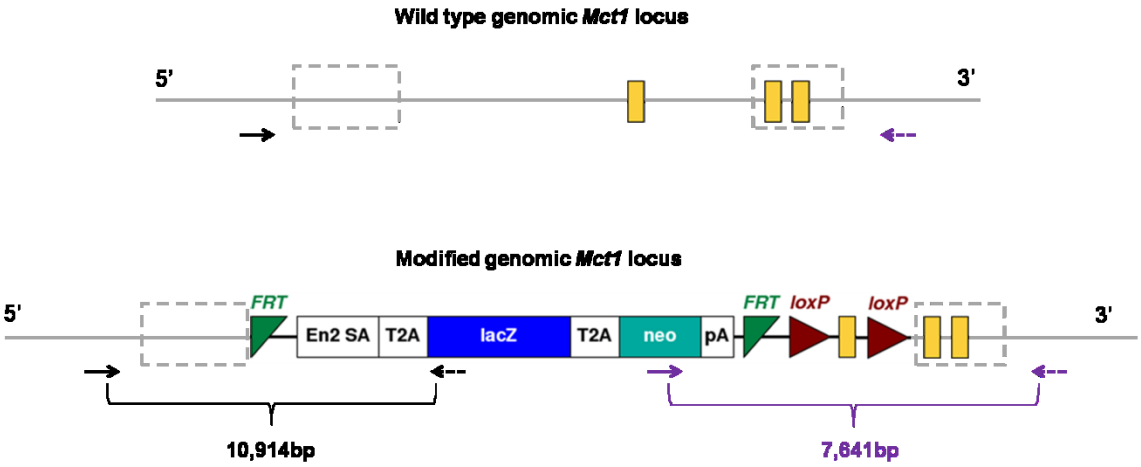

Figure A-7: Long range LA PCR. Both the 5' and 3' ends are screened by LA PCR for positive homologous recombination. At 5' end, its forward primer (→) anneals upstream of 5' homologous arm, whereas the reverse primer (<---) pairs with sequence from the targeting vector after correct homologous recombination, generating a PCR product of 10,914bp. For the 3' end, its reverse primer (<---) anneals downstream of 3' homologous arm, whereas the forward primer (→) pairs with sequence from targeting vector after correct homologous recombination, generating a PCR product of 7,641bp. Neither of the two primer pairs amplifies any DNA fragments in the wild type genomic locus.

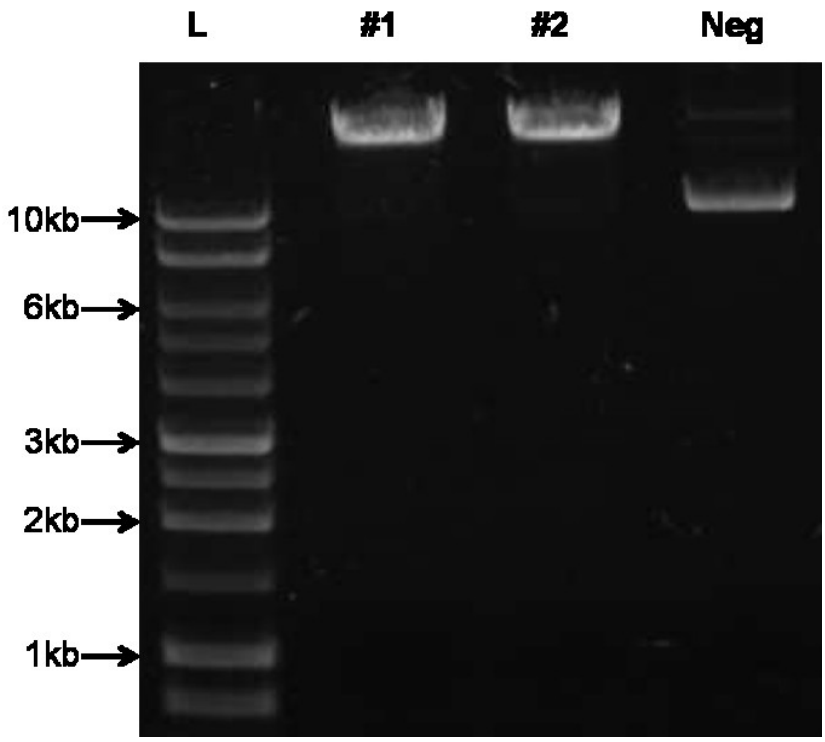

Figure A-8: Linearized *Mct1* targeting vector by the restriction enzyme SgrAI. Our *Mct1* targeting vector was cut once and thus linearized by SgrAI, which was demonstrated by electrophoresis on a 0.5% agarose gel. The supercoil conformation, a key structural characteristic of native plasmids, caused a faster migration on the gel (Neg) than linearized DNA of the same size (lane #1 and lane #2). L: 1kb DNA ladders; #1 and #2: duplicate loadings of digested DNA by SgrAI; Neg: *Mct1* targeting vector negative control without any restriction enzyme digestion.

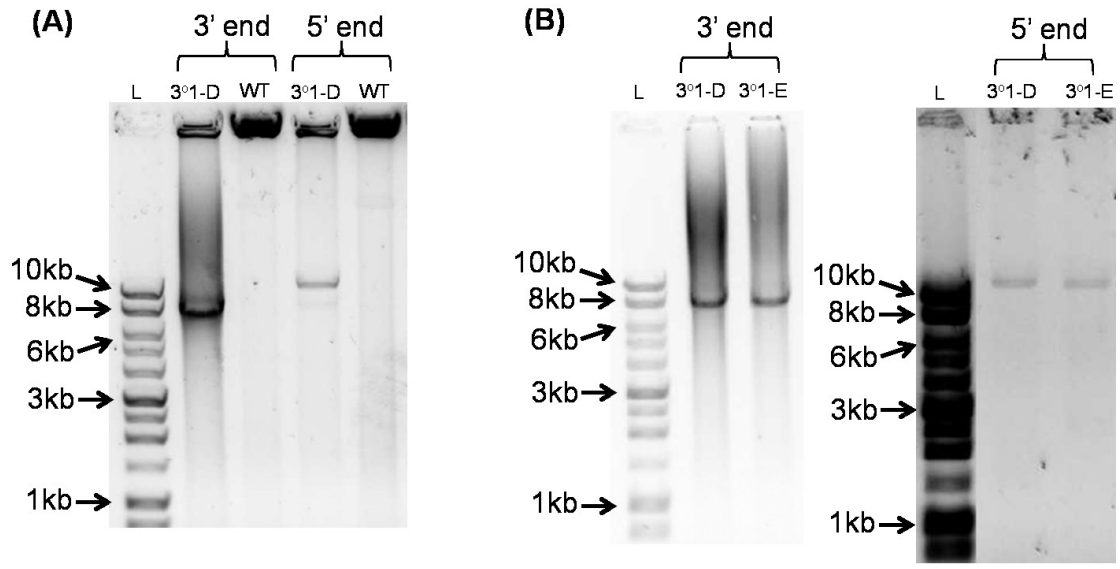

Figure A-9: Identification of positive colonies that were correctly targeted as revealed by LA PCR. LA PCR using both 5' and 3' end screening primers was performed on either wild type control DNA (WT) or DNA prepared from positive colonies (3^{o}1-D and 3^{o}1-E). The products were then run on 0.5% agarose gel for analysis. (A) 3^{o}1-D colony DNA showed correct targeting at both the 5' and 3' ends, generating the expected band of ~10.9kb and 7.6kb, respectively, whereas neither end gave any signals in WT control DNA. (B) Identical to colony 3^{o}1-D, 3^{o}1-E DNA generated a PCR product of ~7.6kb at the 3' end, as well as a band of ~10.9kb at the 5' end, demonstrating that 3^{o}1-E was also correctly targeted. L: 1kb DNA ladders.

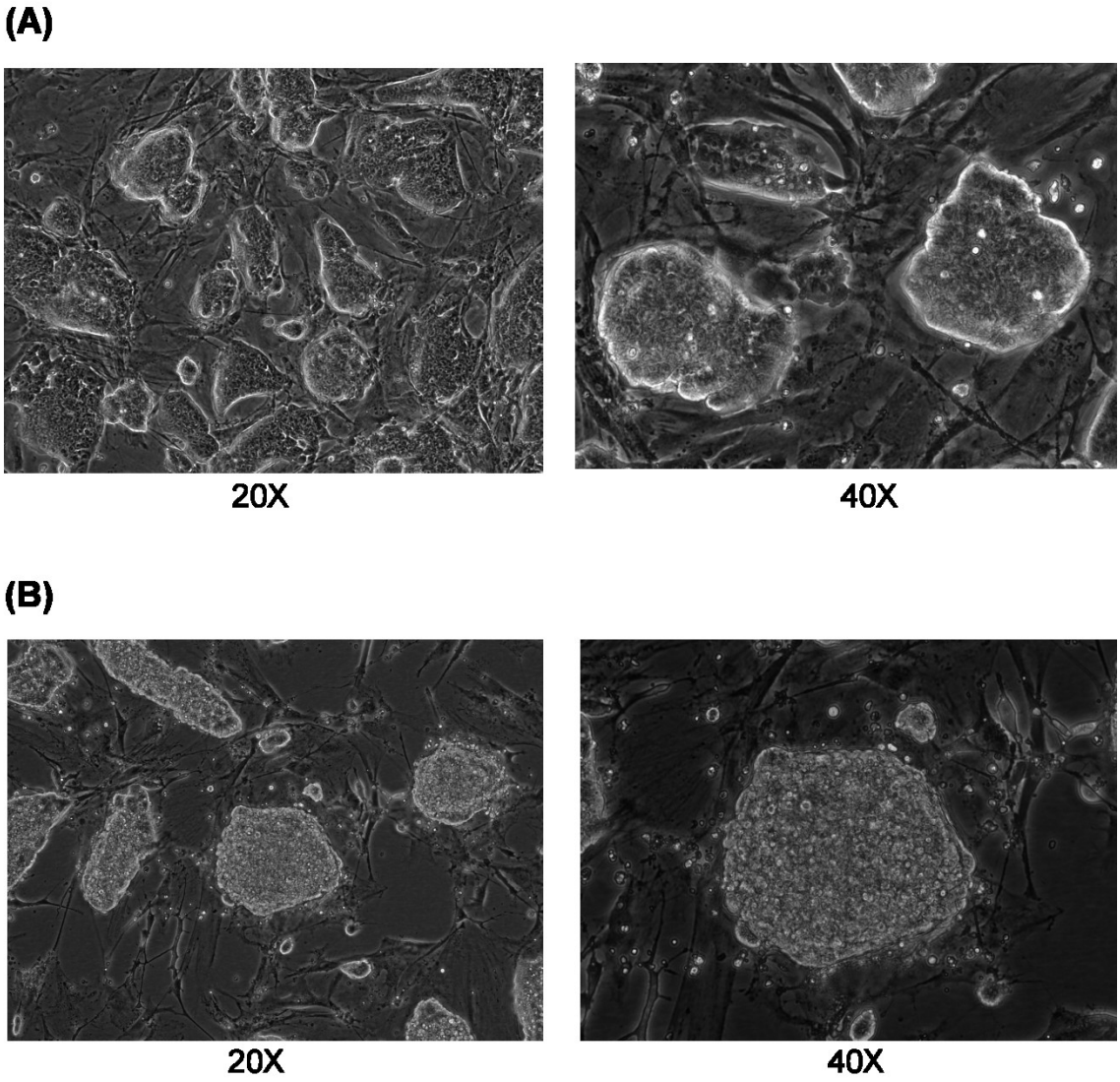

Figure A-10: Morphology of targeted colonies under light microscope. The positively targeted ES colonies of 3^{o}1-D (A) and 3^{o}1-E (B) were examined under microscope (at both 20X and 40X magnifications) to verify the characteristics of an undifferentiated state. The well established hallmarks include: compact and cobblestone shaped colonies with multiple cells, a high nucleus-cytoplasm ratio and a distinct colony border.

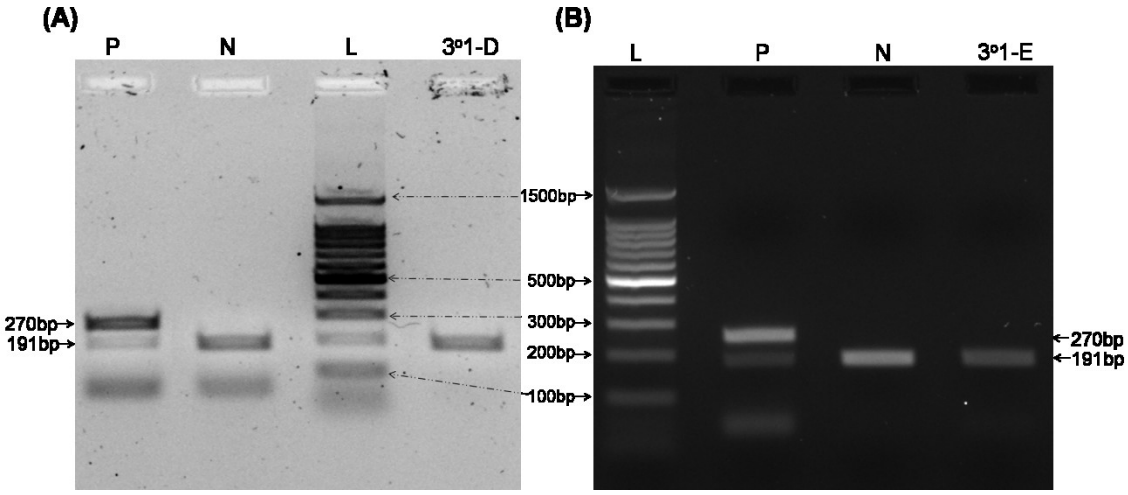

Figure A-11: Both targeted colonies 3°1-D and 3°1-E were mycoplasma negative. Enriched culture supernatant from each colony was collected and processed to serve as template DNA in subsequent PCR based detection of mycoplasma species. A successful PCR always generates a band of ~191bp due to the presence of internal control DNA in the reaction system. Negative control (N) only yields the internal control PCR band, whereas positive control (P) generates an additional band of ~270bp because of the presence of mycoplasma DNA. All the PCR products were analyzed on 1.5% agarose gel. Our results indicated that neither 3°1-D (A) nor 3°1-E (B) colony was contaminated by mycoplasma. L: 100bp DNA ladders

(A)

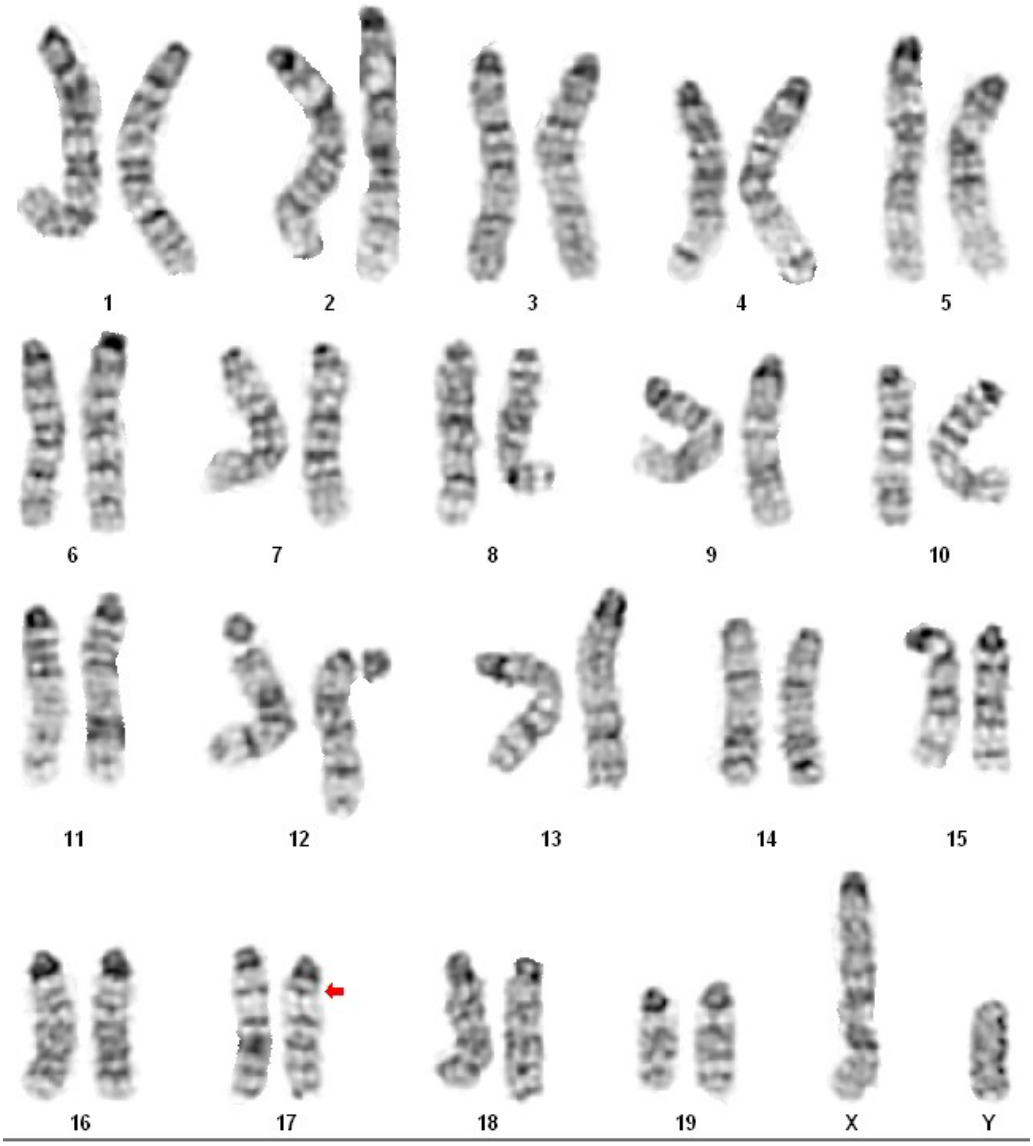

Figure A-12: Karyotyping analysis of the targeted positive colonies. ES cells were first treated for 3 hours with colcemid, before being harvested according to standard cytogenetic protocol. (A) 20 metaphases from 3^{o}1-D colony were completely analyzed by G-banding. All 20 of the metaphase cells analyzed had a male karyotype (38 total autosomes plus sex chromosomes of X and Y) including one normal chromosome 17 and one abnormal chromosome 17 with a small deletion within the proximal long arm (indicated by red arrow). (Panel B and its legends continued on the next page)

(B)

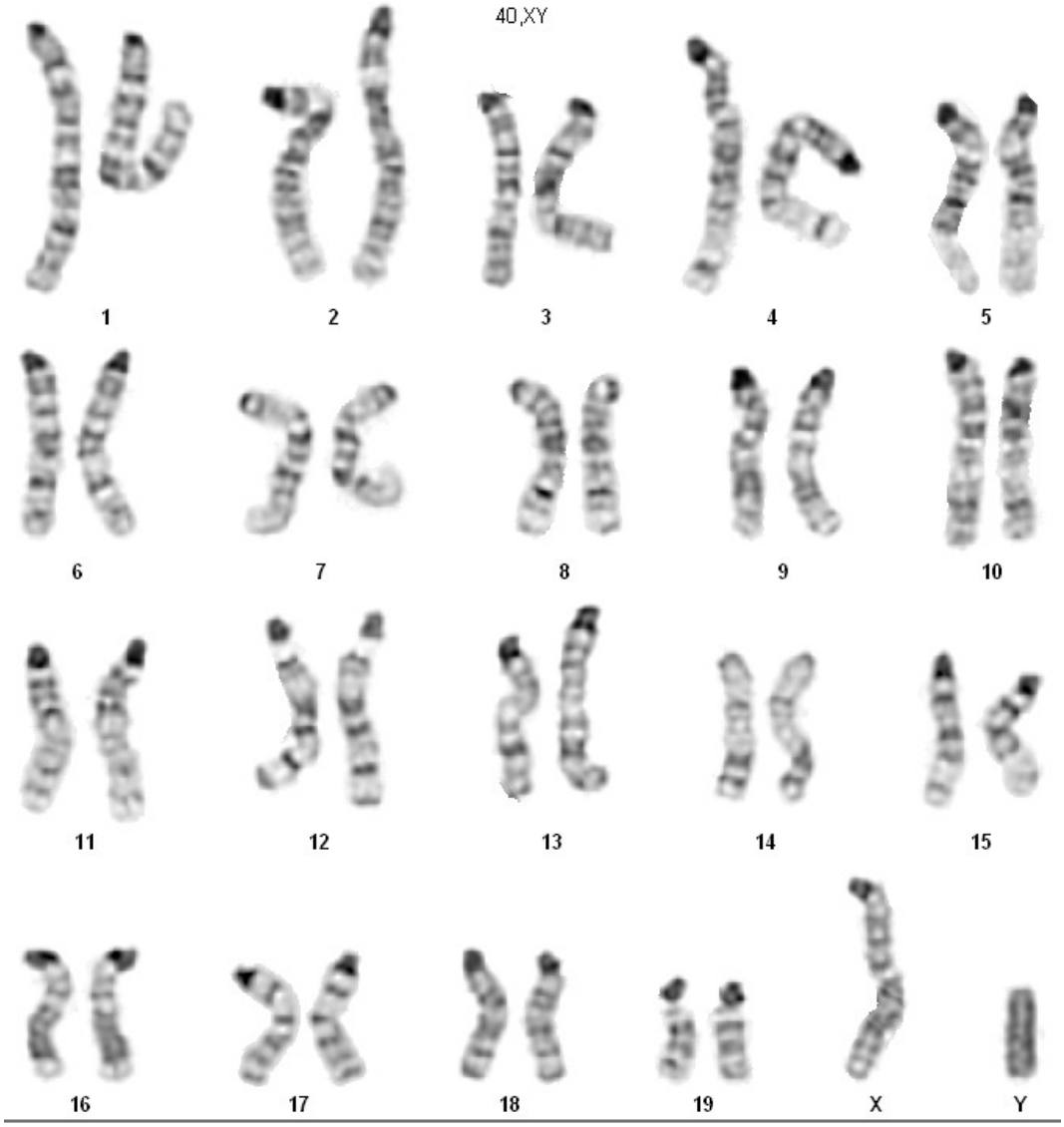

(B) 20 metaphases from 3°1-E colony were completely analyzed by G-banding. 19 metaphases had a normal 40,XY male karyotype. The remaining single metaphase had 42 chromosomes including one extra copy each of chromosomes Y and 8. To rule out the presence of a cell line with +Y and +8, an additional 30 metaphases were screened. All of them had only one Y and two #8 chromosomes present. Thus, the single cell finding with +Y and +8 was considered nonclonal, and this study was interpreted as normal 40,XY.

(A)

(B)

(C)

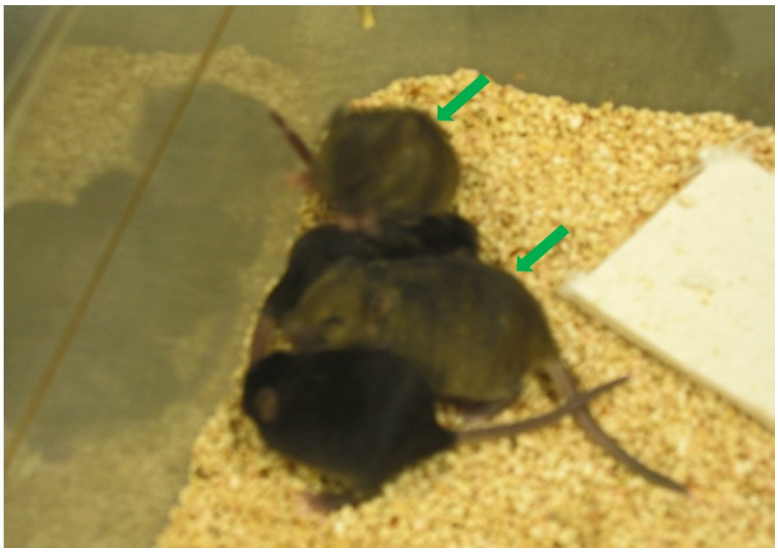

Figure A-13: Chimeric mice generated from blastocysts injected with 3^{o}1-E ES cells. Blastocysts of C57BL/6 strain (black coat color; panel A, adapted from the Jackson Laboratory) were injected with our genetically modified 3^{o}1-E ES cells originally derived from 129S1/SvImJ strain (white-bellied agouti coat color; panel B, adapted from the Jackson Laboratory), and implanted into pseudopregnant C57BL/6 females. The resulting chimeras, generated from blastocysts containing both C57BL/6 and CJ129 ES cells, exhibited streaked black color across agouti (as indicated by green arrows in panel C). A total of 8 such chimeras were obtained, 2 of which were females and 6 were males.

Discussion:

To study the multiple roles of MCT1 in various biological conditions, such as brain energy metabolism, long term memory, diabetes and cancers, we attempted to generate *Mct1* conditional knockout mouse model. However, all the chimeras failed in producing desired offspring that inherited one copy of the knocked-out allele. Several possible reasons can account for the unsuccessful initiative, including: (1) one functional copy of MCT1 is not sufficient for normal germ cells (e.g. sperms) development and future fertilization; (2) the relatively long period of culture and high passage number of ES cells before injection may compromise their potency of inserting into germ line during embryonic development; (3) the presence of large foreign DNA sequence (e.g. NeoR, LacZ) in the animal's genome may impose genetic perturbations that lead to reduced germ cells functionality; (4) injection of multiple positive colonies is recommended and has been shown to increase ES cells germline transmission.

The design of our targeting vector ensures of generating a modified *Mct1* allele that is inactivated and knocked-out upon correct homologous recombination, due to the presence of a polyadenylation signal pA right after Neo^R gene. Therefore, transcription machinery stops immediately after the pA, leaving a truncated version of *Mct1* mRNA. This is so called "Knockout-first" strategy (392). Although *LoxP* sites are still intact after homologous recombination in the modified allele, that *Mct1* gene is already disrupted before embryonic injection. As a consequence, removal of the selective cassette before injection via *Flp-FRT* system will fix the knocked-out allele and restore two normal *Mct1* alleles, which may help improve the generation of desired offspring after chimeras. The necessity of maintaining a functional copy of *Mct1* in germ cells comes from the observation that sperms, which usually contain half of a diploid genome and thus only one allele of a gene, expresses high quantity of MCT1 (53, 393). As a result, sperms carrying the allele copy derived from modified ES cells may not be functional as well as, if not lethal, than the wild type ones. Future efforts of removing selective cassette via *Flp-FRT* first before injecting blastocysts are likely beneficial to eliminate the adverse effect of knockout-first on sperm cells homeostasis.

As a golden rule of all cell culture, reduced incubation time in culturing dishes *in vitro* as well as maintaining a lower passage number of cells, can help preserve their functional performances and cellular characteristics. The long *in vitro* gene targeting process (about 4 weeks) and a relatively high passage number of ES cells before injection (P19) may compromise the inherent capacity of our cells to incorporate into germ line layers. Besides, the presence of large foreign DNA sequences (e.g. LacZ and Neo^R gene) and their products, especially neomycin resistant protein, may exert unexpected stress on the recipient's genome. In fact, insertion of Neo^R gene into mouse genome for gene targeting purpose was found to interfere with neighboring off-target genes expression (394). So, removal of extra alien DNA sequences may help maintain ES cells normal health and improve reproductive efficiency. Finally, injecting multiple ES cell lines that have all gone homologous recombination and quality control tests, is believed to improve the chance for ES cells to translocate into inner cell mass where they will develop into reproductive system (395). Possible explanations include that: (1) multiple ES cells from different colonies injected into a host blastocyst provide some paracrine factors which support their initial survival; (2) not every single ES cell line is fully potent to support embryogenesis due to both genetic and epigenetic changes occurring during cultivation process (396). In this regard, the low efficiency of generating desired mice with single cell colony injection can be a likely reason to explain the absence of heterozygous mice in our current study.

A recent study reported by Lee et al (38) shows the generation of *Mct1* heterzygous knockout mice. In their study, the first exon of *Mct1* was replaced by LacZ and neomycin resistance gene sequence, thus inactivating *Mct1*'s function in one of the two alleles. This observation supports the idea that sperms or oocytes without MCT1 may still able to survive and fertilize with normal oocytes or sperms respectively, to generate the heterozygous knockout animals. Another possibility that needs to keep in mind is that, their targeting strategy might generate a huge fusion protein (LacZ-Neo^R-ΔMCT1), because all the other exons of *Mct1* gene may be still transcribed and translated into peptides, thus providing some functionality of this transporter. Detailed information and clarifications from their targeting strategy would help resolve this question.

In summary, our study provided a valuable rationale for generating *Mct1* conditional knockout model. Further efforts using modified targeting strategy, identifying more positive colonies, and starting with new ES cells with a low passage number, may greatly help to improve the outcome.